

**STATIC AND DYNAMIC NEURAL NETWORK
MODELING FOR REINFORCED CONCRETE
SLAB**

SEYED VAHID RAZAVI TOSEE

**THESIS SUBMITTED IN FULFILLMENT OF THE
REQUIREMENTS FOR THE DEGREE OF DOCTOR OF
PHILOSOPHY**

**DEPARTMENT OF CIVIL ENGINEERING
FACULTY OF ENGINEERING
UNIVERSITY OF MALAYA
KUALA LUMPUR**

2012

ABSTRAK

Model analisis tradisional untuk konkrit bertulang struktur yang boleh dipercayai dan tingkah laku unsure-unsur struktur boleh Berjaya ditentukan menyelesaikan beberapa persamaan berangka. Satu lagi kaedah pemodelan analisis alternative Artificial neural Network (ANN), yang menguasai persamaan berangka antara nod dan tiada formula rasmi diperhatikandalam tempoh satu generasi rangkaian. Kajian terdahulu ANN dalam Kejuruteraan Struktur terutamanya tertumpu kepada Feed-forward Back-propagation Neural Network (FBNN) menggunakan data yang mencukupi untuk generasi rangkaian. Objektif utama kajian ini adalah untuk melatih ANN untuk meramalkan pertengahanrentang pesongan papak sehalu untuk situasi di mana data yang ada tidak mencukupi tersedia untuk generasi rangkaian. Kajian ini juga dianggap sebagaipemodelan rangkaian dengan ruang dalaman yang dinamik dan kelewatan selaras rakaman untuk analisis pembelotan beban yang sememangnya boleh menghafai datainput manakala proses latihan. La melibatkan ramalan pesongan beban 19 bukan papak diperkukuhkan di bawahpertengahan span menumbuk beban dan 7 Carbon Fiber Reinforced Polymer (CFRP) mengukuhkan papak di bawah baris empat beban titik. Keputusan data eksperimenbebanding dengan analisis unsure terhingga menggunakan perisian LUSAS. Keputusanjuga telah disahkan kod BS dan ISIS bukan diperkukuhkan dan CFRP mengukuhkanpapak masing-masing. Generalized Regression Neural Network (GRNN) sebagai Static Neural Network (SNN) telah dijana daripada keputusan eksperimen manakala terdapat data tidak mencukupi untuk generasi rangkaian. Untuk meramakan pesongan pertengahan rentang papak, duajenis Dynamic Neural Network (DNN) iaitu Focused Feed-forward Time-delay Neural Network (FFTDNN) and Recurrent Neural Network (RNN) telah dijana dengan data yang mencukupi. Kajian ini juga berbanding bersama GRNN yang, FBNN, FFTDNN, dan

RNN untuk situasi di mana data adalah mencukupi untuk generasi rangkaian. Hasil kajian menunjukkan bahawa GRNN di mana menggunakan data mencukupi menyelesaikan masalah dalam teknik yang sesuai dengan ralat min 8 dan 11.3% untuk bukannya diperkukuhkan dan CFRP mengukuhkan papak masing-masing. Yang FFTDNN yang di mana, RNN, FBNN, dan GRNN menggunakan data yang mencukupi meramalkan pesongan dengan kesilapan min 8, 9.7, 10.5, and 14.9% masing-masing untuk CFRP mengukuhkan papak. Ia adalah jelas bahawa menggunakan FFTDNN dan pemodelan RNN menyediakan prestasi cemerlang lebih FBNN dan GRNN untuk analisis beban-pesongan papak.

ABSTRACT

Traditional analysis models for reinforced concrete (RC) structures are reliable and the behavior of structural elements can be successfully determined by solving several numerical equations. Another alternative analytical modeling method is Artificial Neural Networks (ANNs), which capture the numerical equations between its nodes and no formal formula is observable within the network generation. Previous researches of ANNs in Structural Engineering mainly focused on Feed-forward Back-propagation Neural Network (FBNN) using sufficient data for network generation. The key objective of this research is to train ANNs to predict mid-span deflection of RC one-way slabs for situation where insufficient data is available for network generation. This research also considered a network modeling with internal dynamic space and tapped-delay line for load deflection analysis which inherently could memorize the input data while training process. It involves the prediction of load deflection of 19 non-strengthened RC slabs under mid-span punching load and 7 Carbon Fiber Reinforced Polymer (CFRP) strengthened RC slabs under four point line loads. The results of experimental data were compared with finite element analysis using LUSAS software. The results were also validated with BS and ISIS code for non-strengthened and CFRP strengthened RC slab respectively. Generalized Regression Neural Network (GRNN) as Static Neural Network (SNN) was generated from the experimental results while there were insufficient data for network generation. To predict the mid-span deflection of RC slab, two types of Dynamic Neural Network (DNN) namely Focused Feed-forward Time-delay Neural Network (FFTDNN) and Recurrent Neural Network (RNN) were generated with sufficient data. This study also compared together the GRNN, FBNN, FFTDNN, and RNN for situations where data is sufficient for network generation. The results showed that the generated GRNN using insufficient data solve

the problems in suitable techniques with mean error of 8 and 11.3% for non-strengthened and CFRP strengthened RC slab respectively. The generated FFDNN, RNN, FBNN, and GRNN using sufficient data predicted the deflection with mean error of 8, 9.7, 10.5, and 14.9% respectively for non-strengthened RC slab and 7.3, 8.4, 9.3, 14.4% respectively for CFRP strengthened RC slab. It is clear that using FFDNN and RNN modelling provided outstanding performance over the FBNN and GRNN for load-deflection analysis of RC slab.

University of Malaya

ACKNOWLEDGMENT

I owe special thanks to several people for their help, guidance, and support while I worked on my dissertation.

First, I would like to thank my supervisor, Prof. Mohd. Zamin Jumaat, for his motivation, guidance, encouragement, and assistance throughout all aspects of my Ph.D thesis. I would also like to thank my co-supervisor, Associate. Prof. Ahmed EI-Shafie, for his helpful insight, support, and suggestions during all the stages of this work.

My special thanks go to my Wife, Pegah Mohammadi, for always standing by my side. I am grateful for his love, support, and extreme patience throughout this entire research. My deepest thanks go to my sweetie angel 5 years old daughter, Vania. I would also like to thank my parents for always believing in me, support, encouragement, and guidance.

Finally, I want to thanks all of the staffs at the Department of Civil Engineering, UM, for their supports and encouragement during the process of completing this research.

God has truly blessed me and I am so thankful to Him for His blessings, guidance and for surrounding me with such wonderful professors, lecturers, and family members who provided me support and guidance through this entire journey. I also thank God for giving me the ability to complete this research.

Table of Content

1. INTRODUCTION	1
1.1 Research Background	1
1.2 Statement of the Problem.....	4
1.3 Objective of the Thesis	5
2. LITERATURE REVIEW	6
2.1 Introduction.....	6
2.2 Traditional Models for Predicting of Concrete Behaviour	6
2.3 Empirical Models for RC Slab Deflection Analysis.....	8
2.4 Finite Element Models for Analysis of RC Slab	10
2.5 Neural Network as a Modeling Technique	13
2.6 Strengthening of Concrete Structures	21
3. ANALYTICAL MODELING	25
3.1 Empirical Modeling for Non-strengthened RC Slab	25
3.1.1 Mechanical properties of the slab under mid-span punching load	25
3.1.2 BS Code for Non-strengthened RC Slab	32
3.1.2.1 Design moment using BS code	32
3.1.2.2 First crack moment using BS code.....	34
3.1.2.3 Deflection calculation using BS code	34
3.1.2.4 Example for the non-strengthened RC one-way slab.....	37
3.2 Empirical Modeling for CFRP Strengthened RC Slab	38
3.2.1 Design moment using ISIS Canada	38
3.2.2 First crack moment using ISIS Canada	40
3.2.3 Deflection calculation using ISIS Canada.....	41
3.2.4 Example for CFRP strengthened RC one-way slab	42
3.3 Finite Difference Method for Deflection Calculation	44
3.3.1 Example for deflection calculation using finite difference	47
4. FINITE ELEMENT ANALYSIS	51
4.1 Introduction.....	51
4.2 Fundamentals and Theory of Using LUSAS Software.....	53
4.3 Modeling Process.....	54
4.3.1 Geometry modeling for RC slab.....	56
4.3.2 Defining attributes for RC slab.....	56
4.3.2.1 Meshing.....	57
4.3.2.2 Element selection	57
4.3.2.3 Geometric properties	59
4.3.2.4 Material properties	59
4.3.2.5 Support condition	62
4.3.2.6 Loading	63
4.3.3 Analysis and results processing.....	64
5. ANN MODELING FOR RC SLAB	66
5.1 Introduction.....	66
5.2 NN Definition	68
5.3 Neural Network Concept Development.....	70

5.3.1	Network connection type.....	71
5.3.2	Feed-forward back-propagation neural network.....	71
5.3.2.1	Network architecture.....	71
5.3.2.2	Transfer function.....	73
5.3.2.3	Network training and learning function.....	75
5.3.2.4	Data normalization.....	76
5.3.3	General regression neural network.....	77
5.3.3.1	Network architecture.....	77
5.3.3.2	Transfer function.....	78
5.3.3.3	Net algorithm.....	80
5.3.4	Dynamic neural networks.....	81
5.3.4.1	Focused time delay neural network.....	82
5.3.4.2	Recurrent neural network.....	83
5.4	ANN Modelling.....	87
5.4.1	FBNN modeling for CFRP strengthened RC slab.....	88
5.4.2	GRNN modeling for for CFRP strengthened RC slab.....	91
5.4.3	FFTDNN modeling for CFRP strengthened RC slab.....	94
5.4.4	RNN Modeling for CFRP Strengthened RC Slab.....	96
6.	EXPERIMENTAL WORK.....	98
6.1	Material and Experimental Program.....	98
6.1.1	Material used in the study.....	100
6.1.1.1	Cement.....	100
6.1.1.2	Water.....	100
6.1.1.3	Fine aggregate.....	100
6.1.1.4	Coarse aggregate.....	101
6.1.1.5	Formwork.....	101
6.1.1.6	Reinforcing bar.....	102
6.1.1.7	Carbon fiber reinforced polymer.....	103
6.1.1.8	Adhesive.....	103
6.1.2	Concrete mix design and mixing of material.....	104
6.1.3	Preparation of Reinforced Concrete Slabs.....	106
6.1.3.1	Instrumentation.....	107
6.1.3.2	Instrument setup for non-strengthened RC one-way slab.....	108
6.1.3.3	Instrument Setup for CFRP Strengthened RC One-way Slab.....	109
6.2	Experimental Work.....	110
6.2.1	Non-strengthened RC one-way slab.....	110
6.2.1.1	Design and ultimate moment.....	110
6.2.1.2	Load-deflection analysis.....	112
6.2.2	CFRP Strengthened One-Way RC Slab.....	118
6.2.2.1	Design and Ultimate Moment.....	120
6.2.2.2	Cracking.....	121
6.2.2.3	Load-Deflection Analysis.....	130
7.	ANALYSIS AND RESULTS.....	134
7.1	Feed-forward Back-propagation Neural Networks.....	134
7.1.1	Load-deflection analysis of non-strengthened RC slab.....	134
7.1.2	Load-deflection analysis of CFRP strengthened RC slab.....	139
7.2	Generalized Regression Neural Network.....	142
7.2.1	Non-strengthened RC slab.....	142
7.2.1.1	Using GRNN for load-deflection analysis.....	142
7.2.1.2	Using GRNN for maximum mid-span deflection.....	144

7.2.2	CFRP strengthened RC slab	146
7.2.2.1	Using GRNN for load-deflection analysis	146
7.2.2.2	Using GRNN for deflection prediction	149
7.3	Focused Feed-forward Time-delay Neural Network	151
7.3.1	FSTDNN for load-deflection analysis of non-strengthened RC slab	151
7.3.2	FSTDNN for load-deflection analysis of CFRP strengthened RC slab	155
7.3.3	Using FSTDNN for prediction of crack width	160
7.4	Recurrent Neural Network	163
7.4.1	RNN for load-deflection analysis of non-strengthened RC slab	163
7.4.2	RNN for load-deflection analysis of CFRP strengthened RC slab	167
7.4.3	Using RNN for prediction of crack width	170
7.5	Summary	175
8.	CONCLUSION AND RECOMMENDATION	183
8.1	Conclusion	183
8.2	Contribution	185
8.3	Recommendation	185
	REFERENCES	187
A.	MECHANICAL PROPERTIES OF LIGHTWEIGHT MIXTURE	195
A.1	Lightweight Aggregate	195
A.2	Mixture Design	197
A.3	Experimental Results	201
A.3.1.	Lightweight Concrete	201
A.3.2.	Lightweight Mortar	211
A.4	Feed-forward Back-propagation Neural Networks	216
A.4.1.	Lightweight Concrete	216
A.4.2.	Lightweight Mortar	219
A.5	Generalized Regression Neural Network (GRNN)	224
A.5.1.	Lightweight Concrete	224
A.5.2.	Lightweight Mortar	226
B.	FIRST CRACK ANALYSIS OF CFRP STRENGTHENED RC SLAB	231
B.1.	Experimental Results	232
B.2.	General regression neural network	234
C.	OTHER PUBLISHED EXPERIMENTAL WORK	237
C.1.	Prediction of elastic modulus of high strength concrete	237
C.2.	Crack width prediction of RC beam under short time loading	242
C.3.	Load-Deflection Analysis of High Strength Concrete Deep Beam	247
D.	The Results of the LUSAS Finite Element Analysis	251
E.	Normalized Experimental Results Applied for NN	256
E. 1.	Non-strengthened RC Slab	256
E.2.	CFRP Strengthened RC Slab	259
F.	ARTIFICIAL NEURAL NETWORKS	260

List of Figures

Figure 2.1: Process involve in designing structural elements	13
Figure 3.1: Cracking pattern of the small width-length ratio slab.....	26
Figure 3.2: Cracking pattern of the large width-length ratio slab	26
Figure 3.3: The distribution of actual reaction force	26
Figure 3.4: The distribution of actual reaction	27
Figure 3.5: Experimental crack pattern of the non-strengthened RC slab under mid-span punching load	31
Figure 3.6: Non-strengthened RC slab under mid-span punching load after testing	31
Figure 3.7: Simplified stress block method for the non-strengthened RC slab.....	32
Figure 3.8: Simplified stress block method for the CFRP strengthened RC one-way slab	38
Figure 3.9: Un-cracked transformed section for the CFRP strengthened RC slab.....	40
Figure 3.10: The basic definition of finite difference method.....	44
Figure 3.11: Simplified network definition for the Equation 3.48	45
Figure 3.12: Networks for solving two-dimensional problem	46
Figure 3.13: Input data and network numbering for the slab 55-2T10-860	47
Figure 4.1: Configuration of non-strengthened RC slab used in LUSAS modeling	55
Figure 4.2: Configuration of CFRP strengthened RC slab used in LUSAS modeling...	56
Figure 4.3: Meshing applied for the concrete, steel bar, and CFRP.....	57
Figure 4.4: QPM8 surface element used for concrete	58
Figure 4.5: BAR3 line element used for steel bar and CFRP.....	58
Figure 4.6: Simplified stress-strain curve for concrete (Niu, 2006).....	60
Figure 4.7: Simplified stress-strain curve for steel bar and CFRP (Niu, 2006)	62
Figure 4.8: Proposed support condition for the RC slab	62
Figure 4.9: Proposed punching point load assigned on the model for the non- strengthened RC slab	63
Figure 4.10: The line load assigned on the model for the CFRP strengthened RC slab	63
Figure 4.11: Manipulation and visualization in LUSAS software	64
Figure 4.12: A plot of deformed shape for non-strengthened RC slab.....	65
Figure 5.1: The overall process for network modeling	67
Figure 5.2: The biological neuron or a nerve cell(Zhang, 2009).....	68
Figure 5.3: The linear transfer function (Purelin)	73

Figure 5.4: Log-sigmoid transfer function(Logsig).....	74
Figure 5.5: Tan-sigmoid transfer function(Tansig).....	74
Figure 5.6: A model of PNN/GRNN.....	77
Figure 5.7: GRNN with individual terms tending for prediction, $\sigma = 0.1$	80
Figure 5.8: A two-layer focused time-delay neural network (Beale et al, 2011).....	82
Figure 5.9: General architecture presentation for FFTDNN (Abed et al, 2010).....	83
Figure 5.10: The basic RNN architecture.....	84
Figure 5.11: Typical RNN architecture (EI-Shafie et al, 2008).....	86
Figure 5.12: The FBNN architecture for the CFRP strengthened RC one-way slab.....	90
Figure 5.13: The GRNN architecture for the CFRP strengthened RC one-way slab.....	92
Figure 5.14: The FFTDNN architecture for the CFRP strengthened RC one-way slab.....	95
Figure 5.15: The RNN architecture for the CFRP strengthened RC one-way slab.....	96
Figure 6.1: Particle size distribution of the fine and coarse aggregates.....	101
Figure 6.2: The formwork used for casting in the experimental work.....	102
Figure 6.3: The longitudinal reinforcement used for the non-strengthened and CFRP strengthened RC one-way slab.....	102
Figure 6.4: The casting and curing of the slabs.....	107
Figure 6.5: Instrument setup for non-strengthened one-way RC slab under mid-span punching load.....	108
Figure 6.6: Instrument setup for CFRP strengthened one-way RC slabs under linear load.....	109
Figure 6.7: Plot of numerical analysis for the slab 100-3T10-2400.....	111
Figure 6.8: Plot of numerical analysis for the slab 70-3T10-1350.....	112
Figure 6.9: The experimental results of load-deflection curve for the samples 100-3T10-2400 and 120-3T10-2400 in compare with LUSAS results.....	114
Figure 6.10: The experimental results of load-deflection curve for the samples 120-4T10-1800 and 120-3T10-1800 in compare with LUSAS results.....	114
Figure 6.11: The experimental results of load-deflection curve for the samples 100-4T10-1800 and 100-3T10-1800 in compare with LUSAS results.....	115
Figure 6.12: The experimental results of load-deflection curve for the samples 55-2T10-1350, 55-3T10-1350, and 55-4T10-1350 in compare with LUSAS results.....	115
Figure 6.13: The experimental results of load-deflection curve for the samples 70-3T10-1350 and 70-2T10-1350 in compare with LUSAS results.....	116

Figure 6.14: The experimental results of load-deflection curve for the samples 0-3T10-1350 and 90-2T10-1350 in compare with LUSAS results	116
Figure 6.15: The experimental results of load-deflection curve for the samples 55-3T10-860 and 55-2T10-860 in compare with LUSAS results	117
Figure 6.16: The experimental results of load-deflection curve for the samples 70-3T10-860 and 70-2T10-860 in compare with LUSAS results	117
Figure 6.17: RC one-way slab strengthened by different lengths and width of CFRP	118
Figure 6.18: The overall crack pattern of the CFRP strengthened RC slab under four point line load	119
Figure 6.19: CFRP debonding at the CFRP/concrete interface under four point line load	119
Figure 6.20: Crack measuring in each step of applied loading	121
Figure 6.21: Measuring guide for the crack location and width presented in Figures 6.22 to 6.28 and Tables 6.13 to 6.19.....	122
Figure 6.22: The loading and crack presentation for the slab without CFRP	123
Figure 6.23: The loading and crack presentation for the RC slab strengthened by CFRP S512-700.....	124
Figure 6.24: The loading and crack presentation for the RC slab strengthened by CFRP S512-1100.....	125
Figure 6.25: The loading and crack presentation for the RC slab strengthened by CFRP S512-1500.....	126
Figure 6.26: The loading and crack presentation for the RC slab strengthened by CFRP S812-700.....	127
Figure 6.27: The loading and crack presentation for the RC slab strengthened by CFRP S812-1100.....	128
Figure 6.28: The loading and crack presentation for the RC slab strengthened by CFRP S812-1500.....	129
Figure 6.29: Comparison of load-deflection analysis between CFRP strengthened one-way RC slab with different lengths of CFRP-S512 and WCFRP	131
Figure 6.30: Comparison of load-deflection analysis between CFRP strengthened one-way RC slab with different lengths of CFRP-S812 and WCFRPb	132
Figure 6.31: The percentage of the improved maximum applied loading in the RC one-way slabs strengthened by different length of the CFRP-S512 and CFRP-S812.....	132

Figure 6.32: Load-deflection comparison between non-strengthened one-way RC slab and strengthened by CFRP512-1500 and CFRP S812-1500.....	133
Figure 6.33: Failure load for different cross section area of the applied CFRP on slabs	133
Figure 7.1: The FBNN training process for prediction of mid-span deflection in non-strengthened RC slab	136
Figure 7.2: The regression plot for the optimum network after FBNN generation.....	137
Figure 7.3: The FBNN testing error for deflection analysis of slab S812-1100	139
Figure 7.4: The FBNN architecture, algorithm, and training performance.....	140
Figure 7.5: Evaluation between experimental and predicted deflection for slab S812-100 by FFBP	141
Figure 7.6: An evaluation between experimental deflection and predicted by GRNN for non-strengthened RC slab.....	142
Figure 7.7: An evaluation between experimental and predicted deflection of slab 100-3T10-1800 by using GRNN	144
Figure 7.8: The evaluation between experimental and predicted deflections of non-strengthened RC slab in GRNN training phase	145
Figure 7.9: Comparison between predicted maximum deflection and experimental output for the slabs 120-2T10-1800, 100-2T10-1800, and 90-3T10-1350.....	145
Figure 7.10: An evaluation between predicted and target deflections on failure load of CFRP strengthened RC slab in GRNN training phase	147
Figure 7.11: An evaluation between predicted and target deflections of failure load on CFRP strengthened RC slab in GRNN testing phase	147
Figure 7.12: An assessment between experimental load-deflections analysis and predicted by GRNN for slab CFRP S812-1100.....	148
Figure 7.13: An evaluation between normalized target and predicted deflections on the sample CFRP S512-700 in GRNN training phase.....	149
Figure 7.14: An evaluation between normalized target and predicted deflections on the sample CFRP S512-700 in GRNN testing phase	150
Figure 7.15: The FFTDNN architecture for non-strengthened RC slab.....	151
Figure 7.16: The nntaintool running in the FFTDNN training stage for the non-strengthened RC slab	152
Figure 7.17: A plot of correlation of determination R^2 using FFTDNN	153
Figure 7.18: Correlation coefficient R^2 plot for slab 100-3T10-1800 using FFTDNN	155

Figure 7.19: FFTDNN Training process for load-deflection curve prediction of CFRP strengthened RC slab	156
Figure 7.20: A comparison between FFTDNN output and experimental results for deflection of CFRP strengthened RC slab	157
Figure 7.21: An evaluation between predicted and experimental load-deflection analysis in FFTDNN training phase for CFRP strengthened RC slab	158
Figure 7.22: Evaluation between experimental and predicted deflection after FFTDNN testing stage on slab S812-1100	159
Figure 7.23: Load deflection curve from FFTDNN and experimental work for the slab S812-1100.....	160
Figure 7.24: The selected FFTDNN architecture for crack width prediction of CFRP strengthened RC slab at maximum applied load	161
Figure 7.25: Evaluation between experimental and predicted crack width on maximum applied loading on CFRP strengthened RC slab using FFTDNN after training phase.....	162
Figure 7.26: Evaluation between experimental and predicted maximum crack width after FFTDNN testing phase.....	163
Figure 7.27: The selected network architecture for non-strengthened RC slab using RNN.....	164
Figure 7.28: RNN running procedure in training stage for non-strengthened RC slab	164
Figure 7.29: The values of correlation of coefficient in network generation for non-strengthened RC slab	165
Figure 7.30: A comparing between experimental results and RNN output for mid-span deflection of slab 100-3T10-1800	167
Figure 7.31: RNN training for load-deflection prediction of CFRP strengthened RC slab.....	168
Figure 7.32: Evaluation between experimental and predicted deflection on CFRP strengthened RC slab after RNN training phase.....	169
Figure 7.33: Evaluation between experimental and predicted deflection of slab S812-1100 after RNN testing phase.....	170
Figure 7.34: The selected RNN architecture for crack width prediction	171
Figure 7.35: RNN training for crack width prediction in maximum applied loading on CFRP strengthened RC slab	171
Figure 7.36: Evaluation between experimental and predicted crack width after RNN training phase.....	172

Figure 7.37: A comparison between RNN output and experimental results for crack width after training	172
Figure 7.38: Plot of experimental crack width at maximum load versus crack width from RNN	173
Figure 7.39: A comparison between RNN output and experimental results for maximum loading crack width after testing process.....	174
Figure 7.40: The correlation of determination R^2 comparison between generated FBNN and GRNN with sufficient data for various experimental works in Table 7.15.....	180
Figure 7.41: The MSE comparison between FBNN and GRNN modeling for the experimental works in Table 7.15.....	181
Figure 7.42: Mean residual error of various modeling for non-strengthened and CFRP strengthened RC slab	182

University of Malaysia

List of Tables

Table 2.1: The values of α , β and m	9
Table 2.2: Using FBNN in initial structural design.....	14
Table 2.3: Using ANN in initial structural design.....	17
Table 2.4: Application of dynamic neural network in civil engineering.....	20
Table 2.5: Mechanical properties of CFRP (Godonue, 2002).....	22
Table 3.1: The values of the bending moment about y direction due to uneven reaction force	30
Table 5.1: Neuron comparison between biological and artificial neural network.....	69
Table 5.2: Properties of the selected FBNN for CFRP strengthened RC slab	88
Table 5.3: Chosen FFTDNN properties for CFRP strengthened RC slab.....	94
Table 6.1: The characteristics of the non-strengthened RC one-way slab under mid-span punching load	99
Table 6.2: The characteristics of samples for the CFRP strengthened RC one-way slab under four point load	99
Table 6.3: The chemical composition of Ordinary Portland Cement (MS, 1989)	100
Table 6.4: Mechanical properties of the CFRP laminate	103
Table 6.5: Mechanical properties of the adhesive Sikadur-30	104
Table 6.6: The test performed on hardened concrete for non-strengthened and CFRP strengthened RC slab	105
Table 6.7: The fresh and hardened concrete test output for the non-strengthened slab	105
Table 6.8: The fresh and hardened concrete test output for the CFRP strengthened slab	106
Table 6.9: Experimental and predicted moment of the non-strengthened RC slabs in flexure	110
Table 6.10: Experimental deflection at the first crack load and ultimate load for the non-strengthened RC slabs	113
Table 6.11: Experimental and predicted ultimate moment of the CFRP strengthened RC slabs in flexure.....	120
Table 6.12: Experimental and predicted ultimate moment of the slabs in flexure.....	121
Table 6.13: The loading, crack location, and crack width for the slab without CFRP.....	123
Table 6.14: The loading, crack location, and crack width for the RC slab strengthened by CFRP S512-700.....	124

Table 6.15: The loading, crack location, and crack width for the RC slab strengthened by CFRP S512-1100	125
Table 6.16: The loading, crack location, and crack width for the RC slab strengthened by CFRP S512-1500	126
Table 6.17: The loading, crack location, and crack width for the RC slab strengthened by CFRP S812-700	127
Table 6.18: The loading, crack location, and crack width for the RC slab strengthened by CFRP S812-1100	128
Table 6.19: The loading, crack location, and crack width for the RC slab strengthened by CFRP S812-1500	129
Table 6.20: Experimental deflection at the first crack and ultimate load for the CFRP strengthened RC one-way slabs.....	130
Table 7.1: The FBNN specifications for non-strengthened RC slab.....	135
Table 7.2: The FBNN testing error for mid-span deflection of slab 100-3T10-1800 ..	138
Table 7.3: The FBNN testing error for prediction of mid-span deflection of slab S812-1800	141
Table 7.4: The GRNN testing MSE for predicted deflection of slab 100-3T10-1800 ..	143
Table 7.5: The GRNN testing MSE for predicted maximum deflection of slabs 120-2T10-1800, 100-2T10-1800, and 90-3T10-1350	146
Table 7.6: The GRNN testing MSE for predicted deflection of slab S812-1800.....	148
Table 7.7: The GRNN testing MSE for the predicted deflection of S512-700	150
Table 7.8: The FFTDNN testing MSE for deflection prediction of slab 100-3T10-1800	154
Table 7.9: The FFTDNN testing MSE for deflection prediction of slab S812-1100 ...	159
Table 7.10: The testing MSE for maximum crack width predicted by FFTDNN.....	162
Table 7.11: The RNN testing MSE for predicted deflection of slab 100-3T10-1800 ..	166
Table 7.12: The RNN testing MSE for predicted mid-span deflection of slab S812-1100	169
Table 7.13: The RNN testing MSE for crack width prediction of CFRP strengthened slab.....	174
Table 7.14: The generated GRNN using insufficient data for network training	176
Table 7.15: The generated GRNN and FBNN using sufficient data for network training	176
Table 7.16: The generated FFTDNN and RNN using sufficient data for network training.....	177

Table 7.17: A comparison between experimental mid-span deflection and predicted by FEA and GRNN using insufficient data for training	177
Table 7.18: A comparison between experimental mid-span deflection and predicted by FEA, FBNN, GRNN, FFTDNN, and RNN using sufficient data for non-strengthened RC slab (100-3T10-1800)	178
Table 7.19: A comparison between experimental mid-span deflection and predicted by FEA, FBNN, GRNN, FFTDNN, and RNN using sufficient data for CFRP strengthened RC slab	179

University of Malaya

ABBREVIATION

ACI	American Concrete Institute
AFRP	Aramid Fiber Reinforced Polymer
AI	Artificial Intelligent
ANNs	Artificial Neural Networks
BDN	Binary Decision Network
BP	Back-Propagation
BS	British Standard
CFRP	Carbon Fiber Reinforced Polymer
DNNs	Dynamic Neural Networks
DOE	Department of the Environment
FBNNs	Feed-forward Back-propagation Neural Networks
FDM	Finite Difference Method
FEA	Finite Element Analysis
FFTDNNS	Focused Feed-forward Time-delay Neural Networks
FRP	Fiber Reinforced Polymer
GFRP	Glass Fiber Reinforced Polymer
GRNNs	Generalized Regression Neural Networks
ISIS	Intelligent Sensing for Innovative Structures
LM	Levenberg-Marquardt
LVDT	Linear variable differential transducers
MLP	Multi Layer Perception
MNN	Multilayer Neural Network
MSE	Mean Squared Error
NNs	Neural Networks

NSM FRP	Near Surface Mounted FRP
OPC	Ordinary Portland Cement
PNN	Probabilistic Neural Networks
RBF	Radial Basis Function
RC	Reinforced Concrete
RMSE	Root Mean Squared Error
RNN	Recurrent Neural Network
SCGA	Scaled Conjugate Gradients Algorithm
SNNs	Static Neural Networks
SSD	Saturated Surface Dry
TDNNs	Time Delay Neural Networks
TNN	Traditional Neural Network
TSS	Time Series Simulation
UPV	Ultrasonic pulse velocity
XOR	Exclusive OR

SYMBOLS

A	The weight matrix of output layer connected to the hidden layer
A_s	Steel bar cross section area
A_{frp}	CFRP cross section area
a	The height of rectangular block stress
B	Slab width
C_c	Compressive force in concrete
C	Depth of natural axes in ISIS Canada
c	Concrete cover
D	Slab bending stiffness
D_i	The distance between the training data and prediction results
D_t	Data
D_{\max}	The largest amount of data
D_{\min}	The smallest amount of data
d	Slab effective depth
E_c	Modulus of elasticity of concrete
E_s	Modulus of elasticity of steel bar
E_{frp}	Modulus of elasticity of FRP
f	Transfer function
f_c	Stress in concrete
f_{cr}	Tension Stress in Concrete at Stress Level
f'_c	Maximum stress in concrete
f_{cu}	Concrete grade
f_y	Steel Bar Yield Stress
f_r	Modulus of Rapture of Concrete

$g []$	The hidden layer hyperbolic tangent function
$H(t+1)$	The updated hidden layer
h	Total depth of section
h_i	Horizontal division in finite difference method
I	Moment of inertia of the transformed reinforced section
I_{cr}	Moment of inertia of cracked section
I_e	Effective second moment of area
I_g	Second moment of area before crack
I_t	Moment of inertia of the transferred reinforced section (un-cracked)
I_o	Normalized data
I_{omax}	The largest amount of normalized data
I_{omin}	The smallest amount of normalized data
K	Curvature factor
K_1	Coefficient for uneven distributed bending moment about x
K_2	Coefficient for uneven distributed bending moment about y
L	Effective Span Length
M	Applied Moment
M_a	Maximum moment in a member at the load stage at which deflection is being calculated
M_c	Moment of resistance of concrete in tension
M_{cr}	First cracking bending moment
M_R	Slab moment design
M_{max}	Maximum bending moment
M_x	Bending moment about x
M_y	Bending moment about y
\overline{M}_x	Mean bending moment about x
\overline{M}_y	Mean bending moment about y
$M_{x_{max}}$	Maximum bending moment about x

$M_{y_{max}}$	Maximum bending moment about y
NH	The number of neurons in hidden layers
NI	The number of neurons in input layer.
NT	The minimum number of training data
NO	The number of output layer neurons
n_s	Steel modular ratio
n_c	CFRP modular ratio
$q(x)$	Uneven reaction force
$\phi(v)$	Threshold function
P	Punching load
p_i	Punching pressure
S_d	Denominator
S_j	Numerator
T_c	Force in concrete in tension
T_s	Tensile force in steel bar
T_{frp}	Tensile force in FRP
t	Slab thickness
u (n+1)	The externally given input
v_k^x	The equivalent clusters for the inputs
v_k^y	The equivalent clusters for the outputs
W_m	The weights of the m hidden nodes connected to the context units
W_{mo}	The weight matrix of the hidden neurons
W^{in}	The input weight matrices
W^{hi}	Hidden layer weight matrix
W^{back}	Output feedback weight matrix
w_k	The weight of the hidden node k
X	Depth of natural axes in BS code

X_1, X_2, \dots	Network input data
X_n, Y_n	Slab crack location
$X(t+a)$	The input layer
Y_1	Network output data
$Y_i(t+1)$	The RNN output
y_t	Distance from center of un-cracked transformed section to extreme tension fiber.
$\alpha, \beta, \text{ and } m$	Factors empirically on specific rebar
$\alpha_1 \text{ and } \beta_1$	Coefficient for concrete compressive stress block
θ_i	Output from pattern layer in GRNN
γ_m	Concrete safety factor
ε_c	Compressive strain in concrete
ε_0	Strain in maximum stress in concrete
ε_{cu}	Concrete failure strain
ε_{frp}	FRP strain
ε_{frpu}	FRP failure strain
ε_s	Steel bar strain
σ	The smoothness parameter
ν	Concrete poisson coefficient
ϕ_c	Concrete resistance factor
ϕ_s	Steel bar resistance factor
ϕ_{frp}	FRP resistance factor
Δ	Slab mid-span deflection
Δ_{cr}	Deflection in the first crack
Δ_{Exp}	Experimental mid-span deflection
Δ_{Net}	Network mid-span deflection
$\frac{d_z}{d_x}, \frac{d_z}{d_y}$	The first derivatives

$$\frac{\partial^2}{\partial x^2}, \frac{\partial^2}{\partial y^2}$$

The second derivatives

$$z_{n+1}$$

Forward point

$$z_{n-1}$$

Backward point

$$\omega$$

Mid-span deflection under punching load in finite difference method

University of Malaya

CHAPTER 1

1. INTRODUCTION

1.1 Research Background

The traditional models used for reinforced concrete (RC) structures are reliable and can successfully determine the load-deflection analysis of the RC slabs and beams. Wium and Eigeaar (2010) observed that the different available calculation methods produce different deflection results. In addition, these models require solving several numerical equations on determining the deflection of RC slabs. Artificial Neural Networks (ANNs) capture the numerical relationship between its nodes and no formal formula is observable within the model. ANNs are trained based on guidelines and relationships between data. Dutta and Shekar (1993) showed that ANNs are able to identify relationships between data even when the data are unclear, changeable, insufficient and ambiguous. Neural networks (NNs) model the impact of input parameters on a set of output conclusions. They apply the influential learn-by-example technique and generalization system to identify the hidden relationships linking the input to their outputs. NNs have the capability to totally identify any complex nonlinear relationship between the dependent and independent variables. The data could be from a market research effort in the form of questionnaires, an assembly procedure of variable working conditions and guidelines, or the result of experimental and observation works in various industries. Medsker and Jain (2001) showed that the goal of NNs is to emulate the human brain's ability to adapt to the changing circumstances based on past experiences and the knowledge acquired there from. This depends entirely on the

ability to learn, remember, and evaluate multipart data relationships. Moselhi (1992) defined in following some advantages of NNs that enable them to predict many different types of applications:

- (1) NNs are able to process data fast due to their parallel and decentralized structure.
- (2) The memories of NNs are distributed using interconnecting weight spread over all of the processing elements.
- (3) NNs remain efficient and functional even when some processing components become defective.
- (4) NNs are able to learn by example.
- (5) NNs are able to simulate with limited modelling attempts.

The science of NN began in 1943, when McCulloch and Pitts published it in their well-known and modern thesis 'A Logical Calculus of the Ideas Immanent in Nervous Activity'. At the same time, they focused on an entirely new era in computer analysis and Artificial Intelligence (AI). Hebb (1949) introduced the training of NN in his published book 'The Organization of Behaviour'. He suggested that the brain is going through one extremely influential changing in the entire life, and by this means it trains tasks. Frank Rosenblatt (1962) presented how to train a binary decision network (BDN), called perceptron. He proved it by changing in the neurons synaptic strengths. Marvin Minsky and Seymour Papert (1969) showed that the neural network was able to run an XOR operation (a binary operation like AND and OR). After that, the problem was resolved by resolution of the hidden neurons. They showed that current training of the networks caused weaknesses in the neural network. They proved that by increasing the number of inputs, the network training time would increase, thus, causing a limitation in the efficiency of the network. Paul Werbos (1974) solved the problem by introduction of the back propagation

algorithm. This algorithm provided a neuron permission to move its error and propagate back to previous layers of the network. It was possible to reduce bigger problems by using this algorithm in training as the neural networks became a successful operation in industry simultaneously. This method allows analogue networks with three or more layers to be generated.

In the last decade, many articles in various fields of science, and, especially, in Civil Engineering, have been published on the use of Feed-forward Back-propagation Neural Network (FBNN). NNs consist of different methods and equations, which are in competition with each other. It is very important to be familiar with the different characteristics of equations in order to select the best possible approach for system modelling. The number of data used in network training is one of the important parameters to generate the optimum network. The minimum number of data for network training depends to the linear or non-linear relationship between data. Due to the number of training data applied in literature review for FBNN generation, the number of data less than 100 data is considered as insufficient data for network training. Specht (1990) introduced Generalized Regression Neural Network (GRNN) which can be applied as a skilled technique for obtaining accuracy predicted outputs with minimum or limited data for network generation. In addition, Dynamic Neural Networks (DNNs) present a suitable method in network training due to memorizing input and feedback data during network generation. Nelles (2001) stated that the dynamic and nonlinear space in network modeling is applied by using an external dynamics, internal dynamic, and tapped-delay line. External dynamics method applies the time-dependent training data to demonstrate nonlinear space within network generation. The internal dynamics method makes a nonlinear space model without applying the historical information of the training data as

expressed by Ishak (2003) and Yasdi (1999). Lingras (2001) showed that tapped-delay line method employs a sequence of internal delay in network modeling to state nonlinear space within network generation.

FBNN and GRNN as static neural network (SNN) and Focused Feed-forward Time-delay Neural Network (FFTDNN) and Recurrent Neural Network (RNN) as DNN are used in this research for the load-deflection analysis of RC one-way slabs with and without Carbon Fibre Reinforced Polymer (CFRP) strengthening. Previous researches of ANNs in Structural Engineering mainly focused on FBNN using sufficient data for network generation. When the number of data to generate a FBNN is not enough, GRNN is mostly useful with only small number of data for network training. The justification of choosing GRNN is due to the difficulty in acquiring sufficient experimental data for FBNN generation. FFTDNN and RNN are chosen to predict mid-span deflection of RC slab using similar data applied in SNN modelling. FFTDNN and RNN are capable to memorize the input data while training process using tapped-delay line and internal dynamic space model respectively. FBNN is selected as baseline to compare with GRNN, FFTDNN, and RNN modelling in this research.

1.2 Statement of the Problem

ANN system which can be divided into static and dynamic neural networks is an acceptable method in predicting experimental results. In this thesis, FBNN and GRNN are the SNN generated to predict the load-deflection analysis in the one-way non-strengthened and CFRP strengthened RC slab. The GRNN was applied for situation where training data is insufficient for network generation. There is really little research on using DNNs in civil engineering. This study would like to focus on the internal nonlinear space and tapped

delay line which was applied for as internal important DNN parameter to memorize the training data. It is tried to make an internal space dynamic modeling applying similar data used in static neural network modeling to compare with the results of FBNN and GRNN. FFTDNN and RNN are two types of DNNs applied in this research. In addition, FBNN, GRNN, FFTDNN and RNN are also applied for other publication in civil engineering.

1.3 Objective of the Thesis

The main objective of this research is to generate ANNs that will predict the load deflection analysis of the non-strengthened and CFRP strengthened one-way RC slabs. Four networks, namely, FBNN, GRNN, FFTDNN and RNN are applied in this research. The objectives and scopes of this study are as follows:

1. To investigate the potential of utilizing GRNN as a SNN model for situations where insufficient training data are available to predict the load-deflection analysis of non-strengthened and CFRP strengthened RC one-way slabs.
2. To develop and compare FBNN and GRNN as a SNN model for situations where training data are sufficient to predict the load-deflection curve of non-strengthened and CFRP strengthened RC one-way slabs.
3. To investigate the potential of utilizing FFTDNN and RNN as a DNN technique to predict the load-deflection analysis for the non-strengthened and CFRP strengthened RC one-way slab for situations of sufficient data.
4. To compare FFTDNN, RNN, FBNN, and GRNN to predict the load-deflection analysis of the non-strengthened and CFRP strengthened RC one-way slabs.
5. To show that the ANNs approaches can also be applied for other applications in civil engineering.

CHAPTER 2

2. LITERATURE REVIEW

2.1 Introduction

Traditional methods for determining the concrete behavior and reinforced concrete slab analysis are first reviewed to establish a baseline for the use of neural network modeling in this chapter. Then, the past and current research works in the area of neural network applications in structural engineering are highlighted and discussed. Also the motivation for this research and its areas of contribution are highlighted as well. Finally, a abridge literature of strengthening method for RC members using CFRP is reviewed.

2.2 Traditional Models for Predicting of Concrete Behaviour

At present several mathematical models for the mechanical behavior of concrete are in use for analyzing reinforced concrete structures. Meyer (1985) carried out that the mathematical model can be divided into four main groups: orthotropic models, nonlinear elasticity models, plastic models and endochronic models.

The orthotropic model is the simplest of all the aforementioned models. It is able to adequately match experimental data under proportional biaxial loading and approximate the concrete behavior under general biaxial loading. Darwin and Pecknold (1977) showed that the model is also capable of representing the hysteretic behavior of concrete under cyclic loading. It is particularly suitable for the analysis of reinforced concrete beams,

panels and shells where the stress state of these structures is predominantly biaxial. It can also be calibrated against an extensive experimental data base. Chen (1976) presented that the orthopaedic model can also be extended to monotonic triaxial behavior.

The nonlinear elasticity model is based on the concept of variable module and matches well various parameter of the experimental data. In the pre-failure regime, distinct relationships are established between hydrostatic and volumetric strain and between differential stress and strain. From these relationships expressions for the tangent bulk and shear modulus are derived. Thus, the nonlinear elasticity response for concrete is simulated by a piecewise linear elastic model with variable modules. The model is, therefore, computationally simple and is particularly well suited for finite element calculations. During unloading, the behavior can be approximated by the module. This is different from those under loading conditions. As a result, this variable nonlinear elasticity model is unable to describe accurately the behavior of concrete under high stress, near the compressive strength and in the strain softening range.

The plastic model, especially, the strain hardening plastic model can be considered as a generalization of the previous two models. The constitutive relation in the strain hardening plastic model is on the basis of three following fundamental factors:

- i) The shape of the initial yield surface;
- ii) The evolution of the loading surface, i.e. the hardening rule;
- iii) The formulation of an appropriate flow rule.

The plastic model is able to successfully model the behavior in the strain hardening region. However, this classical theory of work-hardening plasticity is not able to explain the strain softening behavior of concrete beyond the peak stress. Therefore, it is unsuitable for use in the analysis of reinforced concrete structures where strain softening occurs. Nevertheless,

Arnesen et al (1980) stated that the model has been extensively applied in the study of concrete behavior with since the introduction of additional assumptions which has made it capable of simulating the behavior of concrete with good accuracy.

The endochronic model is based on the concept of intrinsic time that is used to measure the extent of internal damage in concrete structural elements under general deformation. This theory represents much concrete behavior without the need for loading-unloading conditions. However, for specific material, the loading criteria are necessary and this is accomplished by introducing loading surfaces and plasticity hardening rules.

Though previous applications have proven well the applicability of the endochronic approach, it was necessary to refine the theory and to reduce the number of material constants. Bazant and Ozbolt (1983) achieved this by introducing a refined model called the micro-plane model. It is able to represent adequately several monotonic features and tri-axial behavior of concrete; it is particularly suitable for local analyses of reinforced concrete structures. However, it is very costly and not practical for the large structural element used in this current research.

2.3 Empirical Models for RC Slab Deflection Analysis

In this model, the slab deflection is mainly calculated from the linear elastic analysis equations by assuming the effective second moment of area to be uniform along the slab. The empirical model is based on the use of an effective second moment of area empirically determined on the basis of experimental data. The following relationship is the general expression of the effective second moment of area for slabs and beams:

$$I_e = \alpha\beta I_g \left(\frac{M_{cr}}{M_{max}}\right)^m + I_{cr} \left[1 - \alpha\left(\frac{M_{cr}}{M_{max}}\right)^m\right] \quad (2.1)$$

Where:

I_e , is effective second moment of area

I_g , is second moment of area before crack

I_{cr} , is second moment of area after crack

M_{cr} , is first cracking bending moment

M_{max} , is maximum bending moment

α , β , and m , are factors empirically derived from experimental data on specific rebar

The ACI (1996), Benmokrane et al (1996), and Al-Sayed et al (1996) established models and their respective α , β and m values used are shown in Table 2.1.

Table 2.1: The values of α , β and m

Model	α	β	m
ACI	1.00	$\alpha^* \left(\frac{E_{FRP}}{E_{steel}} + 1\right)$	3.0
Benmokrane	0.84	0.143	3.0
Al-Sayed	1	1	5.5

($\alpha^*=0.5$; E_{FRP} and E_{steel} elastic modulus of FRP and the steel rebar)

Each of the design standards considered provides a different approach for the calculation of the effective second moment of area. ACI (1996) and SABS (1992) use a similar approach, known as Branson's approach (1977). EN 1992-1-1 (2004) uses a different approach, similar to Bischoff's approach (2005).

A different equation for the second moment of area of slabs was introduced by Faza and GangaRao (1993). Their model was based on the assumption that the concrete section

of a slab between load points is fully cracked (I_{cr}) and out of the load points are partially cracked (I_g). For beams with specific loading and supporting condition, the effective second moment of area obtained as a combination of I_g and I_{cr} .

Yost et al (2011) evaluated the flexural performance of simply supported concrete beams under four-point loadings with a 2D fiber-reinforced polymer (FRP) grid. Load-deflection, failure mode, cracking behavior, and reinforcement strain experimental data were compared with theoretical predictions calculated from traditional steel-reinforced concrete procedures. The deflection results of theoretical bilinear model were near to the measured experimental deflections.

The value of the slab deflections is depended on the moment-curvature law and the moment diagram shape and magnitude along slab length; therefore, empirical models cannot be generalized to the analysis of any loading and boundary conditions.

2.4 Finite Element Models for Analysis of RC Slab

Finite element analysis (FEA) is a method to evaluate the response of complex elements to any external loading by dividing the complex elements into lots of smaller and simpler elements. Ngo and Scordelis (1967) published the earliest study of using FEA modeling for analysis of RC structures. The concrete and steel bars were represented by constant strain triangular elements and the connection between concrete and steel bar modeled by a special bond link element. They determined the principal stresses in concrete, stresses in steel bars and bond stresses by using predefined crack patterns and under linear elastic analysis. Since the publication of this new study, many publications have appeared for analysis of reinforced concrete structures. The following literatures will highlight the application of the FEA modeling for the analysis of RC slabs and beams.

Lin and Scordelis (1975) used a layered triangular finite elements model for incorporating the coupling between membrane and bending effects, as well as the tension stiffening effect of concrete between cracks in RC slab analysis.

Dotroppe et al. (1973) utilized a layered finite element method in which slab elements were divided into layers to account the progressive cracking through the slab thickness.

Later Kwak and Kim (2002) developed a new finite element model based on the RC beams moment-curvature relations including the bond-slip and tension softening between cracks. The well established Timoshenko of beam theory was used in this analysis

Jofriet and McNeice (1971) carried out experimental and analytical studies of RC slabs. The analyses were based on a bilinear moment-curvature relation. This derived from an empirically determined effective second moment of area of the cracked slab section and the effect of tension stiffening. They considered on changing of the bending stiffness due to cracking on the slab.

A numerical model for the nonlinear analysis of RC slabs was developed by Jiang and Mirza (1997). Both concrete and steel were considered as nonlinear material. The RC slab was first divided into a number of composite elements, and each of the composite elements was then assembled into a single concrete element and a small number of steel beam elements.

Scanlon and Murray (1974) utilized layered rectangular slab elements to include both cracking and time-dependent effects of creep and shrinkage in RC slabs. They assumed that cracks propagate only parallel and perpendicular to orthogonal reinforcement.

Limam et al (2003) used a simplified layered plate model to describe CFRP strengthened reinforced concrete two-way slabs. The two-way RC slab was supported in four sides subjected to a load in the centre. The model developed by considering the failure mode in layer 1 (compressive concrete), layer 2 (steel), layer 3 (CFRP strips), between CFRP strip and concrete, or the whole thickness of cover concrete. The model gave a simple sufficient conditions and the ultimate load capacity for every collapse mechanism.

Hedong et al (2006) applied a moment-curvature law for investigation related to specific aspects of materials configuration for CFRP strengthening of slabs. Fourteen different experimental works were conducted on concrete slabs using a variety of configurations which results good agreement with the experimental results.

Foret and limam (2008) studied rational method on the composite orthotropic plate using finite element analysis to describe elastic behavior of RC slabs strengthened with near surface mounted (NSM) FRP rods. NSM FRP method provides an increasing in flexural and shear strength in RC members. A good agreement between experimental and numerical results was found.

All the aforementioned numerical models have focused on determining the behavior of mainly slabs and beams and therefore are not applicable for other structural elements. In addition, these models require solving several equations to predict for more than one parameter. Traditional modeling is limited to specific structural elements due to the many formal equations it has to solve; ANN differs in this aspect. Garrete et al (1992) mentioned that ANN is much simpler than traditional modeling because, although the numerical relationship is captured between its nodes, no formal mathematical rules or formula are observable within the model.

2.5 Neural Network as a Modeling Technique

The structural elements are subjected by a wide variety of external forces that have challenged solutions using conventional computational techniques. These can often be resolved using the same computers but with appropriate innovative training and knowledge. The design of a structural element consists of an iterative development as shown in Figure 2.1.

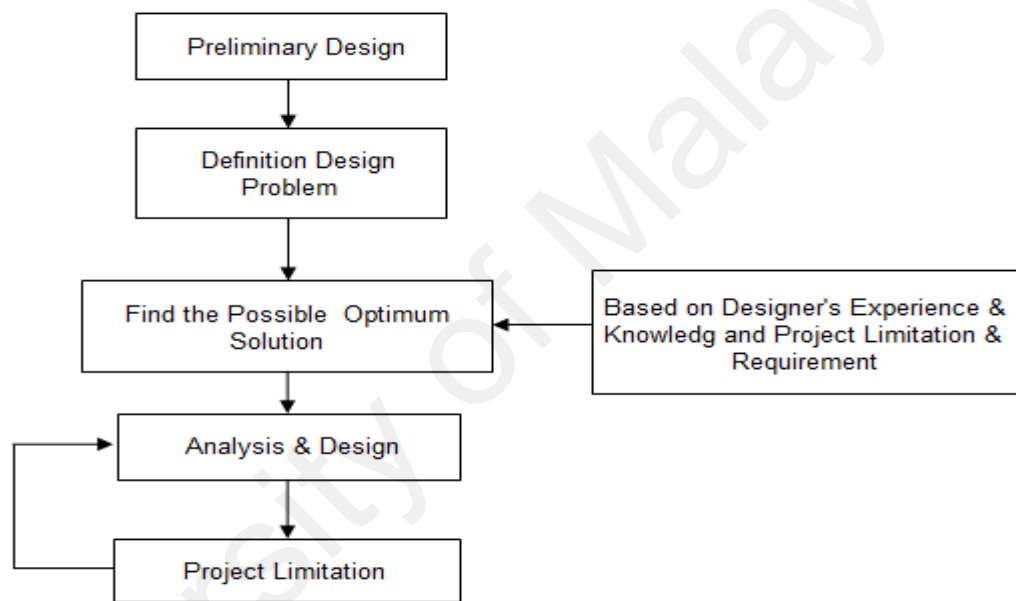


Figure 2.1: Process involve in designing structural elements

A successful design depends on the technical designer's initial understanding of the structural element and the approach towards related problems. The extent of the designer's knowledge and experience will determine the number of analysis-design cycles. Though the design and analysis process is dependent on human intuition and therefore is extremely difficult to computerize. In spite of that, it can be simulated by generating ANN from available experimental results. Previous researches of ANNs in Structural Engineering

mainly focused on FBNNs using sufficient data for network generation. Some well recognized initial structural design using FBNNs are given in Table 2.2.

Table 2.2: Using FBNN in initial structural design

No.	References	Year	Objective	Outline
1	Vanluchene And Roufei	(1990)	Initial design of reinforced concrete beam sections	Prediction the depth of a RC beam
2	Liu and Gan	(1991)	A preliminary structural design expert system	Space grid structures
3	Mukherjee	(1995)	Preliminary design of a simple & multi span reinforced concrete beam	Minimum cost design of a simply supported concrete beam.
4	Rajasekaran	(1995b)	Initial Design	Cross-sectional area of a steel truss for a given geometry

Other researchers have done some study about the effect of network parameters upon network output in structural design. Adhikary and Mutsuyoshi (2006) applied ANN models to predict the ultimate shear strength in steel fiber RC beams. The back-propagation was utilized as learning algorithm in feed-forward neural network. They studied on the effect of the number of input layer upon the network accuracy by comparing with the analytical formulation given in literature. The analysis shows that the generated FBNN with five input layers can predict the ultimate shear strength more accurately than the network with 4 input layers. Also the results show that FBNN presents the underlying shear behavior very well in beam.

Naci Caglar et al (2007) utilized the dynamic analysis results of 165 buildings to generate a multilayer perception (MLP) with a back-propagation (BP) algorithm. Different properties in network employed to find the optimum network. The output results specified that the

produced ANN can determine the 3D response of buildings subjected to earthquake as a user friendly computational tool.

In other research by Jamal et al (2007), FBNN with different transfer functions and vast training data is applied for shear resistance of rectangular RC beams predicted and compared together. The BPNN with sigmoid function was the last iteration to predict the shear strength of RC beam accurately.

Kerh and Yee (2000) applied energy function as minimization key in back propagation neural networks to analyze the deformed behaviors for culvert structure under a static loading. The stiffness matrix and force vector of the structure were replaced with weighting matrix and bias vector in the neural networks calculations.

Mehmet (2007) tried to model FBNN to predict ultimate deformation capacity of RC columns. Different network architecture investigated on the 682 column tests in un-axial bending with or without axial force and the N 9-12-1, N 9-14-1, N 9-16-1, N 9-18-1 and N 9-20-1 were the best five networks when MSE of testing data was considered. The results from the generated network presented the feasibility of using ANN models for deformation prediction of RC columns.

101 data was employed by Cevik and Guzelbey (2008) to generated ANN to predict mechanical strength of cylindrical samples reinforced by CFRP. The training algorithm was quasi-Newton back propagation with 4–15–1 NN architecture and hyperbolic tangent sigmoid transfer function (tansig). The outcomes of the produced NN model in MATLAB programming compared to experimental results are found to be pretty acceptable.

Mansour et al (2004) used multi-layered back-propagation neural network for ultimate shear strength prediction of RC beams with stirrups. The experimental result on 176 RC beams was applied for network generation. They used 80% of total data for

training and 20% for testing. The results of generated network indicated that the network requires the error tolerance settled to 3%.

Investigation on the other researcher's experimental study as given in Table 2.3, shows FBNN can be very useful to apply experimental results to improve analytical expressions. FBNN can reasonably predict the laws of material mechanic, if the neural networks are trained with a comprehensive set of experimental output.

Guang and Zong (2000) proposed a method by using multi-layer feed-forward neural networks to predict 28-day compressive strength of concrete. The model was created to find a relationship between the complex nonlinear inputs and the output. The generated neural network models gave high prediction accuracy.

Dias and Pooliyadda (2001) have shown that FBNN is appropriate method to predict the strength and slump of ready mixed concrete and high strength concrete. They tried to adjust network parameters to find the optimum network with minimum error and maximum coefficient of determination in training and testing data. 137 data was used for network learning and testing.

Table 2.3: Using ANN in initial structural design

No	References	Year	Objective	Network
1	Ghabousi et al	(1991)	Modeling the stress-strain behavior of concrete to investigate the biaxial actions of plain concrete	Architecture: 2-40-40-2 Feed-forward Back-propagation Algorithm
2	Mukherjee and Nag	(1995a)	Stress-strain relationship of the material under un-axial loading	Feed forward network and back-propagation algorithm
3	Kasperkiewicz et al	(1995)	Predicting strength of high-performance concrete	ARTMAP architecture
4	Yeh	(2007)	Slump flow prediction for high-performance concrete	Architecture: 7-7-1 Feed-forward Back-propagation Algorithm
5	Topcu and Saridemir	(2007)	The hardened concrete properties of waste AAC aggregate concrete	Architecture: 7-7-8-4 23 data for training & 22 data for testing Momentum & Learning rate 0.99 & 0.96
6	Demir	(2007)	Predict elastic modulus of both normal and high strength concrete	Architecture: 1-3-1, 1-5-1, and 1-3-3-1 Sigmoid Activation Function
7	Manish and Rajiv	(2005)	Ultrasonic pulse velocity (UPV) as a measure of compressive strength of concrete	Learning rate = 0.5, mutation rate = 0.04, population size = 50, and cross over rate = 0.2.
8	Guneyisi et al	(2007)	Effects of cement type, curing condition, and testing age on the chloride permeability of concrete	Architecture: 5-8-1 Learning algorithms: Conjugate Gradient and Levenberg Marquaet
9	Oztas et al	(2006)	Predicting the compressive strength and slump of high strength concrete	Architecture: 7-5-3-2 Learning algorithm: scaled conjugate gradients algorithm (SCGA).
10	Pala et al	(2005)	Effects of fly ash and silica fume replacement content on the strength of concrete cured for a long-term period of time	Architecture: 8-9-1 Learning algorithm: scaled conjugate gradients algorithm (SCGA)

Most of the research in literature used FBNN in situation where sufficient data is available for network training. The use of the FBNN for large structural elements is limited due to

the difficulty in acquiring sufficient experimental data. Specht (1990) expressed that GRNN is mostly useful with only small number of data for network training when the number of data to generate a back-propagation neural network is not enough. GRNNs have been proved to be a capable method for many scientific and engineering problems prediction such as sigma processing by Kendrick (1994), chemical processing by Mukesh (1996), and assessment of high power systems by Wehenkel (1996). But, the technique has not been widely applied in the field of structural engineering.

Williams and Gucunski (1995) have been studied to develop GRNN and FBNN to predict elastic module and layer thicknesses for pavement and soil systems. They developed the artificial neural by using ninety-eight cases of synthetic dispersion-curve data for network training and testing. The results of the generated neural networks were close to the practical outputs.

Mahesh and Surinder (2008) have generated GRNN for pile capacity modeling. Totally 105 data set collected from the pre-stressed spun pipe piles made with precast high strength concrete have applied for network training and testing. A coefficient of determination value of 0.977 was reached for the pile capacity prediction by GRNN.

In another study by Mahmut and Mahmud (2009), GRNN and FFNN have used for scour depth prediction around circular bridge piers. Hundred and sixty five data collected from different experimental studies employed for network generation. They tried to make equilibrium between the scour depth around bridge piers as net output and the grain size, flow depth, pier diameter, average velocity of the approach flow, the critical velocity, the dynamic viscosity of fluid, and the fluid density as net input. The output of the produced network has shown the successfully prediction of the scour depth around circular bridge piers.

In another research, GRNNs were used in the area of the transportation engineering by Hilmi and Cigizoglu (2006). They tried to model daily trip for available transportation modes by GRNN in compared with both an FFNN and a stochastic model. The generated GRNN presented successfully prediction in this area.

Pannirselvan et al (2008) utilized the GRNN system to generate a neural network for predicting the yield load, ultimate load, yield deflection, ultimate deflection, deflection ductility and energy ductility of 6 RC beams strengthened with Glass FRP and 3 beams without GFRP. The normalized root mean square error values for training data and testing data were in the range of 0.0635-0.2414 and 0.0104-0.1274 respectively.

In this research, GRNN has applied for the load-deflection prediction in RC slab and mechanical properties forecasting of lightweight concrete and mortar in case of enough and small data for training.

There are many important causes to have knowledge for network generation in time-varying pattern by making internal dynamic space and tapped-delay line. In following are two important properties of ANN that make it valuable to predict data generated in sequential pattern. (Abed et al, 2010):

- 1) ANN is capable to learn from examples without prior knowledge of the regularities or consistency in data.
- 2) ANN is able generalize from a previous state to a new one by modifying their behavior in response to new information. Therefore, they can be suitable for sequential pattern modeling.

There is really little research on using DNNs in civil engineering. Some of the limited uses of DNNs are shown in Table 2.4.

Table 2.4: Application of dynamic neural network in civil engineering

No.	References	Year	Network Type	Application
1	Pana et al	(2007)	Recurrent	To explain the transition of the rainfall–runoff processes
2	Hilmi and Cigizoglu	(2007)	Delay	Traffic Engineering
3	Barari and Pandey	(1996)	Time-delay	Damage detection of railway bridges
4	Yun et al	(1998)	Time-delay	Traffic volume forecasting.
5	Li et al	(1999)	Time series simulation(TSS)	Prediction of amplitude damping in buildings
6	Chen et al	(1995)	TSS	Identify structural dynamic model
7	EI-Shafie et al	(2008)	Recurrent	Predicting creep deformation in masonry structures

In a research, the traditional neural network (TNN) and time delay neural network (TDNN) has been employed to detect damage in bridge structures (Barari and Pandey, 1996). A multilayer perceptron with the back-propagation learning algorithm has been implemented to train TDNNs and TNNs. The architecture for TDNN and TNN was 345-(21-21)-21 and 69-(21-21)-21 with two hidden layers and 21 nodes in each hidden layer. It is found that the results of generated TDNN are more effective than TNN to detect damage in the bridge structure.

Graf et al (2010) showed a numerical prediction for future structural responses in dependency of uncertain load processes and environmental influences using ANN. The generated ANN was based on RNN trained by time-dependent measurement results. The approach presents a capability for prediction of the long-term structural behavior of a reinforced concrete plate strengthened by a textile reinforced concrete layer.

Abed et al (2010) applied focused Time Delay Neural Network (FFTDNN) to consider the time dependency of creep in masonry structures by using external dynamic space within network training. The architecture of the generated network was 4-8-4-1. It means, the produced network consisted of an input layer with four neurons, two hidden

layers with eight and four neurons and an output layer with one neuron. They compared the capability of the created network for creep prediction with the other model which is employed RNN by El-Shafie et al (2008). They presented that the created model in FTDNN has a comparatively small prediction error compared to the RNN model and other theoretical models. In this research, FTDNN and RNN are applied for load-deflection and crack width prediction of RC slab strengthened by CFRP.

Freitag et al (2011) introduced a model for prediction of time-dependent structural behaviour using RNN. The time-dependent data for RNN generation was obtained from measurements or numerical analysis. The RNN new approach was verified by a fuzzy fractional rheological material model to predict the long-term behaviour of a textile strengthened reinforced concrete structure

2.6 Strengthening of Concrete Structures

The different applications of structures depend on how they were initially designed and the causes of upgrading and repair are relative to structural changes, degradation, and loading separately or in combination. It is not always economically pragmatic to change the presented structure with a new one. The challenge is to evaluate effective and economical techniques for strengthening and upgrade of the existing construction. They need to strengthen and upgrade because of increasing service loads and/or structurally or functionally degradation of existing concrete structures. So, the strengthening and rehabilitation of the presented structures can be classified into strengthening methods for protection, upgrading, and increasing the load-bearing capacity. It is important to evaluate the suitable repair and upgrading method for structures to detect deficiencies. Strengthening and upgrading of reinforced concrete structures using bonded steel plate is an effective, suitable and economic method. But, because of some disadvantage of using

steel plate such as managing of the heavy steel plates and corrosion of the steel plate have enthused study to evaluate alternative upgrading and strengthening method in reinforced concrete structures. Wang et al (2004) defined FRP as high strength and light weight alternative material to steel plate due to its effective characteristics such as adaptability to the design of systems, easy surface preparation, reduced mechanical fixing, permanence of strengthening system, improved fire resistance, reduced risk of damage due to freeze/thaw, protection of strengthening system, reduced construction phase, capability to pre stress, and resistance to electrochemical corrosion.

Three kinds of FRP are carbon (CFRP), aramid (AFRP) and glass (GFRP). Meier (1987) and Kaiser (1989) established that CFRP plate as a non-corrosive, lightweight, and no length limited material could be used in strengthening of reinforced concrete structures. CFRP becomes popular to strengthen and rehabilitate of reinforced concrete slabs because of its good durability, long-term fatigue properties and do not need to be maintained over time. CFRP is made of carbon atoms and involved by very thin fiber about 0.005-0.010 mm in diameter. It used for applications where high mechanical properties and low weight are the important requirements. The typical mechanical properties of CFRP are given in Table 2.5.

Table 2.5: Mechanical properties of CFRP (Godonue, 2002)

Fiber type	Elastic modulus [GPa]	Tensile strength[MPa]	Failure strain [%]
Carbon (HS/S)	160 - 250	1400 - 4930	0.8 – 1.9
Carbon (IM)	276 - 317	2300 - 7100	0.8 – 2.2

Some of the applications of CFRP for strengthening of RC beam and slab are discussed in follow:

Tan and Zhao (2004) done experimental work on six one-way reinforced concrete slabs with openings strengthened with CFRP composite. The samples were subjected to concentrated line loads. The experimental results were compared to those of a one-way slab with a non-strengthened opening and a one-way slab without opening. They concluded that the CFRP composite confirmed to be effective in increasing in the load-carrying capacity and stiffness of one –way reinforced concrete slabs with an opening.

Chamai et al (2007) investigated on Twenty-six reinforced concrete beams with dimensions $100 \times 150 \times 1800$ mm, with and without bonded CFRP laminates. They studied on the time-dependent behavior of carbon FRP-strengthened concrete beam.

Amen et al (2008) done an experimental and theoretical analysis on the bending behavior of square shape of reinforced concrete slab with dimension $1250 \times 1250 \times 100$ mm strengthened with CFRP and supported on one direction as one-way slabs. In this study, the low quality of the concrete cover on the steel bar on the efficiency of the externally-bonded CFRP strips was investigated. They presented that a reduction in the quality of the concrete cover causes to lessen the effectiveness of thin CFRP strips and so leads to bending failure. They concluded that the CFRP composite significantly increases punching failure stress and so decreases the slab rotation around the loading column.

Waleed (2005) has done a study about repair of initially cracks in reinforced concrete slabs. This paper investigates the structural behavior of cracked reinforced concrete one-way slab, which is repaired using different techniques. Five different techniques are used for the purpose of repair in the cracked concrete slab namely; cement grout, epoxy injection, ferrocement layer, carbon fiber strip and section enlargement. All repair techniques are found to be able to restore or enhance the structural capacity of cracked concrete slabs. The strengthening of the slab by using the CFRP at its soffit improves the

crack width without repairing the initial cracks. In this specimen, new cracks are developed at slightly lower load compared to the original slab. The slab which is repaired by CFRP show 77.4% higher ultimate load capacities compared to the control slab.

Christopher et al (2002) completed an experimental study on the similar reinforced concrete beams in depth ranging from 0.2 m to 0.8 m strengthened by 2 to 8 layers of CFRP sheets to achieve the same CFRP/concrete area ratio. The results were in good agreement with the theoretical models.

Carlos and Maria (2006) applied a numerical method for failure loading prediction of RC beam strengthened by different type of FRP. The results of numerical method compared with the results of experimental data obtained from 19 beams.

In another study, Hedong et al (2006) investigated on the effect of material configuration such as strength, failure mechanisms and ductility. These properties achieved through the use of pultrusion and wet layup fabricated strips, both adhesively bonded to the fourteen different concrete slabs. The initial results of materials are compared to an analytical fracture based model.

So, it is obvious that CFRP is a strengthening material with good durability, long-term fatigue properties, excellent mechanical properties, superior structural performance, and low weight for RC structures.

CHAPTER 3

3. ANALYTICAL MODELING

In this part of study, the mechanical property of non-strengthened RC slab under mid-span punching load is studied. After that, the empirical method using BS code for non-strengthened RC slab under mid-span punching load and ISIS Canada for CFRP strengthened RC slab under four point line loads is discussed. For the more, the mid-span deflection of one sample of non-strengthened RC slab is checked by using finite difference method.

3.1 Empirical modeling for Non-strengthened RC Slab

3.1.1 Mechanical properties of the slab under mid-span punching load

The mechanical properties of the one-way slab are similar to beam in situation where the slab width-length ratio is small and the influence of the bending moment along simply support (M_y) is ignored. The crack pattern for the slab with large width-length and small width-length ration is shown in Figures 3.1 and 3.2 respectively.

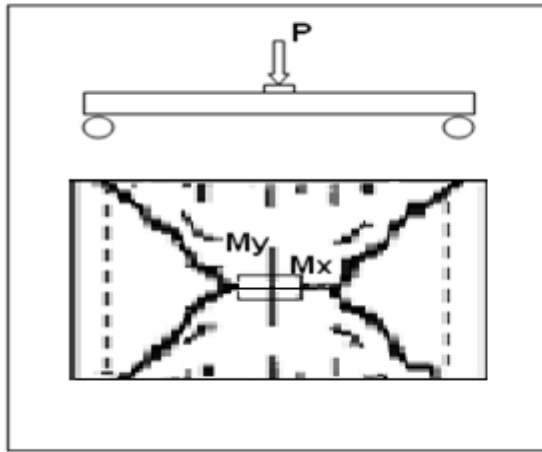


Figure 3.1: Cracking pattern of the large width-length ratio slab

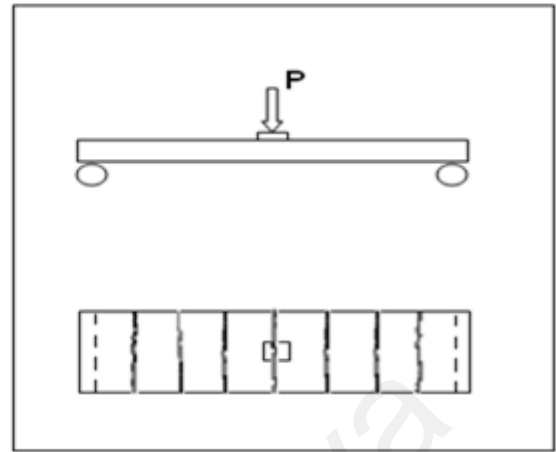


Figure 3.2: Cracking pattern of the small width-length ratio slab

Due to different width-length ratio of the experimental samples for non-strengthened RC slab, the influence of the M_y on mechanical properties of the slab is studied in follow.

Zhang (2009) expressed that the reaction force along the simply supported one-way slab under punching load is uneven (Figure 3.3).

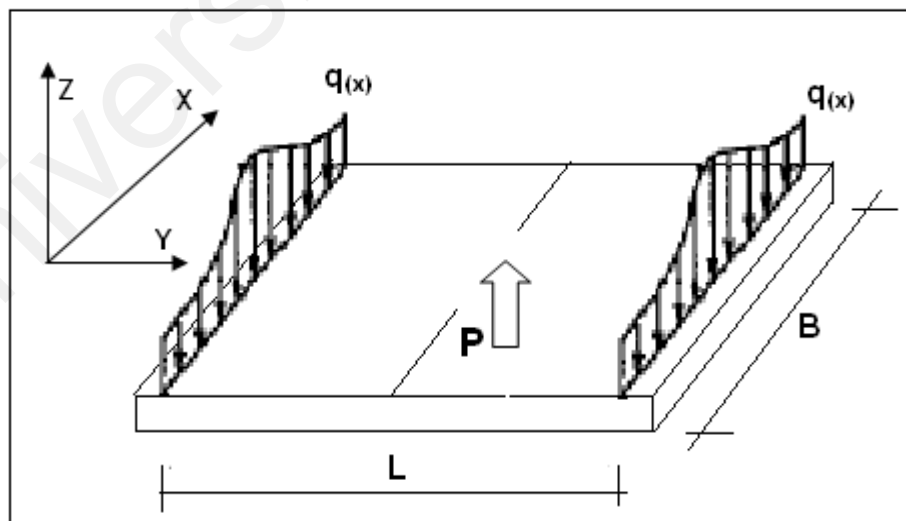


Figure 3.3: The distribution of actual reaction force

The reaction force along simply support defines by following equation:

$$\int q(x).dy = \frac{P}{2} \quad (3.1)$$

Where:

$q(x)$, is the uneven reaction force

B , is the slab width

P , is the punching load

Due to uneven reaction force, the center of the reaction forced moves towards the outside and the moment arm will be increased. So, it is much safer to use the following simplified calculation method.

The uneven reaction force presented in equation (3.2) can be defined as following uniform reaction force (Figure 3.4):

$$q(x) = \frac{P}{2B} \quad (3.2)$$

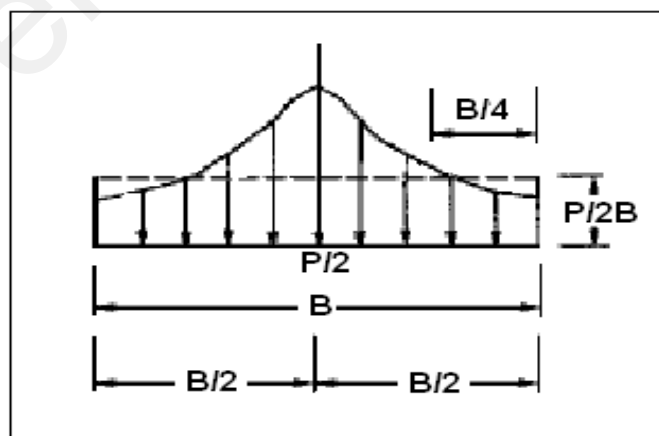


Figure 3.4: The distribution of actual reaction

The bending moment (M_x) defines by following equations:

$$\int_0^L M_x dy = \frac{P}{2} \times \frac{L}{2} = \frac{P \times L}{4} \quad (3.3)$$

The mean moment about x direction is shown in equation 3.4.

$$\overline{M_x} = \frac{P \times L}{4B} \quad (3.4)$$

The bending moment (M_y) is calculated based on uniform reaction force in Figure 4.4, as well as shown by following equation:

$$\int_0^B M_y dx = 2 \times \frac{P}{2B} \times \frac{B}{2} \times \frac{B}{4} \quad (3.5)$$

The mean moment about y direction is shown in equation 3.4

$$\overline{M_y} = \frac{P \times B}{8L} \quad (3.6)$$

The distribution of the M_x and M_y of the one-way slab is uneven. The following K_1 and K_2 are set to describe the uneven distributed M_x and M_y respectively. Thus, the maximum bending moment about x direction, $M_{x_{max}}$, and the bending moment about y direction, $M_{y_{max}}$, are defined by following equations:

$$M_{x_{max}} = K_1 \times \overline{M_x} = K_1 \times \frac{P \times L}{4B} \quad (3.7)$$

$$M_{y_{max}} = K_2 \times \overline{M_y} = K_2 \times \frac{P \times B}{8L} \quad (3.8)$$

Thus:

$$\frac{M_{y_{max}}}{M_{x_{max}}} = \frac{1}{2} \times \frac{K_2}{K_1} \times \frac{B^2}{L^2} \quad (3.9)$$

Zhang (2009) shows that the distribution of the M_x is quite uniform ($K_1=1$) and the value of the K_2 is between 1 and 1.2. Since reinforcement along simply support is not the main reinforcement for slabs, the ratio of K can be set to 1 approximately. So, the equation (3.9) is summarized to following equation:

$$\frac{M_{y_{max}}}{M_{x_{max}}} = \frac{1}{2} \times \frac{B^2}{L^2} \quad (3.10)$$

The values of M_y for the non-strengthened RC slabs under punching load are shown in Table 3.1. The value of the bending moment about y direction, M_y , is less than bending moment about x direction, M_x . So, the mechanical properties of non-strengthened RC slabs are similar to the structural behavior of beams and the influence of the bending moment about y direction on the mid-span deflection was ignored. In addition, the experimental crack pattern of the non-strengthened RC slabs was similar to crack pattern for the slabs with small width-length ratio (Figures 3.5 and 3.6). So, the results of the analytical method and experimental crack width proved that the structural behavior of the non-strengthened RC slabs under mid-span punching load were similar to structural behavior of beams

Table 3.1: The values of the bending moment about y direction due to uneven reaction force

Slab	Slab Clear Span Length (mm)	$\frac{B^2}{2L^2}$	Experimental M_x (kN-m)		$M_y = \frac{B^2}{2L^2} \times M_x$ (kN-m)	
			At First Crack	At Max. Load	At First Crack	At Max. Load
120-3T10-2400	2250	0.0158	3.49	11.25	0.06	0.18
100-3T10-2400	2250	0.0158	3.21	8.16	0.05	0.13
120-4T10-1800	1650	0.0294	3.55	13.61	0.10	0.40
120-3T10-1800	1650	0.0294	3.51	10.31	0.10	0.30
120-2T10-1800	1650	0.0294	3.51	8.25	0.10	0.24
100-4T10-1800	1650	0.0294	2.27	9.9	0.07	0.29
100-3T10-1800	1650	0.0294	2.27	7.84	0.07	0.23
100-2T10-1800	1650	0.0294	2.10	6.81	0.06	0.20
55-2T10-1350	1200	0.0555	0.66	1.95	0.04	0.11
55-3T10-1350	1200	0.0555	0.54	3	0.03	0.17
55-4T10-1350	1200	0.0555	0.75	3.9	0.04	0.22
70-2T10-1350	1200	0.0555	1.14	3.6	0.06	0.20
70-3T10-1350	1200	0.0555	1.20	5.1	0.07	0.28
90-2T10-1350	1200	0.0555	1.77	5.4	0.10	0.30
90-3T10-1350	1200	0.0555	1.86	6.9	0.10	0.38
55-2T10-860	710	0.158	0.73	2.1	0.11	0.33
55-3T10-860	710	0.158	0.73	2.45	0.11	0.39
70-2T10-860	710	0.158	1.15	3.68	0.18	0.58
70-3T10-860	710	0.158	1.22	4.38	0.19	0.69



Figure 3.5: Experimental crack pattern of the non-strengthened RC slab under mid-span punching load



Figure 3.6: Non-strengthened RC slab under mid-span punching load after testing

3.1.2 BS Code for Non-strengthened RC Slab

3.1.2.1 Design moment using BS code

The following section describes the simplified stress block method of BS 8110: Part 1:1997 (BS, 1997) used for designing and ultimate moment calculation of the non strengthened RC one-way slab. The strain and stress block diagrams on the cross section of the RC one-way slab is shown in Figure 3.7.

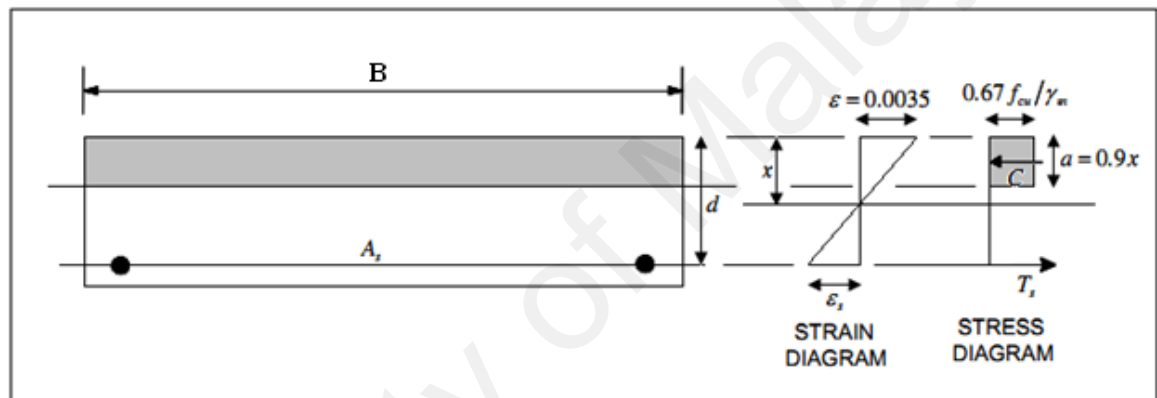


Figure 3.7: Simplified stress block method for the non-strengthened RC slab

The concrete stress is given by following equation using the partial safety, γ_m of 1.5 for concrete.

$$\frac{0.67 f_{cu}}{\gamma_m} = \frac{0.67 f_{cu}}{1.5} = 0.447 f_{cu} = 0.45 f_{cu} \quad (3.11)$$

Using partial safety factor of 1.05 for reinforcement, the steel stress is given as:

$$\frac{f_y}{1.05} = 0.95 f_y \quad (3.12)$$

The compressive force in concrete and tensile force in steel bar shown in Figure 3.7 are:

Compressive Force in Concrete:

$$C_c = 0.45 \times f_{cu} \times 0.9X \times B \quad (3.13)$$

Tensile Force in Steel Bar:

$$T_s = 0.95 \times f_y \times A_s \quad (3.14)$$

Equating the compressive force in concrete and tensile force in steel bar for the equilibrium of the forces in the section:

$$C_s = T_s \quad (3.15)$$

$$0.45f_{cu} \times 0.9X \times B = 0.95f_y \times A_s \quad (3.16)$$

$$X = \frac{0.95f_y \times A_s}{0.45f_{cu} \times 0.9 \times B} \quad (3.17)$$

The moment design of the slab:

$$M_R = 0.95f_y A_s \left(d - \frac{0.9X}{2} \right) \quad (3.18)$$

The ultimate moment was calculated using ultimate strength found experimentally for reinforcement and also without partial safety factor for the concrete and reinforcement.

Depth of natural axes:

$$X = \frac{f_t \times A_s}{0.67f_{cu} \times 0.9 \times B} \quad (3.19)$$

$$M_{ult} = f_t A_s \left(d - \frac{0.9X}{2} \right) \quad (3.20)$$

3.1.2.2 First crack moment using BS code

The first cracking moment in BS code is given by:

$$M_{cr} = \frac{f_r I}{h - X} \quad (3.21)$$

Where:

f_r = Modulus of rupture of concrete

I = Moment of inertia of the transformed reinforced section

h = total depth of section

X = depth of natural axes

The value of the second moment of area and depth of natural axes can be calculated from the following equations:

$$X = \frac{\frac{1}{2}bh^2 + n_s A_s d}{bh + n_s A_s} \quad (3.22)$$

$$I = \frac{bh^3}{12} + bh\left(\frac{h}{2} - X\right)^2 + n_s A_s (d - X)^2 \quad (3.23)$$

3.1.2.3 Deflection calculation using BS code

As described in BS 8110: Part 2: 1985, the deflection calculation is based on the curvature obtained. The curvature for the slab was taken from maximum curvature of cracked and un-cracked section.

(1). Curvature for cracked section:

The curvature for the cracked section is defined by the equation 3.24.

$$\phi_{curve} = \frac{M_r}{E_c I_{cr}} \quad (3.24)$$

The term M_r is given by following equations:

$$M_r = M - M_c \quad (3.25)$$

$$M_c = \frac{2T_c(h - X_{cr})}{3} \quad (3.26)$$

$$T_c = \frac{0.5f_{cr}(h - X_{cr})^2}{d - X_{cr}} \quad (3.27)$$

Where,

M = applied moment,

M_c = moment of resistance of concrete in tension

E_c = modulus of elasticity of concrete

I_{cr} = moment of inertia of cracked section

T_c = force in concrete in tension, and

f_{cr} = tensile stress in concrete at stress level

(2). Curvature for un-cracked section:

The curvature for the un-cracked section is defined by the equation 3.28.

$$\phi_{curve} = \frac{M}{E_c I_x} \quad (3.28)$$

Where,

M = applied moment,

E_c = modulus of elasticity of concrete

I_x = moment of inertia of un – cracked transformed section

Deflection can be calculated using following expression:

$$\Delta = kL^2\phi_{curve} \quad (3.29)$$

Where:

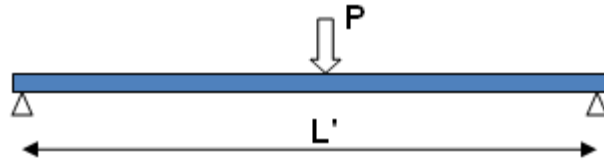
ϕ_{curve} = Maximum Curvature from Cracked and Un-cracked Section

L = effective span of the member

K = a coefficient, which depends on the shape of the bending moment diagram. (Table 3.1 of BS8110:Part2: 1995)

3.1.2.4 Example for the non-strengthened RC one-way slab

One-way slab marking: 120-3T10-2400



Section Width
 Section Thickness
 Span Length,
 Clear Length
 Effective Depth
 Concrete Elasticity Modulus
 Steel Elasticity Modulus
 CFRP Elasticity Modulus
 Cover
 Steel Rebar
 Concrete tensile strength,
 Concrete cube strength,
 Strength of reinforcement,

$$(d = H - c - \frac{10}{2})$$

3T10

B =	400	mm
H =	120	mm
L =	2400	mm
L' =	2250	mm
d =	90	mm
Ec =	26313	Mpa
Es =	215000	Mpa
ECF =	165000	Mpa
c =	25	mm
As =	235.5	mm ²
Fct =	6.35	N/mm ²
Fcu =	44.75	N/mm ²
Fy =	610	N/mm ²

[A] Ultimate Moment

Depth of natural axis
 Moment of Resistance

$$X = \frac{A_s \cdot f_t}{(0.67 \cdot f_{cu} \cdot b \cdot 0.9)}$$

$$M_u = f_y \cdot A_s \cdot (d - 0.9X/2)$$

X =	13.31	mm
M _u =	12.1	kNm

[B] First Crack Moment

Natural axis
 Second moment of area before crack
 Crack Moment Capacity
 First Crack Load

X =	58.81	mm
I =	59598397	mm ⁴
M _r =	6.18	kNm
P =	5.50	kN

[C] Deflection

Maximum Curvature
 Deflection

φ =	0.00408074
Δ =	2.07

3.2 Empirical Model for CFRP Strengthened RC Slab

3.2.1 Design moment using ISIS Canada

The following procedure illustrates the analysis of an externally-strengthened reinforced concrete beam and one-way slab (with tension steel only) using ISIS Canada. The strain and stress block diagrams on the cross section of the CFRP strengthened RC one-way slab is shown in Figure 3.8.

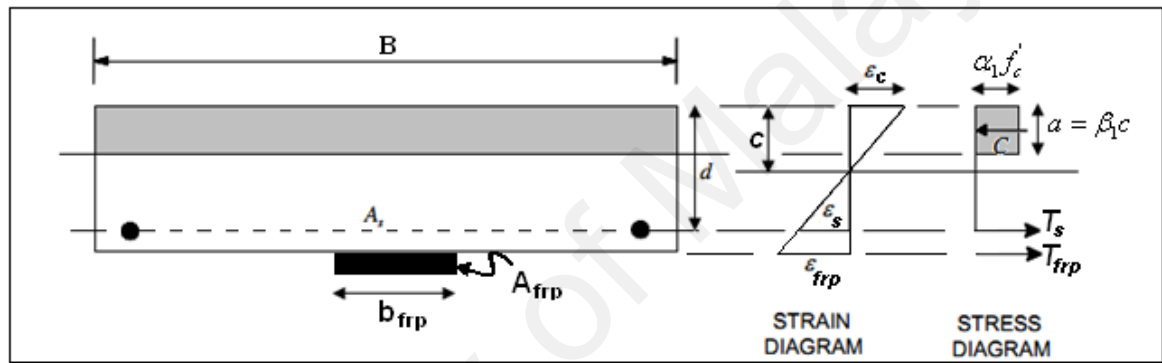


Figure 3.8: Simplified stress block method for the CFRP strengthened RC one-way slab

1. Assume the failure strain for concrete is in compression. Thus we get the following result from strain compatibility:

$$\varepsilon_{f_{rp}} = \varepsilon_{cu} \frac{h-c}{c} \quad \text{and} \quad \varepsilon_s = \varepsilon_{cu} \frac{d-c}{c} \quad (3.30)$$

Assume that the steel has yielded so that $f_s = f_y$

2. Determine the concrete compressive stress block factors

$$\alpha_1 = 0.85 - 0.0015 f'_c \geq 0.67 \quad (3.31)$$

$$\beta_1 = 0.97 - 0.0025 f'_c \geq 0.67 \quad (3.32)$$

3. Determine the depth of the neutral axis

$$C = T + T_{frp} \quad \phi_c \alpha_1 f_c' \beta_1 b c = \phi_s f_y A_s + \phi_{frp} E_{frp} A_{frp} \epsilon_{frp} \quad (3.33)$$

4. Once c is known, check to see if the strain in the FRP has exceeded its tensile failure strain

$$\epsilon_{frp} = \epsilon_{cu} \frac{h-c}{c} > \epsilon_{frpu} \quad (3.34)$$

5. The factored moment resistance can be obtained from the following equation

$$M_c = \phi_s f_y A_s \left(d - \frac{a}{2} \right) + \phi_{frp} E_{frp} A_{frp} \epsilon_{frp} \left(h - \frac{a}{2} \right) \quad \text{where } a = \beta_1 c \quad (3.35)$$

To avoid sudden and brittle failure of the externally strengthened member, we ensure that the internal steel reinforcement has yielded.

$$\epsilon_s = \epsilon_{cu} \frac{d-c}{c} > \epsilon_y \quad (3.36)$$

It will be correct if yes otherwise we should reduce the amount of FRP and recalculate by ensuring the steel reinforcement yields in the final design.

6. Assume that failure occurs by tensile failure of the FRP. This means that the strain in the FRP at failure is equal to $\epsilon_{frp} = \epsilon_{frpu}$, and the strain in the extreme concrete compression fibre is somewhat less than ϵ_{cu} .

7. Determine the depth of the neutral axis, c , using:

$$C = T + T_{frp} \quad \phi_c \alpha_1 f_c' \beta_1 b c = \phi_s f_y A_s + \phi_{frp} E_{frp} A_{frp} \epsilon_{frpu} \quad (3.37)$$

8. Verify that the strain at the extreme compression fibre is less than ϵ_{cu} :

$$\epsilon_c = \epsilon_{frpu} \frac{c}{h-c} < \epsilon_{cu} \quad (3.38)$$

9. Calculate the factored moment resistance of the cross-section using:

$$M_c = \phi_s f_y A_s \left(d - \frac{a}{2} \right) + \phi_{frp} E_{frp} A_{frp} \varepsilon_{frp} \left(h - \frac{a}{2} \right) \quad (3.39)$$

3.2.2 First crack moment using ISIS Canada

The first cracking moment in ISIS Canada is given by:

$$M_{cr} = \frac{f_{cr} I_t}{y_t} \quad (3.40)$$

Where:

$$f_{cr} = 0.4 \sqrt{f'_c}$$

I_t = Moment of inertia of the transformed reinforced section (un – cracked)

y_t = Distance from center of un-cracked transformed section to extreme tension fiber.

The un-cracked transformed slab section is shown in Figure 3.9.

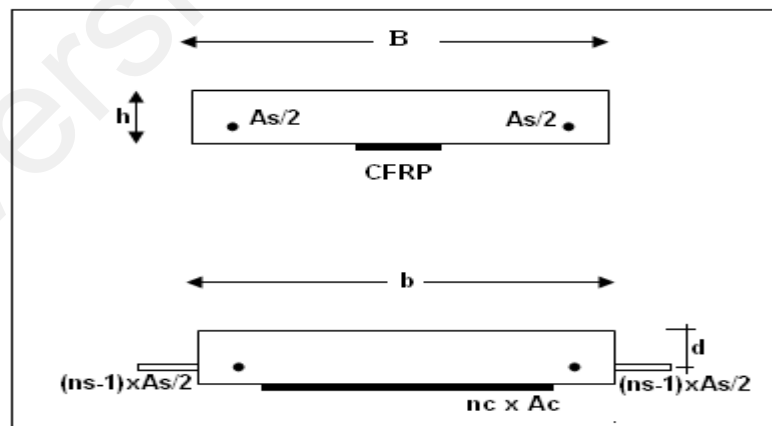


Figure 3.9: Un-cracked transformed section for the CFRP strengthened RC slab

The second moment of area of the transformed un-cracked section for the CFRP strengthened RC one-way slab was calculated using following equations:

$$X = \frac{\left[\frac{bh^2}{2} + ((n_s - 1) \times A_s \times (h - d))\right]}{[(B \times h) + (n_s - 1) \times A_s + (n_c \times A_{cfrp})]} \quad (3.41)$$

$$I_t = \frac{B \times (h - X)^3}{3} + (B \times h) \times \left(\frac{h}{2} - X\right)^2 + (n_c - 1) \times A_s \times (d - X)^2 + (n_s \times A_s) \times X^2 \quad (3.42)$$

3.2.3 Deflection calculation using ISIS Canada

If a member remains un-cracked under service loads, then deflection requirements can be checked using the concept of transformed gross sections. However, if the member is cracked under service load, the effective second moment of area should be calculated (for a rectangular section) using the following equation, which was empirically derived from test data on FRP-reinforced concrete members:

$$I_e = \frac{I_t I_{cr}}{I_{cr} + \left(1 - 0.5 \left(\frac{M_{cr}}{M_a}\right)^2\right) (I_t - I_{cr})} \quad (3.43)$$

Where:

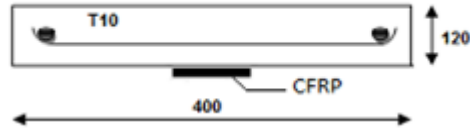
I_{cr} = moment of inertia of the cracked section transformed to concrete

I_t = moment of inertia of a un – cracked section transformed to concrete

M_{cr} = cracking moment (N.mm)

M_a = maximum moment in a member at the load stage at which deflection is being calculated (N.mm)

3.2.4 Example for CFRP strengthened RC one-way slab



CFRP S512

CFRP Width = 50 mm

CFRP Thk = 1.2 mm

As = 2 T10

Slab Thk = 120 mm

Slab Width = 400 mm

$$f_g = 610 \text{ N/mm}^2$$

$$f_{cu} = 45.5 \text{ N/mm}^2$$

$$f_t = 6.19 \text{ N/mm}^2$$

$$E_{cfRP} = 165000 \text{ N/mm}^2$$

$$E_c = 25881 \text{ N/mm}^2$$

Solution:

$$\alpha_1 = 0.85 - 0.0015 \times 0.85 \times 45.5 = 0.792 \geq 0.67$$

$$\beta_1 = 0.97 - 0.0025 \times 0.85 \times 45.5 = 0.87 \geq 0.67$$

$$\phi_c \alpha_1 f_c' \beta_1 bc = \phi_s f_y A_s + \phi_{frp} E_{frp} A_{frp} \varepsilon_{frp}$$

$$0.6 \times 0.792 \times 0.85 \times 45.5 \times 0.87 \times 400 \times C = 0.85 \times 610 \times 157$$

$$+ 0.75 \times 165000 \times 60 \times 0.0035 [(120 - C)/C]$$

$$C = 27.91 \text{ mm}$$

$$\varepsilon_{frp} = \varepsilon_{cu} \frac{h - c}{c} \quad \varepsilon_{frp} = 0.0035 \times \frac{120 - 27.91}{27.91} = 0.0115 \leq \frac{3100}{165000} = 0.0187$$

$$\varepsilon_s = \varepsilon_{cu} \frac{d - c}{c} \quad \varepsilon_s = 0.0035 \times \frac{100 - 27.91}{27.91} = 0.009 \geq 0.002$$

$$M_r = 0.85 \times 610 \times 137 \left(100 - \frac{0.87 \times 27.91}{2}\right) + 0.75 \times 165000 \times 60 \times 0.0115 \times \left(120 - \frac{0.87 \times 27.91}{2}\right)$$

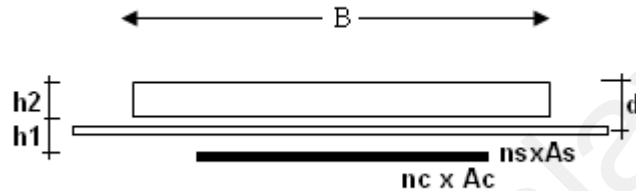
$$M_r = 17.36 \text{ kNm}$$

Second moment of area for un-cracked section:

$$I_t = 3.31 \times 10^7 \text{ mm}^4$$

$$M_{cr} = \frac{6.19 \times 3.31 \times 10^7}{60} \times 10^{-6} = 3.42 \text{ kNm}$$

Second moment of area for cracked section:



$$\frac{Bh_2^2}{2} = n_s A_s (d - h_2) + n_c A_c (H - h_2)$$

$$h_2 = 24.76 \text{ mm}$$

$$I_{cr} = \frac{Bh_2^3}{12} + n_s \times A_s \times (d - h_2)^2 + n_c \times A_c \times h_1^2 = 1.052 \times 10^7 \text{ mm}^4$$

$$I_e = \frac{2(1.052 \times 10^7 \times 3.31 \times 10^7)}{1.052 \times 10^7 + 3.31 \times 10^7} = 1.6 \times 10^7$$

$$\Delta = \frac{0.5PL^3}{6E_c I_e} \left[\frac{3a_s}{4L} - \left(\frac{a_s}{L} \right)^3 \right] = \frac{0.5 \times 5.26 \times 10^3 \times (1650)^3}{6 \times 25881 \times 1.6 \times 10^7} \left[\frac{3 \times 0.65}{4 \times 1.65} - \left(\frac{0.65}{1.65} \right)^3 \right]$$

$$= 1.113 \text{ mm}$$

3.3 Finite Difference Method for Deflection Calculation

Finite difference method (FDM) is a numerical technique based on mathematical discretization of the boundary problem equations. In this method, the continuous process is investigated in a finite number of adequately small time intervals. So, the function is estimated by approximate expression. FDM is an approximation to the first and second derivatives as well as shown in Figure 3.10 and defined in following equations.

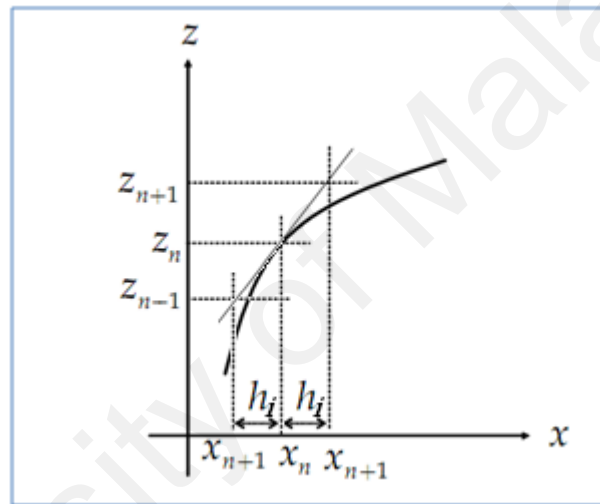


Figure 3.10: The basic definition of finite difference method

$$\left. \frac{dz}{dx} \right|_n^{backward} \approx \frac{z_n - z_{n-1}}{h_j} \quad (3.44)$$

$$\left. \frac{dz}{dx} \right|_{n+1}^{forward} \approx \frac{z_{n+1} - z_n}{h_j} \quad (3.45)$$

$$\left. \frac{d^2z}{dx^2} \right|_n = \frac{d}{dx} \left[\frac{dz}{dx} \right] = \frac{\left(\frac{dz}{dx} \right)_{n+1} - \left(\frac{dz}{dx} \right)_n}{h_j} = \frac{\frac{z_{n+1} - z_n}{h_j} - \frac{z_n - z_{n-1}}{h_j}}{h_j}$$

$$\left. \frac{d^2 Z}{dx^2} \right|_n = \frac{1}{h_x^2} (Z_{n+1} - 2Z_n + Z_{n-1}) \quad (3.46a)$$

and:

$$\left. \frac{d^2 Z}{dy^2} \right|_n = \frac{1}{h_y^2} (Z_{m+1} - 2Z_m + Z_{m-1}) \quad (3.46b)$$

$$\nabla^2 Z = \frac{\partial^2 Z}{\partial x^2} + \frac{\partial^2 Z}{\partial y^2} \quad (3.47)$$

$$\nabla^2 Z = \frac{1}{h^2} (Z_{n+1} - 2Z_n + Z_{n-1} + Z_{m+1} - 2Z_m + Z_{m-1}) \quad (3.48)$$

Equation 3.48 is simplified in Figure 3.11 and Equation 3.49.

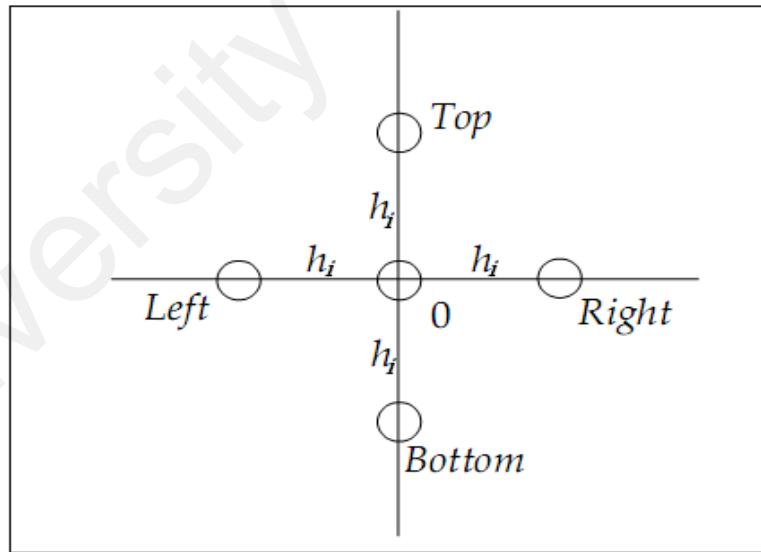


Figure 3.11: Simplified network definition for the Equation 3.48

$$\nabla^2 Z = \frac{1}{h_i^2} (Z_{Top} + Z_{Bot} + Z_{Left} + Z_{Right} - 4Z_0) \quad (3.49)$$

The FDM method for the two-dimension problem is defined by following equation as well as shown in Figure 3.12.

$$\frac{\partial^4 \omega}{\partial x^4} + 2 \frac{\partial^4 \omega}{\partial x^2 \partial y^2} + \frac{\partial^4 \omega}{\partial y^4} = \frac{P}{D} \quad (3.50)$$

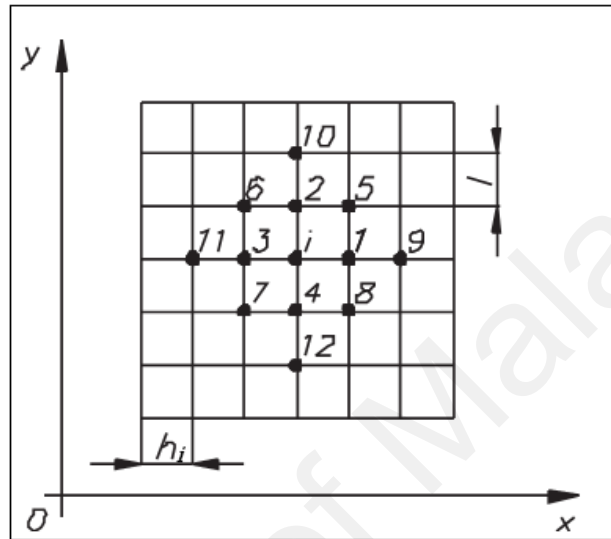


Figure 3.12: Networks for solving two-dimensional problem

Using derivatives of third and fourth order we have:

$$(6\alpha^2 + 8\alpha + 6)\omega_i - 4\alpha(\alpha + 1)(\omega_1 + \omega_3) - 4(\alpha + 1)(\omega_2 + \omega_4) + 2\alpha(\omega_5 + \omega_6 + \omega_7 + \omega_8) + \alpha^2(\omega_9 + \omega_{11}) + \omega_{10} + \omega_{12} = \frac{p_i l}{D} \quad (3.51)$$

Where:

$$D = \frac{Et^3}{12(1-\nu^2)} \quad : \text{Plate bending stiffness}$$

t and ν are slab thickness and poisson coefficient respectively.

$$p_i = \frac{P}{h_i l} \quad : P, \text{ is Concentrated Load}$$

3.3.1 Example for deflection calculation using finite difference

The slab width-length ratio of the samples investigated in this research satisfied following expression for the thin plate which is expressed by Timoshinko and Goodier (1951).

$$\frac{t}{L} \leq \frac{1}{10} \quad (3.52)$$

Slab: 55-2T10-860

The slab information data and network numbering is shown in Figure 3.13.

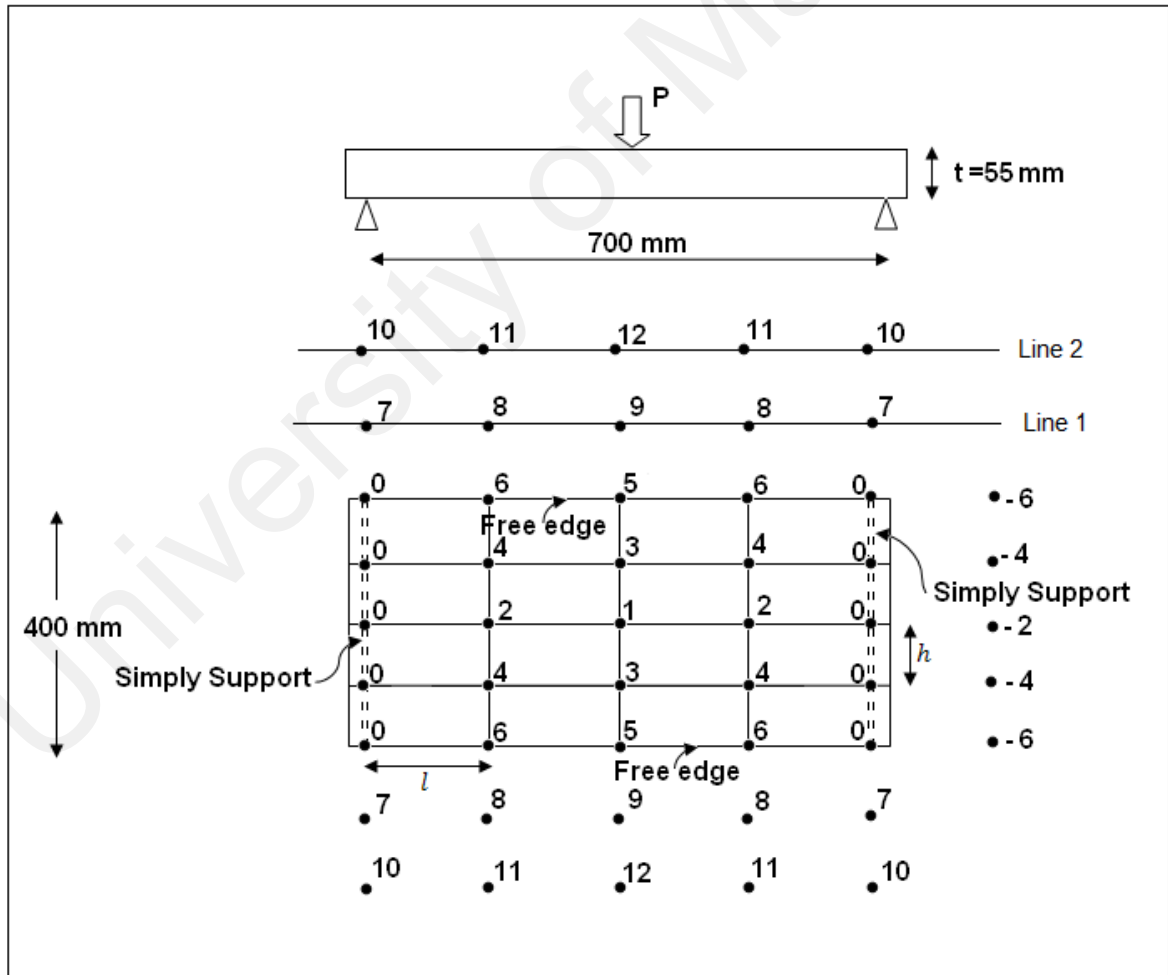


Figure 3.13: Input data and network numbering for the slab 55-2T10-860

$$l = \frac{L}{4} = \frac{700}{4} = 175 \text{ mm} \quad h_i = \frac{B}{4} = \frac{400}{4} = 100 \text{ mm} \quad \alpha = \frac{l^2}{h_i^2} = \frac{(175)^2}{(100)^2} = 3.0625$$

$$D = \frac{Et^3}{12(1-\nu^2)} = \frac{26313 \times 10^3 \times (55 \times 10^{-3})^3}{12(1-(0.2)^2)} = 3.8 \times 10^2 \text{ Nm}$$

$$p_i = \frac{P}{hl} = \frac{4.1}{0.175 \times 0.100} = 234.3 \times 10^3 \frac{\text{N}}{\text{m}^2}$$

$$\frac{p_i \times l^4}{D} = \frac{234.3 \times 10^3 \times 0.175^4}{3.8 \times 10^2} = 5.78 \times 10^{-1} \text{ m}$$

$$6\alpha^2 + 8\alpha + 6 = 88.77; \quad 4\alpha(\alpha + 1) = 12.44; \quad 4(\alpha + 1) = 16.25; \quad 2\alpha = 6.125 \quad \alpha^2 = 9.38$$

Equation in node 1:

$$88.77 \omega_1 - 12.44 \times 2 \times \omega_3 - 16.25 \times 2 \times \omega_2 + 6.125 \times 4 \times \omega_4 + 9.38 \times 2 \times \omega_5 = 5.78 \times 10^{-1}$$

Equation in node 2:

$$88.77 \omega_2 - 12.44 \times 2 \times \omega_4 - 16.25 \times \omega_1 + 6.125 \times 2 \times \omega_3 + 9.38 \times 2 \times \omega_6 + \omega_2 = 0$$

Equation in node 3:

$$88.77 \omega_3 - 12.44 \times (\omega_1 + \omega_5) - 16.25 \times 2 \times \omega_4 + 6.125 \times 2 \times (\omega_2 + \omega_6) + 9.38 \times (\omega_9 + \omega_3) = 0$$

Equation in node 4:

$$88.77 \omega_4 - 12.44 \times (\omega_2 + \omega_6) - 16.25 \times \omega_3 + 6.125 \times (\omega_1 + \omega_5) + 9.38 \times (\omega_4 + \omega_8) = 0$$

Equation in node 5:

$$88.77 \omega_5 - 12.44 \times (\omega_3 + \omega_9) - 16.25 \times 2 \times \omega_6 + 6.125 \times 2 \times (\omega_4 + \omega_8) + 9.38 \times (\omega_1 + \omega_{12}) = 0$$

Equation in node 6:

$$88.77 \omega_6 - 12.44 \times (\omega_4 + \omega_8) - 16.25 \times \omega_5 + 6.125 \times 2 \times (\omega_7 + \omega_9 + \omega_3) + 9.38 \times (\omega_2 + \omega_{11}) = 0$$

Helpfully dimensions:

$$\frac{v}{\alpha} = \frac{0.2}{3.0625} = 0.065; \quad 2 \left(1 + \frac{v}{\alpha}\right) = 2.13; \quad 2 \frac{2-v}{\alpha} = 2 \times \frac{2-0.2}{3.0625} = 1.176$$

$$4 \left(1 + \frac{2-v}{\alpha}\right) = 4 \times \left(1 + \frac{2-0.2}{3.0625}\right) = 6.35; \quad \frac{2v-v^2}{\alpha^2} = \frac{2 \times 0.2 - 0.2^2}{3.0625^2} = 0.038$$

$$4 \left(\frac{1}{\alpha} - \frac{2v-v^2}{\alpha^2}\right) = 4 \times \left(\frac{1}{3.0625} - \frac{2 \times 0.2 - 0.2^2}{3.0625^2}\right) = 1.15$$

$$4 \left(1 + \frac{2}{\alpha} + \frac{3}{2} \frac{2v-v^2}{\alpha^2}\right) = 4 \times \left(1 + \frac{2}{3.0625} + \frac{3}{2} \times \frac{2 \times 0.2 - 0.2^2}{3.0625^2}\right) = 6.84$$

Equations in Line 1:

$$\omega_7 = 2.13 \times \omega_6 - \omega_4 - 0.065(\omega_6 - \omega_6) = 0$$

$$\omega_8 = 2.13 \times \omega_6 - \omega_4 - 0.065\omega_5$$

$$\omega_9 = 2.13 \times \omega_5 - \omega_3 - 0.065(\omega_6 + \omega_6)$$

Equations in Line 2:

$$\omega_{11} = 6.84 \times \omega_6 - 6.35\omega_4 - 1.15\omega_5 + 1.176\omega_3 + \omega_2 + 0.0038 \times 2 \times \omega_6$$

$$\omega_{12} = 6.84 \times \omega_5 - 6.35\omega_3 - 1.15 \times 2 \times \omega_6 + 1.176 \times 2 \times \omega_4 + \omega_1 + 0.0038 \times \omega_5$$

Substitute helpfully dimensions and equations in line 1 and line 2 into equations node1 to node 6:

$$1) \quad 88.76\omega_1 - 32.5\omega_2 - 24.88\omega_3 + 24.5\omega_4 + 18.76\omega_5 = 5.78 \times 10^{-4}$$

$$2) \quad -16.25\omega_1 + 89.77\omega_2 + 12.25\omega_3 - 24.88\omega_4 + 18.76\omega_6 = 0$$

$$3) \quad -12.44\omega_1 + 12.25\omega_2 + 79.38\omega_3 - 32.58\omega_4 + 75.4\omega_5 + 11\omega_6 = 0$$

$$4) \quad 6.1254\omega_1 - 12.44\omega_2 - 16.25\omega_3 + 88.74\omega_4 + 5.51\omega_5 + 7.5\omega_6 = 0$$

$$5) \quad 18.76\omega_1 + 59.5\omega_3 + 22\omega_4 + 125.6\omega_5 - 29.6\omega_6 = 0$$

$$6) \quad 18.76\omega_2 + 11\omega_3 - 59.6\omega_4 - 0.136\omega_5 + 124.9\omega_6 = 0$$

Solving equations to determine deflection:

$$\omega_1 = 0.543 \text{ mm}; \quad \omega_2 = 0.0696 \text{ mm}; \quad \omega_3 = 0.3402 \text{ mm}; \quad \omega_4 = 0.0518 \text{ mm}; \quad \omega_5 = \omega_6 = 0$$

CHAPTER 4

4. FINITE ELEMENT ANALYSIS

4.1 Introduction

Courant (2008) developed the Finite Element Analysis (FEA) that is perhaps the most accepted numerical technique used nowadays. He employed the Ritz method of numerical analysis and minimization of variation calculation to achieve estimated key for vibration systems. But, the FEA was limited to the case study related to automotive, aeronautics, defense and nuclear industries caused by expensive cost of obtaining a computer by the early 70's. While the increasing accessibility of high speed processor have caused structural engineers to apply FEA as a practicable technique to solve complex engineering problems in recent years. FEA applies the method to divide the structural system into a mesh of finite sized element of simple shapes. The variation of displacement is analyzed by using simple polynomial shape functions and nodal displacements within each element. The analyzed equations for the strains and stresses are developed in case of the unidentified nodal displacements. The mentioned equations of equilibrium are collected in a matrix form which can simply be defined and solved with a computer. The nodal displacements are calculated after applying the suitable boundary conditions and solving the matrix stiffness equation. Then the strains and stressed of the element can be found after nodal displacement calculation.

The development of procedures in a FEA by Melosh (2007) is as follows:

- 1) Idealization of the physical system of the model that consisted of selection and exactly definition of the mathematical models of the system. These definitions involve of the geometry, the boundary conditions, material behavior, stress equilibrium, and displacement continuity.
- 2) Dividing the mathematical model that includes separating the members into randomly selected piece in the structure. This also involves choosing the behavior approximations of each piece of the structure. The model dividing will be completed when numerical amounts have been allocated to the stiffness matrix and equivalent loading vector coefficients of all elements in the model.
- 3) Processing the FEA calculation that converts the stiffness matrix equation into the constrained stiffness equations of element for the structures. It considers continuity and balance conditions of the engineering system as well.
- 4) Solving of the equations by using Gauss elimination method to find the nodal displacements.
- 5) Evaluation of stress that needs developing numerical amounts for element stress matrices represented by the nodal loading equations and the interior loading stress equations.
- 6) Explanation of FEA results consisted of determining the meaning of the behavior calculation of the discredited model regarding the physical system of interest.

Most of FEA software package such as ABAQUS, ANSYS, ADINA, LUSAS, NASTARAN, and DIANA give different one-, two- or three-dimensional elements to solve problems like straight and curved beams, plane stress, plane strain, shell and three-dimensional solid elements. In this study, LUSAS software package applied for the

purpose of non-linear analysis of non-strengthened and CFRP strengthened RC one-way slab. LUSAS software is selected because of its flexibility in material and geometry modeling. This chapter includes the fundamental of LUSAS software and step by step definition of non-linear modeling from geometry until the determination of the slab mid-span deflection.

4.2 Fundamentals and Theory of Using LUSAS Software

LUSAS is a FEA software that can evaluate the most of complex models using linear or non linear analysis. In LUSAS software the model geometry is defined as features which are sub-divided into finite elements in order to do the analysis. By increasing the number of elements in the meshed member the accuracy of the analysis usually is increased but the time required for analysis will be also increased.

In case of using LUSAS Software to analyze reinforced concrete structures, the model of structure must be first defined and then the characteristics of the structure need to be inputted. Actually, the model process of LUSAS software as graphical representation consisted of geometry feature and assigned characteristic. The geometry feature is represented by points, lines, surfaces and volumes. The major basis of geometry drawing is started by a number of points, which by connection together will create the lines. Combined lines will make a surface and combined surfaces will create a volume. LUSAS software can do either global analysis of whole structure or local analysis of the different elements of structures. The attributes assigning mean inputting the information or properties of the structural model. The attributes of a structural model, as explained in the following, consisted of the meshing, geometry, materials, support and loading. In the modeling process by LUSAS several assumptions are made that are very important in

model creation to make it similar to the actual experiment configuration. These assumptions are:

- 1) The linear strain distribution is considered over the depth;
- 2) No any slip existed between the longitudinal steel bar and the surrounded concrete around steel bar;
- 3) No any slip between the external CFRP and the surface of the concrete;
- 4) Early separation and shear failure of the CFRP is not allowable;
- 5) The tensile strength of the adhesive is ignored,
- 6) No any tensile stress is carried by concrete after cracking.

4.3 Modeling Process

In order to analyze the load-deflection study of non-strengthened and CFRP strengthened RC one-way slab, the LUSAS software is employed in this research. Pre-processing, solving, and results-processing are three complete stages in finite element method. In the pre-processing stage, the geometry of the structure is modeled and then the material properties are assigned to the created model. The model solution can be started by clicking on the solve bottom. LUSAS software makes a data file and solves the matrix software. Finally, the mid-span deflection of RC slab under loading is found in the result-processing stage. For model creation, the geometry structure is identified and drawn using geometry features such as Points, Lines, Combined Lines, Surfaces, and Volumes. After that, the structure attribute such as Material, Loading, Supports, Mesh are defined by making an attribute dataset. The defined dataset is then assigned to the selected features.

The general view of the proposed model used in LUSAS software for the non-strengthened and CFRP strengthened RC slab are illustrated in Figures 4.1 and 4.2 respectively. In the

first part, the non-strengthened RC one-way slabs with different length, thickness, and steel bar were modeled for the load-deflection analysis under mid-span point punching load. In second part, the one-way RC slabs with similar dimension and steel bar and strengthened with different length and width of CFRP was modeled for the load-deflection analysis under four points line load. All the slabs were modeled with width of 400 mm.

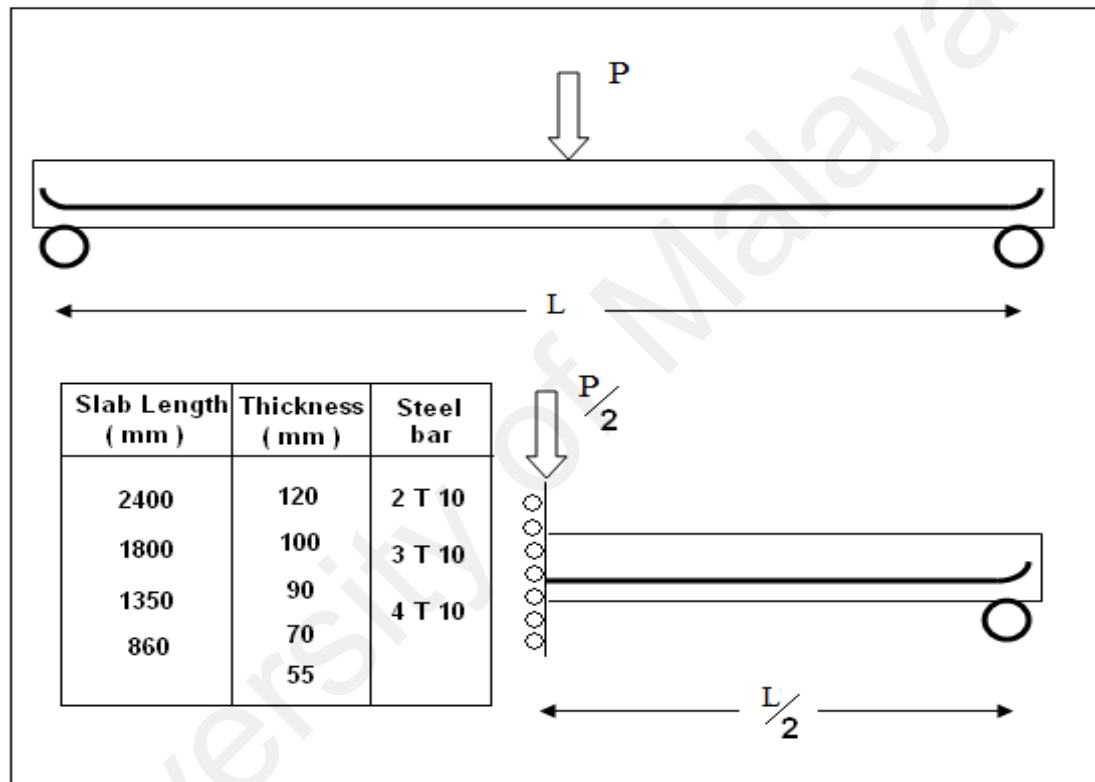


Figure 4.1: Configuration of non-strengthened RC slab used in LUSAS modeling

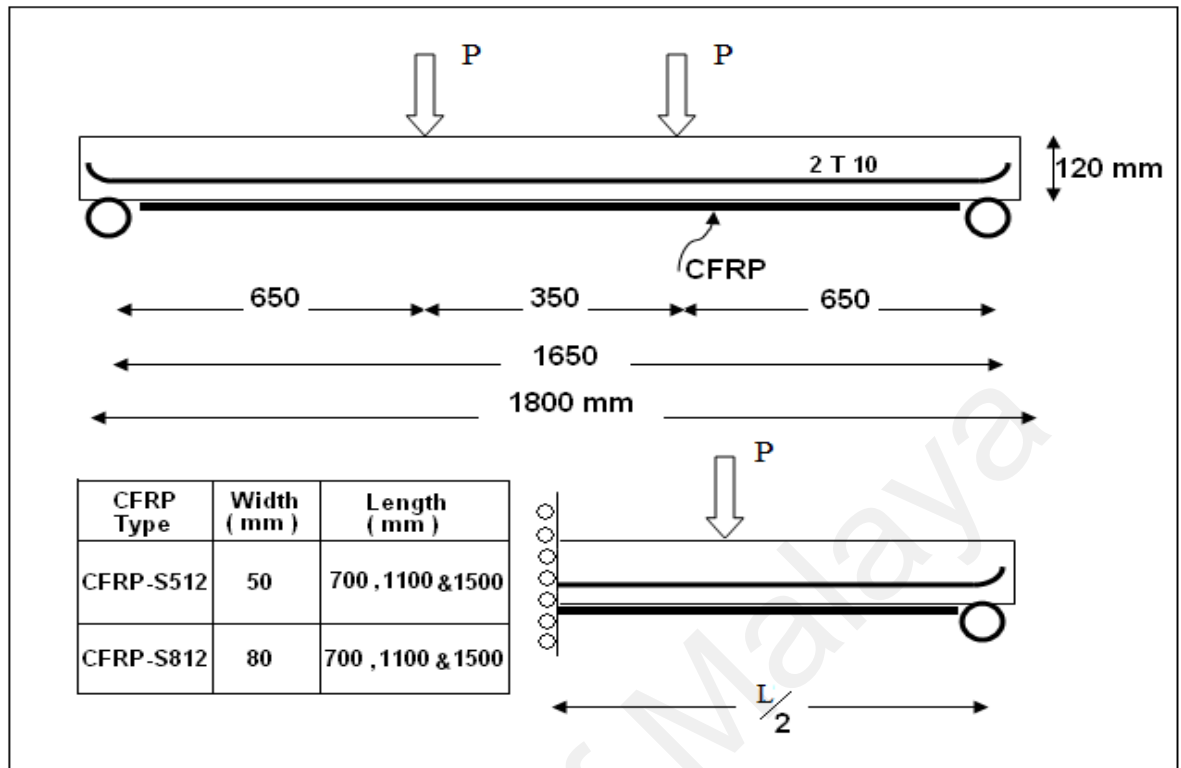


Figure 4.2: Configuration of CFRP strengthened RC slab used in LUSAS modeling

Only the right-hand span of the slab is modeled with simply support in the right hand end and with a symmetry support at the left-hand axis of symmetry.

4.3.1 Geometry modeling for RC slab

Point, Line, and Surface are three geometry feature types in LUSAS software used in this study for slab modeling. Both the non-strengthened and CFRP strengthened RC slabs were of surface feature type defined by lines and points.

4.3.2 Defining attributes for RC slab

Meshing, element selection, geometric properties, material properties, loading, and support conditions are necessary attributes for 2D modeling in a finite element method.

4.3.2.1 Meshing

The method of finite element analysis lies in the development of an appropriate mesh arrangement to provide an accurate analysis results and reasonable analysis time. The process of subdividing a geometry model into FEA named meshing. The number of division in geometry feature will determine how dense is the mesh in each geometry feature and hence mean how accurate the element will be analyzed. LUSAS software gives many mesh patterns which can be applied in analysis of structures. In this study, regular mesh applied for the non-strengthened and CFRP strengthened RC slab. The applied meshing for the concrete, steel bar, and CFRP is illustrated in Figure 4.3.

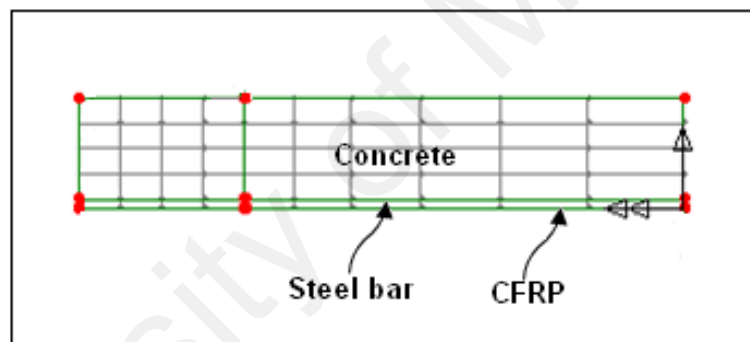


Figure 4.3: Meshing applied for the concrete, steel bar, and CFRP

4.3.2.2 Element selection

The concrete section for the both non-strengthened and CFRP strengthened RC slab is defined by plane stress (QPM8) as well as shown in Figure 4.4. The continuum surface element applied for concrete modeling as the normal stress (σ_z) and shear stress (σ_{xz} and σ_{yz}) directed perpendicular to the xy plan are were assumed equal zero.

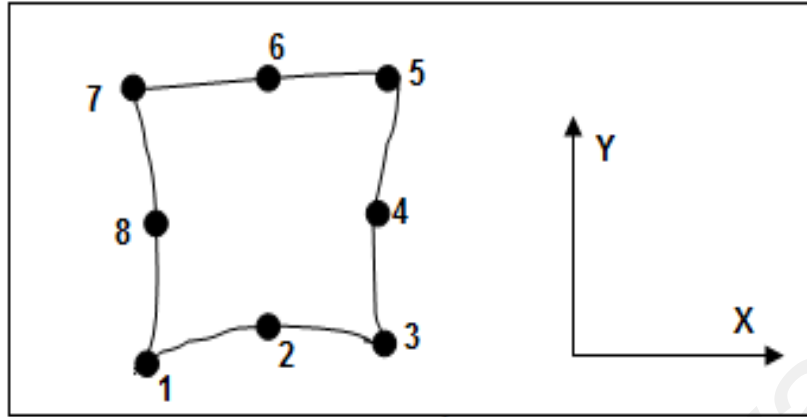


Figure 4.4: QPM8 surface element used for concrete

The steel bar and CFRP are modeled by line element (BAR3). BAR3 is an isoperimetric element that can only cover longitudinal displacement and force (Figure 4.5). The number of dimension and interpolation order for the steel bar and CFRP meshing was 2 dimensional and quadratic respectively.

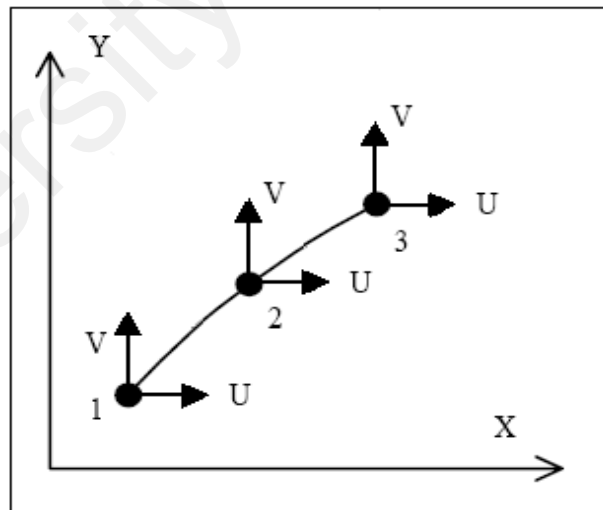


Figure 4.5: BAR3 line element used for steel bar and CFRP

4.3.2.3 Geometric properties

The geometry attributes such as slab thickness, cross sectional area of steel bar and CFRP are defined in geometry property paradigms. The thickness of slabs for non-strengthened and CFRP strengthened were 400 mm. The cross sectional area defined for 2T10, 3T10, and 4T10 was 158, 237, and 316 mm² respectively. The CFRP cross sectional area for S-512 and S812 were 60 and 96 mm² respectively. The defined geometry properties have to assign to the corresponded features.

4.3.2.4 Material properties

A material property dataset must be assigned to each part of models in FEA. The nonlinear material with isotropy property for the concrete, steel bar, and CFRP assumed as following three groups for the both non-strengthened and CFRP strengthened RC slab.

Group 1: Nonlinear Concrete

Compressive strength	:	45 N/mm ²
Tensile Strength	:	6 N/mm ²
Modulus of elasticity	:	2.6×10^4 N/mm ²
Mass density	:	2.4×10^{-2} N/mm ²
Poisson's ratio	:	0.2

Group 2: Nonlinear Steel Bar

Yield strength	:	6.1×10^2 N/mm ²
Modulus of elasticity	:	2.0×10^5 N/mm ²
Mass density	:	7.8×10^{-5} N/mm ²
Poisson's ratio	:	0.3

Group 3: Nonlinear CFRP

Tensile Strength	:	$3.1 \times 10^3 \text{ N/mm}^2$
Modulus of elasticity	:	$1.65 \times 10^5 \text{ N/mm}^2$
Poisson's ratio	:	0.25

The stress-strain curve for the concrete is assumed as proposed by Hognestad (2006) as well as shown in Figure 4.6.

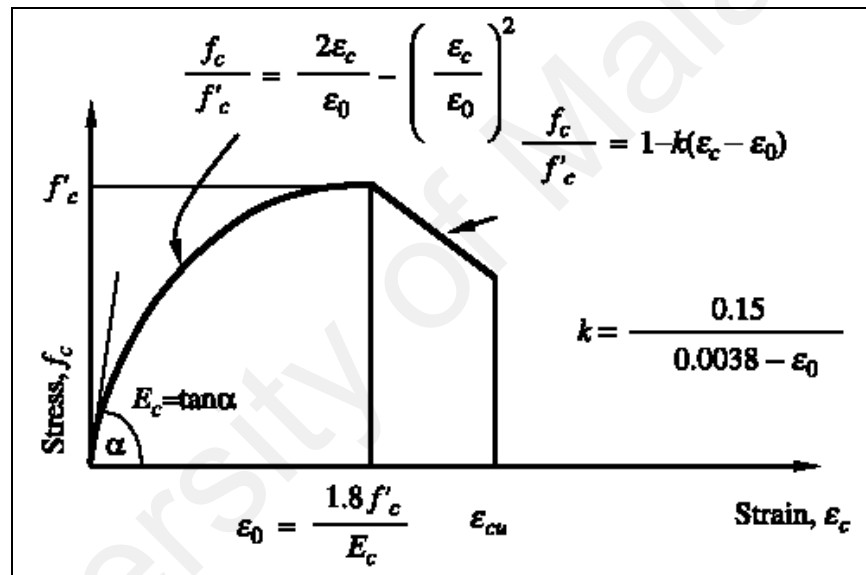


Figure 4.6: Simplified stress-strain curve for concrete (Niu, 2006)

The concrete feature assumptions in current study are as following:

- i) The maximum stress in concrete in the first crack is equal $0.3f'_c$
- ii) The relationship between stress and strain in the elastic area is defined as $f_c = E_c \varepsilon_c$
- iii) The ultimate concrete compressive strain is equal 0.003.
- iv) The relationship between stress and strain after first crack and before ε_0 is defined as following formula:

$$\frac{f_c}{f'_c} = \frac{2\varepsilon_c}{\varepsilon_0} - \left(\frac{\varepsilon_c}{\varepsilon_0}\right)^2 \quad (4.1)$$

$$\varepsilon_0 = \frac{1.8f'_c}{E_c} \quad (4.2)$$

The relationship between stress and strain after ε_0 and before ε_{cu} is defined as following formula:

$$\frac{f_c}{f'_c} = 1 - K(\varepsilon_c - \varepsilon_0) \quad (4.3)$$

$$K = \frac{0.15}{0.0038 - \varepsilon_0} \quad (4.4)$$

Where:

f_c = Stress in concrete

f'_c = Maximum stress in concrete

ε_c = Compressive strain in concrete

ε_0 = Strain in maximum stress in concrete

E_c = Concrete module of elasticity

The reinforcing steel bar is assumed to have bilinear strain hardening and the CFRP is model having linear elastic behavior till failure as well as shown in Figure 4.7.

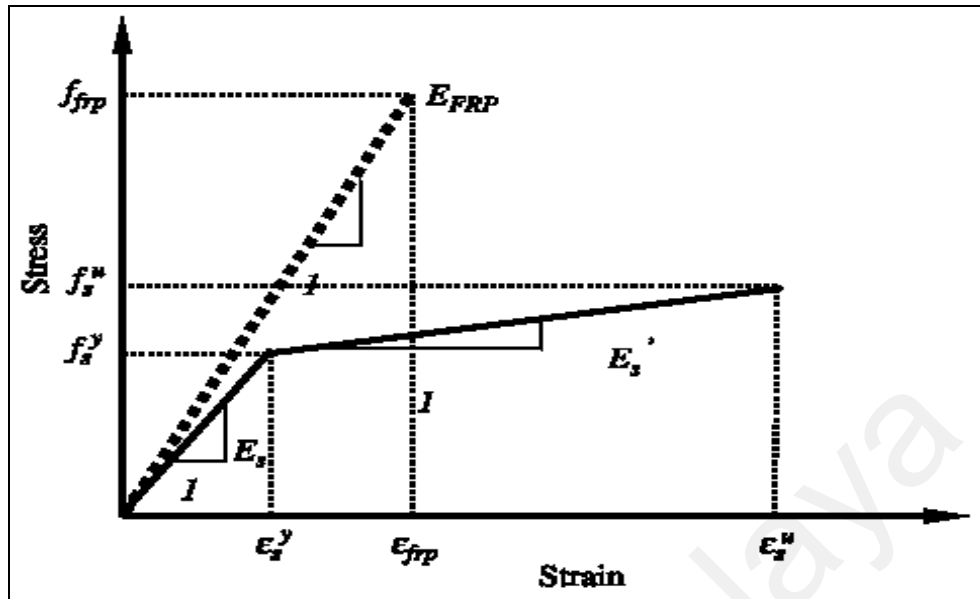


Figure 4.7: Simplified stress-strain curve for steel bar and CFRP (Niu, 2006)

4.3.2.5 Support condition

The support conditions in FEA are defined for the way in which the proposed model is supported or restrained. The dataset for support conditions includes information about the restrains applied to each degree of freedom. In this study, simply support in Y direction at the right-hand end and a horizontal restraint in X direction was applied for the slab as well as shown in Figure 4.8. The proposed horizontal restraint in mid-span was required to satisfy the symmetry requirement for half span modeling.

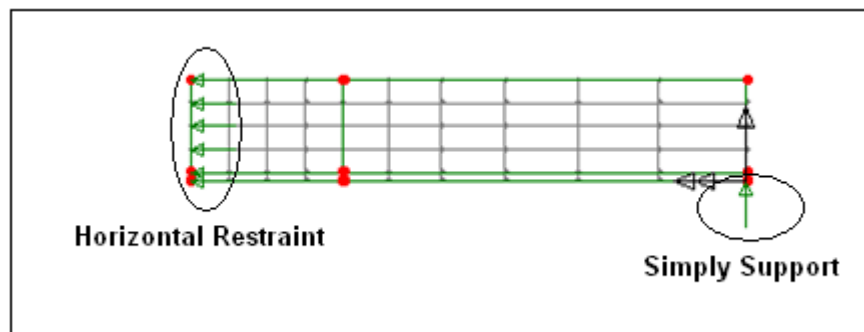


Figure 4.8: Proposed support condition for the RC slab

4.3.2.6 Loading

The external influence on the model describes by loading dataset. The applied loading for the non-strengthened and CFRP strengthened RC slab was mid-span punching point load and four point line load respectively. In this study, the loading applied on the both types of slabs was considered as line load and the effect of punching load on the perpendicular direction due to small slab width was ignored. The proposed loading on the non-strengthened RC slab and CFRP strengthened RC slab is shown in Figures 4.9 and Figure 4.10 respectively.

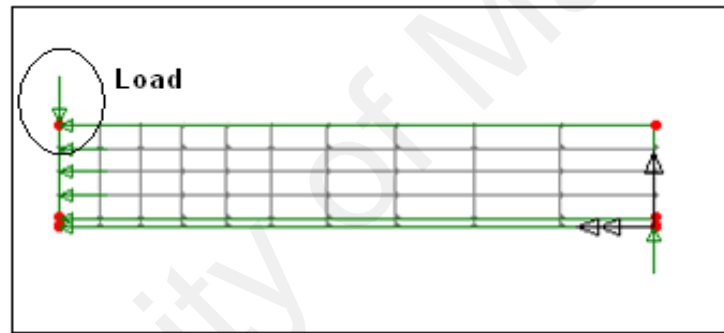


Figure 4.9: Proposed punching point load assigned on the model for the non-strengthened RC slab

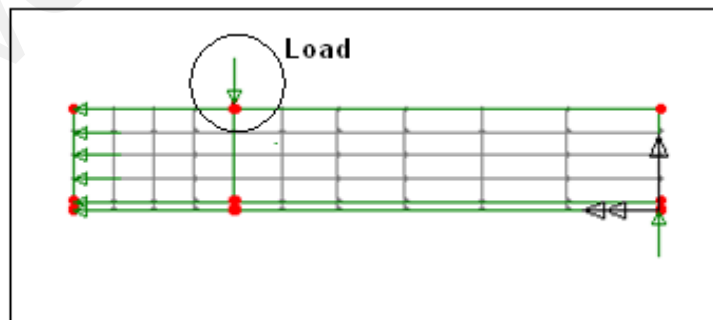


Figure 4.10: The line load assigned on the model for the CFRP strengthened RC slab

4.3.3 Analysis and results processing

Post-processing or results processing is the manipulation and visualization of the outputs produced by FEA software during an analysis. A general view of the LUSAS abilities in manipulation and visualization is presented in Figure 4.11. In this research, mid-span deflection versus loading for non-strengthened and CFRP strengthened RC slabs was analyzed and printed out. A plot of deformed shape after applied loading for the non-strengthened RC slab is shown in Figure 4.12. The load-deflection graph for slabs was provided using step-by-step selection in graph wizard section.

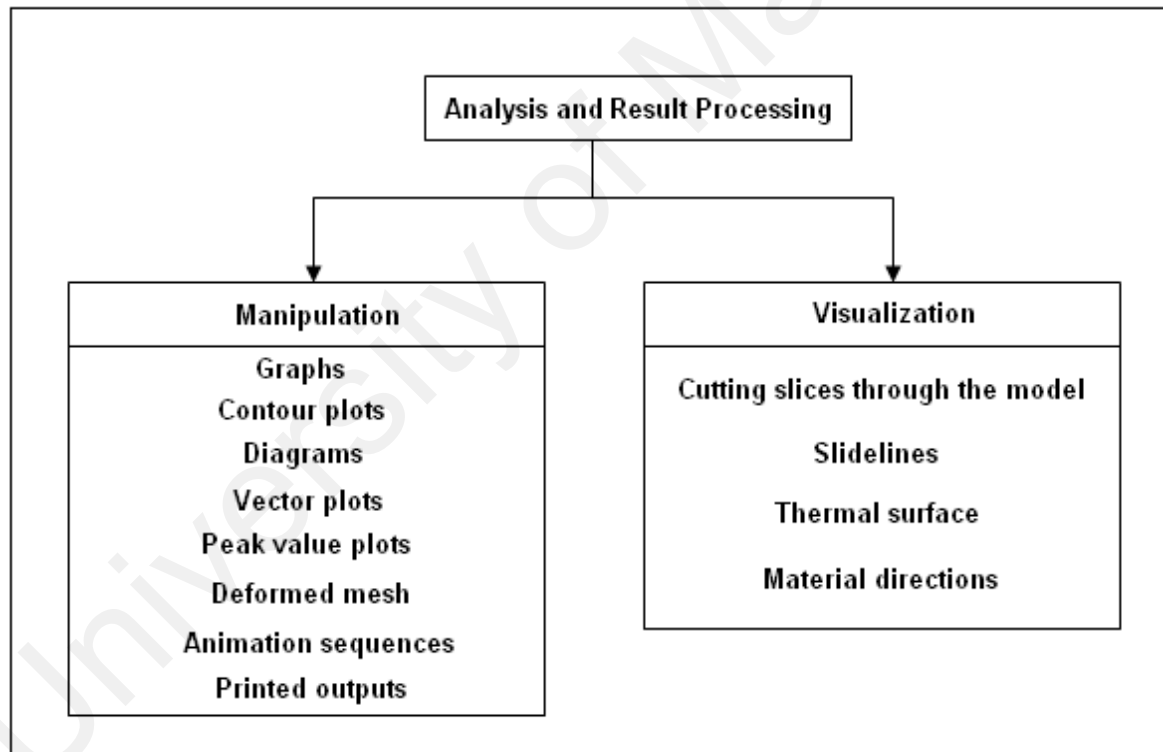


Figure 4.11: Manipulation and visualization in LUSAS software

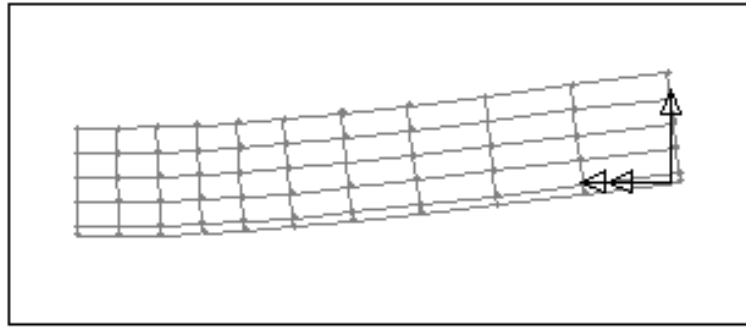


Figure 4.12: A plot of deformed shape for non-strengthened RC slab

The load-deflection analysis results for the both non-strengthened and CFRP strengthened RC one-way slab were collected to compare with experimental load-deflection results.

University of Malaya

CHAPTER 5

5. ANN MODELING FOR RC SLAB

5.1 Introduction

To generate ANNs for situations where training data is sufficient, and insufficient, several key steps must be met. Firstly, data needs to be gathered and the quality of data is evaluated and decided if it is adequate. Data gathering consist of data specification, organization, and analysis. Secondly, the data is then used to generate ANNs which are fitted to apply a computerizing methodology by learning from examples from prior understanding of the nature of the problem. Creating an NN engages definition of a primary network, selecting a package of input properties, arranging the model, and identifying the best net architecture during the training process. If the generated neural network does not present an acceptable minimum error, the program loops back to adjust the network data in pre-processing step to improve the training data. These steps are shown in Figure 5.1. The flow chart is applied to generate FBNN, GRNN, FFTDNN and RNN to determine the relationship from experimental results obtained in this research and those published by other recognized researchers in the field of structural engineering. MATLAB software was used for network simulations.

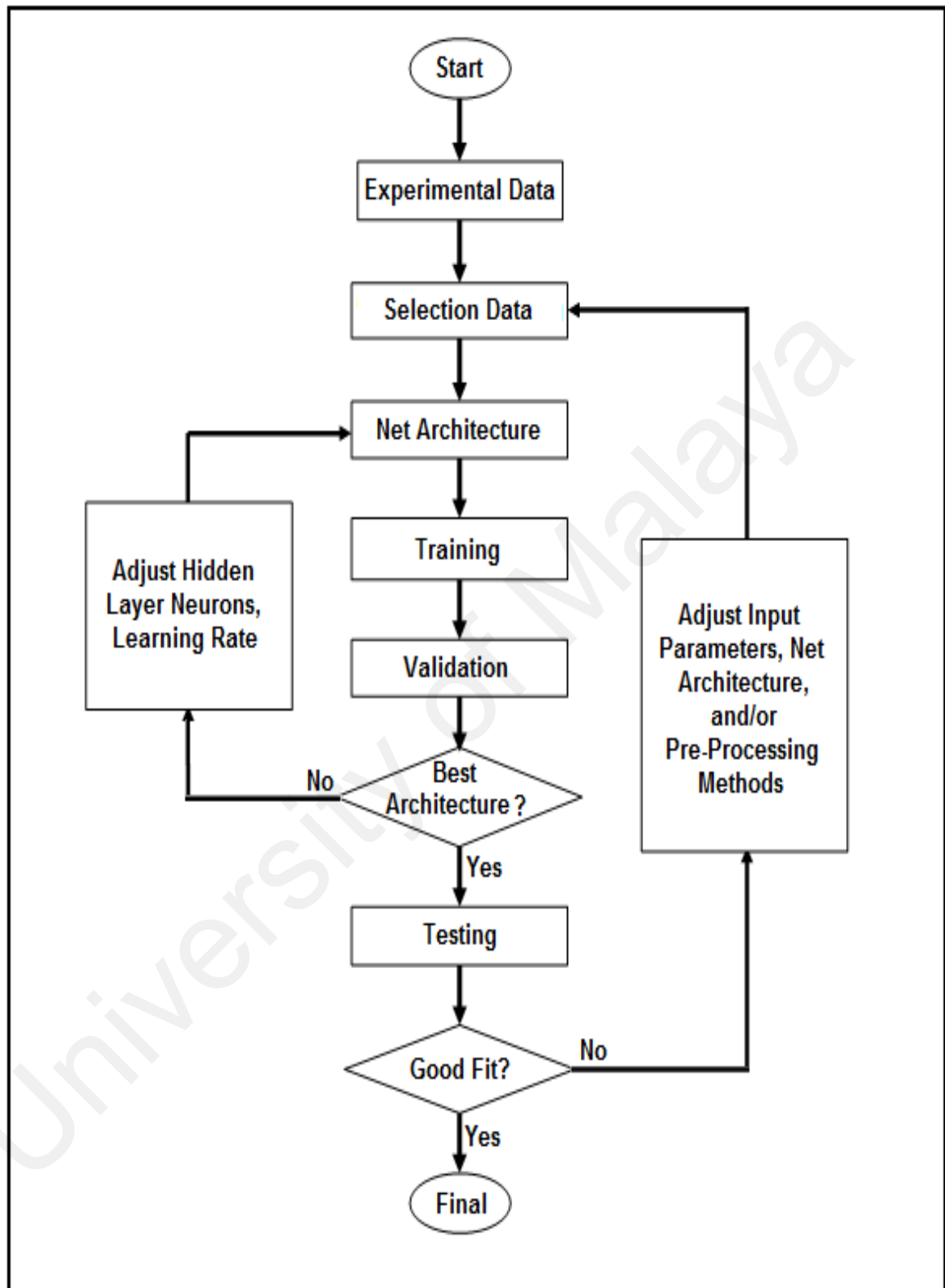


Figure 5.1: The overall process for network modeling

5.2 NN Definition

The master unit of the human brain is neuron that each neuron works like a numerical processing. Brains consist of a number of multi million of neuron that have connected together extremely complex and operate parallel. Normally neurons in the brain receive information from other neuron and send the output to other layers. The biological neuron or a nerve cell consists of synapse, dendrites, the cell body (soma), and the axon shown in Figure 5.2.

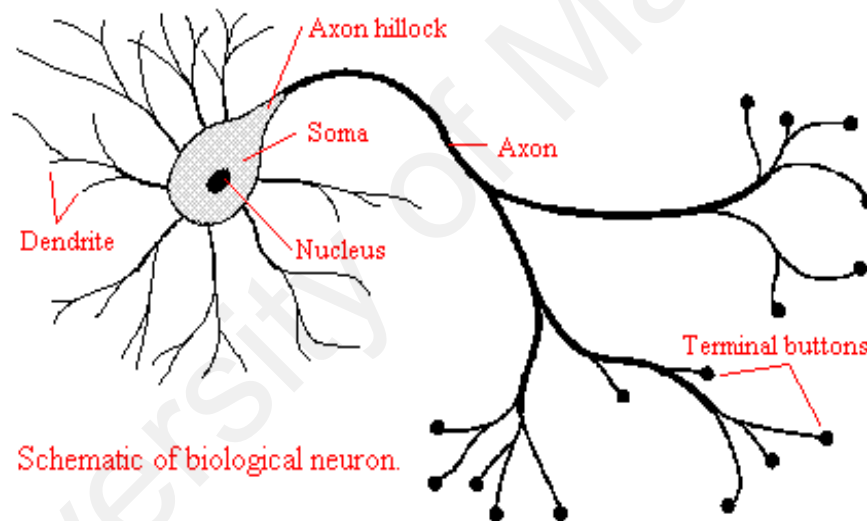


Figure 5.2: The biological neuron or a nerve cell(Zhang, 2009)

The human brain includes almost 10 billion neurons and 60 trillion synapses (connections) between them. The brain can make its purposes much quicker than the best computers in reality by using multiple neurons at the same time.

Scientists of biological science have recently discovered how neural networks work. They have found that the performance of biological neurons such as storage and memorizing information depends on the neurons and relationship. Actually, it infers that learning plays

as important role in creating new communication between neurons and regulates the existing communication.

In a similar method, ANNs are extremely simplified models of biological neural system, displaying capabilities such as learning, abstraction and generalization. ANNs are kinds of data information giving out method whose architecture are enthused by the construction of human nervous structure. Hawely et al (1990).expressed that the fundamental purposes of biological neurons are simulated by artificial neurons. A neuron comparison between biological and ANN is given in Table 5.1.

Table 5.1: Neuron comparison between biological and artificial neural network

Biological Neural Network		Artificial Neural Network
Neuron elements	Definition	
Soma	The sum of the all incoming signals	Neuron
Dendrite	Receives signals from other neurons	Input
Axon	It transmits the received signals from cell body to other neuron	Output
Synapse	The electrochemical contact between neurons	Weight

ANNs are similar to biological systems that transfer the relationship and function between data to a network structure by processing of the experimental data. These systems learn based on the calculation of numerical data or examples and are, therefore, referred to as intelligent systems. These systems endeavour to model the human brain structure based on intelligent calculation. The aim of ANN is to emulate the human ability to adjust to changing conditions and the current situation. This largely relies on being able to learn

from events that have happened in the past and being able to request this information for future action. Similar to biological networks, the ANN modelling is simple and the network function is determined based on relation between data.

5.3 Neural Network Concept Development

A NN performs of a lot of nodes that connected together by equations. The layer between input and output layer named hidden layer. The information data enters to network named input neurons, then connect to hidden layers by transfer function and finally the network output concludes from output layer. The selection of network type is the first and important part of ANN modeling. Then the network architecture means the number of hidden layers, neurons in input, hidden, and output layers, the kind of transfer function for neurons, and the network training and learning function will be determined. The selected network type and network architecture is applied to generate network using experimental data. Limam et al (2003) divided the gathered data for network generation in following three phases:

(1) Training phase: Using all training data set for network learning to fit the weight of the neurons within network generation.

(2) Validation phase: A set of data to adjust the parameters of a generated network, such as the number of hidden layer and neurons in each hidden layer. In this phase, the necessary training iteration is determined to avoid of overtraining.

(3) Test phase: A set of data for fully assessment of the network performance.

5.3.1 Network connection type

The network connections are divided in static and dynamic network connections. In static or feed-forward connection, the information moves in only forward direction from input to output. The output of any layer does not have any effect on the same layer. FBNN and GRNN are two kinds of SNN that are discussed in this study.

In dynamic or feed-back connection, the signal moves in both directions, forward and backward. These kinds of networks are very powerful and can get the results performance over the SNN. FFTDNN and RNN are two kinds of DNN that is applied for mid-span deflection prediction of non-strengthened and CFRP strengthened RC slab.

5.3.2 Feed-forward back-propagation neural network

FBNN is the first and perhaps simplest artificial neural network for output prediction of different objective in science. In FBNN, the information moves in only one way, forward, from the input, through the hidden nodes (if any), and to the output node. In this network, the connections between the units are no cycles or loops. FBNN can easily be built with an easy optimizing and is the most common neural network architecture in use nowadays.

5.3.2.1 Network architecture

The network architecture is the first important stage to construct network modeling. Normally, a trial and error method is assumed to select the optimum network architecture. It is because, there is not any rules to define the network architecture in back-propagation neural network as stated by Al-Sayed et al (1996). The neuron layers linking the input and the output layers are defined as hidden layers. Oztas et al (2006) expressed that there is not any theory to discuss how many hidden layers need to predict any given function. More of

times, the linear model are applicable for a widely range of prediction purposes. If the number of input layer is one, it appears to have no improvement to using in the network more than one hidden layer. But, when the number of input layers are more than one input, the case get much more complex. The number of hidden layers and neurons can be randomly selected and changed to find the optimum results in each try. Although increasing the number of hidden layers improve the generalization capacity. Yost et al (2011) showed that one or two hidden layers with a randomly large number of neurons may be enough to approximate any function. Also, Mukherjee and Deshpande (1995) confirmed that network with a single hidden layer with sufficient number of neurons can be generated for linear equations. The number of neurons in hidden layer should be between the average and the sum of the input and output data as defined by Hajala and Breke (1992). Jofriet and Mcneice (1971) defined the following formula for the minimum number of neurons in hidden layer:

$$NH = NI + 1 \quad (5.1)$$

Where, NH is the number of neurons in hidden layers and NI is the number of neurons in input layer.

The number of training data is the second important part to define network modeling. Although increasing the number of training data increase the time required to train network, the number of prototype in the training step considerably influence in ability of a network generation. Scanlon and Murray (1974) showed that the minimum number of training data is defined by following equation:

$$NT = NH * (NI + 1) + NO * (NH + 1) \quad (5.2)$$

Where:

NT, is the minimum number of training data

NH, is the number of hidden layer neurons

NI, is the number of input layer neurons

NO, is the number of output layer neurons

5.3.2.2 Transfer function

A suitable transfer function should be chosen for numerical representation of the relation among the input and output of a network modeling. Dotroppe et al (1973) expressed that the type of transfer function in hidden layer is the main difference between the network types. Over the last few years, many transfer functions have been initiated by researchers using in ANNs. Only three following transfer functions are usually used in multilayer neural network:

(1) **Linear:** In this kind of transfer function, the output action is proportional to the total weighted of output. The linear transfer function (Purelin) is shown in Figure 5.3.

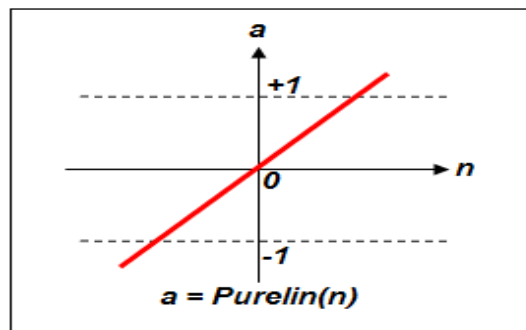


Figure 5.3: The linear transfer function (Purelin)

(2) **Threshold:** Depending on whether the whole input is bigger than or less than some entrance amount, the data in the output place at one of two points in following equation :

- If the input is less than a certain threshold value implies $\varphi(v) = 0$
- If the input is greater than or equal to the threshold value implies $\varphi(v) = 1$

$$\varphi(v) = \begin{cases} 1 & \text{if } v \geq 0 \\ 0 & \text{if } v < 0 \end{cases} \quad (5.3)$$

(3) **Sigmoid:** In the sigmoid transfer function, the output differs constantly but not linearly as the changes of input data. Sigmoid units such as log-sigmoid (Figure 5.4) and tan-sigmoid (Figure 5.5), provide a better similarity to actual neurons.

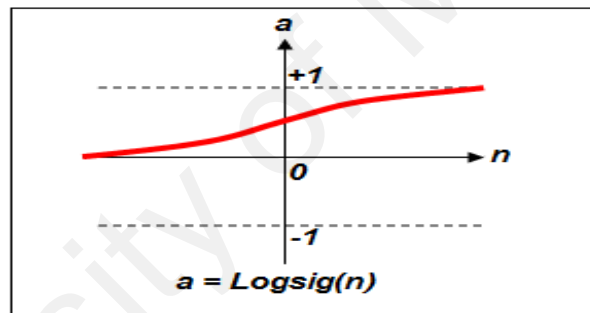


Figure 5.4: Log-sigmoid transfer function(Logsig)

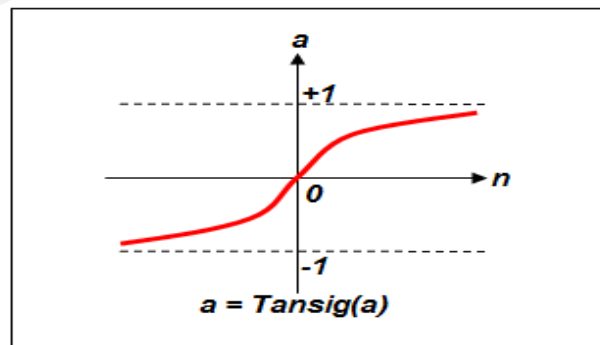


Figure 5.5: Tan-sigmoid transfer function(Tansig)

The following equations are the log-sigmoid (Logsig) and tan-sigmoid (Tansig) transfer function.

$$\text{Log-sigmoid (Logsig): } a > 0 \quad f(x) = \frac{1}{1 + e^{-ax}} \rightarrow f'(x) = \sigma f(x) \cdot [1 - f(x)] \quad (5.4)$$

$$\text{Tan-sigmoid (Tansig): } g(x) = 2f(x) - 1 = \frac{1 - e^{-ax}}{1 + e^{-ax}} \rightarrow g'(x) = \frac{\sigma}{2} [1 + g(x)] \quad (5.5)$$

In multilayer neural network, sigmoid transfer function is a common type of activation function used by the hidden neurons. The linear transfer function (Pureline) uses in output layer.

5.3.2.3 Network training and learning function

Learning and training functions are numerical measurement used for automatically change the weights and biases of the system. The training function applies a comprehensive algorithm that concerns all weights and biases of a network. But, the learning function can be used to apply individual weights and biases inside a system.

NN Toolbox consists of a range of training algorithms, including several class extraction methods, the Levenberg-Marquardt algorithm (LM), conjugate gradient technique, and the strong back propagation algorithm. The toolbox's modular system leads us directly improve training algorithms that can be included with basic algorithms. The training algorithms can be applied from the command line or due to graphical instrument. Back-propagation is the popular algorithm for network training. A back-propagation network normally starts out with a casual set of weight. The weight will be changed in each process of input-output pair. The back-propagation algorithm revises the weights in each input-output set by propagation the error back to the network using a widely used learning mechanism to change the weights and biases. The Input-output pairs are used to

train a network until the network can approximate a function. After training the generated network can be tested for the new input-output pairs.

5.3.2.4 Data normalization

Normally for more performance, all input and outputs data have to be normalized between 0 and 1 or -1 and 1. Hedong et al (2006) stated that the generated networks tend to work best when the data have been normalized. Also, it is important to apply similar normalization method for training data as well as for testing data. The formula for the data normalization is given in follow:

$$I_o = I_{o\min} + (I_{o\max} - I_{o\min}) * (D_t - D_{t\min}) / (D_{t\max} - D_{t\min}) \quad (5.6)$$

Where:

I_o = Normalized data

D_t = data

$D_{t\max}$ = the largest amount of data

$D_{t\min}$ = the smallest amount of data

$I_{o\max}$ = the largest amount of normalized data

$I_{o\min}$ = the smallest amount of normalized data

5.3.3 General regression neural network

GRNN introduced by Nadaraya (2008) and Watson (1992), discovered by D. F. Specht (1971), reinvented by Schiøler (2001), and approached asymptotically from an increasing number of samples to the optimal regression surface. When, the number of data to generate a back-propagation neural network is not enough, GRNN is mostly useful with only a small number of training data available. It is because; GRNN has capability to connect to the primary function of the data. This makes GRNN an extremely useful tool to achieve predictions and comparisons of system performance in practice. The learning method is similar to finding a table in a multidimensional space that provides a perfect fit to the training data. The generalization is correspondent to the use of this multidimensional way to include the test data. The sample model of GRNN is given in Figure 5.6.

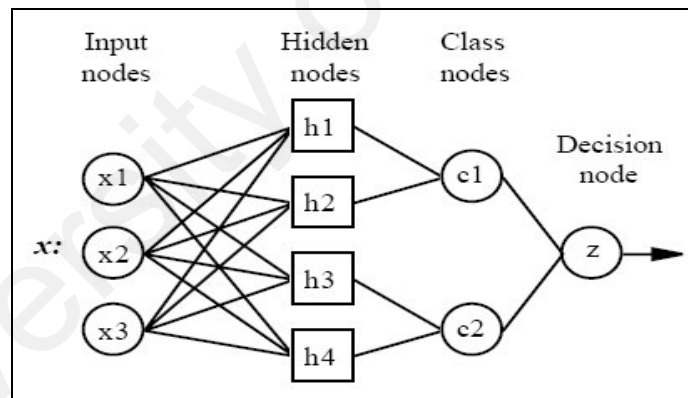


Figure 5.6: A model of PNN/GRNN

5.3.3.1 Network architecture

GRNN has following four layers:

- (1) Input layer:** For each predictor variable, one neuron is in the input layer. In the case of categorical variables, “ $n-1$ ” neurons use in hidden layer where, “ n ” is the number of categories. The neurons in input layer are standardized by subtracting

the median and dividing by the inter quartile range. The input layer then send the input value to each of neurons in the hidden layer.

- (2) **Pattern layer:** There is one neuron for each variable defined in the training information collection. The neuron supplies the values of the predictor variables for the case along with the object value. The output from pattern layer will transfer to the summation layer.
- (3) **Summation layer:** There are two neurons in the summation layer. One neuron is the numerator summation part and another is the denominator summation part. The denominator summation part inserts the weight values coming from each of neurons in the hidden layer. The numerator summation part applies the weight values multiplied by the real target value for each neuron in the hidden layer.
- (4) **Output layer:** The decision or output layer separates the value accumulated in the numerator summation section by the value in the denominator summation section and uses the result as the predicted target value.

5.3.3.2 Transfer function

The most popular choice for the function in hidden layer is a multivariate Gaussian function with an appropriate mean and auto covariance matrix. The following equation presents the outputs from hidden layer:

$$\phi_k[x] = \exp [-(x - v_k^x)^T (x - v_k^x)/(2\sigma^2)] \quad (5.7)$$

When, v_k^x are the equivalent clusters for the inputs, v_k^y are the equivalent clusters for the outputs. The v_k^y obtain by applying a clustering technique of the input/output information that make the K as cluster centers. v_k^y define by following formula:

$$v_k^y = \sum_{y(p)=clusterk} y(p) \quad (5.8)$$

N_k is the number of input information in the cluster center k, and

$$d(x, v_k^x) = (x, v_k^x)^T (x, v_k^x) \quad (5.9)$$

With

$$v_k^x = \sum_{x(p)=clusterk} x(p) \quad (5.10)$$

The node output of the hidden layer multiple by fitting interconnection weights to create the network output. The weight of the hidden node k (i.e., w_k) is equivalent to following equation:

$$w_k = \frac{v_k^y}{\sum_{k=1}^K N_k \exp \left[-\frac{d(x, v_k^x)^2}{2\sigma^2} \right]} \quad (5.11)$$

The selection of a sufficient number of training data is extremely influential in order to get suitable generalization properties. All the gathered information applies in two sets: training and testing. The information data using in training and testing phase is not the same.

5.3.3.3 Net algorithm

The normal distribution is as probability density function used in GRNN and each X_j , as training sample is defined as the mean of a normal distribution. The behavior of systems can be predicted by using these following equations based on few training samples. This can predict smooth multi-dimensional curves, and interpolate between training samples.

$$Y(X) = \frac{\sum_{i=1}^n Y_i \exp\left(\frac{-D_i^2}{2\sigma^2}\right)}{\sum_{i=1}^n \exp\left(\frac{-D_i^2}{2\sigma^2}\right)} \quad (5.12)$$

$$D_i^2 = (X - X_i)^T \cdot (X - X_i) \quad (5.13)$$

Where:

D_i , is the distance between the training data and prediction results

σ , is the smoothness parameter

A prediction carried out by GRNN is given in Figure 5.7. The position of training data shows by circle sign. The predicted results due to GRNN presented by solid line going through most of the circles sign. Also, the bell shaped curves are the individual terms due to net algorithm equation.

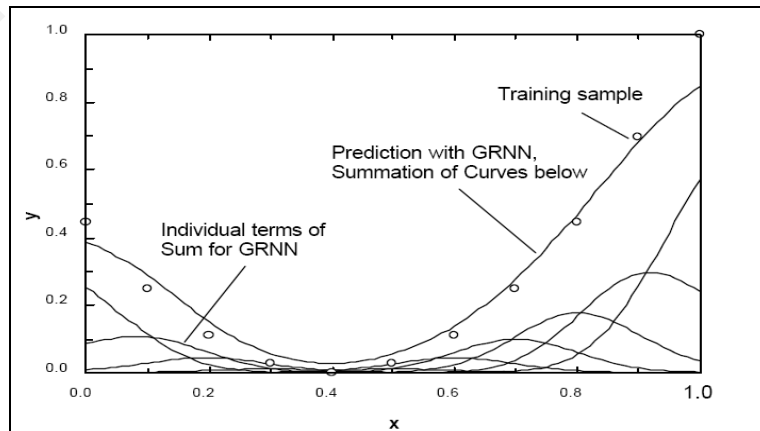


Figure 5.7: GRNN with individual terms tending for prediction, $\sigma = 0.1$

At each position outline values of the individual terms give up the value of the prediction. The smoothness parameter was randomly chosen to $\sigma=0.1$.

5.3.4 Dynamic neural networks

DNN is a kind of ANN that can modify its own topology to acceptable and also changeable data. In the other word, learning process in DNNs never finishes. In DNN, the network output belongs to the present input data and present or previous inputs, outputs, or status of the network. Nelles (2001) stated that the dynamic case of network can be communicated by using an external dynamic, internal dynamics and tapped-delay line. External dynamics method applies the historical information of output to demonstrate dynamics and makes autoregressive type neural network. The internal dynamics type takes in a nonlinear condition space model without any information regarding the true process state as expressed by Ishak (2003) and Yasdi (1999). Lingras (2001) showed that tapped-delay line method employs a sequence of delay to state dynamics and create time-delay neural network.

The training process of dynamic neural networks is similar to the training process of static feed-forward networks. However, the dynamic type of neural networks is normally more powerful than static case of neural networks. It is because; the dynamic neural network has memory and can be trained using sequential pattern for the results prediction.

In this research, FFTDNN and RNN as DNNs are applied for prediction of the load-deflection of non-strengthened and CFRP strengthened RC slab.

5.3.4.1 Focused time delay neural network

FFTDNN is a kind of time delay neural network consisted of a feed-forward network with a tapped delay line at the input. In this method the dynamics appear only at the input layer of a static multilayer feed-forward network. A two-layer FFTDNN has shown in Figure 5.8. FTDNN basically consisted of two following components (Abed et al, 2010):

(1)**Memory Structure:** is a time delay line which contains the p most recent inputs generated by the delay element represented by the operator D .

(2)**Non Linear Associate:** is the conventional feed-forward network and uses the memory to predict future occasions.

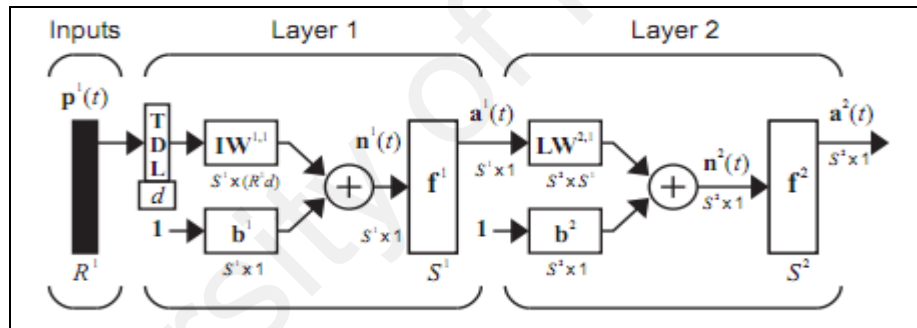


Figure 5.8: A two-layer focused time-delay neural network (Beale et al, 2011)

In the FFTDNN the memory structure is focused on the input layer. It makes particular characteristic of the FFTDNN to be different from the general Time Delay Neural Network (TDNN). A major advantage of the FFTDNN is that it is less complex than the conventional TDNN and has the same temporal patterns processing capability.

The general presentation of the FTDNN architecture is illustrated in Figure 5.9.

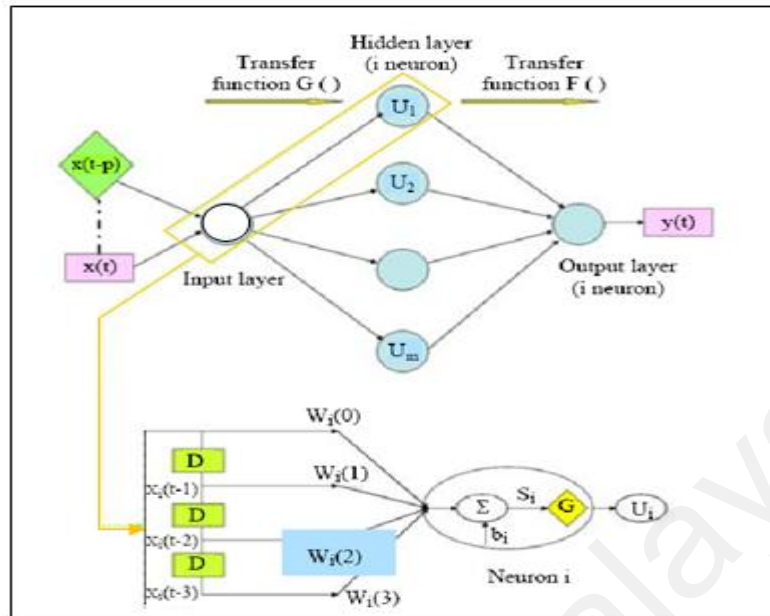


Figure 5.9: General architecture presentation for FFDNN (Abed et al, 2010)

5.3.4.2 Recurrent neural network

Feedback structure is added in the FBNN to memorize incoming data using internal sequential pattern. This incorporation called RNN which has feedback connections between units of different layers or connections of self-loop type. RNN has feed-forward fully connection for all neurons and so, the connections permit the network show the dynamic behavior. RNN mathematically realizes dynamical systems by memorizing the events. Many types of RNN architectures have been applied for modeling data in sequential pattern. Three general type of RNN depend to network architecture are:

- 1) Jordan RNN, which consisted of feedback connections from the output layer to its inputs.
- 2) Locally RNN, which only applies local feedback.
- 3) Globally connected RNN, which has feedback connection from neurons in hidden layer to neurons in input layer.

The basic elements of a RNN are neurons which connected by synaptic links and strengthened by weight. The RNN architecture included of Input, hidden, and output layers. At a given time, each layer or unit has activation vector. The activations vector of input, hidden, and output layer are indicated by $u(n)$, $x(n)$, and $y(n)$ respectively as following equations.

$$u(n) = (u_1(n), \dots, u_K(n))^t \quad (5.14)$$

$$x(n) = (x_1(n), \dots, x_N(n))^t \quad (5.15)$$

$$y(n) = (u_1(n), \dots, y_L(n))^t \quad (5.16)$$

The basic RNN architecture with k input layer, N hidden layer, and L output layer are shown in Figure 5.10.

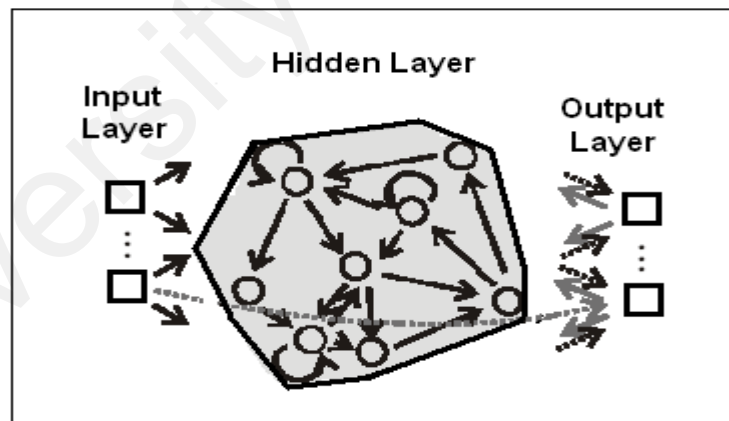


Figure 5.10: The basic RNN architecture

The connection weight for input, hidden and output layer in following equations is defined in $N \times K$, $N \times N$, and $L \times (K+N)$ weight matrices respectively.

$$\left. \begin{aligned} W^{in} &= (w_{ij}^{in}) \\ W^{hi} &= (w_{ij}^{hi}) \\ W^{out} &= (w_{ij}^{out}) \end{aligned} \right\} \quad (5.17)$$

As shown in following formula, the output units may arbitrary go back hidden layer with connections whose weights are collected in $N \times L$ back-projection weight matrix.

$$W^{back} = (w_{ij}^{back}) \quad (5.18)$$

The output units may have connections not only from hidden layer but also from input layer and from output layer. The activation vector of hidden layer is updated according to following equation:

$$x(n+1) = f(W^{in}u(n+1) + Wx(n) + W^{back}y(n)) \quad (5.19)$$

Where:

$u(n+1)$ = the externally given input

f = transfer function,

The output is calculated as following formula:

$$y(n+1) = f^{out}(W^{out}(u(n+1), x(n+1), y(n))) \quad (5.20)$$

Where; $(W^{out}(u(n+1), x(n+1), y(n)))$ is the concatenated vector made from input, internal, and output activation vectors.

In this research, the globally connected RNN or Elman RNN is considered for load-deflection curve prediction of non-strengthened and CFRP strengthened RC slab. In addition, the use of RNN for crack width prediction of CFRP strengthened RC slab is studied. The architecture of the general connection RNN is shown in Figure 5.11.

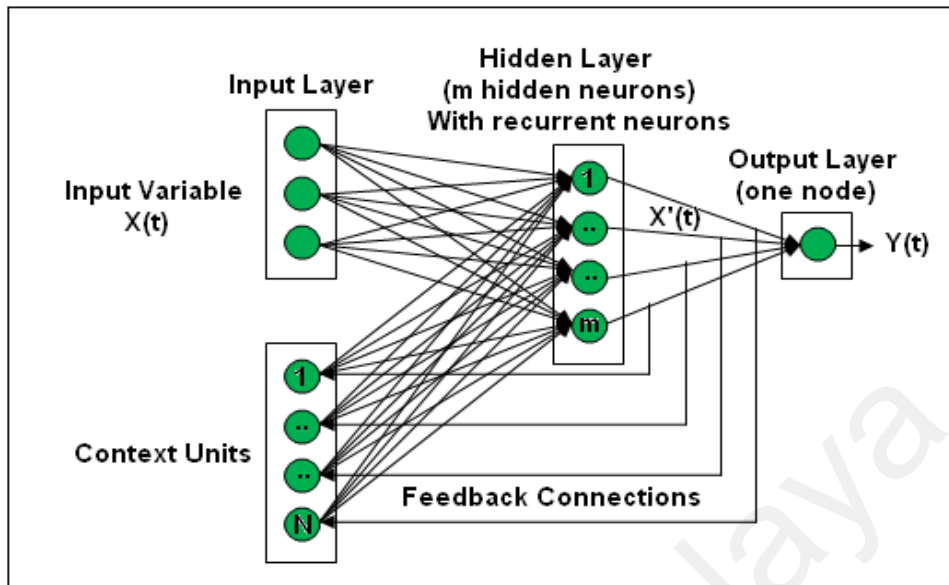


Figure 5.11: Typical RNN architecture (EI-Shafie et al, 2008)

EI-Shafie et al (2008) expressed that the input vector $x(t)$ and $x'(t)$, the output of the hidden layer at time t , the dynamic behavior of the model in Figure 5.11 may be described by the following equations:

$$Y_i(t+1) = A_x^e(t+1) \quad (5.21)$$

$$X^e(t+1) = g[W_m(t) + W_{mo}x(t)] \quad (5.22)$$

Where:

$Y_i(t+1)$ = The RNN output

A = The weight matrix of output layer connected to the hidden layer

$g []$ = The hidden layer hyperbolic tangent function

W_m = The weights of the m hidden nodes connected to the context units

W_{mo} = The weight matrix of the hidden neurons connected to the input nodes.

The main property of the mentioned model on RNN was relied on the interaction of the context unit with the hidden nodes.

5.4 ANN Modelling

The load-deflection analysis of the non-strengthened and CFRP strengthened RC one-way slab can be quantitatively modeled in a number of different methods. The philosophy of modeling using ANN is similar to a number of conventional statistical models in the sense that both are challenging characteristics to find the relationship between inputs and corresponding outputs. ANNs modeling do not need any prior knowledge between input and output data, which is one of the benefits that ANNs have compared with most empirical models.

In this research, four artificial neural networks, namely, Feed-forward Back-propagation FBNN, GRNN, FFTDNN and RNN were developed to predict load-deflection analysis of the non-strengthened and CFRP strengthened RC one-way slab. Development of the reliable ANN model is fundamental for the appropriate prediction of load-deflection analysis of the RC slabs. On the other hand, the appropriate selection of different elements of neural network must be conducted to generate the network with maximum accuracy in prediction of the problem. The number of hidden layers, the number of neurons in each hidden layer, the number of data to create a network, training function, adaption learning function and performance function are impressible parameters to create a network. A trial and error method for selection of these impressible parameters was applied to implement the model. In this research, the process and development details of the network modeling are beyond the scope of the methodology. The processing elements are usually applied between input layer, output layer and hidden layers. In this part, the completion of the process and development detail of the FBNN, GRNN, FFTDNN, and RNN for the load-deflection analysis of the CFRP strengthened RC one-way slab is focused. The processing

elements used for deflection prediction of non-strengthened RC slab are discussed in Chapter 7.

5.4.1 FBNN modeling for CFRP strengthened RC slab

The data gathered from load-deflection experimental work on the CFRP strengthened RC slabs was applied for the generation of FBNN. Many input elements of the FBNN were tried to find the best network based on the maximum agreement between the network output and target output. The properties of the optimum network are presented in Table 5.2.

Table 5.2: Properties of the selected FBNN for CFRP strengthened RC slab

No.	parameters	Property
1	Training Algorithms	Lonberg-Markorat
2	Adaption Learning Function	LEARNGDM
3	Network Transfer Function	LOGSIG-TANSIG- PURELIN
4	Network Architecture	3-15-5-1
5	The totally number of data	103
6	The number of data for network generation	93=75(training)+9(verifying)+9(testing)
7	The number of second testing data	10
8	Network function	Feed Forward Backprop

From 103 load-deflection experimental data, 93 data were used for network generation and 10 data for testing. The training, verifying, and testing data were normalized between 0 and +1 and created in a form of matrix equation. The data for each part of training, verifying, and testing were divided into two parts of input and output matrix data. The following

matrix equations present the input and output matrix data used on the CFRP strengthened RC one-way slab:

i) *Training Data:*

$$\begin{array}{c}
 \text{73 Input Data} \\
 \left[\begin{array}{cccc} \vdots & \vdots & \vdots & \dots & \vdots \\ \vdots & \vdots & \vdots & \dots & \vdots \\ \vdots & \vdots & \vdots & \dots & \vdots \end{array} \right] \begin{array}{l} \leftarrow \text{Loading} \\ \leftarrow \text{CFRPLength} \\ \leftarrow \text{CFRPWidth} \end{array} \\
 T_{r_input} = \\
 \left[\begin{array}{cccc} \vdots & \vdots & \vdots & \dots & \vdots \\ \vdots & \vdots & \vdots & \dots & \vdots \\ \vdots & \vdots & \vdots & \dots & \vdots \end{array} \right] \leftarrow \text{Deflection} \\
 \text{73 Output Data}
 \end{array} \quad (5.23)$$

ii) *Verifying Data*

$$\begin{array}{c}
 \text{10 Input Data} \\
 \left[\begin{array}{cccc} \vdots & \vdots & \vdots & \dots & \vdots \\ \vdots & \vdots & \vdots & \dots & \vdots \\ \vdots & \vdots & \vdots & \dots & \vdots \end{array} \right] \begin{array}{l} \leftarrow \text{Loading} \\ \leftarrow \text{CFRPLength} \\ \leftarrow \text{CFRPWidth} \end{array} \\
 V_{r_input} = \\
 \left[\begin{array}{cccc} \vdots & \vdots & \vdots & \dots & \vdots \\ \vdots & \vdots & \vdots & \dots & \vdots \\ \vdots & \vdots & \vdots & \dots & \vdots \end{array} \right] \leftarrow \text{Deflection} \\
 \text{10 Output Data}
 \end{array} \quad (5.24)$$

iii) *Testing Data*

$$\begin{array}{c}
 \text{10 Input Data} \\
 \left[\begin{array}{cccc} \vdots & \vdots & \vdots & \dots & \vdots \\ \vdots & \vdots & \vdots & \dots & \vdots \\ \vdots & \vdots & \vdots & \dots & \vdots \end{array} \right] \begin{array}{l} \leftarrow \text{Loading} \\ \leftarrow \text{CFRPLength} \\ \leftarrow \text{CFRPWidth} \end{array} \\
 T_{s_input} = \\
 \left[\begin{array}{cccc} \vdots & \vdots & \vdots & \dots & \vdots \\ \vdots & \vdots & \vdots & \dots & \vdots \\ \vdots & \vdots & \vdots & \dots & \vdots \end{array} \right] \leftarrow \text{Deflection} \\
 \text{10 Output Data}
 \end{array} \quad (5.25)$$

The network architecture for the selected network is shown in Figure 5.12. Loading, CFRP length and width were input data and deflection was output data. Fifteen and five neurons were provided for the first and second layer of the hidden layers respectively.

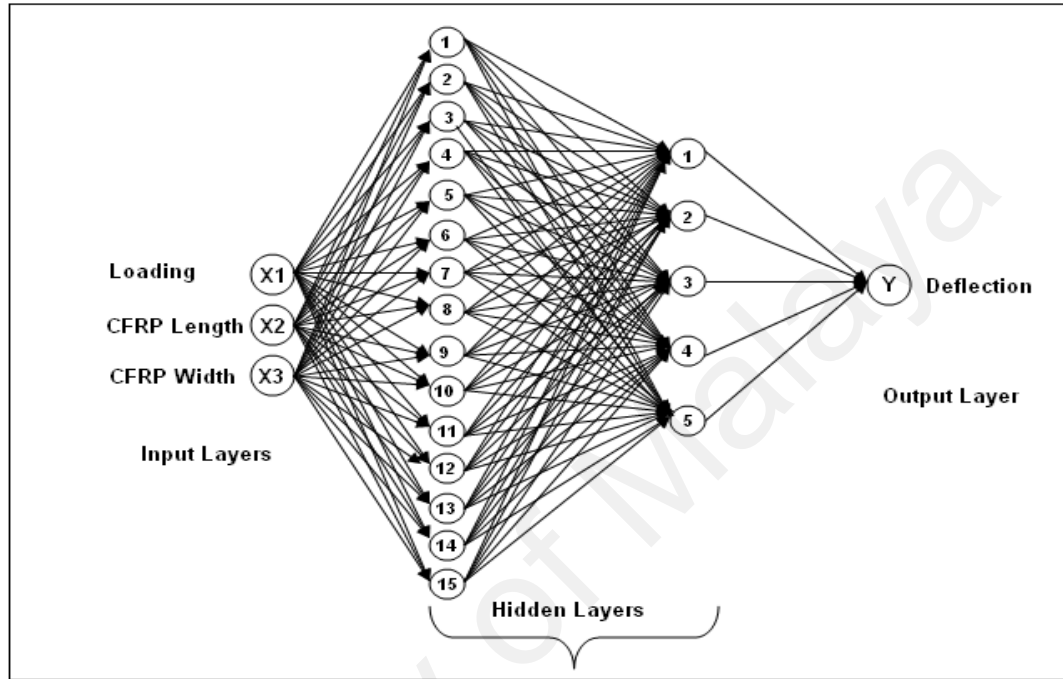


Figure 5.12: The FBNN architecture for the CFRP strengthened RC one-way slab

The loading, CFRP length and width as input layers (X_1 , X_2 , and X_3) are multiplied by an adjustable connection weight ($W(X_i)_j$) and then the weighted input signals are summed and a bias (b) is added.

$$I_j = \sum_{i=1}^R X_i W(X_i)_j + b \quad (5.26)$$

This combined input (I_j) is then passed through the following Logsig and Tansig transfer function in first and second hidden layer, respectively, to produce the output of the hidden layer.

LOGSIG in first hidden layer:

$$f(x) = \frac{1}{1 + e^{-a(\sum_{i,j=1}^R W_{(x_i)j} X_i)}} \quad (5.27)$$

TANSIG in second hidden layer:

$$g(x) = \frac{1 - e^{-a(\sum_{i,j=1}^R W_{(x_i)j} X_i)}}{1 + e^{-a(\sum_{i,j=1}^R W_{(x_i)j} X_i)}} \quad (5.28)$$

Then, each hidden layer sums all the weighted signals from input and applies the PURLIN to calculate the output signals on output layer. The output layer calculates the error by comparing the target patterns and the response of the training pattern in case of supervised training. The back-propagation algorithm revises the weights in each input-output set by propagation the error back to the network using a widely used learning mechanism to change the weights and biases. The effect of back-propagation algorithm starts at the input layer where the input data are presented. The network adjusts its weights on the 73 training data and uses the LEARNNGDM as learning rule to find a set of weights that will produce the input/output mapping with maximum accuracy in training. The performance of the generated network has to be validated using testing data.

5.4.2 GRNN modeling for for CFRP strengthened RC slab

Totally 104 load-deflection data gathered from 7 samples applied for network generation. 93 data were utilized for training and 10 data of strengthened RC slab S812-1100 used for testing. The GRNN architecture for predicting load-deflection analysis of

CFRP strengthened RC one-way slab was involved of four following layers as well as shown in Figure 5.13:

- i) Input layer: Contains three neurons for the loading, CFRP length, and CFRP width
- ii) Pattern neurons: Includes three neurons for each training case
- iii) Summation neurons: Includes one neuron equal to neuron in output layer
- iv) Output neurons: Contains one neuron for the deflection

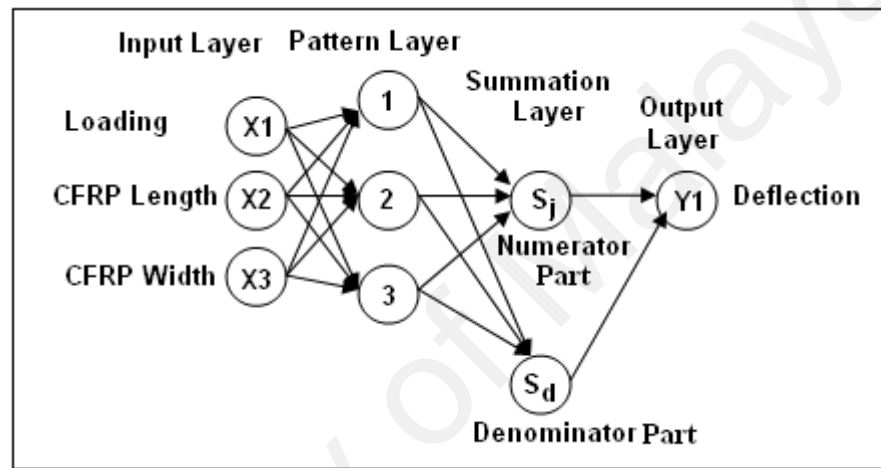


Figure 5.13: The GRNN architecture for the CFRP strengthened RC one-way slab

The input layer of processing units is responsible for reception of information from load-deflection experimental work. For each input variable, a unique input neuron is defined in the model. No processing of data for loading, CFRP length and width is conducted at the input neurons. Then, the input neurons present the data to the pattern neurons. The data from input layer are combined in the pattern layer and then the outputs are computed using transfer function. The amount of the smoothing parameter plays important role in the computed output from pattern layer. The smoothing parameter determines how closely the function implemented by the GRNN and fits the training data. A trial and error method was followed to find the optimum smoothing parameter.

After that, the outputs from patten layer are forwarded to the summation layer. The summation layer includes of numerator and denominator neurons which compute the weighted and simple arithmetic sum respectively. The denominator, S_d , and numerator, S_j , are defined by following equations:

$$S_d = \sum_i \theta_i \quad (5.29)$$

$$S_j = \sum_i w_i \theta_i \quad (5.30)$$

The calculated summation neurons are subsequently sent to the output neuron. Finally, the output neuron carries out the following division to calculate the slab deflection.

$$Y_1 = S_j / S_d \quad (5.31)$$

5.4.3 FFTDNN modeling for CFRP strengthened RC slab

The data is loaded and normalized in MATLAB software. The properties of selected network during generation are shown in Table 5.3.

Table 5.3: Chosen FFTDNN properties for CFRP strengthened RC slab

The Number of Data	103
Input Layer	Loading, CFRP Length and Width
The number of Neurons in Hidden Layer	13-5-1
Output Layer	Slab Deflection
Net Architecture	(3-13-5-1-1)
Network Type	Feed-Forward
Net Algorithm	Back-Propagation
Training Function	Trainlm
Learning Function	LEARNGDM
Output Transfer Function	PURELIN
Hidden Transfer Function	Tansig-Logsig-Purelin
Performance Function	MSE

FFTDNN consisted of a static feed-forward network with a tapped delay line at the input layer. The process and development details of the FFTDNN modeling is similar to FBNN modeling with a tapped delay line that involves the most recent inputs. In this method, the tapped delay line appears only at the input without any back-propagation to compute the network gradient. The FFTDNN architecture for the CFRP strengthened RC one-way slab is shown in Figure 5.14.

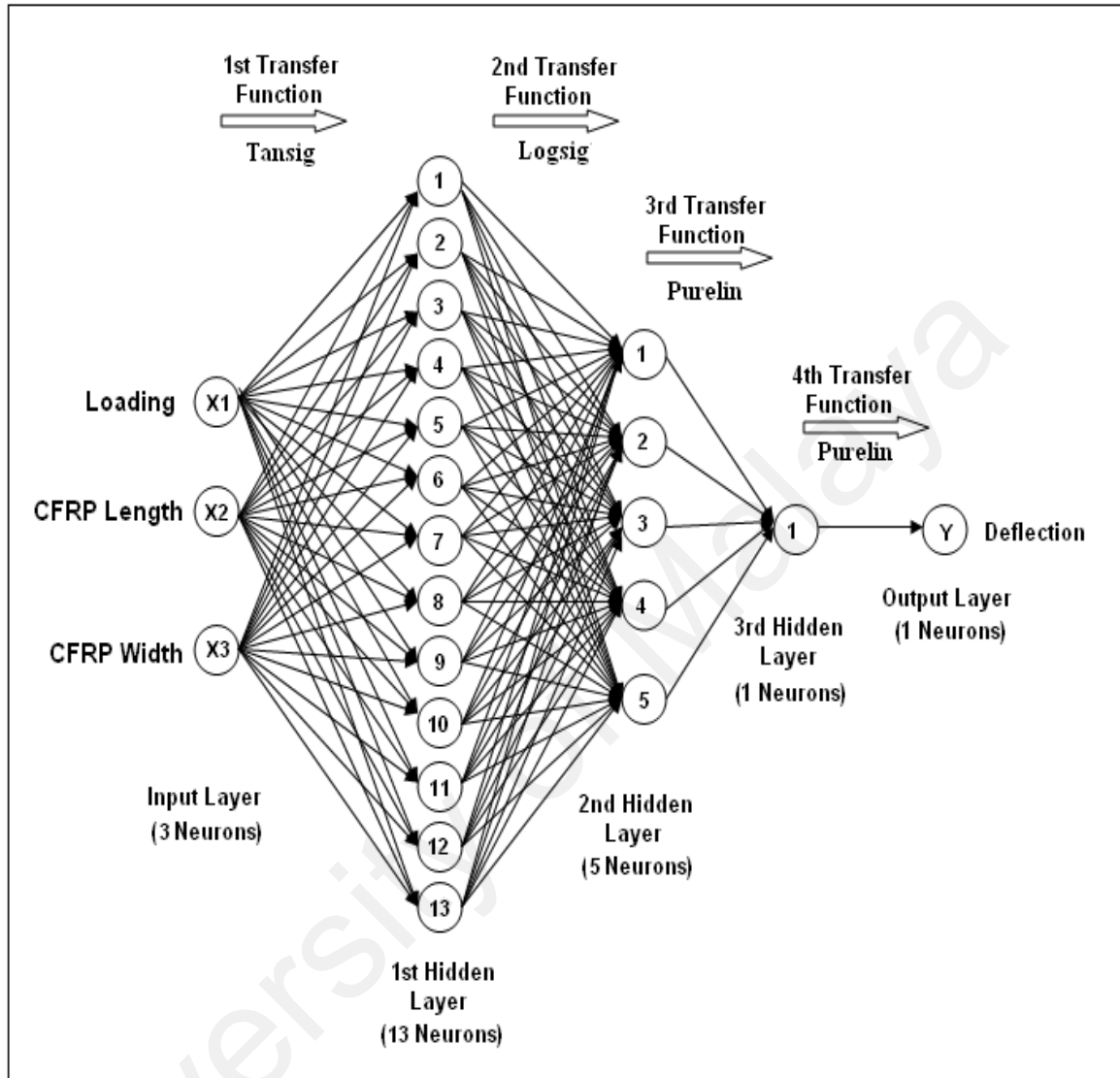


Figure 5.14: The FFTDNN architecture for the CFRP strengthened RC one-way slab

The first, second, and third transfer function in hidden layer were TANSIG, LOGSIG, and PURELIN respectively. The transfer function as activation function for the output layer was PURELIN.

5.4.4 RNN Modeling for CFRP Strengthened RC Slab

The architecture of selected RNN is consisted of one hidden layer with 11 neurons as well as shown in Figure 5.15. The transfer function in hidden layer and output were TANSIG and PURELIN respectively.

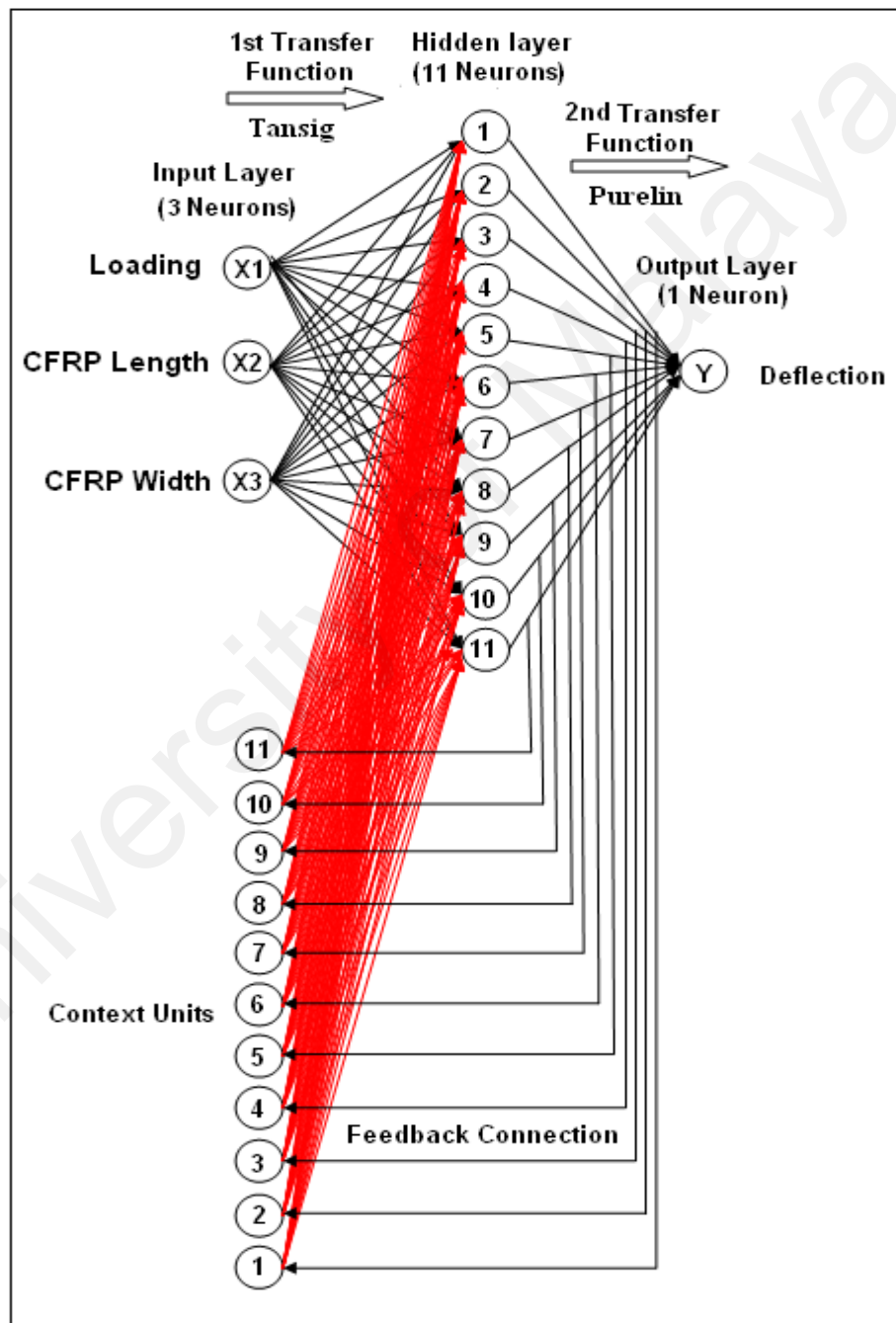


Figure 5.15: The RNN architecture for the CFRP strengthened RC one-way slab

The loading, CFRP length and width as three input layers (X_1 , X_2 , and X_3) are multiplied by an (11×3) weight matrices. The results of combined input are then passed through the TANSIG transfer function in the hidden layer to produce the output of the hidden layer using PURELIN activation function. In the RNN, the neurons in hidden layer have feedback connection to neurons in input layer by context unit. The number of neurons in context unite is equal to neurons in hidden layer. The neurons in hidden layer feedback and then the activation vector of hidden layer is updated using following equation:

$$H(t+1) = \frac{1}{1 + e^{-a(W^{in}X(t+1) + W^{hi}H(t) + W^{back}Y(t))}} \quad (5.32)$$

Where:

$H(t+1)$, is the updated hidden layer

W^{in} , is the input weight matrices

$X(t+a)$, is the input layer

W^{hi} , is the hidden layer weight matrix

W^{back} , is the output feedback connection of 11×1 weight matrix

The updated neurons in hidden layer make again the output layer using PURELIN activation function and then feedback to context unit to update the activation vector of hidden layer. The cycle between hidden layer and input layer is repeated to maximize the accuracy in network training.

CHAPTER 6

6. EXPERIMENTAL WORK

This part firstly explains the properties of material used in this study and the experimental program adopted with a view to gathering data for network generation. Then, the experimental results of the non-strengthened and CFRP strengthened one-way RC slab are presented. These results were applied to generate FBNN, GRNN, FFTDNN, and RNN. These NNs will be discussed in detail in Chapter 7.

6.1 Material and Experimental Program

The experimental work is divided into two parts. The first part deals with load-deflection analysis of 19 non-strengthened RC one-way slabs, while the second part discussed on structural behavior of the CFRP strengthened RC one-way slab. The characteristics of samples for the non-strengthened RC one-way slab and CFRP strengthened RC one-way slab are shown in Tables 6.1 and 6.2 respectively.

Table 6.1: The characteristics of the non-strengthened RC one-way slab under mid-span punching load

No.	Slab	Slab Thickness (mm)	Slab Steel Bar	Slab Span Length (mm)
1	120-3T10-2400	120	3T10	2400
2	100-3T10-2400	100	3T10	2400
3	120-4T10-1800	120	4T10	1800
4	120-3T10-1800	120	3T10	1800
5	120-2T10-1800	120	2T10	1800
6	100-4T10-1800	100	4T10	1800
7	100-3T10-1800	100	3T10	1800
8	100-2T10-1800	100	2T10	1800
9	55-2T10-1350	55	2T10	1350
10	55-3T10-1350	55	3T10	1350
11	55-4T10-1350	55	4T10	1350
12	70-2T10-1350	70	2T10	1350
13	70-3T10-1350	70	3T10	1350
14	90-2T10-1350	90	2T10	1350
15	90-3T10-1350	90	3T10	1350
16	55-2T10-860	55	2T10	860
17	55-3T10-860	55	3T10	860
18	70-2T10-860	70	2T10	860
19	70-3T10-860	70	3T10	860

Table 6.2: The characteristics of samples for the CFRP strengthened RC one-way slab under four point load

No.	Slab	CFRP Width (mm)	CFRP Length (mm)
1	S512-700	50	700
2	S512-1100	50	1100
3	S512-1500	50	1500
4	S812-700	80	700
5	S812-1100	80	1100
6	S812-1500	80	1500
7	WCFRP*	-	-

*Without CFRP

The dimension of the CFRP strengthened RC one-way slab was 1800×400×120 mm (1800 mm length, 400 mm width, and 120 mm thickness) with similar steel bar of 2T10. The concrete cover was 25 mm.

6.1.1 Material used in the study

6.1.1.1 Cement

Ordinary Portland Cement (OPC) derived from one source, with a relative density and a specific surface of 3.1 and 335 m².kg⁻¹, respectively, and was used for all mixed respectively. The chemical composition of OPC is presented in Table 6.3.

Table 6.3: The chemical composition of Ordinary Portland Cement (MS, 1989)

Oxide Composition	CaO	SiO ₂	Al ₂ O ₃	Fe ₂ O ₃	MgO	SO ₃	K ₂ O	Na ₂ O	LOI
%	63.4	19.8	5.1	3.1	2.5	2.4	1	0.19	1.8

6.1.1.2 Water

Portable water, free from chemical contaminants was used both mixing and curing. It satisfies the requirements of BS 8110 (BS, 1997).

6.1.1.3 Fine aggregate

The fine aggregate used in this research was the mining sand sieved to a particle size range between 0.15 and 2.36 mm. The specific gravity of fine aggregate was 2.61 in saturated surface dry (SSD) condition. The sieve analysis of sand is shown in Figure 6.1.

6.1.1.4 Coarse aggregate

The coarse aggregate used in this study was crushed granite with maximum size of 19 mm. The particle size distribution of the coarse aggregate used in this research is shown in Figure 6.1. The specific gravity of coarse aggregate was 2.65.

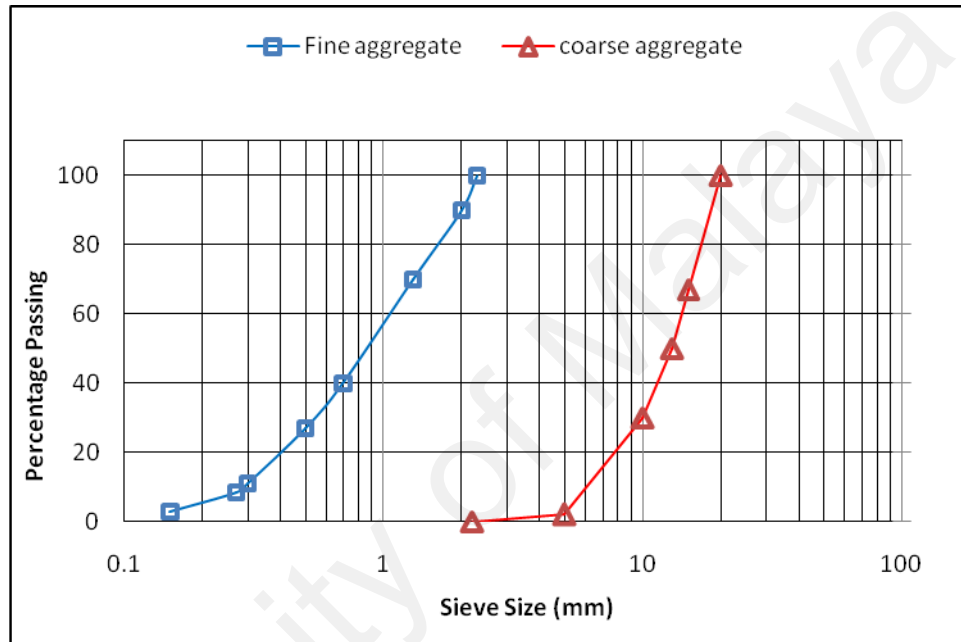


Figure 6.1: Particle size distribution of the fine and coarse aggregates

6.1.1.5 Formwork

The formwork used build on site out of plywood as well as shown in Figure 6.2. The formwork interior dimension was 400 and 120 mm in width and thickness respectively. The formwork interior length was 2400, 1800, 1350, and 860 mm. All the formworks were brushed with oil from inside to make easy their removal after the concrete casting and curing.



Figure 6.2: The formwork used for casting in the experimental work

6.1.1.6 Reinforcing bar

The longitudinal reinforcement for the non-strengthened and CFRP strengthened RC one-way slab consisted of high tensile hot rolled deformed bar of 10 mm diameter. The yield strength and module of elasticity of the steel bar used in this study were 610 and 215000 N/mm² respectively. The longitudinal reinforcement used for the non-strengthened and CFRP strengthened RC one-way slab is shown in Figure 6.3.



Figure 6.3: The longitudinal reinforcement used for the non-strengthened and CFRP strengthened RC one-way slab

6.1.1.7 Carbon fiber reinforced polymer

CFRP is made of carbon atoms and involved by very thin fiber about 0.005-0.010 mm in diameter. CFRP has a high strength to weight ratio, favorable fatigue behavior and excellent resistance to electrochemical corrosion, which make it practically suited for concrete structural application (Clarke, 1996). It was used for applications where high mechanical properties and low weight are the important requirements. The pultruded carbon fiber reinforced polymer (CFRP) laminates used in this research was from Sika company designed for strengthening concrete structures. The mechanical properties of the CFRP laminate are given in Table 6.4.

Table 6.4: Mechanical properties of the CFRP laminate

Laminate Type	Elastic modulus [GPa]	Tensile strength [MPa]	Failure strain [%]
Sika CarboDur Plates	165	3100	1.7

6.1.1.8 Adhesive

The adhesive used for CFRP installing on the RC slab was Sikadur-30. It consisted of epoxy resins and special filler, designed for use at normal temperatures between +8°C and +35°C. The mechanical properties of the adhesive Sikadur-30 used in this research are given in Table 6.5.

Table 6.5: Mechanical properties of the adhesive Sikadur-30

Adhesive type	Service temperature	Elastic modulus [GPa]	Tensile strength[MPa] (7 days curing)	
			Curing at +15°C	Curing at +35°C
Sikadur-30	-40°C to +45°C (when cured at >+23°C)	11.2 (at +23°C)	24-27	26 - 31

6.1.2 Concrete mix design and mixing of material

Concrete mix design is the method for determining the proportions of the concrete ingredients, to achieve the desired properties in the most economical way. The mix design used in the investigation was DOE method published by the British Department of the Environment (Teychenne et al, 1988). The determined concrete ingredients mixed together and then the concrete specimens casted and placed in the required curing conditions. The concrete slump measured on the fresh concrete as well as the compressive strength, tensile strength, and modulus of elasticity determined in hardened concrete. Table 6.6 shows the test performed on the hardened concrete for non-strengthened and CFRP strengthened RC slab. The results of slump, compressive strength, tensile strength, and modulus of elasticity for the 19 non-strengthened RC one-way slabs and 7 CFRP strengthened RC one-way slabs are given in Tables 6.7 and 6.8 respectively.

Table 6.6: The test performed on hardened concrete for non-strengthened and CFRP strengthened RC slab

No.	Test and references	Specimens and size	Age of testing (day)
1	Compressive strength BS EN 12390-3:2002	Cubes of 100 mm	7 and 28
2	Splitting tensile strength BS EN 1390-6:2000	Cylinder of 150 mm diameter × 300 mm height	28
3	Modules of elasticity BS EN 1881-121:1983	Cylinder of 150 mm diameter × 300 mm height	28

Table 6.7: The fresh and hardened concrete test output for the non-strengthened slab

No.	Slab	Slump (mm)	Compressive Strength (MPa)	Tensile Strength (MPa)	Modulus of Elasticity (MPa)
1	120-3T10-2400	46	35	5.7	31214
2	100-3T10-2400	46	35	5.7	31214
3	120-4T10-1800	45	41	6.8	27104
4	120-3T10-1800	45	41	6.8	27104
5	120-2T10-1800	45	41	6.8	27104
6	100-4T10-1800	40	54	5.8	23514
7	100-3T10-1800	40	54	5.8	23514
8	100-2T10-1800	40	54	5.8	23514
9	55-2T10-1350	41	50	6	25101
10	55-3T10-1350	41	50	6.3	25101
11	55-4T10-1350	41	50	6.3	25101
12	70-2T10-1350	42	45	6.6	28112
13	70-3T10-1350	42	45	6.6	28112
14	90-2T10-1350	42	43	7	25258
15	90-3T10-1350	42	43	7	25258
16	55-2T10-860	48	45	6.1	23889
17	55-3T10-860	48	45	6.1	23889
18	70-2T10-860	48	45	6.1	23889
19	70-3T10-860	48	45	6.1	23889
Mean			45	6.4	26313

Table 6.8: The fresh and hardened concrete test output for the CFRP strengthened slab

No.	Slab Market	Slump (mm)	Compressive Strength (MPa)	Tensile Strength (MPa)	Modulus of Elasticity (MPa)
1	S512-700	40	46	6.8	25842
2	S512-1100	41	47	5.5	28101
3	S512-1500	44	42	6.3	25963
4	S812-700	46	41	5.9	26028
5	S812-1100	44	47	5.7	24567
6	S812-1500	40	49	6.8	26789
7	WCFRP	42	46	6.4	23879
Mean			45	6.2	25880

6.1.3 Preparation of Reinforced Concrete Slabs

The precaution of clear cover and interior dimension of formwork was provided using 25 mm mortar block and checking with measuring tape, respectively, before the casting of the concrete. After casting of the concrete, the slabs were kept in the formwork for 3 days. After that, the slabs were cured by wet gunny for 7 days and then kept in the uncontrolled condition of concrete laboratory until the day of testing (Figure 6.4).



Figure 6.4: The casting and curing of the slabs

6.1.3.1 Instrumentation

The following equipment and instrumentations were provided and used in the testing program:

i) Linear variable differential transducers (LVDT)

The LVDT that could measure a maximum deflection of 50 mm was used to measure the deflection in the middle of the slab. The LVDT was connected to a data logger to record the mid-span deflection at the load increments.

ii) Data Logger

The mid-span deflection was recorded using a TS-TDS-302 data logger, manufactured by Tokyo Sokki Kenkyujo Co. Ltd, Japan.

iii) Hand Held Microscope

The flexural cracks at the level of the main steel bar were measured using a handy microscope. The microscope used for crack measuring had a magnification of 40 times with an accuracy of 0.02 mm.

6.1.3.2 Instrument setup for non-strengthened RC one-way slab

In this part, the sample size was nineteen with different length, thickness, and steel bar which were tested and mid-span deflection calculated and classified to use in network generation. All the slabs were simply supported and were loaded under mid-span point punching load. The loading and instrument setup are shown in Figure 6.5.

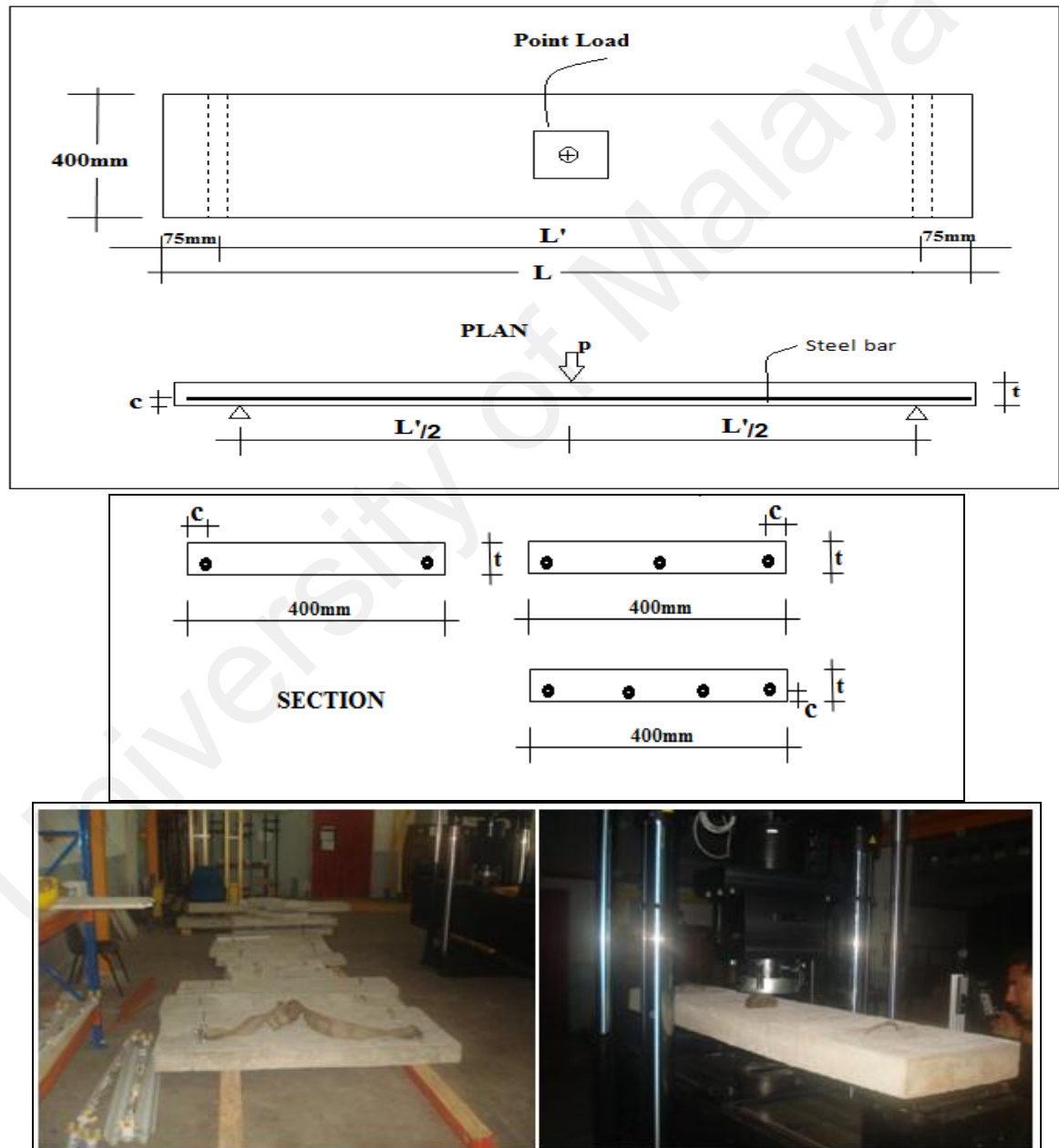


Figure 6.5: Instrument setup for non-strengthened one-way RC slab under mid-span punching load

6.1.3.3 Instrument Setup for CFRP Strengthened RC One-way Slab

In this part of the experimental work, six reinforced concrete slabs having dimension $1800 \times 400 \times 120$ mm with similar steel bar of 2T10 and strengthened using different length and width of CFRP were tested and compared with similar samples without CFRP. All the slabs were simply supported and were loaded under four point bending load with line load. The loading and instrument setup are shown in Figures 6.6.

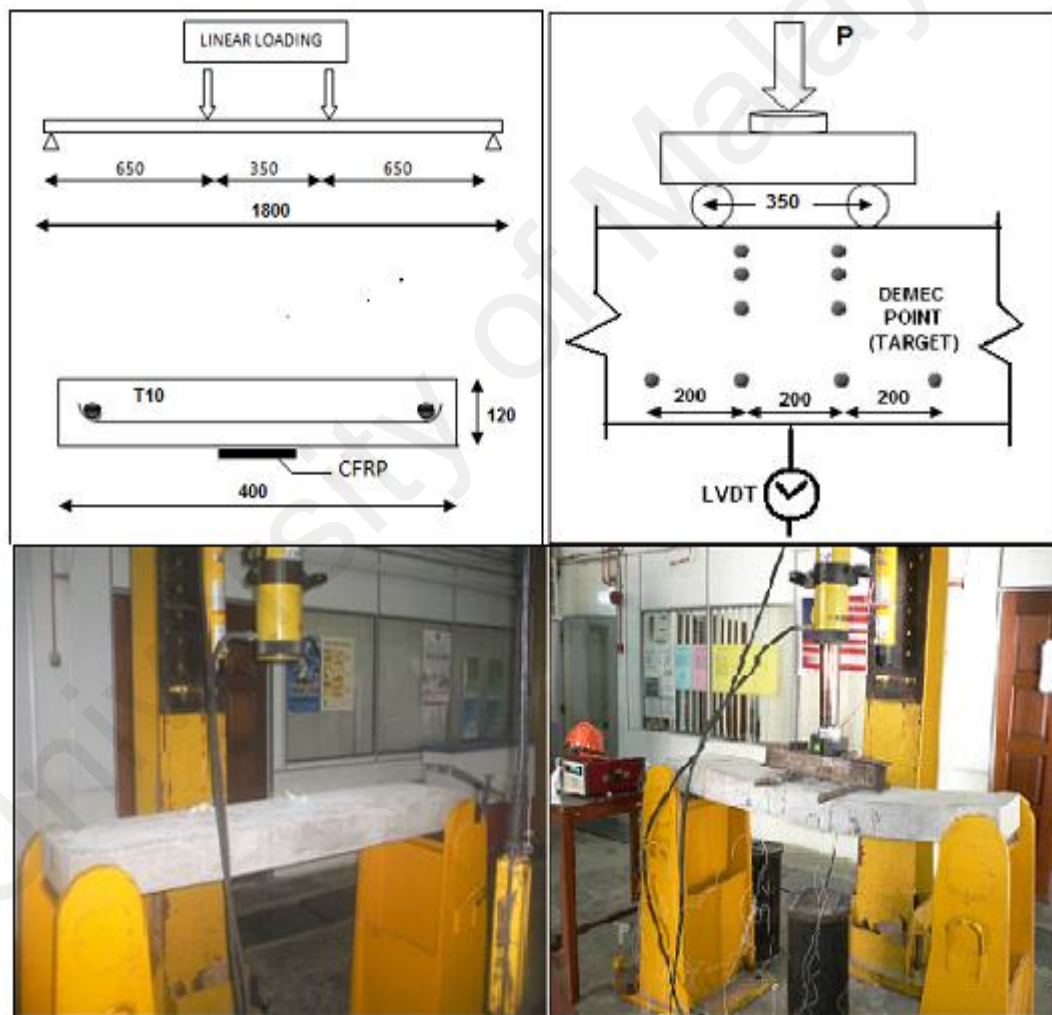


Figure 6.6: Instrument setup for CFRP strengthened one-way RC slabs under linear load

6.2 Experimental Work

6.2.1 Non-strengthened RC one-way slab

6.2.1.1 Design and ultimate moment

All the slabs were designed as under-reinforced section based on rectangular stress block of BS-8110 (BS, 1997). In the failure mode of the slabs, the yielding of the steel took place before the failure of concrete in the compression zone. The comparison of experimental and predicted ultimate moment by BS code and FEA is shown in Table 6.9.

Table 6.9: Experimental and predicted moment of the non-strengthened RC slabs in flexure

Slab	Exp. Ultimate Load (kN)	Exp. Ultimate Moment (M_u) (kNm)	Predicted Ultimate Moment (kNm)		M_u/M_{BS}	M_u/M_{FEA}	Curvature (10^{-2})
			M_{BS}	M_{FEA}			
120-3T10-2400	20	11.25	12.07	10.25	0.932	1.097	0.408
100-3T10-2400	14.5	8.16	9.20	7.75	0.887	1.052	0.487
120-4T10-1800	33	13.61	15.71	12.40	0.867	1.098	0.392
120-3T10-1800	25	10.31	12.07	9.90	0.855	1.042	0.394
120-2T10-1800	20	8.25	8.24	7.84	1.002	1.052	0.397
100-4T10-1800	24	9.90	11.88	9.49	0.834	1.044	0.470
100-3T10-1800	19	7.84	9.20	7.63	0.852	1.027	0.473
100-2T10-1800	16.5	6.81	6.32	6.38	1.077	1.067	0.476
55-2T10-1350	6.5	1.95	2.01	2.02	0.970	0.968	0.874
55-3T10-1350	10	3.00	2.73	2.64	1.099	1.136	0.872
55-4T10-1350	13	3.90	3.26	3.54	1.197	1.102	0.870
70-2T10-1350	12	3.60	3.45	4.11	1.044	0.876	0.682
70-3T10-1350	17	5.10	4.89	4.80	1.044	1.063	0.678
90-2T10-1350	18	5.40	5.36	5.10	1.007	1.059	0.529
90-3T10-1350	23	6.90	7.76	6.47	0.889	1.066	0.526
55-2T10-860	12	2.10	2.01	1.93	1.044	1.091	0.874
55-3T10-860	14	2.45	2.73	2.41	0.897	1.015	0.872
70-2T10-860	21	3.68	3.45	3.20	1.066	1.147	0.682
70-3T10-860	25	4.38	4.89	4.20	0.896	1.042	0.678

The ratio between the experimental ultimate moment and the values predicted by BS code (M_u/M_{BS}) and finite element analysis (M_u/M_{FEA}) varied in the range of 0.834 to 1.197 and 0.876 to 1.147 respectively. The prediction by BS code and finite element analysis showed agreement results to experimental results.

After testing, all of the load-deflection experimental output data are evaluated and compared with the results of finite element method. The results of the ultimate load for the slab 100-3T10-2400 and 70-3T10-1350 obtained from finite element analysis shows in Figures 6.7 and 6.8 respectively.

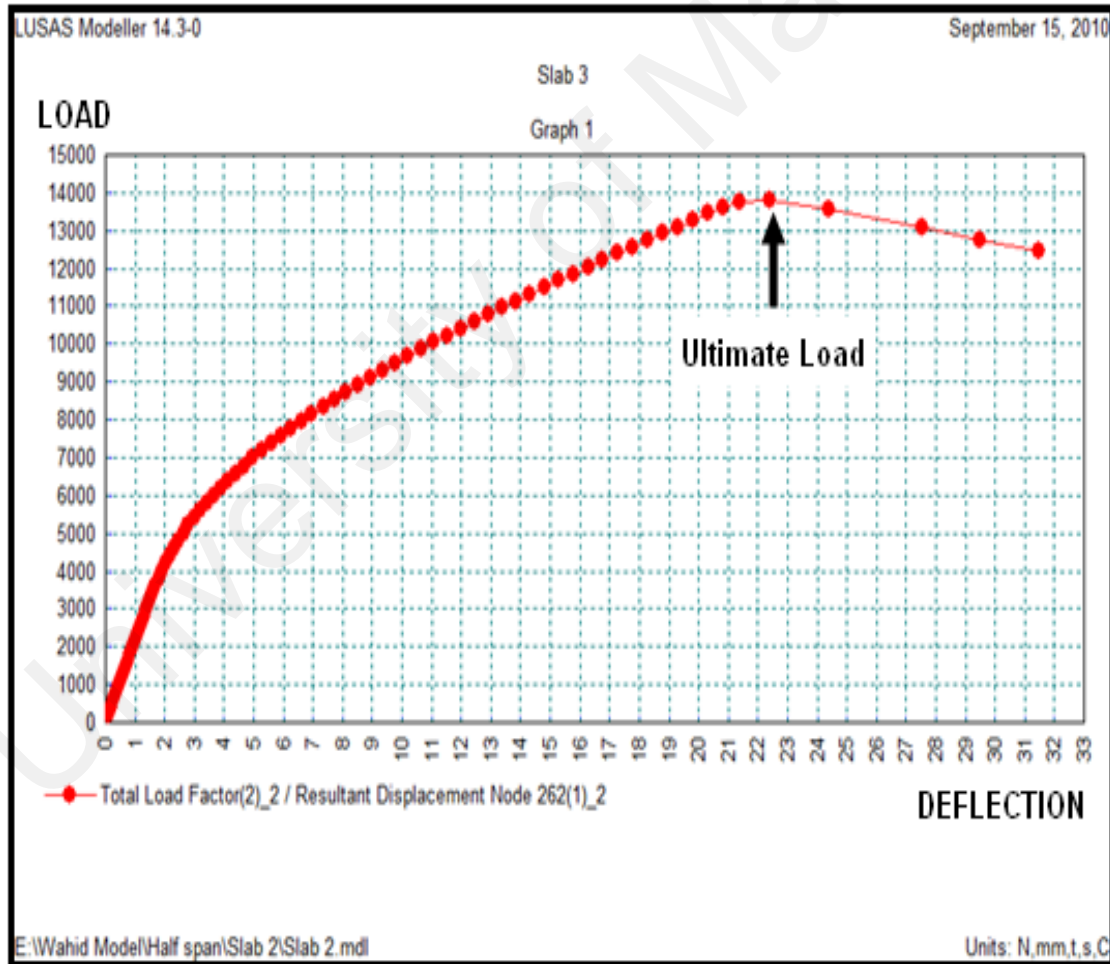


Figure 6.7: Plot of numerical analysis for the slab 100-3T10-2400

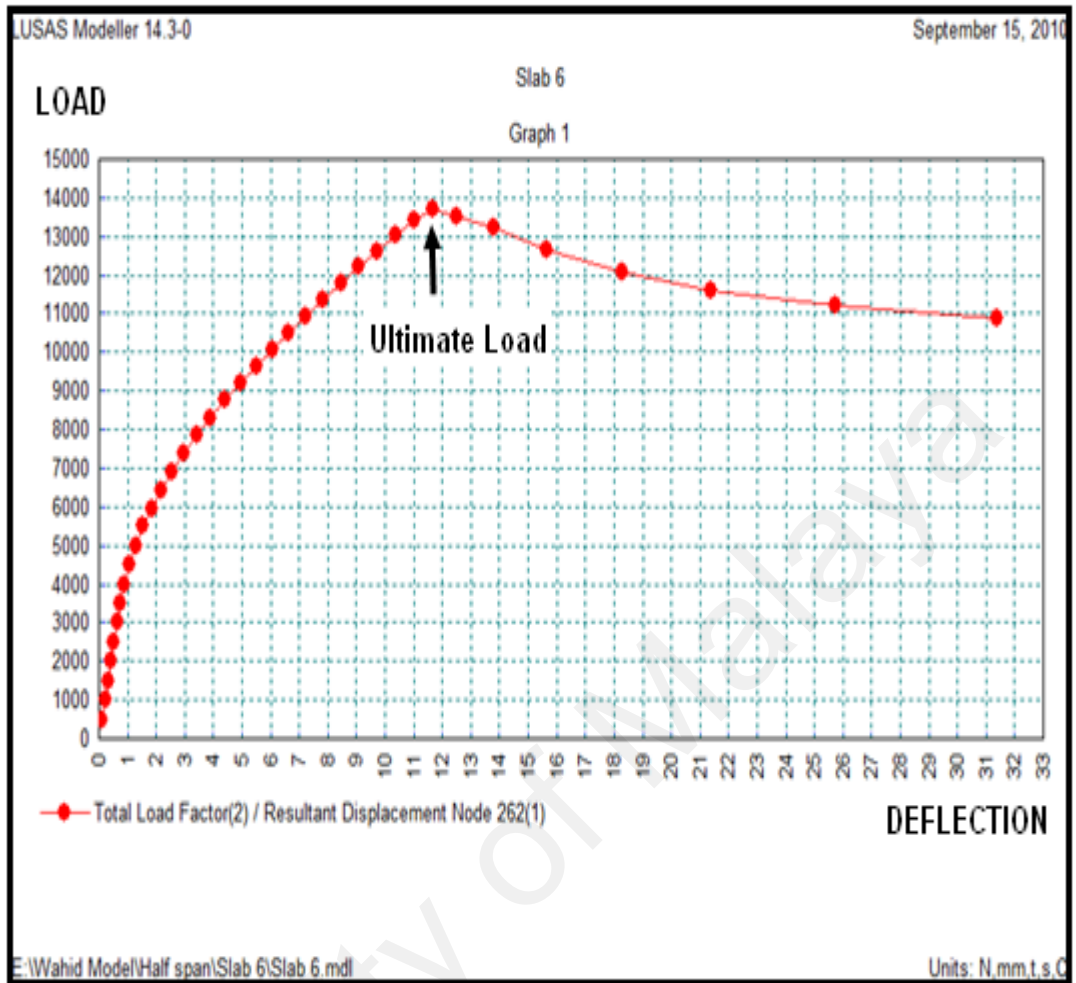


Figure 6.8: Plot of numerical analysis for the slab 70-3T10-1350

6.2.1.2 Load-deflection analysis

The experimental load-deflection analysis at the first crack and ultimate load shows in Table 6.10. The ratio between the experimental deflection at first crack and the values predicted by BS code and finite element analysis varied in the range of 0.74 to 2.03 and 0.75 to 1.92 respectively. Also, the load-deflection curve of the 19 slabs is shown in Figures 6.9 to 6.16. The experimental mid-span deflections were in acceptable agreement with the results of finite element method and BS code (1997).

Table 6.10: Experimental deflection at the first crack load and ultimate load for the non-strengthened RC slabs

Slab	Exp. First Crack Load (kN)	Def. at First Crack (mm)			Span / Def	Def. Ratio at First Crack		Ultimate Load (kN)		
		Exp	BS	FEA		Exp / BS	Exp / FEA	Exp	BS	FEA
120-3T10-2400	6.2	1.56	2.10	2.08	1442	0.74	0.75	20	21.5	18.2
100-3T10-2400	5.7	3.06	2.50	2.45	735	1.22	1.25	14.5	16.3	13.8
120-4T10-1800	8.60	1.46	1.06	1.11	1130	1.38	1.32	33	38.1	30.1
120-3T10-1800	8.5	1.36	1.06	1.11	1213	1.28	1.23	25	29.3	24.0
120-2T10-1800	8.5	2.17	1.07	1.13	760	2.03	1.92	20	20.0	19.0
100-4T10-1800	5.5	1.22	1.26	1.29	1352	0.97	0.95	24	28.8	23.0
100-3T10-1800	5.5	1.98	1.27	1.32	833	1.56	1.50	19	22.3	18.5
100-2T10-1800	5.1	1.7	1.28	1.34	971	1.33	1.27	16.5	15.3	15.5
55-2T10-1350	2.2	1.67	1.25	1.33	719	1.34	1.26	6.5	6.7	6.7
55-3T10-1350	1.8	1.6	1.24	1.31	750	1.29	1.22	10	9.1	8.8
55-4T10-1350	2.5	1.55	1.23	1.3	774	1.26	1.19	13	10.9	11.8
70-2T10-1350	3.8	1.37	0.97	1.11	876	1.41	1.23	12	11.5	13.7
70-3T10-1350	4	1.1	0.96	1.06	1091	1.15	1.04	17	16.3	16.0
90-2T10-1350	5.9	1.31	0.75	0.85	916	1.75	1.54	18	17.9	17.0
90-3T10-1350	6.2	1.52	0.75	0.82	789	2.03	1.85	23	25.9	21.6
55-2T10-860	4.1	0.65	0.42	0.49	1077	1.55	1.33	12	11.5	11.0
55-3T10-860	4.1	0.62	0.42	0.46	1129	1.48	1.35	14	15.6	13.8
70-2T10-860	6.5	0.39	0.33	0.38	1795	1.18	1.03	21	19.7	18.3
70-3T10-860	6.9	0.34	0.33	0.35	2059	1.03	0.97	25	27.9	24.0

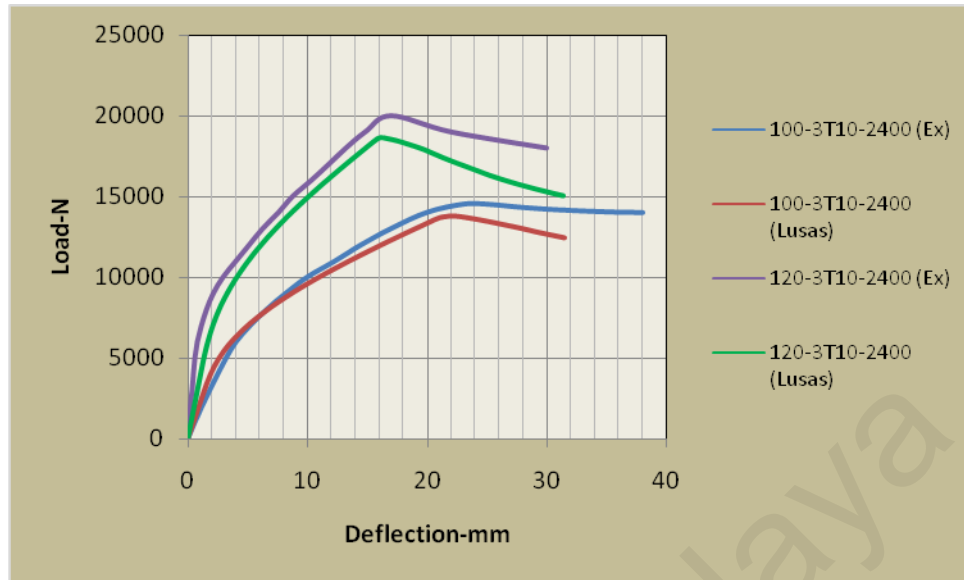


Figure 6.9: The experimental results of load-deflection curve for the samples 100-3T10-2400 and 120-3T10-2400 in compare with LUSAS results

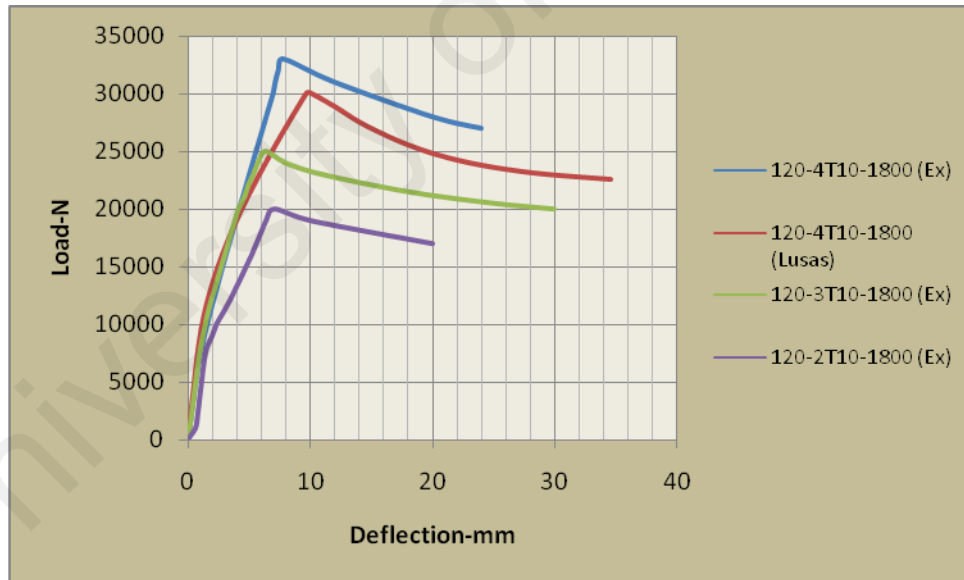


Figure 6.10: The experimental results of load-deflection curve for the samples 120-4T10-1800, 120-3T10-1800 and 120-2T10-1800 in compare with LUSAS results

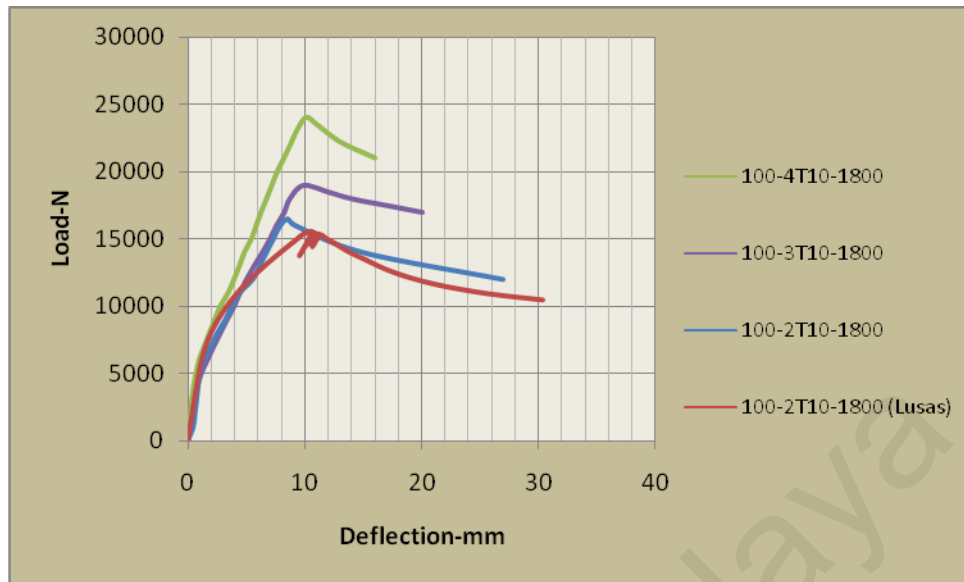


Figure 6.11: The experimental results of load-deflection curve for the samples 100-4T10-1800, 100-3T10-1800 and 100-2T10-1800 in compare with LUSAS results

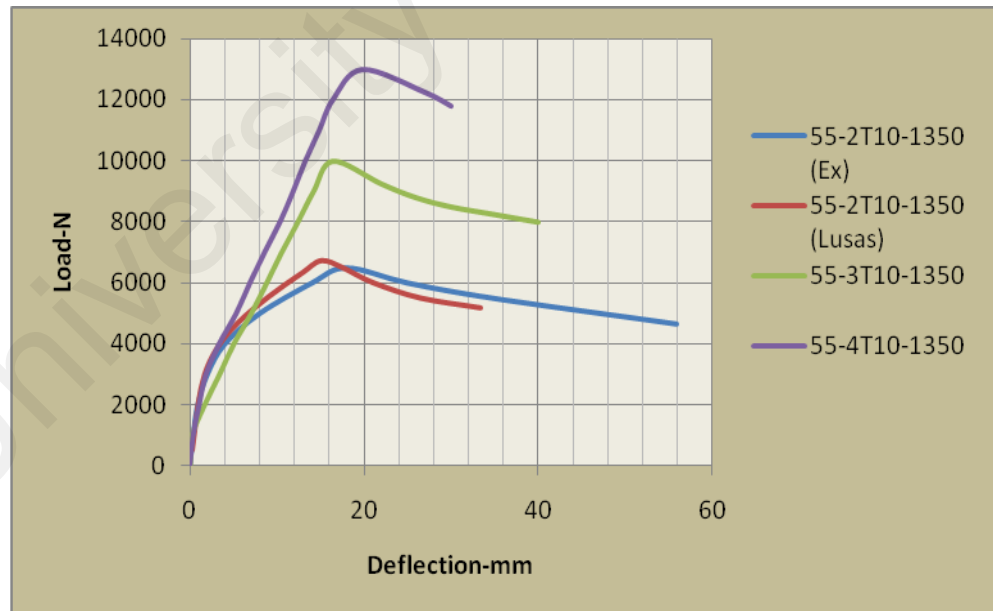


Figure 6.12: The experimental results of load-deflection curve for the samples 55-2T10-1350, 55-3T10-1350 and 55-4T10-1350 in compare with LUSAS results



Figure 6.13: The experimental results of load-deflection curve for the samples 70-3T10-1350 and 70-2T10-1350 in compare with LUSAS results

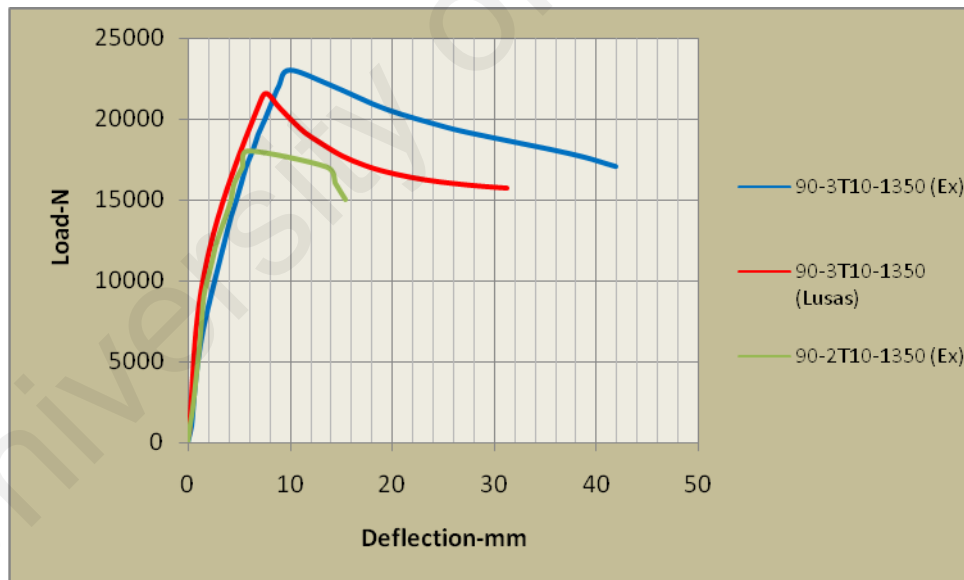


Figure 6.14: The experimental results of load-deflection curve for the samples 90-3T10-1350 and 90-2T10-1350 in compare with LUSAS results

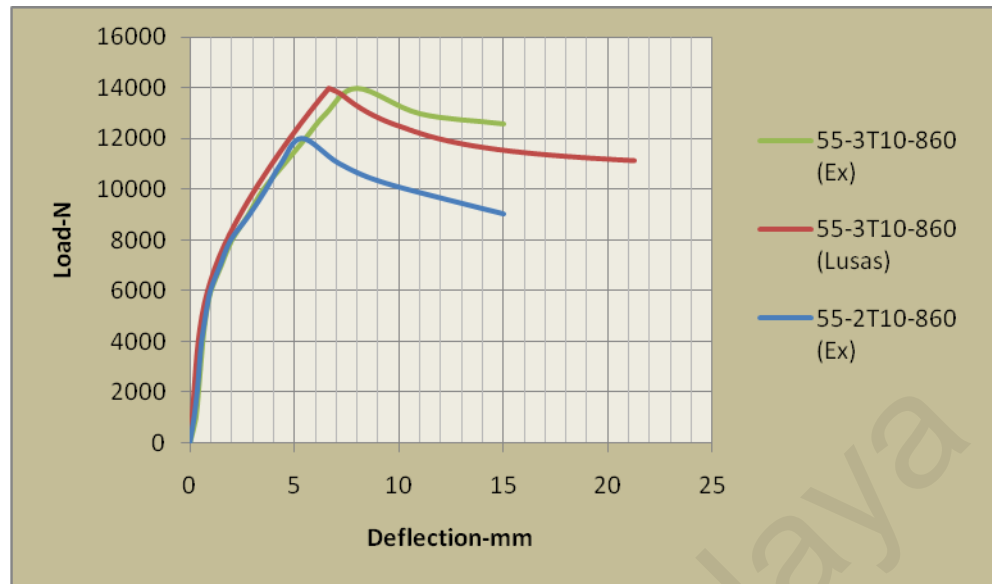


Figure 6.15: The experimental results of load-deflection curve for the samples 55-3T10-860 and 55-2T10-860 in compare with LUSAS results

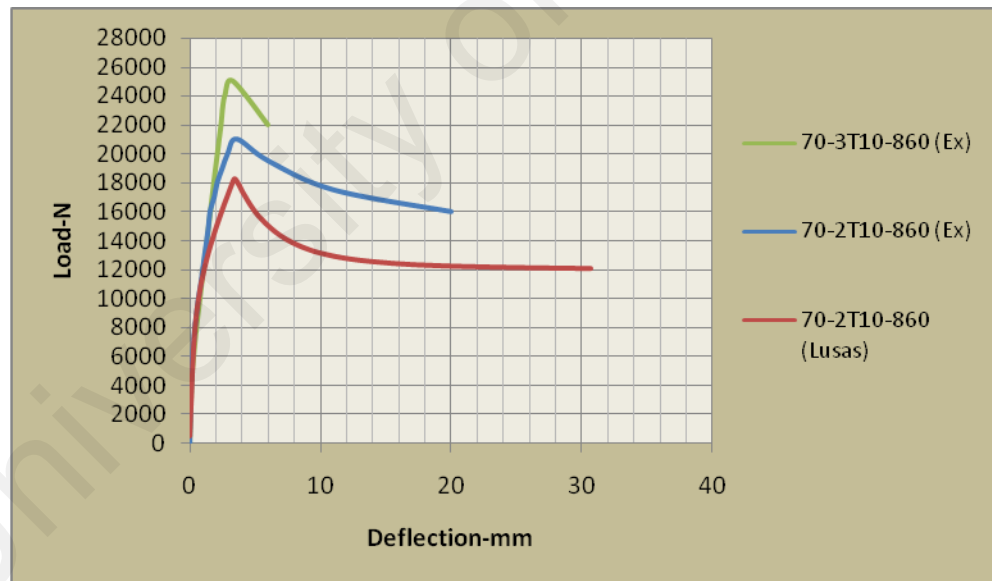


Figure 6.16: The experimental results of load-deflection curve for the samples 70-3T10-860 and 70-2T10-860 in compared with LUSAS results

6.2.2 CFRP Strengthened One-Way RC Slab

In this part, six CFRP strengthened RC one-way slab was designed, fabricated and tested in flexure. All the slabs had the same dimensions and internal steel reinforcement, with the main test parameters being the length and width of CFRP reinforcement (Figure 6.17).



Figure 6.17: RC one-way slab strengthened by different lengths and width of CFRP

All the CFRP strengthened RC slabs were designed as under- reinforced section based on rectangular stress block of ISIS (Intelligent Sensing for Innovative Structures) Canada Research Network (2001). The crack pattern of the strengthened slabs is shown in Figure 6.18. In the failure mode of the slabs, the yielding of the steel took place before the failure of concrete in the compression zone. Debonding of the CFRP plate was occurred at the CFRP/concrete interface before the yielding of the steel reinforcement (Figure 6.19). The structural behavior of the CFRP strengthened RC slabs were compared with similar slab without CFRP.

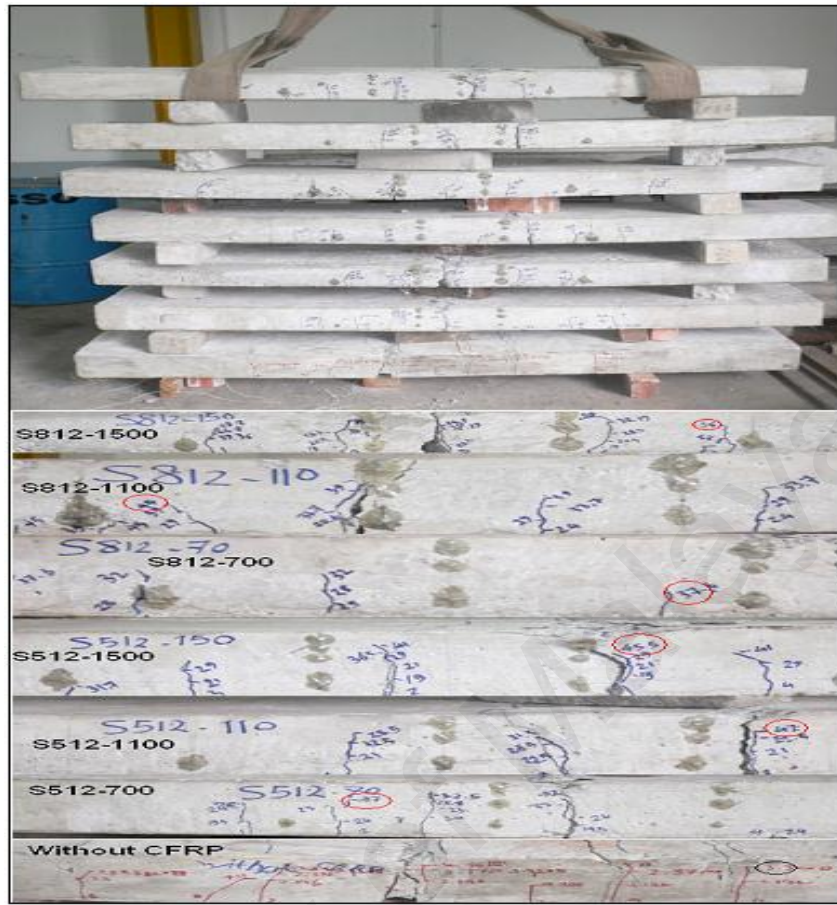


Figure 6.18: The overall crack pattern of the CFRP strengthened RC slab under four point line load



Figure 6.19: CFRP debonding at the CFRP/concrete interface under four point line load

The structural behavior of the CFRP strengthened RC one-way slab discussed in design and ultimate moment, cracking, and mid-span deflection. In each part, the theoretical service and ultimate capacity based on ISIS are compared to the corresponding experimental results. The load-deflection curve of the CFRP strengthened slabs obtained from the experimental work is validated with the corresponding finite element analysis.

6.2.2.1 Design and Ultimate Moment

Table 6.11 shows a comparison between experimental and predicted ultimate moment. . The predicted ultimate moment for the CFRP strengthened RC one-way slabs calculated based on the ISIS (2001). The ratio between the experimental ultimate moment and the values predicted by ISIS (M_u/M_{ISIS}) and FEA (M_u/M_{FEA}) varied in the range of 0.85 to 1.04 and 0.97 to 1.03 respectively. The prediction by finite element analysis showed closer results to experimental results.

Table 6.11: Experimental and predicted ultimate moment of the CFRP strengthened RC slabs in flexure

Slab	Exp. Ultimate Load (kN)	Exp. Ultimate Moment (M_u) (kN-m)	Predicted Ultimate Moment (kN-m)		M_u/M_{ISIS}	M_u/M_{FEA}
			M_{ISIS}	M_{FEA}		
S512-700	37	12	17.4	11.4	0.69	1.05
S512-1100	42	13.7	17.4	13.2	0.79	1.04
S512-1500	45.5	14.8	17.4	15.3	0.85	0.97
S812-700	37	12.1	17.3	12.5	0.70	0.97
S812-1100	45	14.6	17.3	15.9	0.84	0.92
S812-1500	54	17.8	17.3	18.5	1.03	0.96
WCFRP	33.3	10.8	10.4	10.5	1.04	1.03

6.2.2.2 Cracking

Flexural cracks of CFRP strengthened RC slab were investigated and measured in each step of applied loading (Figure 6.20). Table 6.12 gives the applied load at the initiation of flexural cracking in the region of constant moment between the two bending line loads.



Figure 6.20: Crack measuring in each step of applied loading

Table 6.12: Experimental and predicted ultimate moment of the slabs in flexure

Slab	Exp. Load at First Crack (kN)	Moment at First Crack M_{cr} (kNm)			M_{cr} / M_{ISIS}	M_{cr} / M_{FEA}	Ultimate Stage			M_u / M_{cr}
		Exp	ISIS	FEA			Load (kN)	Moment (kNm)	Crack Width (mm)	
S512-700	7.5	4.9	5.26	5.95	0.93	0.82	37	12	0.75	2.46
S512-1100	10	6.5	5.26	5.95	1.24	1.04	42	13.7	0.80	2.11
S512-1500	10	6.5	5.26	5.95	1.24	1.04	45.5	14.78	0.75	2.27
S812-700	9.5	6.2	5.45	6.31	1.14	0.97	37	12.07	0.65	1.95
S812-1100	10.3	6.7	5.45	6.31	1.23	1.05	45	14.62	0.75	2.18
S812-1500	10.5	6.8	5.45	6.31	1.25	1.07	54	17.87	0.95	2.62
WCFRP	7	4.6	4.93	5.23	0.93	0.88	33.3	10.8	0.75	2.37

In addition, the location and the width of the cracks out of constant moment were investigated and measured. The measured crack width and location in loading process are presented on Figures 6.22 to 6.28 and Tables 6.13 to 6.19. The measuring guide for the crack width and location is shown in Figure 6.21. The location of the cracks (X and Y) was measured from the left-hand coordinate shown in Figure 6.21. The crack width in each step of applied loading is measured on the steel bar level. The loading in Tables 6.13 to 6.19 is selected during experimental testing for visible cracks on the concrete surface.

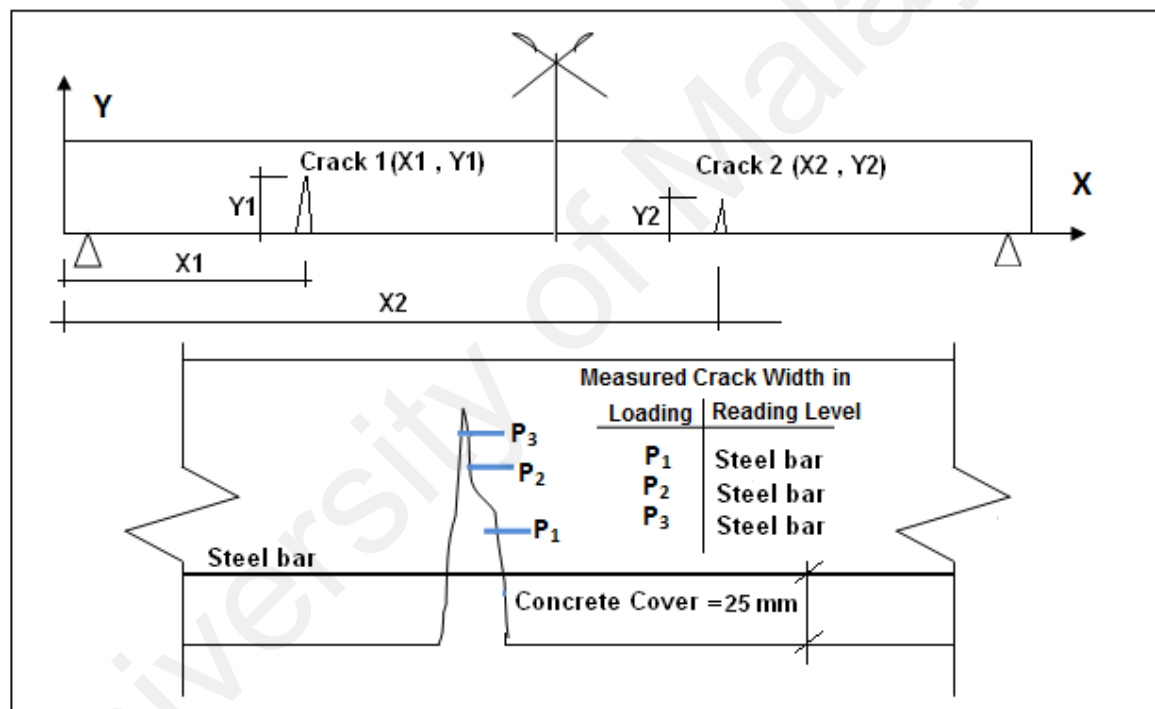


Figure 6.21: Measuring guide for the crack location and width presented in Figures 6.22 to 6.28 and Tables 6.13 to 6.19.

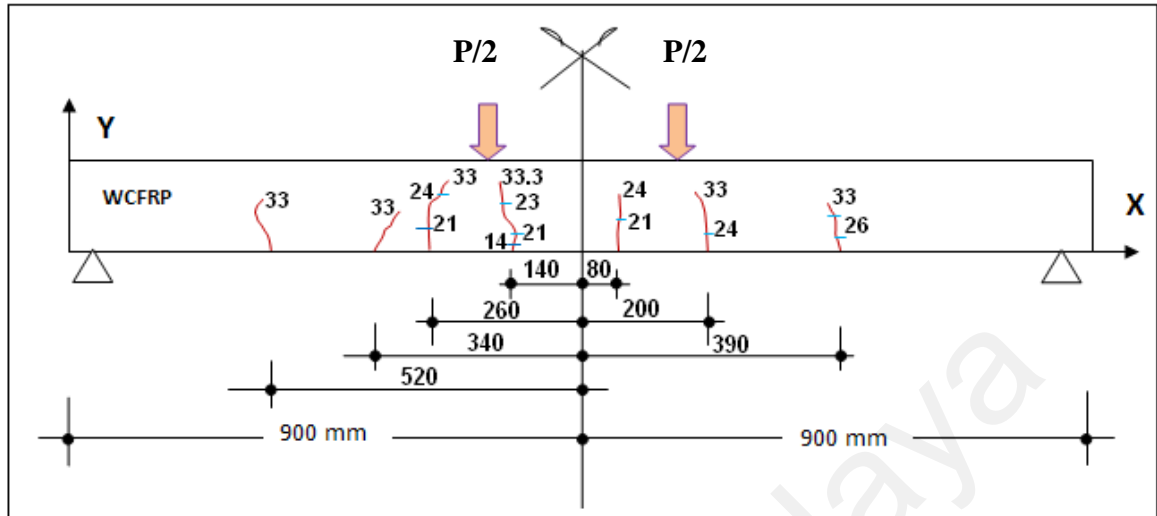


Figure 6.22: The loading and crack presentation for the slab without CFRP

Table 6.13: The loading, crack location, and crack width for the slab without CFRP

No.	Loading-KN	X-mm	Y-mm	Crack Width-mm
1	21	640	30	0.25
2	21	760	34	0.30
3	21	980	41	0.30
4	23	750	62	0.35
5	24	647	54	0.30
6	24	990	66	0.35
7	24	1100	35	0.15
8	26	1285	30	0.20
9	33	680	80	0.45
10	33	1080	75	0.25
11	33	1270	55	0.40
12	33	590	40	0.35
13	33	380	60	0.40
14	33.3	740	95	0.75

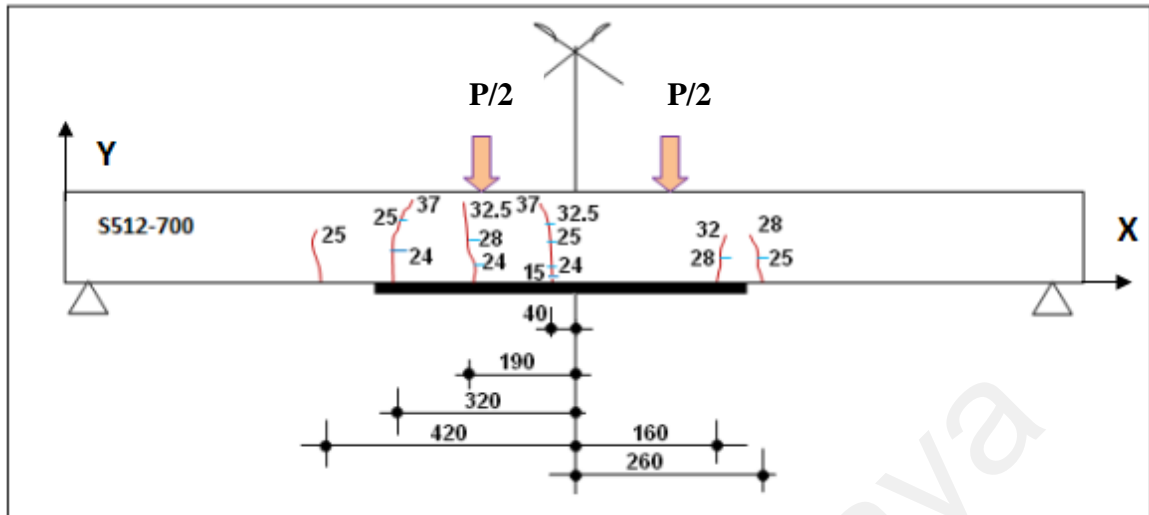


Figure 6.23: The loading and crack presentation for the RC slab strengthened by CFRP S512-700

Table 6.14: The loading, crack location, and crack width for the RC slab strengthened by CFRP S512-700

No.	Loading-KN	X-mm	Y-mm	Crack Width-mm
1	24	580	35	0.20
2	24	710	40	0.15
3	24	860	40	0.25
4	25	850	63	0.45
5	25	1160	35	0.20
6	25	480	75	0.30
7	25	550	85	0.40
8	28	700	70	0.30
9	28	1060	45	0.25
10	28	1140	65	0.40
11	32	1040	60	0.30
12	33	700	85	0.45
13	33	830	80	0.65
14	37	820	95	0.75

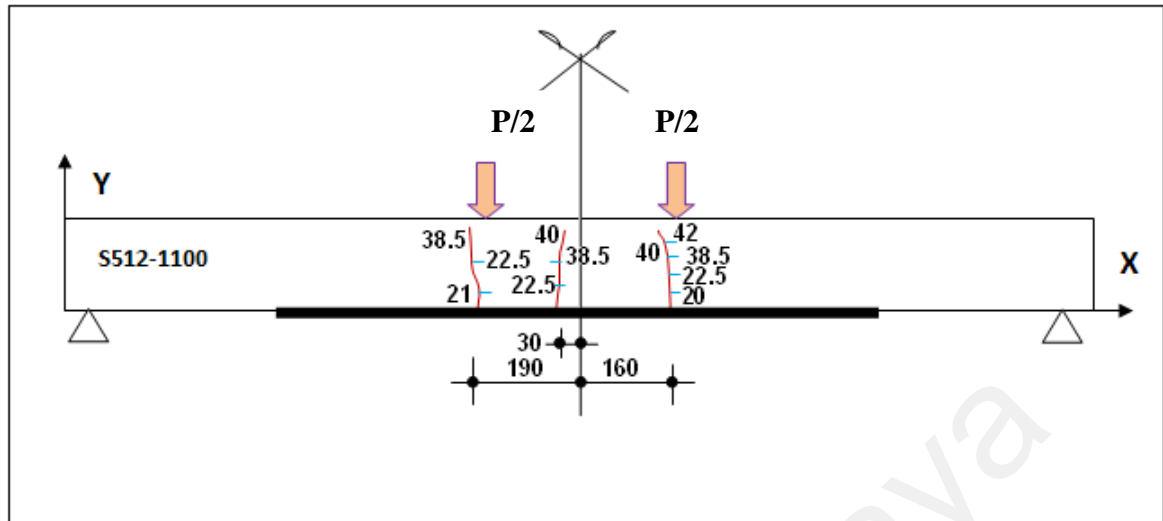


Figure 6.24: The loading and crack presentation for the RC slab strengthened by CFRP S512-1100

Table 6.15: The loading, crack location, and crack width for the RC slab strengthened by CFRP S512-1100

No.	Loading-KN	X-mm	Y-mm	Crack Width-mm
1	20	710	35	0.20
2	21	1060	45	0.15
3	23	870	30	0.25
4	23	720	70	0.30
5	23	1060	75	0.25
6	39	855	65	0.45
7	39	1060	80	0.50
8	39	735	85	0.55
9	40	850	70	0.50
10	40	1060	85	0.65
11	42	1060	95	0.80

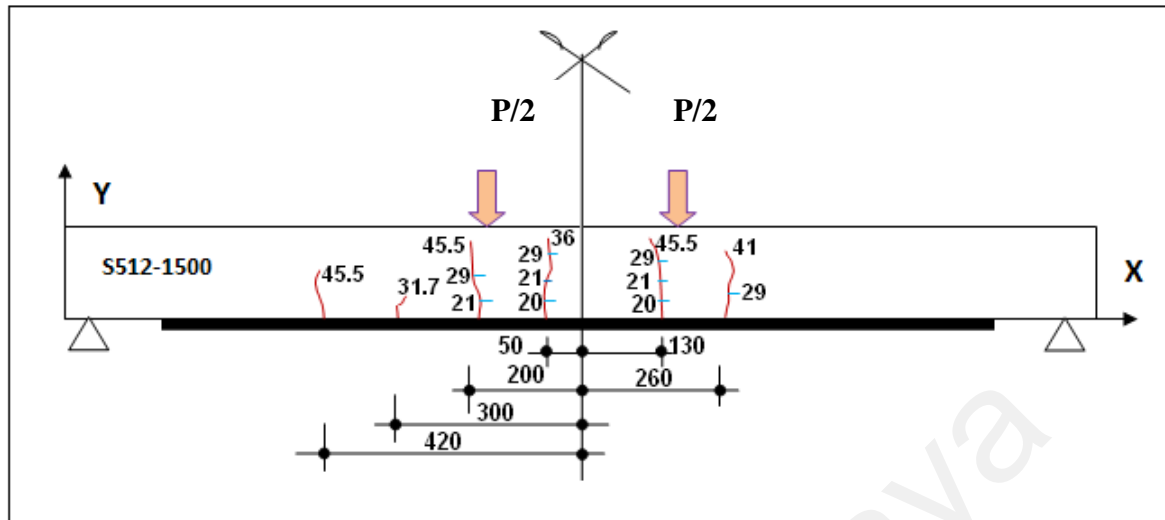


Figure 6.25: The loading and crack presentation for the RC slab strengthened by CFRP S512-1500

Table 6.16: The loading, crack location, and crack width for the RC slab strengthened by CFRP S512-1500

No.	Loading-KN	X-mm	Y-mm	Crack Width-mm
1	20	1030	40	0.10
2	20	850	30	0.15
3	21	700	25	0.25
4	21	850	50	0.20
5	21	1050	50	0.15
6	29	700	40	0.30
7	29	850	70	0.30
8	29	1030	65	0.25
9	29	1160	60	0.15
10	32	600	20	0.25
11	36	850	75	0.45
12	41	1140	85	0.45
13	45.5	480	55	0.35
14	45.5	690	85	0.55
15	45.5	1000	85	0.75

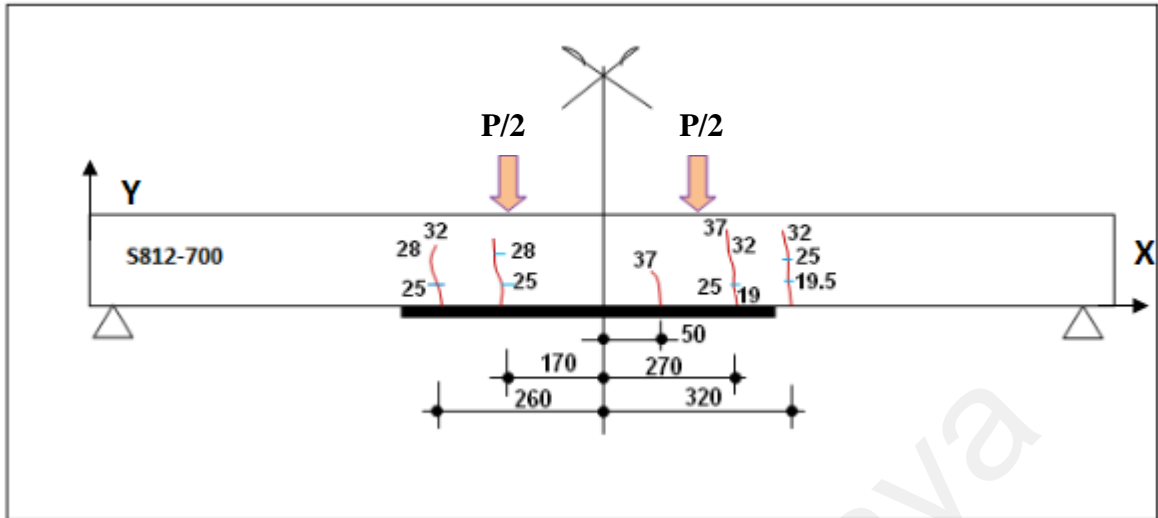


Figure 6.26: The loading and crack presentation for the RC slab strengthened by CFRP S812-700

Table 6.17: The loading, crack location, and crack width for the RC slab strengthened by CFRP S812-700

No.	Loading-KN	X-mm	Y-mm	Crack Width-mm
1	19.5	1220	35	0.25
2	25	640	25	0.15
3	25	730	20	0.20
4	25	1170	30	0.25
5	25	1215	55	0.20
6	28	635	60	0.30
7	28	730	65	0.25
8	32	640	70	0.32
9	32	1170	45	0.45
10	32	1220	80	0.45
11	37	950	45	0.35
12	37	1170	85	0.65

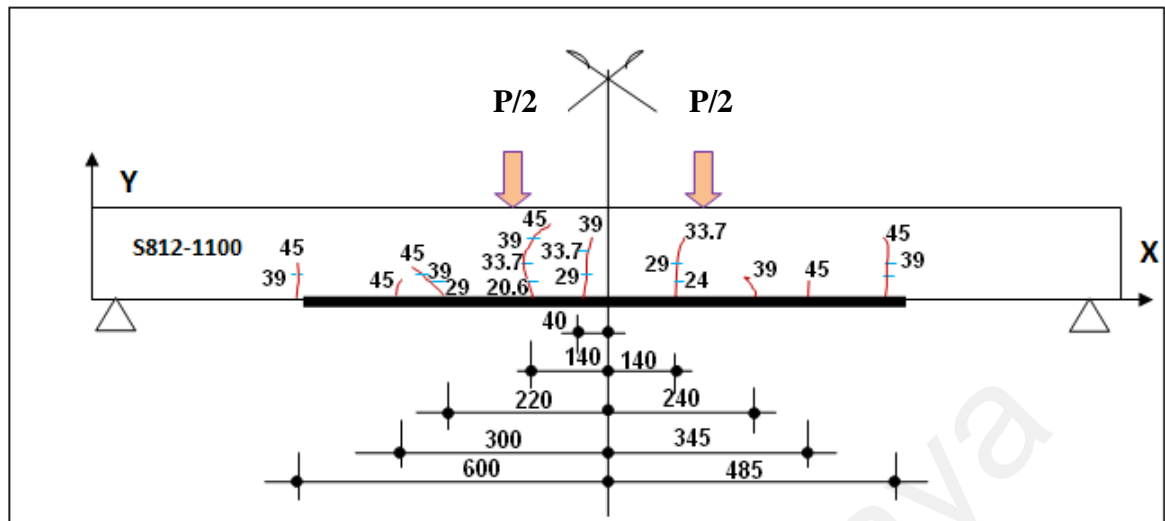


Figure 6.27: The loading and crack presentation for the RC slab strengthened by CFRP S812-1100

Table 6.18: The loading, crack location, and crack width for the RC slab strengthened by CFRP S812-1100

No.	Loading-KN	X-mm	Y-mm	Crack Width-mm
1	21	760	25	0.10
2	24	1040	10	0.15
3	29	680	20	0.20
4	29	860	30	0.15
5	29	1045	45	0.20
6	34	760	35	0.20
7	34	860	40	0.25
8	34	1055	75	0.45
9	39	300	10	0.20
10	39	630	40	0.25
11	39	775	75	0.50
12	39	860	60	0.45
13	39	1140	35	0.10
14	39	1385	45	0.15
15	45	300	20	0.30
16	45	600	20	0.25
17	45	650	70	0.50
18	45	790	90	0.75
19	45	1245	25	0.20
20	45	1385	60	0.40

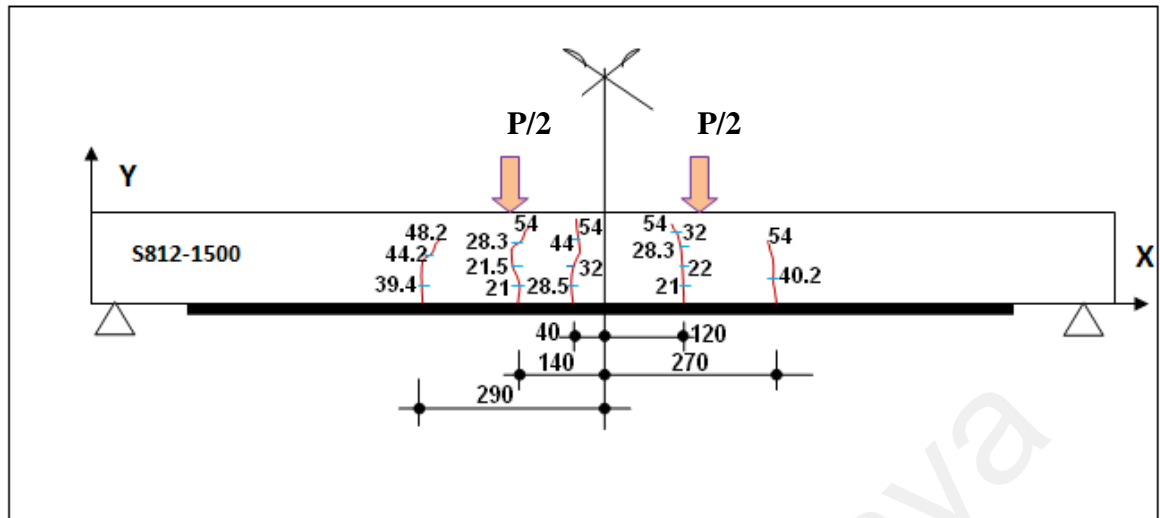


Figure 6.28: The loading and crack presentation for the RC slab strengthened by CFRP S812-1500

Table 6.19: The loading, crack location, and crack width for the RC slab strengthened by CFRP S812-1500

No.	Loading-KN	X-mm	Y-mm	Crack Width-mm
1	21	760	20	0.10
2	21	1020	25	0.15
3	21.5	755	40	0.20
4	22	1035	30	0.25
5	28	760	55	0.30
6	28	1045	60	0.30
7	29	860	25	0.15
8	32	860	55	0.30
9	32	1055	80	0.40
10	39	610	35	0.10
11	40	1170	40	0.15
12	44	625	60	0.50
13	44	860	85	0.55
14	48	640	75	0.65
15	54	860	95	0.85

6.2.2.3 Load-Deflection Analysis

Deflections of the all CFRP strengthened RC one-way slab were measured using linear variable displacement transducer (LVDT) and recorded using a data logger. Table 6.20 gives the mid-span deflection at the first crack and ultimate load for each slab. The ratio between the experimental deflection at first crack and the values predicted by ISIS Canada and FEA varied in the range of 0.56 to 1.33 and 0.50 to 1.20 respectively.

Table 6.20: Experimental deflection at the first crack and ultimate load for the CFRP strengthened RC one-way slabs

Slab	Exp. First Crack Load (kN)	Def. at First Crack (mm)			Span / Def	Def. Ratio at First Crack		Ultimate Load (kN)		
		Exp	ISIS	FEA		Exp / ISIS	Exp / FEA	Exp	ISIS	FEA
S512-700	7.5	0.62	1.11	1.23	2674	0.56	0.50	37	53.5	35.1
S512-1100	10	1.22	1.11	1.23	1352	1.10	0.99	42	53.5	40.6
S512-1500	10	1.25	1.11	1.23	1320	1.13	1.02	45.5	53.5	47.1
S812-700	9.5	1.05	1.14	1.27	1571	0.92	0.83	37	53.2	38.5
S812-1100	10.3	1.19	1.14	1.27	1387	1.04	0.94	45	53.2	48.9
S812-1500	10.5	1.52	1.14	1.27	1086	1.33	1.20	54	53.2	56.9
WCFRP	7	1.17	1.15	1.13	1404	1.02	1.04	33.3	32.0	32.3

In Figure 6.29, the load-deflection of the one-way RC slab strengthened by CFRP S512 with lengths 700, 1100, and 1500 mm have been compared with the non-strengthened one-way RC slab. The non-strengthened one-way slab failed at load 33kN. After the strengthening using CFRP, the one-way RC showed an increased failure load of 37 kN, 42

kN, 45.5 kN for S512-700, S512-1100 and S512-1500 respectively. These results indicated that using CFRP for strengthening improves the failure load. It also shows that by increasing the lengths of CFRP, the failure load increases by 10.8%, 21.5% and 27.5% for the 512-700, S512-1100, and S512-1500 respectively.

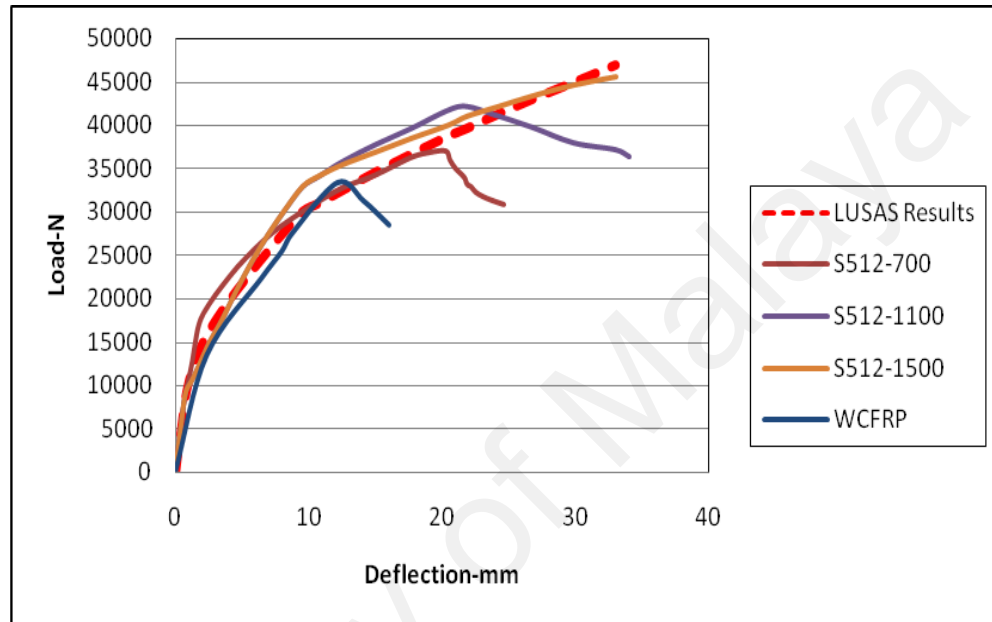


Figure 6.29: Comparison of load-deflection analysis between CFRP strengthened one-way RC slab with different lengths of CFRP-S512 and WCFRP

Also noted on Figure 6.29 is that the experimental results of load-deflections analysis are in agreement with the results of the LUSAS leading to an acceptable finding of this research. The comparison between the results of the experimental work on the strengthened one-way RC slab using CFRP-S812 with CFRP lengths 700mm, 1100mm and 1500 mm and the non-strengthened one-way RC slab are presented in Figure 6.30. By increasing the lengths of the CFRP, the loading capacity improved by 13.2%, 26.7% and 40% for S812-700, S812-1100 and S812-1500 respectively

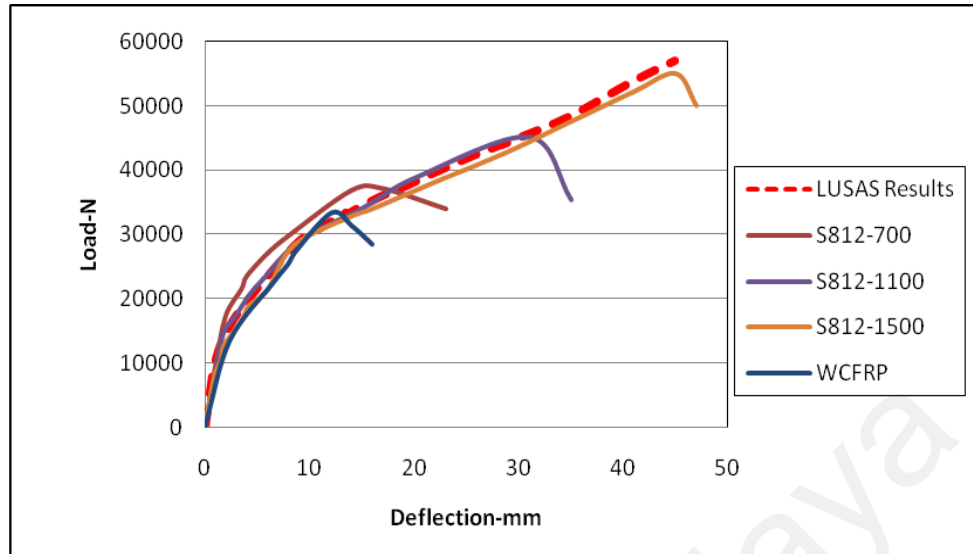


Figure 6.30: Comparison of load-deflection analysis between CFRP strengthened one-way RC slab with different lengths of CFRP-S812 and WCFRPb

The use of CFRP improved the load-deflection relationship and failure load in one-way RC slab. The percentage of the improved failure load is shown in Figure 6.31.

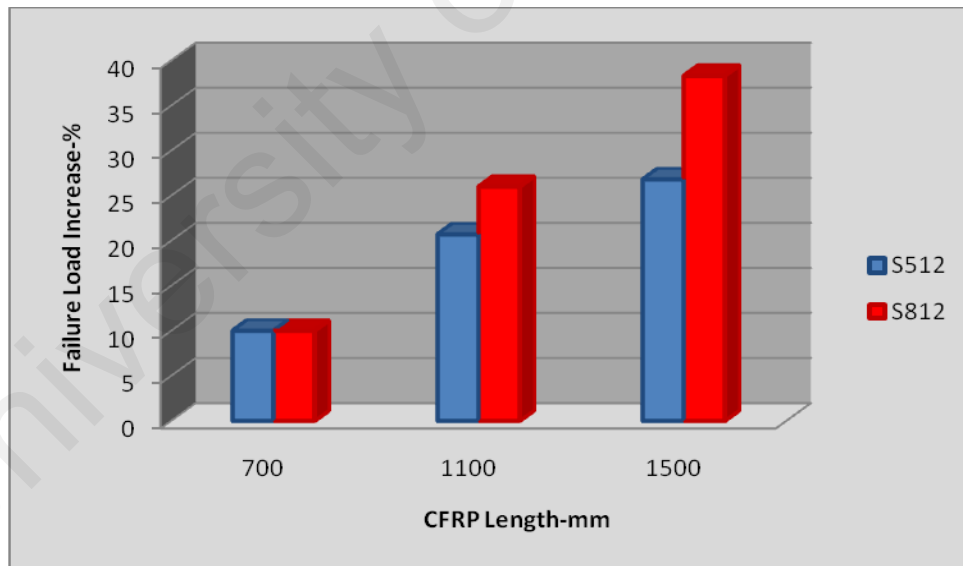


Figure 6.31: The percentage of the improved maximum applied loading in the RC one-way slabs strengthened by different length of the CFRP-S512 and CFRP-S812.

By increasing the CFRP cross section area from 60 mm^2 (S512-1500) to 96 mm^2 (S812-1500), the maximum load capacity increased from 45.5 KN to 54 KN as shown in Figure 6.32.

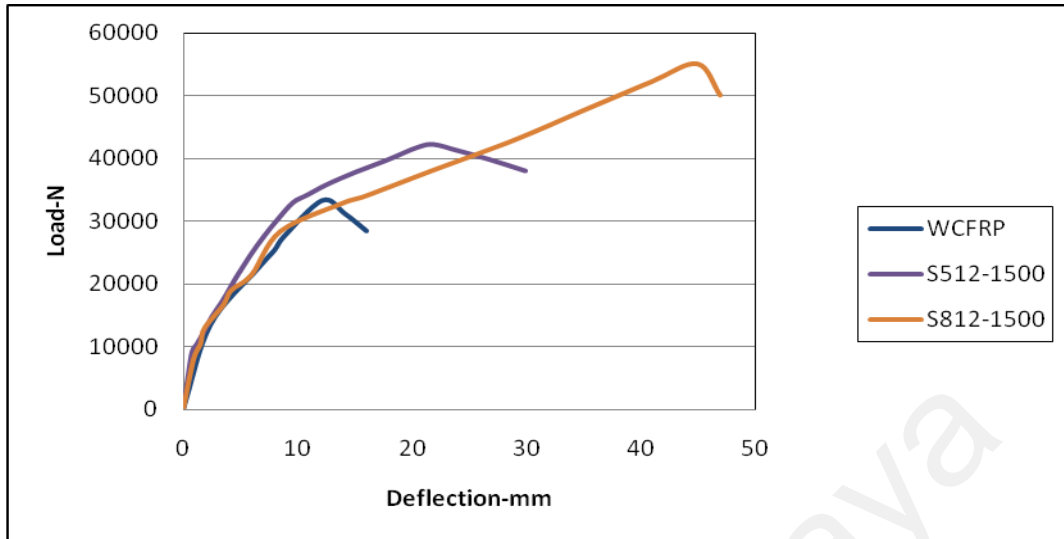


Figure 6.32: Load-deflection comparison between non-strengthened one-way RC slab and strengthened by CFRP512-1500 and CFRP S812-1500

It was also presented in Figure 6.33 that by increasing the CFRP cross sectional area from 60 to 96 mm², the slab maximum applied load improved 6.67 and 15.7% for the CFRP length of 1100 and 1500 mm respectively.

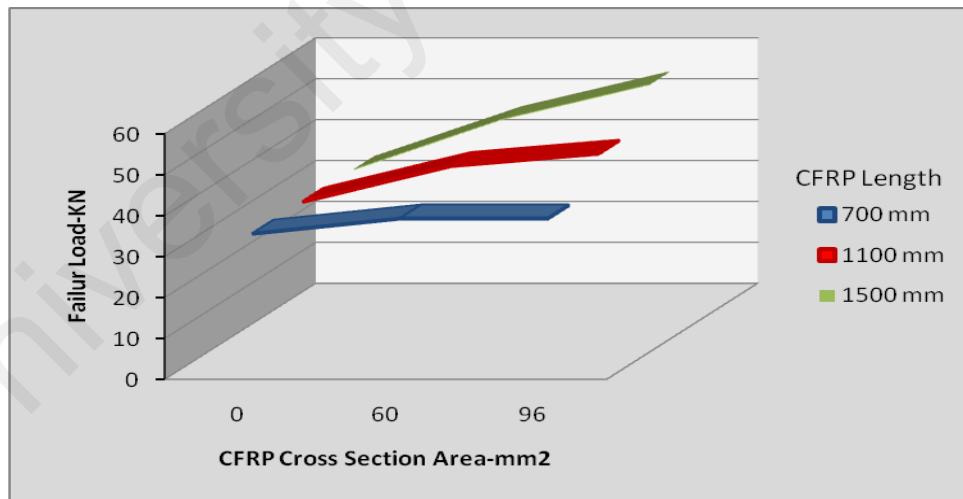


Figure 6.33: Failure load for different cross section area of the applied CFRP on slabs

CHAPTER 7

7. ANALYSIS AND RESULTS

The results of the generated networks are presented and discussed in this chapter. The experimental data discussed in Chapter 6 are managed using the EXCEL software. This data then were analysed with the NNTOOL and coding function in MATLAB software to create network for prediction. The FBNN, GRNN, FFDNN, and RNN are the four networks trained using the experimental data from this research. The validity of these networks is then checked again using the remainder of the data. The comparison between network outputs and targets are presented as Mean Squared Error (MSE) and as coefficient of determination.

7.1 Feed-forward Back-propagation Neural Networks

FBNN was applied for the load-deflection analysis of non-strengthened and CFRP strengthened one-way RC slab.

7.1.1 Load-deflection analysis of non-strengthened RC slab

The data gathered from load-deflection analysis of the 19 non-strengthened RC slabs with different lengths, thicknesses, and steel bar applied for the FBNN generation. From 35 networks, an optimum network is chosen and this is presented in Table 7.1.

Table 7.1: The FBNN specifications for non-strengthened RC slab

The Totally Number of Data	378 data
The number of data for network generation	362=290(training)+36(verifying)+36(testing)
The number of data for testing	16 data selected from slab 100-3T10-1800
The number of neurons in hidden layers(HNs)	$5 \leq \text{HNs} \leq 25$
Input layers	Slab length and thickness, steel bar, and loading
Output layer	Mid-span deflection
Net Architecture	(4-15-7-1)
Network Type	Multilayer feed-forward
Net Algorithm	Back-propagation
Training Function	Trainlm
Learning Function	LEARNGDM
Output Transfer Function	Purelin
Hidden Transfer Function	Tansig and Logsig
Performance Function	MSE

The selected network was generated with 290, 36, and 36 data for training, validation, and testing, respectively. Furthermore, 16 mid-span deflection of slab 100-3T10-1800 was applied for network testing. The slab length, thickness, steel bar, and loading were the input data and the mid-span deflection was the output data. The architecture of the generated network is included of two hidden layers with 15 neurons in the first hidden layer and 7 neurons in the second hidden layer. The transfer function for the first and second hidden layer and output layer were Tansig, Logsig, and Purelin respectively. The

network training and related information are shown in Figure 7.1. It is observed that the network training MSE performance function is 0.000356. The regression curves for network training, testing, and validation are shown in Figure 7.2. The coefficient of determination for network training, testing, and validation were close to 1.

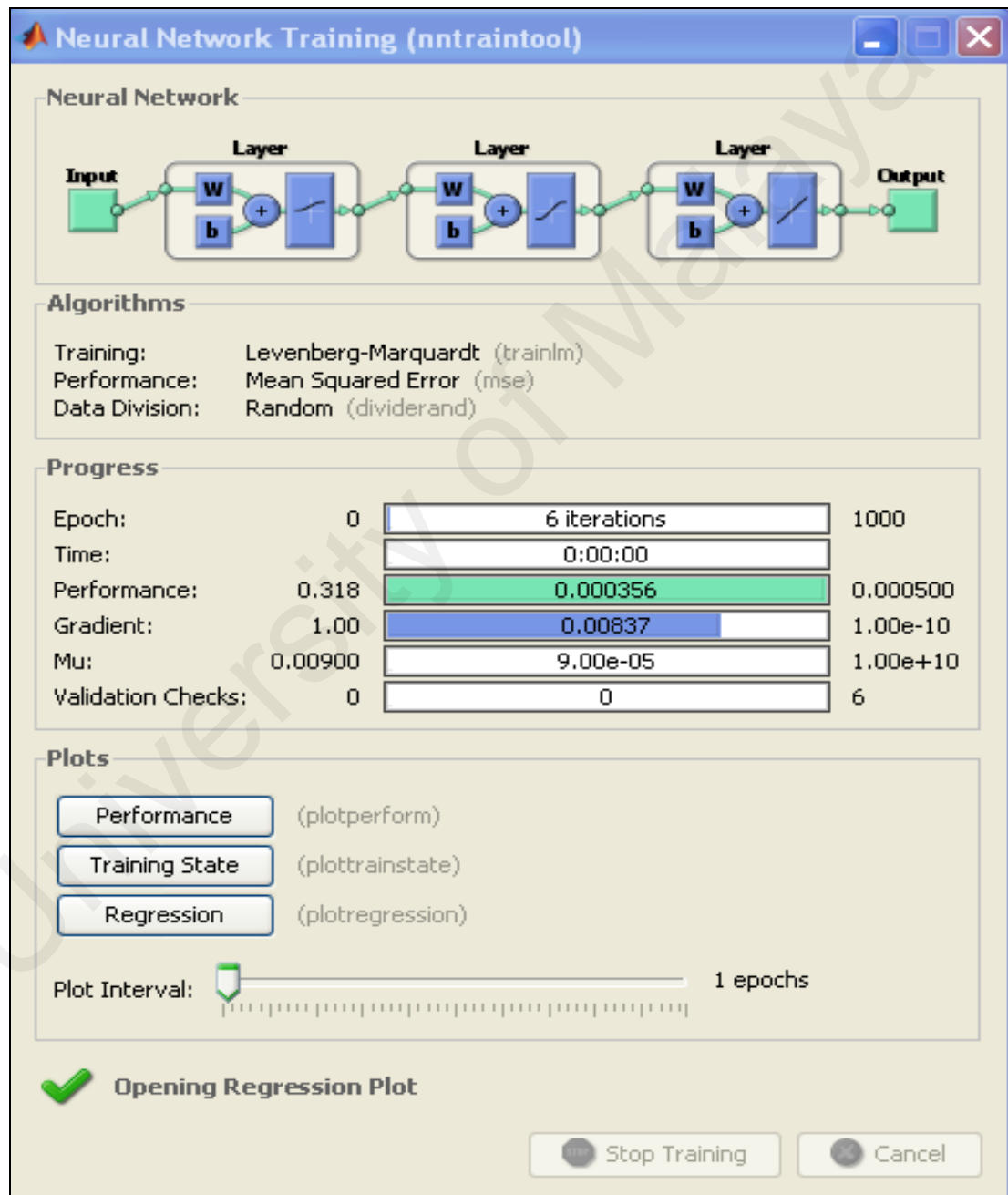


Figure 7.1: The FBNN training process for prediction of mid-span deflection in non-strengthened RC slab

After network simulation, the testing MSE performance function for slab 100-3T10-1800 was calculated by comparing network outputs and experimental deflection as well as shown in Table 7.2. The created network predicted the mid-span deflection with maximum MSE performance function of 0.000219 and correlation of determination R^2 of 0.97.

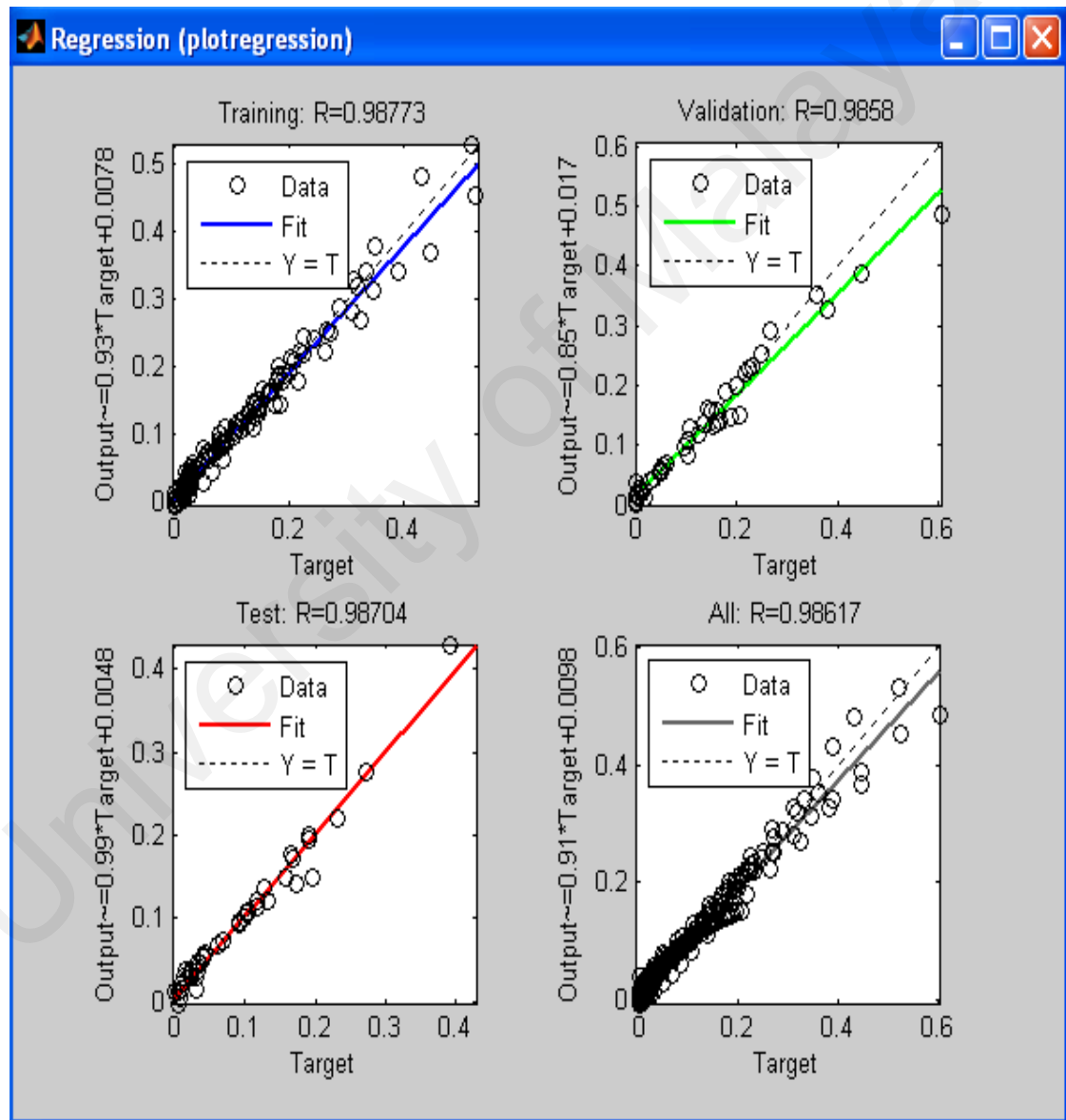


Figure 7.2: The regression plot for the optimum network after FBNN generation

Table 7.2: The FBNN testing error for mid-span deflection of slab 100-3T10-1800

Neurons (n)	Exp. Deflection Δ_{Exp} (mm)		Network Deflection Δ_{Net} (mm)		$\frac{\Delta_{Net}}{\Delta_{Exp}}$	$E = \Delta_{Exp} - \Delta_{Net}$	E^2
	Real	Normalized	Real	Normalized			
1	0.00	0	0.00	0	-	0.0000	0
2	0.53	0.014	0.39	0.010	0.73	0.0038	0.00001
3	0.84	0.022	0.66	0.017	0.79	0.0046	0.00002
4	1.14	0.030	0.91	0.024	0.80	0.0060	0.00004
5	1.52	0.040	1.38	0.036	0.90	0.0038	0.00001
6	2.17	0.057	1.99	0.052	0.92	0.0046	0.00002
7	3.15	0.083	2.73	0.072	0.86	0.0113	0.00013
8	4.18	0.110	3.63	0.096	0.87	0.0144	0.00021
9	5.28	0.139	4.55	0.120	0.86	0.0193	0.00037
10	6.35	0.167	5.68	0.149	0.89	0.0176	0.00031
11	7.52	0.198	6.81	0.179	0.91	0.0187	0.00035
12	8.44	0.222	7.83	0.206	0.93	0.0159	0.00025
13	9.50	0.250	9.02	0.237	0.95	0.0127	0.00016
14	10.75	0.283	10.17	0.268	0.95	0.0153	0.00023
15	12.08	0.318	12.65	0.333	1.05	-0.0149	0.00022
16	13.30	0.350	14.60	0.384	1.10	-0.0342	0.00117
$MSE = \sum E^2/n$							0.000219

7.1.2 Load-deflection analysis of CFRP strengthened RC slab

The load-deflection analysis of six CFRP strengthened RC slabs and one non-strengthened RC slab was applied for the generation of FBNN. The 93 data used in network generation applied for network training, verifying, and testing. For the more, another 10 data were selected from slab S812-1100 for network testing. The loading, CFRP length and width were the neurons in input layer and the deflection at each loading was the neuron in output layer. The architecture of the generated network is included of two hidden layers with 15 neurons in the first hidden layer and 5 neurons in the second hidden layer as well as presented in Figure 5.12. The transfer function for the first and second hidden layer and output layer were Logsig, Tansig, and Purelin respectively. The maximum testing and network generation performance function were 0.00084 and 0.00697 respectively, extracted from MSE method. The calculated MSE for the testing and training stage are shown in Figures 7.3 and 7.4 respectively.

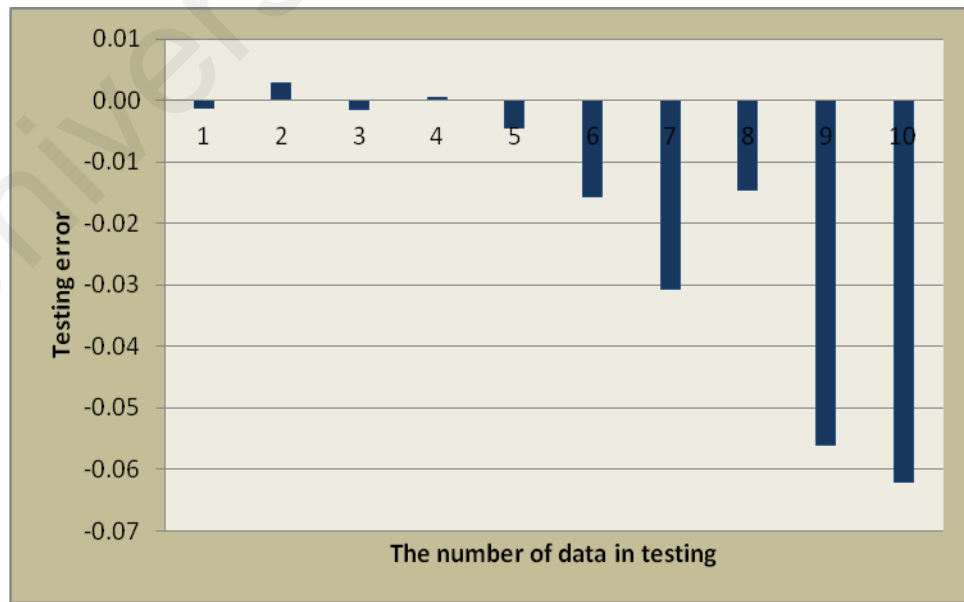


Figure 7.3: The FBNN testing error for deflection analysis of slab S812-1100

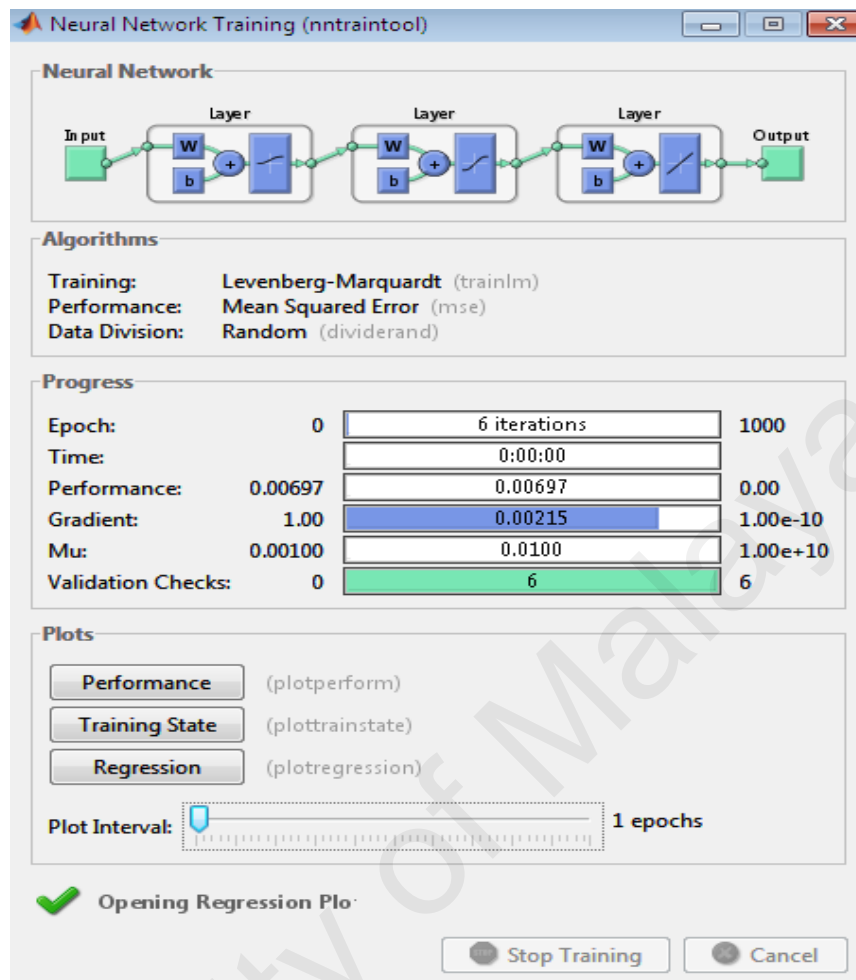


Figure 7.4: The FBNN architecture, algorithm, and training performance

Table 7.3 presents the MSE calculation for predicted deflection by FBNN on slab S812-1800. The coefficient of determination between data in training stage was 0.95. The evaluation between experimental and predicted deflection on slab S812-1800 in testing stage is shown in Figure 7.5. The coefficient of determination in testing stage of generated network was 0.99.

Table 7.3: The FBNN testing error for prediction of mid-span deflection of slab S812-1800

Neurons (n)	Exp. Deflection Δ_{Exp} (mm)		Network Deflection Δ_{Net} (mm)		$\frac{\Delta_{Net}}{\Delta_{Exp}}$	E= $\Delta_{Exp}-\Delta_{Net}$	E^2
	Real	Normalized	Real	Normalized			
1	0	0.1	0.1	0.10	-	-0.0013	1.8E-06
2	1.32	0.12	1.0	0.12	0.76	0.0028	7.9E-06
3	1.83	0.13	1.9	0.13	1.01	-0.0016	2.4E-06
4	3	0.15	2.9	0.15	0.97	0.0004	1.5E-07
5	4.2	0.17	4.4	0.17	1.04	-0.0045	2.0E-05
6	5.8	0.19	6.2	0.21	1.07	-0.0157	2.5E-04
7	9.1	0.25	10.6	0.28	1.17	-0.0306	9.4E-04
8	15.1	0.36	16.1	0.37	1.07	-0.0147	2.2E-04
9	20.3	0.44	23.3	0.50	1.15	-0.0561	3.1E-03
10	31	0.63	34.8	0.69	1.12	-0.0620	3.8E-03
MSE= $\sum E^2/n$							0.00084

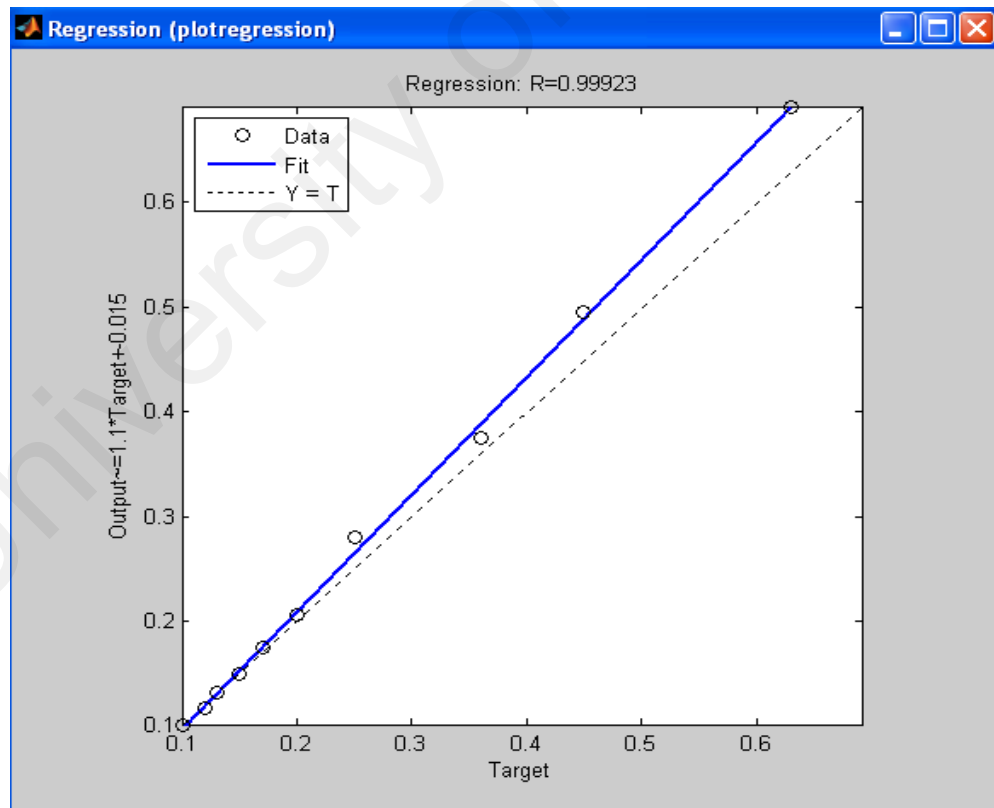


Figure 7.5: Evaluation between experimental and predicted deflection for slab S812-100 by FFBP

7.2 Generalized Regression Neural Network

In this part, GRNN is utilized for the prediction of the load-deflection analysis of non-strengthened and CFRP strengthened RC one-way slab.

7.2.1 Non-strengthened RC slab

The GRNN applied in the two following applications:

7.2.1.1 Using GRNN for load-deflection analysis

The number of data for network generation and network testing was similar to the number of data used in FBNN method as well as presented in Table 7.1. Many networks in similar number of input and output layer and various network spread were tested and the optimum network was selected with the network spread of 0.1. The slab length, thickness, steel bar, and loading were input layer and the mid-span deflection of slab under applied loading was output layer. The results of data training for the generated network presented in Figure 7.6.

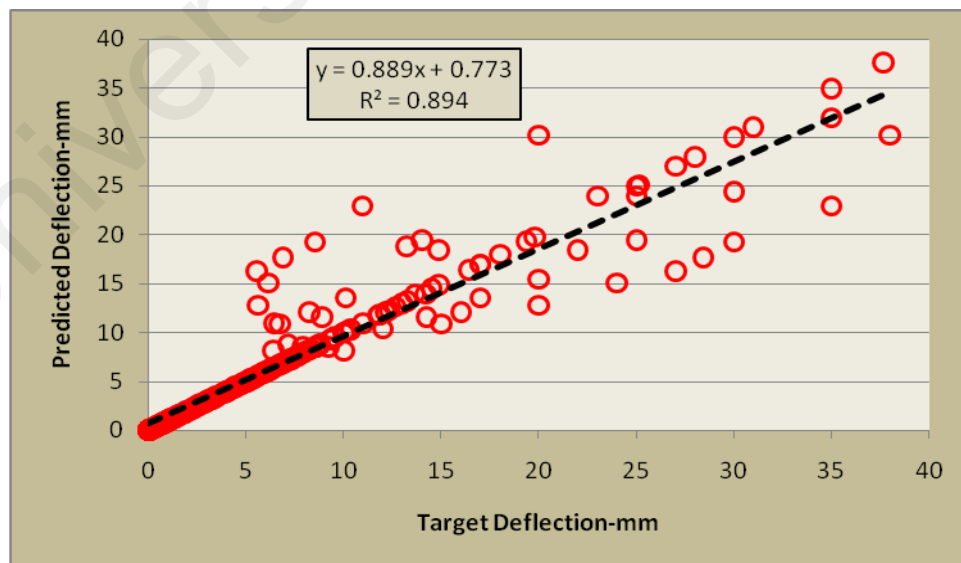


Figure 7.6: An evaluation between experimental deflection and predicted by GRNN for non-strengthened RC slab

The results of network training showed the mean squared error and coefficient of determination of 0.00083 and 0.894 respectively. After network simulation, the testing errors were calculated by comparison between GRNN output for mid-span deflection and experimental results for the slab 100-3T10-1800. The testing error and mean square error are given in Table 7.4. The MSE performance function for the 16 neurons in output layer was 0.00128

Table 7.4: The GRNN testing MSE for predicted deflection of slab 100-3T10-1800

Neurons (n)	Exp. Deflection Δ_{Exp} (mm)		Network Deflection Δ_{Net} (mm)		$\frac{\Delta_{Net}}{\Delta_{Exp}}$	E= $\Delta_{Exp}-\Delta_{Net}$	E^2
	Real	Normalized	Real	Normalized			
1	0.00	0	0.54	0.0142	-	0	0
2	0.53	0.014	0.57	0.0188	1.07	-0.0048	1.23E-05
3	0.84	0.022	0.98	0.0258	1.17	-0.0038	1.43E-05
4	1.14	0.030	1.37	0.0361	1.20	-0.0061	3.73E-05
5	1.52	0.040	1.79	0.0514	1.18	-0.0114	0.00013
6	2.17	0.057	2.47	0.0715	1.14	-0.0145	0.000211
7	3.15	0.083	3.63	0.0956	1.15	-0.0126	0.00016
8	4.18	0.110	4.51	0.1186	1.08	-0.0086	7.34E-05
9	5.28	0.139	4.90	0.1289	0.93	0.0101	0.000102
10	6.35	0.167	5.53	0.1455	0.87	0.0215	0.000464
11	7.52	0.198	6.12	0.1611	0.81	0.0369	0.001358
12	8.44	0.222	6.79	0.1786	0.80	0.0434	0.001881
13	9.50	0.250	7.86	0.2069	0.83	0.0431	0.001857
14	10.75	0.283	8.72	0.2296	0.81	0.0534	0.002852
15	12.08	0.318	9.44	0.2485	0.78	0.0695	0.00483
16	13.30	0.350	10.23	0.2693	0.77	0.0807	0.006518
MSE= $\sum E^2/n$							0.00128

The coefficient of determination between experimental and predicted data in testing phase was 0.96 as well as shown in Figure 7.7.

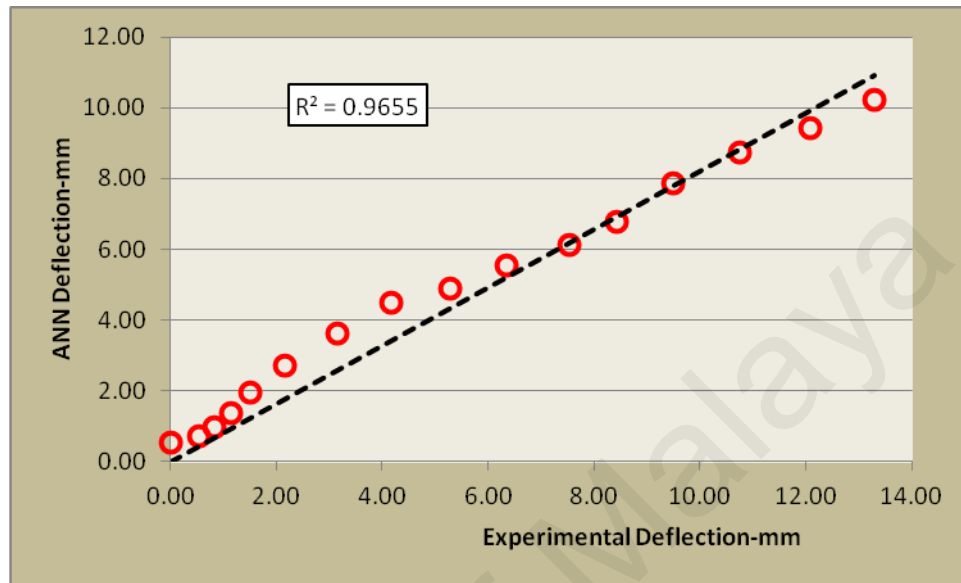


Figure 7.7: An evaluation between experimental and predicted deflection of slab 100-3T10-1800 by using GRNN

7.2.1.2 Using GRNN for maximum mid-span deflection

The values of deflection due to maximum applied loading during experimental testing were selected for training and testing in GRNN generation. The numbers of selected data were 19 sets gathered from 19 samples. GRNN is mostly useful with only a small number of training data available (Specht, 1990). The 16 maximum deflections applied for training and the maximum mid-span deflection of slabs 120-2T10-1800, 100-2T10-1800, and 90-3T10-1350 used for testing. The last try for the network generation to find the best network was found for network spread of 0.2. The evaluation between predicted results and experimental outputs in training phase is presented in Figure 7.8. The MSE performance function in training process was 0.0074. The coefficient of determination between data in training phase was 0.82. In training stage, the predicted outputs were in good agreement with experimental results as well as shown in Figure 7.9. The MSE

performance function and coefficient of determination in testing stage were 0.0011 and 0.854 respectively. The testing MSE performance function calculation for the three output neurons is given in Table 7.5.

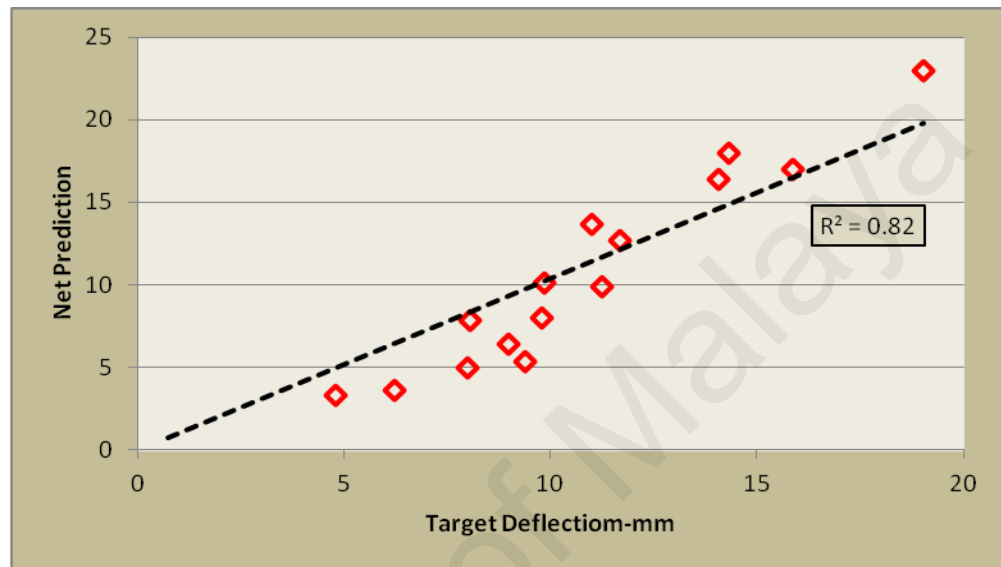


Figure 7.8: The evaluation between experimental and predicted deflections of non-strengthened RC slab in GRNN training phase

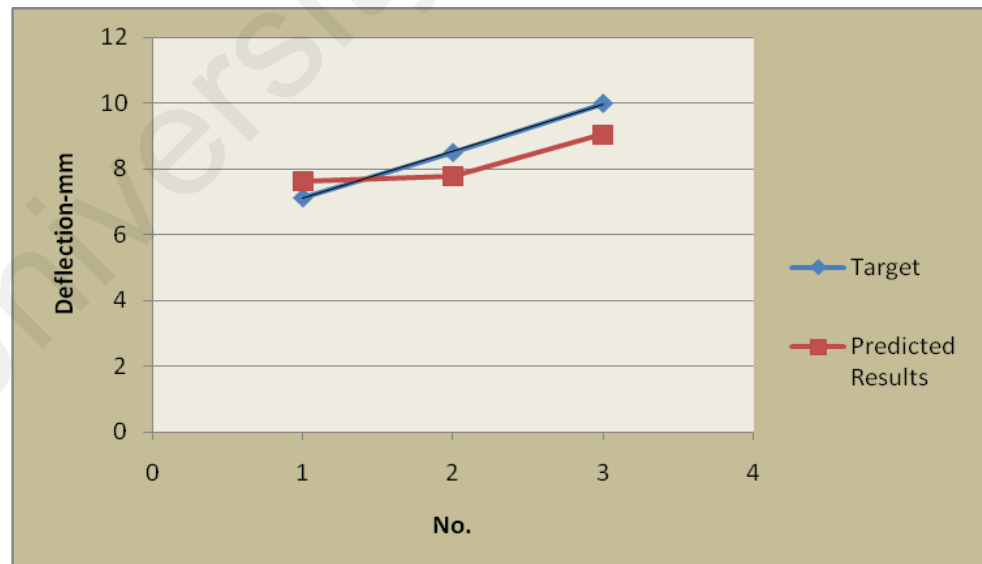


Figure 7.9: Comparison between predicted maximum deflection and experimental output for the slabs 120-2T10-1800, 100-2T10-1800, and 90-3T10-1350

Table 7.5: The GRNN testing MSE for predicted maximum deflection of slabs 120-2T10-1800, 100-2T10-1800, and 90-3T10-1350

Slab	Exp. Deflection Δ_{Exp} (mm)		Network Deflection Δ_{Net} (mm)		$\frac{\Delta_{Net}}{\Delta_{Exp}}$	E= $\Delta_{Exp}-\Delta_{Net}$	E ²
	Real	Normalized	Real	Normalized			
120-2T10-1800	7.13	0.31	7.63	0.33	1.07	-0.022	0.0005
100-2T10-1800	8.51	0.37	7.80	0.34	0.92	0.031	0.0009
90-3T10-1350	10	0.44	9.06	0.39	0.91	0.041	0.0017
MSE= $\sum E^2/n$							0.0011

7.2.2 CFRP strengthened RC slab

In this part, GRNN applied to predict the load-deflection analysis of CFRP strengthened one-way RC slab in two following applications:

7.2.2.1 Using GRNN for load-deflection analysis

Totally, 103 load-deflection data gathered from 7 samples applied for network generation. 93 data were utilized for network generation and 10 data of strengthened RC slab S812-1100 used for testing. A comparison between experimental deflection and predicted in training stage is evaluated on Figure 7.10. A coefficient of determination and MSE performance function equal to 0.83 and 0.00089, respectively, presented in training stage between predicted and experimental deflection. The created network is tested for the 10 deflection data (S812-1100) by evaluation between experimental and predicted deflection as well as shown in Figure 7.11 and Table 7.6. The coefficient of determination and MSE performance function were 0.776 and 0.0014 respectively. The load-deflection of slab S812-1100 was evaluated with the load-deflection predicted by GRNN (Figure 7.12).

The comparison results between experimental and predicted load-deflection showed an appropriate agreement between them.

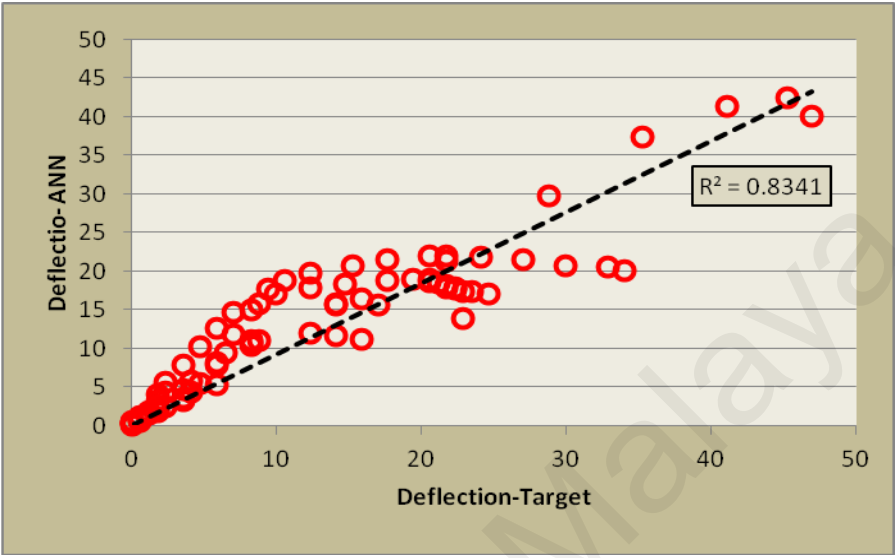


Figure 7.10: An evaluation between predicted and target deflections on failure load of CFRP strengthened RC slab in GRNN training phase

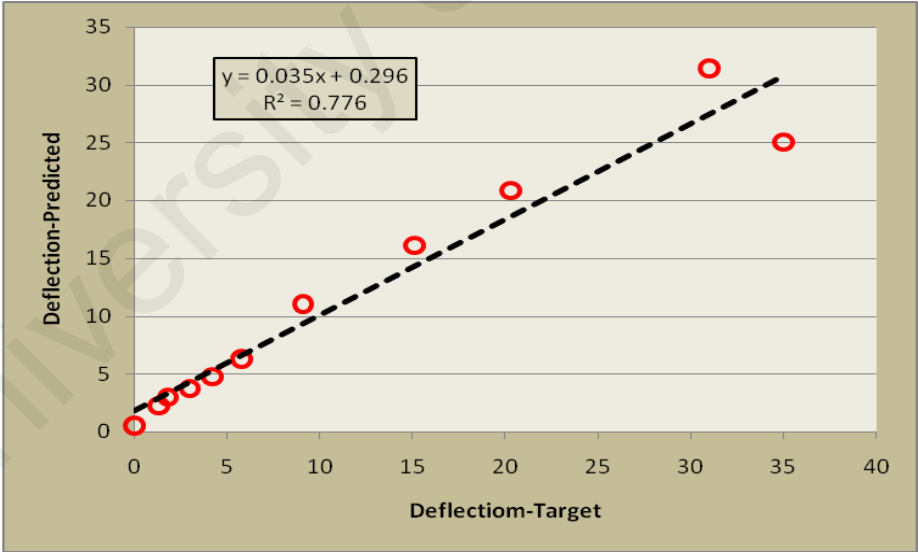


Figure 7.11: An evaluation between predicted and target deflections of failure load on CFRP strengthened RC slab in GRNN testing phase

Table 7.6: The GRNN testing MSE for predicted deflection of slab S812-1800

Neurons (n)	Exp. Deflection Δ_{Exp} (mm)		Network Deflection Δ_{Net} (mm)		$\frac{\Delta_{Net}}{\Delta_{Exp}}$	E= $\Delta_{Exp}-\Delta_{Net}$	E ²
	Real	Normalized	Real	Normalized			
1	0	0.1	-0.5	0.09	-	0.0088	7.8E-05
2	1.32	0.12	0.99	0.11	0.75	0.0055	3.0E-05
3	1.83	0.13	2.3	0.14	1.26	-0.0091	8.3E-05
4	3	0.15	3.69	0.17	1.23	-0.0157	2.5E-04
5	4.2	0.17	4.9	0.18	1.17	-0.0139	1.9E-04
6	5.8	0.19	6.2	0.21	1.07	-0.0157	2.5E-04
7	9.1	0.25	10.0	0.27	1.10	-0.0210	4.4E-04
8	15.1	0.36	14.0	0.34	0.93	0.0220	4.9E-04
9	20.3	0.44	18.2	0.41	0.90	0.0295	8.7E-04
10	31	0.63	25.0	0.53	0.81	0.1048	1.1E-02
MSE= $\sum E^2/n$							0.0014

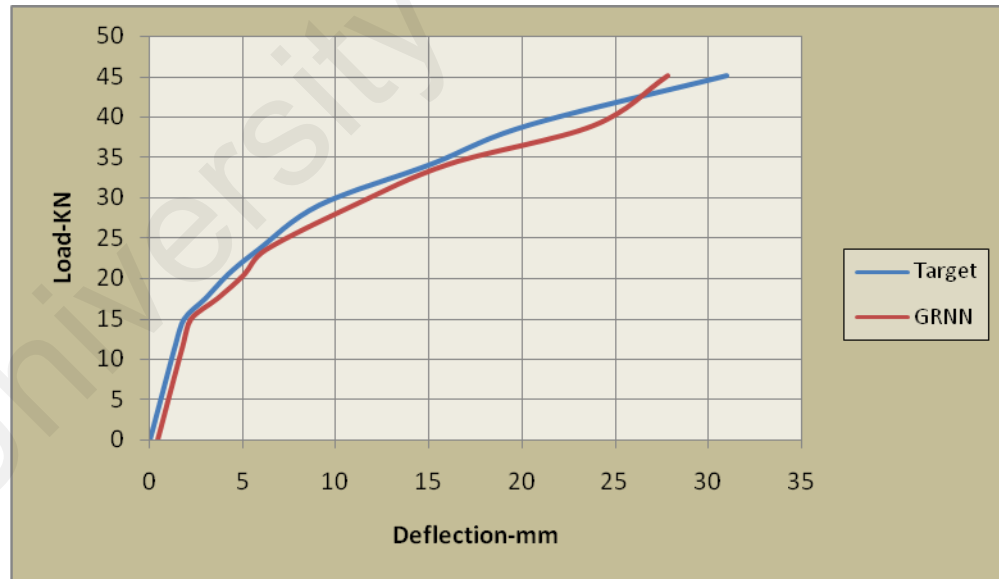


Figure 7.12: An assessment between experimental load-deflections analysis and predicted by GRNN for slab CFRP S812-1100

7.2.2.2 Using GRNN for deflection prediction

Totally, 28 deflection data due to applied loading on the sample CFRP S512-700 are randomly selected for training and testing in GRNN method. 23 data were utilized for training and 5 data for testing. A comparison between normalized experimental results and predicted by GRNN in training stage is shown in Figure 7.13. The coefficient of determination and MSE performance function in training stage was 0.873 and 0.0051 respectively. The created network is tested for the 5 data by evaluation between experimental and predicted deflection (Figure 7.14). The coefficient of determination and MSE were 0.838 and 0.0043 respectively. The selected network had a network spread equal to 0.2. The testing MSE performance function calculation for the five neurons in testing stage is shown in Table 7.7.

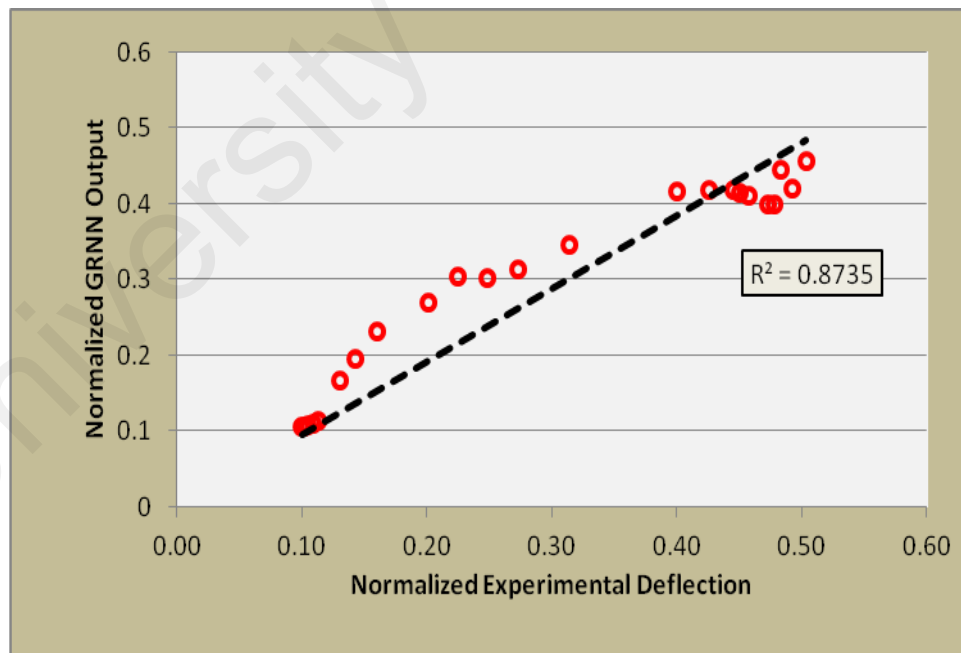


Figure 7.13: An evaluation between normalized target and predicted deflections on the sample CFRP S512-700 in GRNN training phase

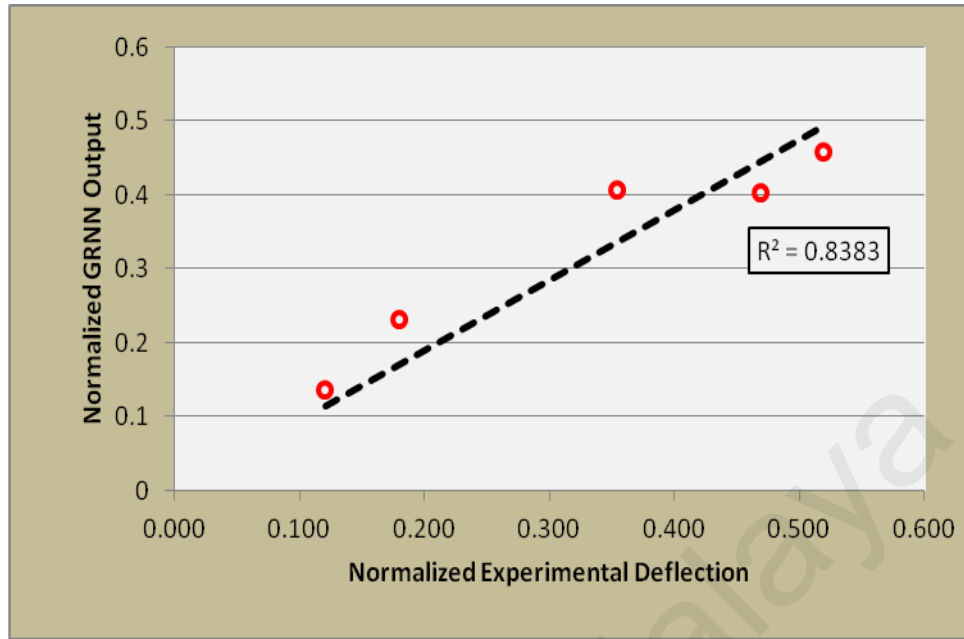


Figure 7.14: An evaluation between normalized target and predicted deflections on the sample CFRP S512-700 in GRNN testing phase

Table 7.7: The GRNN testing MSE for the predicted deflection of S512-700

Neurons (n)	Exp. Deflection Δ_{Exp} (mm)		Network Deflection Δ_{Net} (mm)		$\frac{\Delta_{Net}}{\Delta_{Exp}}$	E= $\Delta_{Exp}-\Delta_{Net}$	E ²
	Real	Normalized	Real	Normalized			
1	1.22	0.12	1.15	0.03	0.95	0.09	0.0081
2	4.68	0.18	5.3	0.13	1.13	0.05	0.0025
3	14.96	0.35	17.1	0.41	1.14	-0.053	0.00278
4	21.16	0.47	19.83	0.40	0.93	0.065	0.00423
5	24.1	0.52	21.03	0.46	0.87	0.061	0.00377
MSE= $\sum E^2/n$							0.0043

7.3 Focused Feed-forward Time-delay Neural Network

7.3.1 FFTDNN for load-deflection analysis of non-strengthened RC slab

In this part, FFTDNN is applied for load-deflection analysis of non-strengthened RC slab by using an internal tapped delay to make dynamic space during network generation. From 378 data, 362 data used for network generation and 16 selected data from slab 100-3T10-1800 applied for network testing. The network generation is included of network training, verifying, and testing. The architecture of selected network is shown in Figure 7.15. The selected network have 3 hidden layer with 12, 7, and 3 neurons in first, second, and third hidden layer respectively. The transfer functions from input layer to output layer were Tansig, Logsig, Tansig, and Purelin. The slab length, thickness, steel bar, and loading were neurons of input layer and the slab mid-span deflection was neuron in output layer.

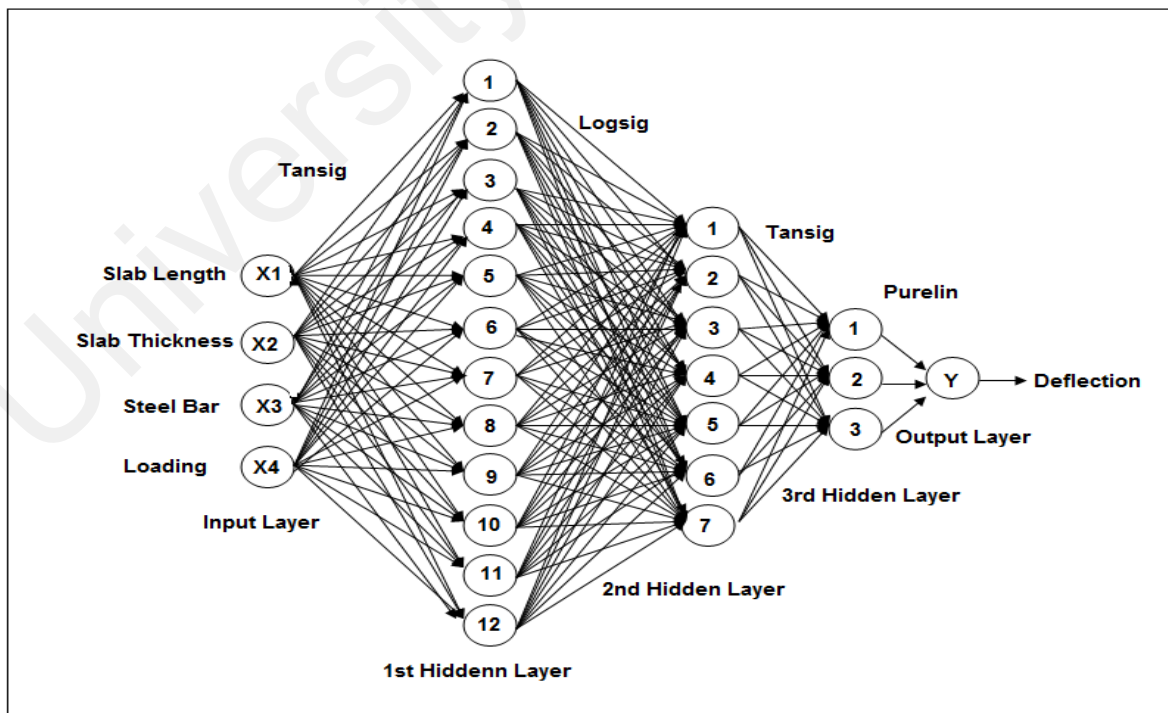


Figure 7.15: The FFTDNN architecture for non-strengthened RC slab

The MSE performance function and correlation of determination R^2 of created network were $9.65e-05$ and 0.995 , respectively, as well as shown in Figures 7.16 and 7.17.

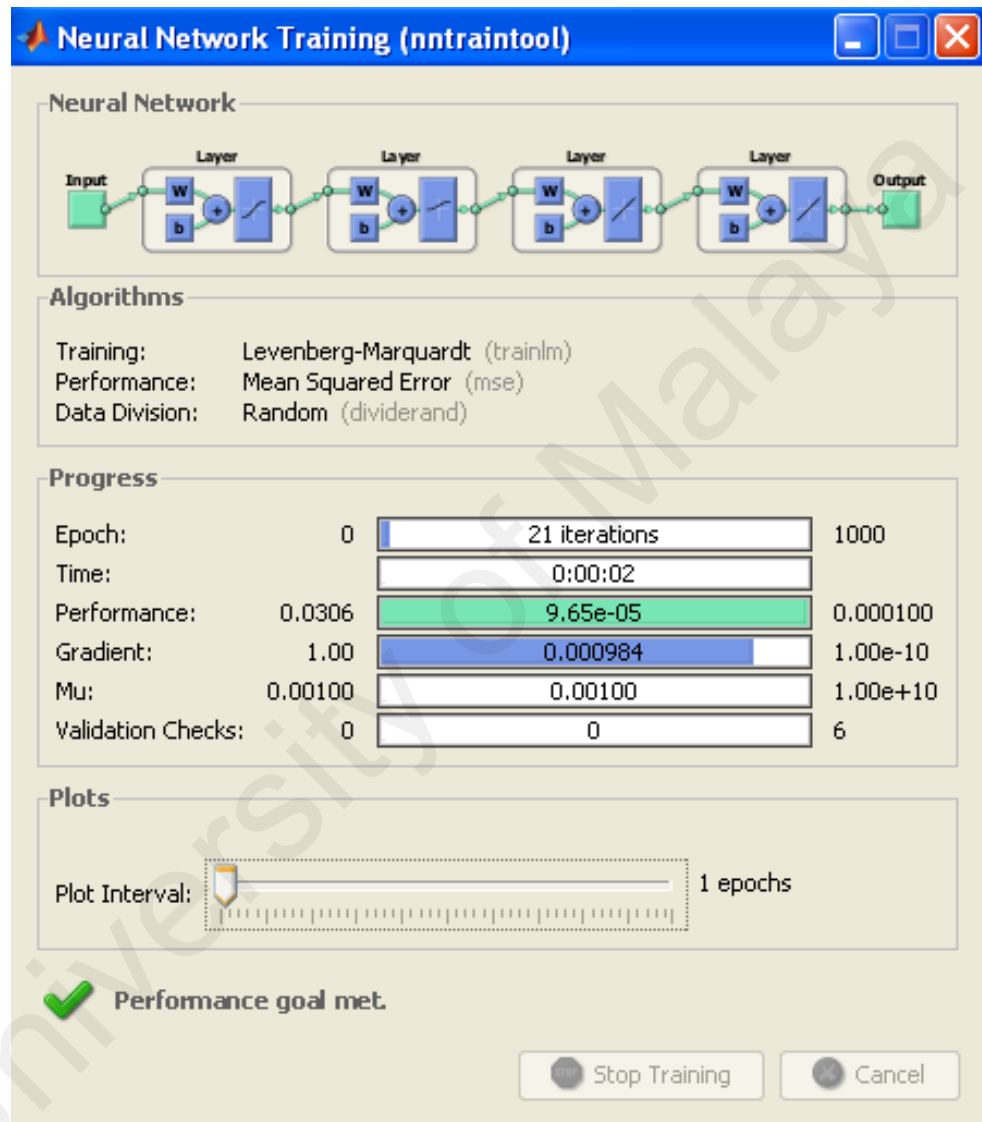


Figure 7.16: The nntraintool running in the FFDNN training stage for the non-strengthened RC slab

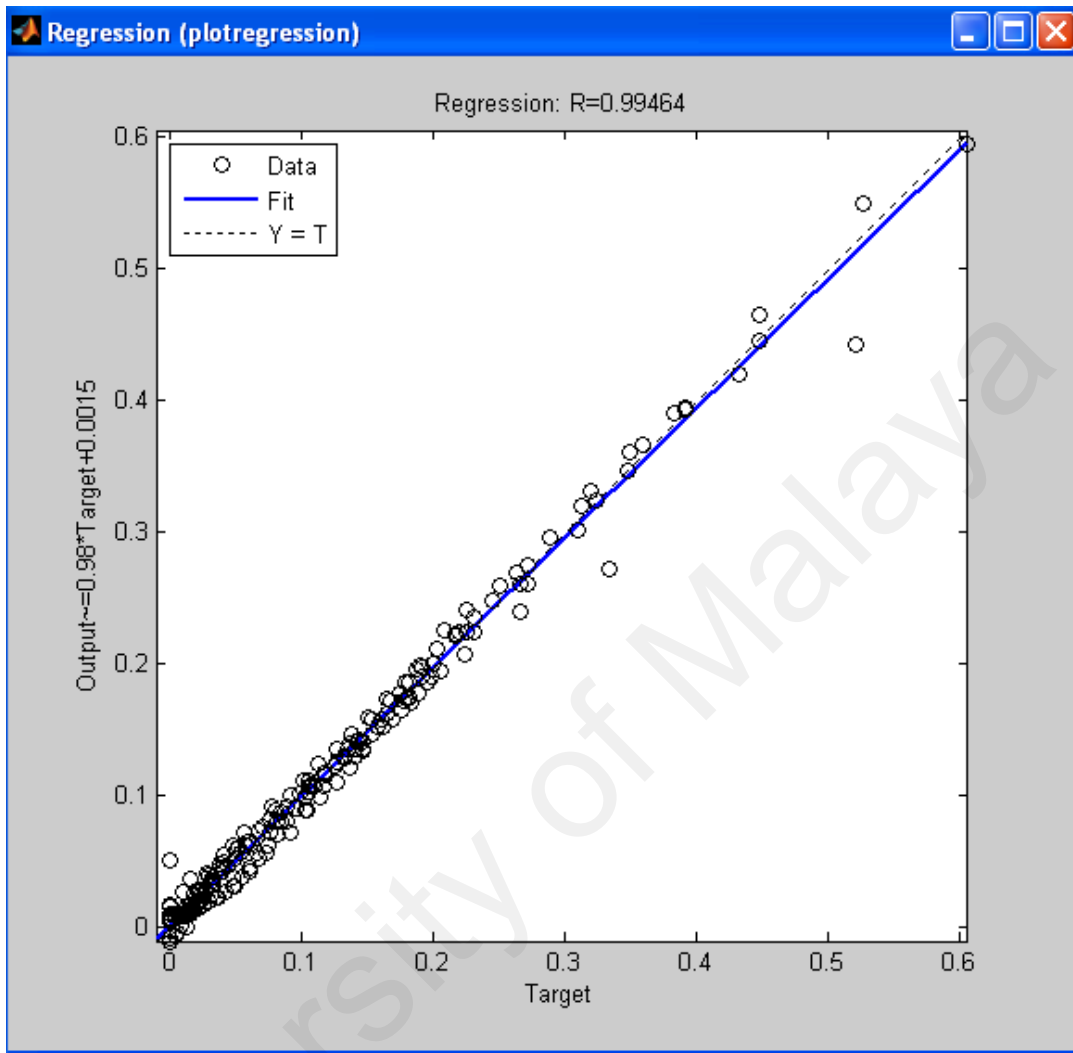


Figure 7.17: A plot of correlation of determination R^2 for FFTDNN training stage

The generated network was simulated for 16 data of slab 100-3T10-1800 and the MSE performance function and correlation of determination R^2 in testing stage were 0.00008 and 0.998 respectively.

Table 7.8: The FFTDNN testing MSE for deflection prediction of slab 100-3T10-1800

Neurons (n)	Exp. Deflection Δ_{Exp} (mm)		Network Deflection Δ_{Net} (mm)		$\frac{\Delta_{Net}}{\Delta_{Exp}}$	$E = \Delta_{Exp} - \Delta_{Net}$	E^2
	Real	Normalized	Real	Normalized			
1	0	0	0	0	-	0	2.0E-09
2	0.53	0.014	0.48	0.012569	0.90	0.0014	2.0E-06
3	0.84	0.022	0.74	0.019383	0.88	0.0026	6.9E-06
4	1.14	0.03	0.97	0.025499	0.85	0.0045	2.0E-05
5	1.52	0.04	1.61	0.042356	1.06	-0.0024	5.6E-06
6	2.17	0.057	2.43	0.064028	1.12	-0.0070	4.9E-05
7	3.15	0.083	3.42	0.090115	1.09	-0.0071	5.1E-05
8	4.18	0.11	4.47	0.117612	1.07	-0.0076	5.8E-05
9	5.28	0.139	5.55	0.146022	1.05	-0.0070	4.9E-05
10	6.35	0.167	6.63	0.174504	1.04	-0.0075	5.6E-05
11	7.52	0.198	7.72	0.203246	1.03	-0.0052	2.8E-05
12	8.44	0.222	8.92	0.23462	1.06	-0.0126	1.6E-04
13	9.5	0.25	10.24	0.269377	1.08	-0.0194	3.8E-04
14	10.75	0.283	11.69	0.30758	1.09	-0.0246	6.0E-04
15	12.08	0.318	13.33	0.350716	1.10	-0.0327	1.1E-03
16	13.3	0.35	15.06	0.396395	1.13	-0.0464	2.2E-03
MSE = $\sum E^2/n$							0.00008

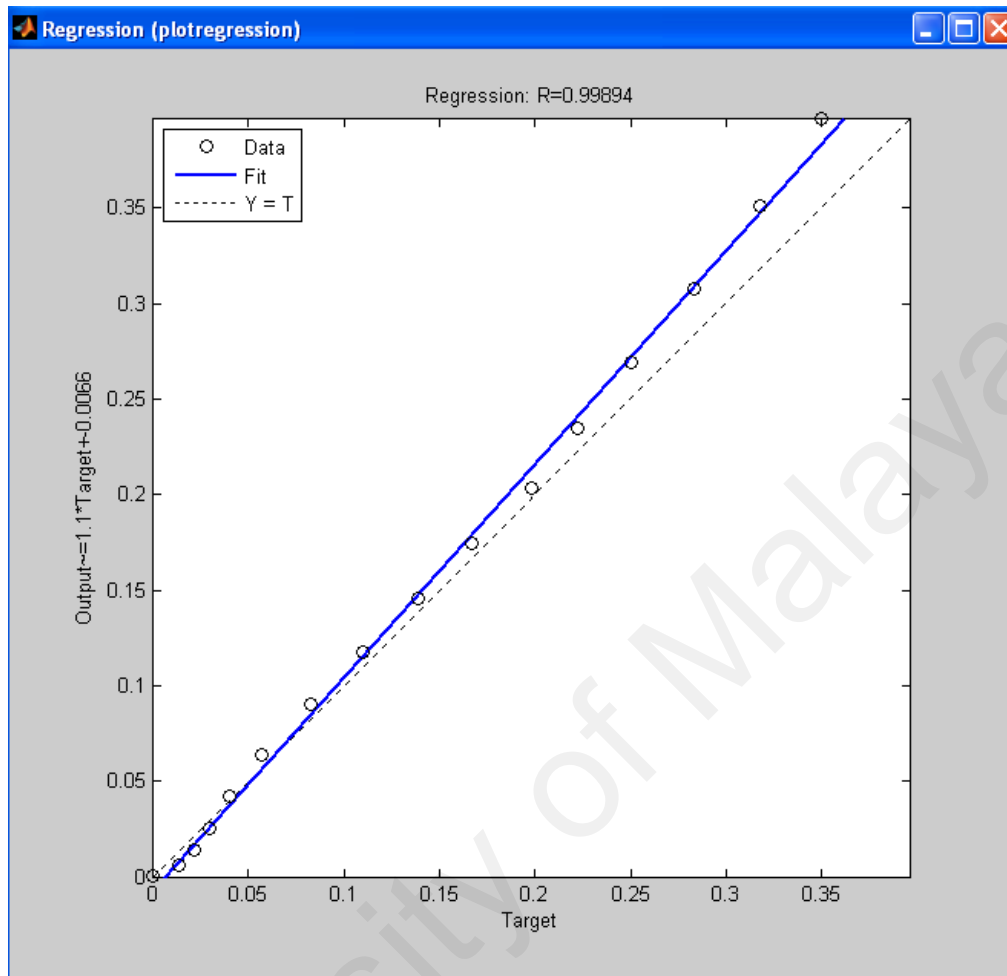


Figure 7.18: Correlation coefficient R^2 plot for slab 100-3T10-1800 using FFTDNN

7.3.2 FFTDNN for load-deflection analysis of CFRP strengthened RC slab

In this part, FFTDNN is applied to predict mid-span deflection of CFRP strengthened RC one-way slab. Totally 103 input data were uploaded and normalized in MATLAB software. Loading, CFRP length and width was input layer and mid-span deflection was output layer. The back-propagation algorithm was trained by TRAINLM training function and validated by MSE performance function. The generated network gave

MSE performance functions of $8.4\text{e-}5$ in training stage (Figure 7.19). The network response after training was compared with the training input (Figure 7.20).

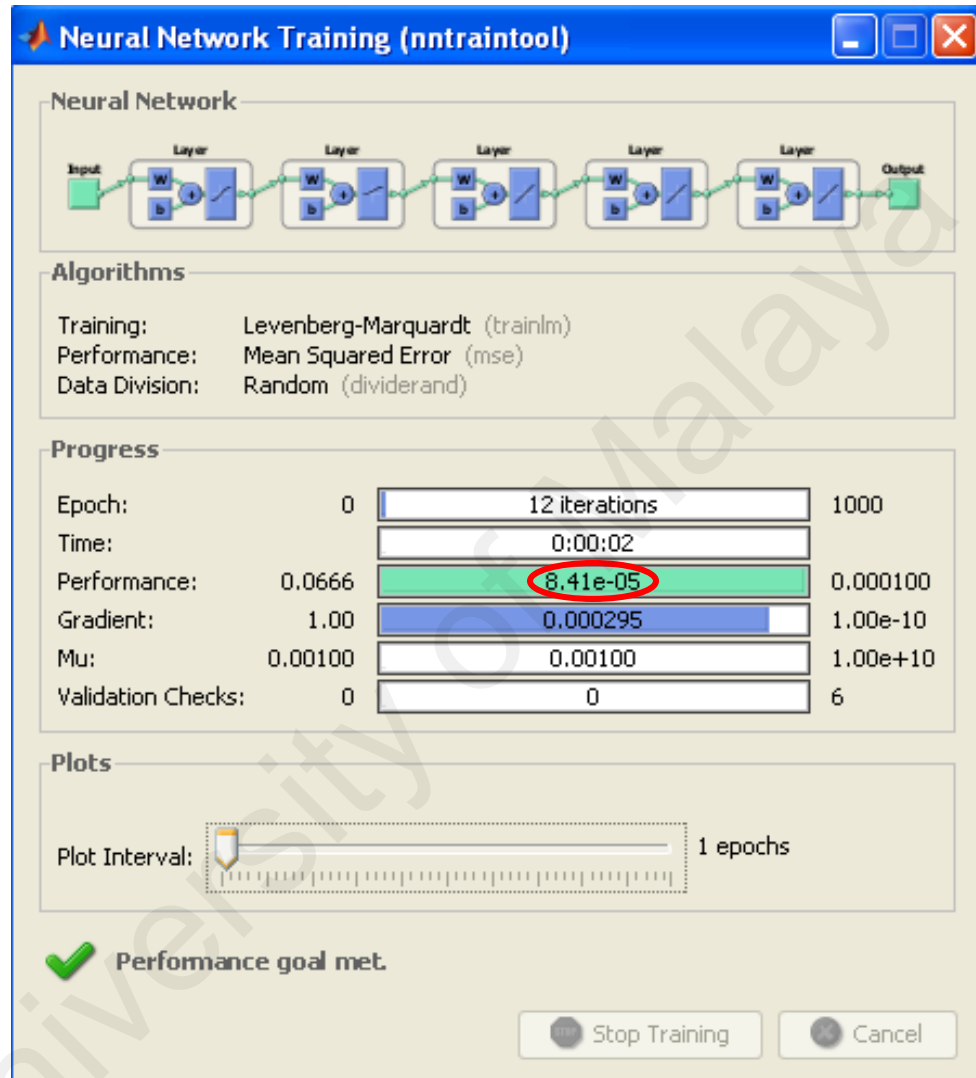


Figure 7.19: FFDNN training process for load-deflection curve prediction of CFRP strengthened RC slab

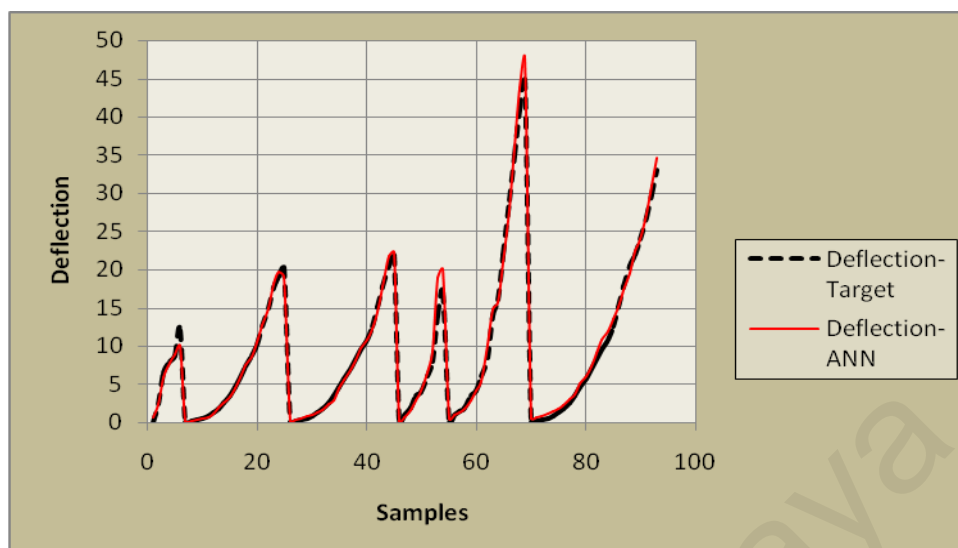


Figure 7.20: A comparison between FFTDNN output and experimental results for deflection of CFRP strengthened RCslab

The generated load-deflection analysis by network shows good correlation with the experimental results (Figure 7.21). The coefficient of determination in training phase was 0.987. After training and validation, 10 load-deflection data of samples S812-1100 were utilized for network testing. The network output after training was compared with the input data for testing stage. The MSE calculation for the load-deflection of slab S812-1100 in testing stage is shown in Table 7.9. The MSE performance function between the experimental and predicted outputs after the testing process was 0.00021. The coefficient of determination of 0.977 is an acceptable relationship between experimental results and predicted by FFTDNN in the testing process for slab S812-1100 (Figure 7.22). A comparison between real load-deflection curve and predicted by FFTDNN for the slab S812-1100 is shown in Figure 7.23.

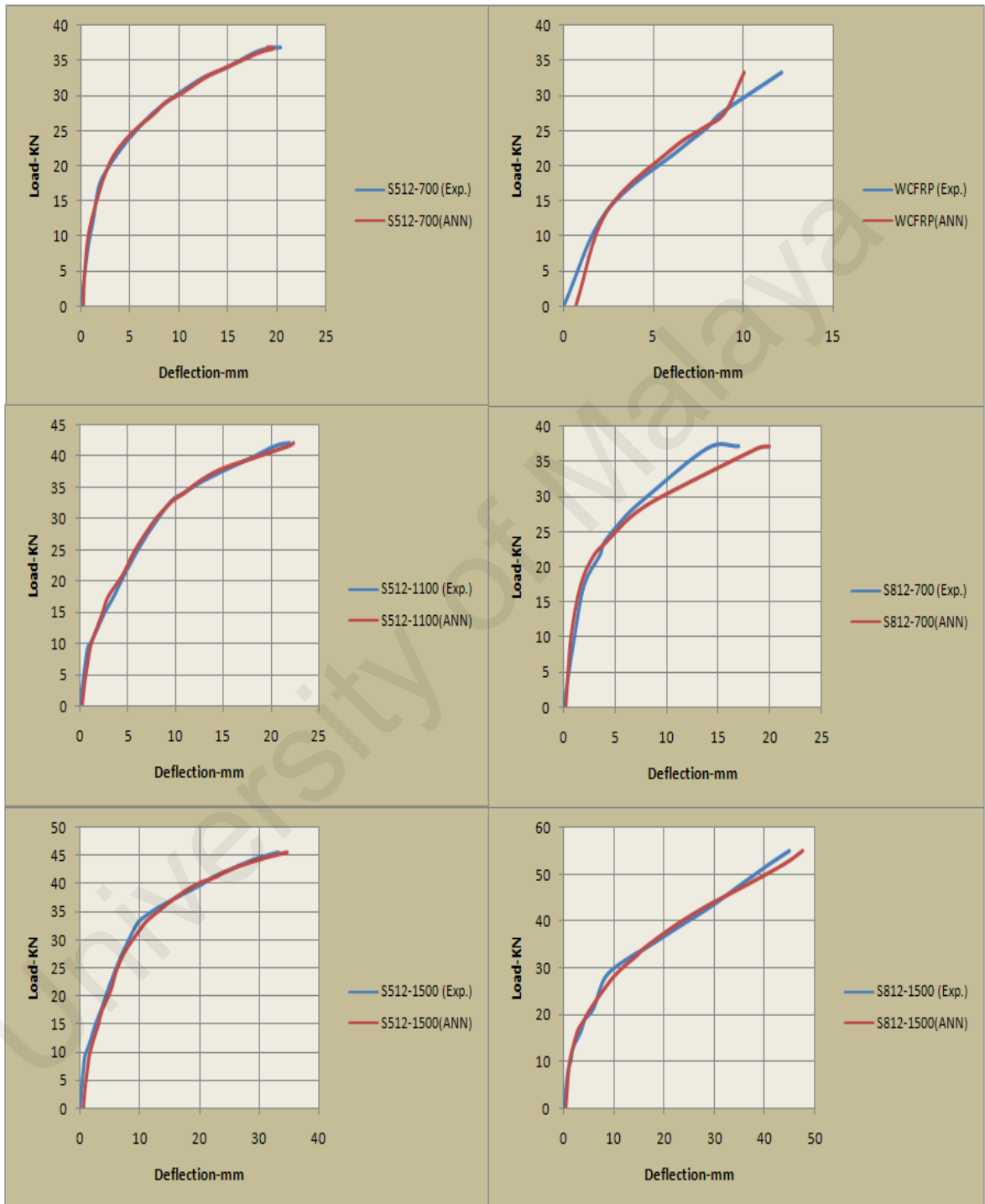


Figure 7.21: An evaluation between predicted and experimental load-deflection analysis in FFDNN training phase for CFRP strengthened RC slab

Table 7.9: The FFTDNN testing MSE for deflection prediction of slab S812-1100

Neurons (n)	Exp. Deflection Δ_{Exp} (mm)		Network Deflection Δ_{Net} (mm)		$\frac{\Delta_{Net}}{\Delta_{Exp}}$	E= $\Delta_{Exp}-\Delta_{Net}$	E^2
	Real	Normalized	Real	Normalized			
1	0	0.1	0.75	0.11	-	-0.0127	1.6E-04
2	1.32	0.12	1.28	0.12	0.97	-0.0010	1.0E-06
3	1.83	0.13	2.10	0.13	1.15	-0.0040	1.6E-05
4	3	0.15	3.33	0.16	1.11	-0.0067	4.5E-05
5	4.2	0.17	4.02	0.17	0.96	0.0016	2.5E-06
6	5.8	0.19	4.95	0.18	0.85	0.0058	3.4E-05
7	9.1	0.25	8.04	0.24	0.88	0.0131	1.7E-04
8	15.1	0.36	13.75	0.33	0.91	0.0260	6.8E-04
9	20.3	0.44	20.82	0.45	1.03	-0.0144	2.1E-04
10	31	0.63	30.47	0.62	0.98	0.0113	1.3E-04
MSE= $\sum E^2/n$							0.00021

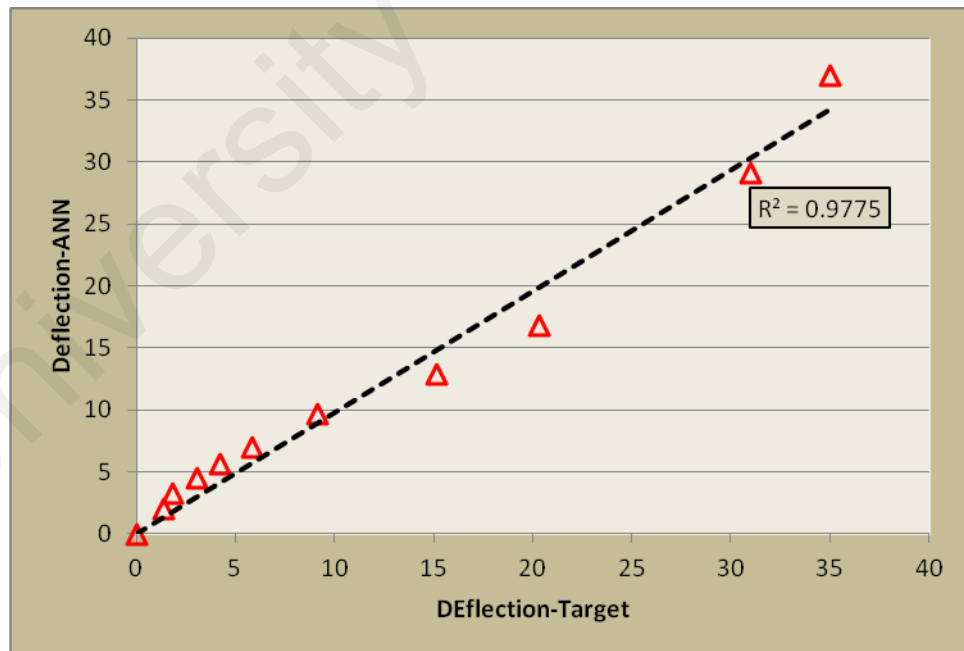


Figure 7.22: Evaluation between experimental and predicted deflection after FFTDNN testing stage on slab S812-1100

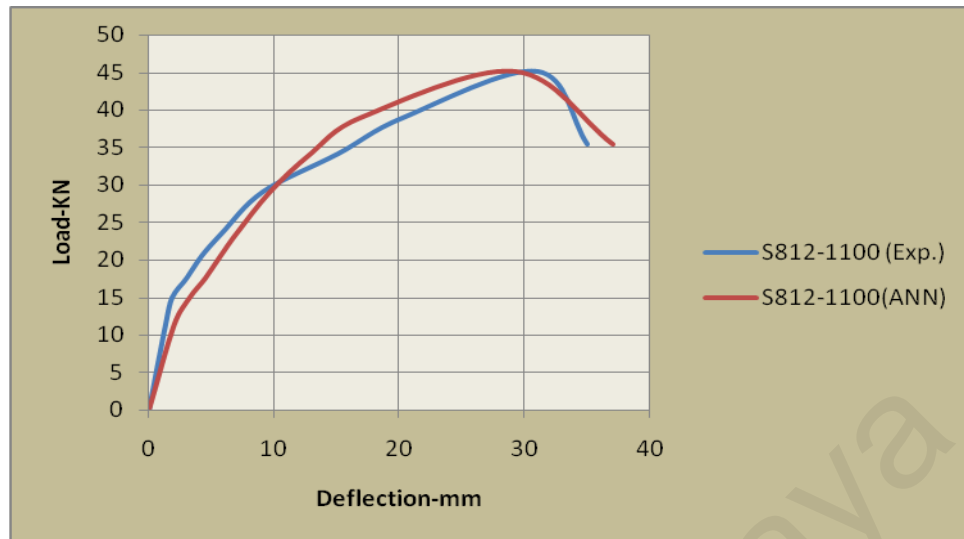


Figure 7.23: Load deflection curve from FFTDNN and experimental work for slab S812-1100

7.3.3 Using FFTDNN for prediction of crack width

Several networks with different architecture were tested to determine the optimum network with the minimum error and acceptable correlation of determination. The architecture of the selected network is shown in Figure 6.21. The loading, CFRP length and width, and crack location X and Y were used as input layers and the crack width at maximum loading applied on the slab was the output layer. The selected architecture was trained and validated with 86 data. The generated network was tested for the crack width at maximum loading of the 7 experimental samples. The transfer functions in hidden layer were Tansig, Logsig, and Pureline.

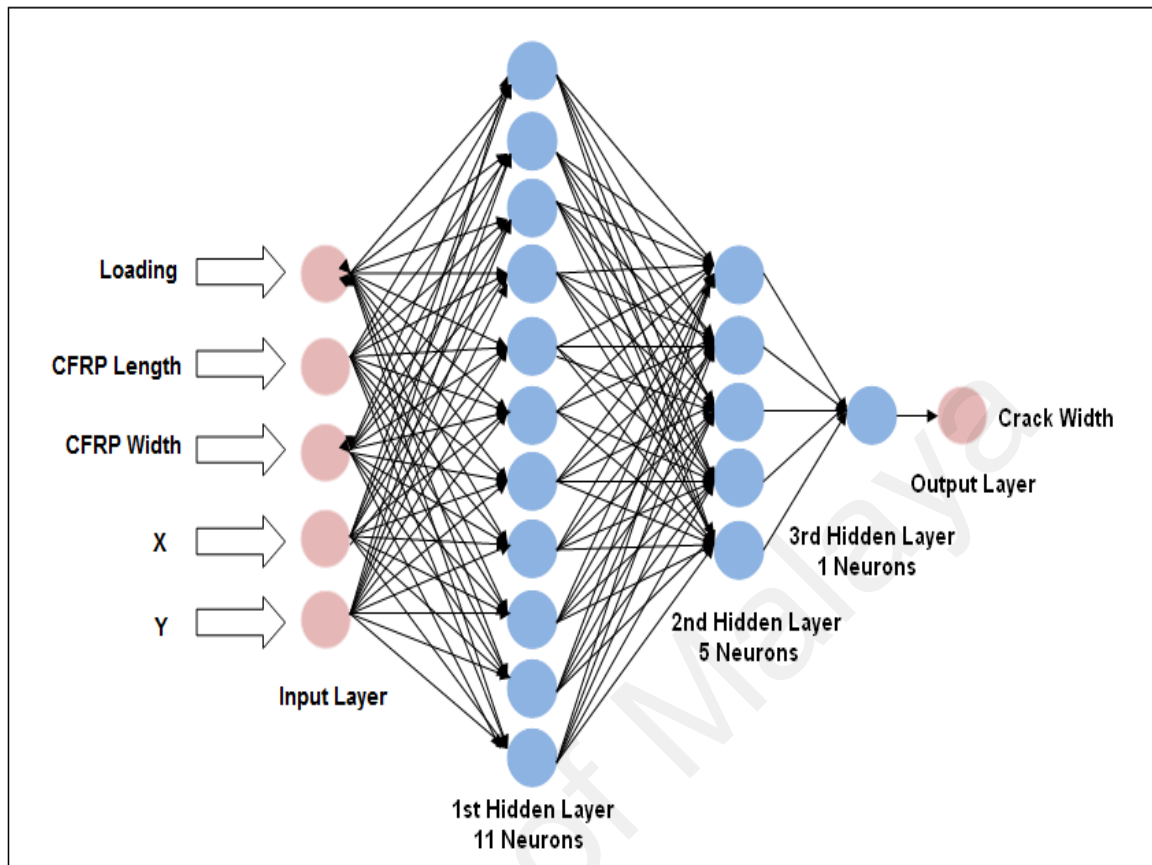


Figure 7.24: The selected FFDNN architecture for crack width prediction of CFRP strengthened RC slab at maximum applied load

The MSE performance function for the generated network in training phase was 0.00238. An evaluation between the target and predicted crack width at various loading during the training phase gave a correlation of determination R^2 of 0.815 shown in Figure 7.25. After training, the network was tested to predict the crack width at maximum load. The error calculation in testing phase is presented in Table 7.10. The network predicted a maximum crack width with performance function of 0.008. The correlation of determination R^2 in testing phases was 0.97 respectively (Figure 7.26).

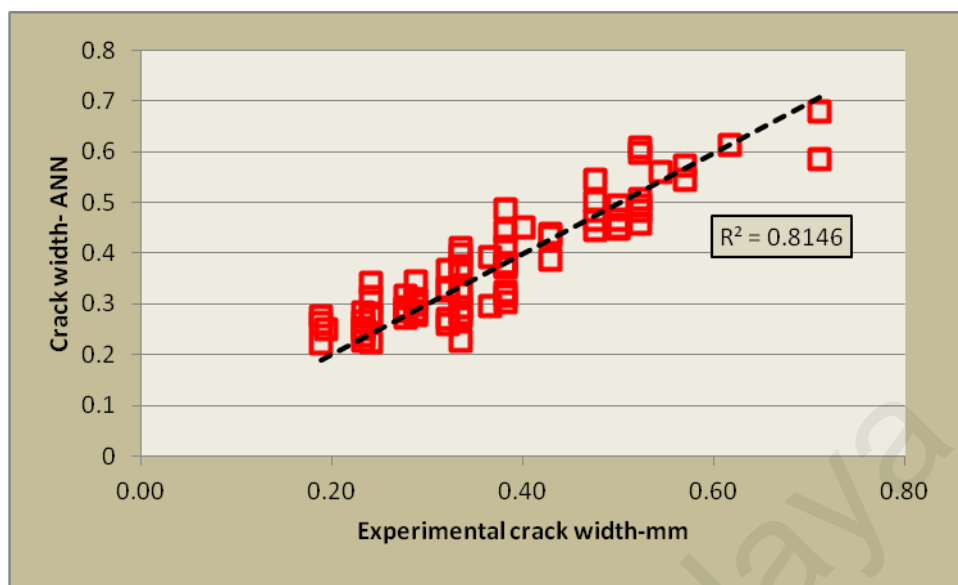


Figure 7.25: Evaluation between experimental and predicted crack width on maximum applied loading on CFRP strengthened RC slab using FFTDNN after training phase

Table 7.10: The testing MSE for maximum crack width predicted by FFTDNN

Slab	Exp. Deflection Δ_{Exp} (mm)		Network Deflection Δ_{Net} (mm)		$\frac{\Delta_{Net}}{\Delta_{Exp}}$	$E = \Delta_{Exp} - \Delta_{Net}$	E^2
	Real	Normalized	Real	Normalized			
S512-700	0.75	0.81	0.65	0.71	0.87	0.093	0.0087
S512-1100	0.75	0.81	0.65	0.72	0.87	0.090	0.0082
S512-1500	0.8	0.85	0.63	0.69	0.79	0.159	0.0253
S812-700	0.35	0.43	0.32	0.40	0.91	0.024	0.0006
S812-1100	0.35	0.43	0.35	0.43	1.00	-0.005	0.0000
S812-1500	0.3	0.38	0.25	0.34	0.83	0.045	0.0020
WCFRP	0.85	0.90	0.74	0.79	0.87	0.106	0.0112
$MSE = \sum E^2/n$							0.008

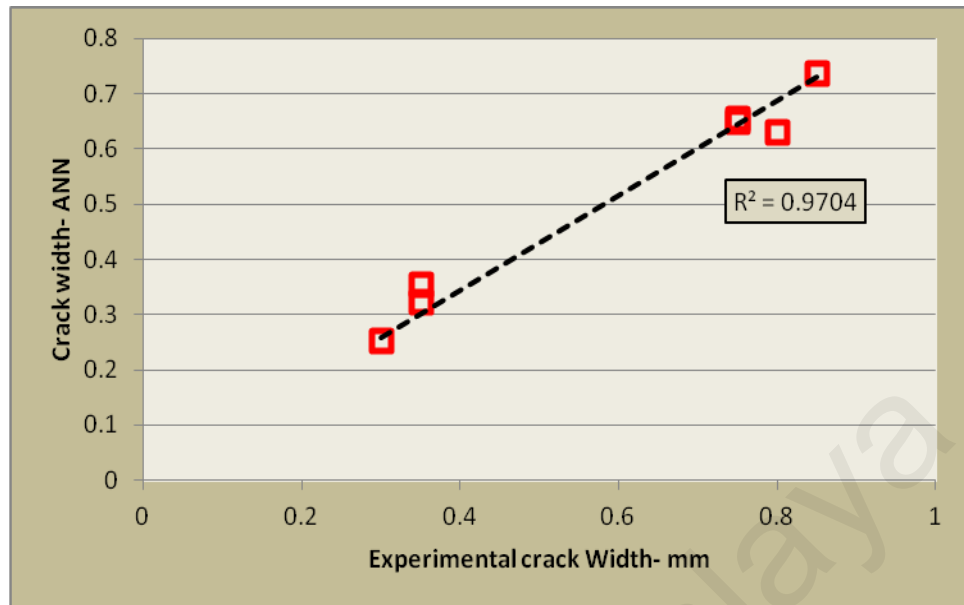


Figure 7.26: Evaluation between experimental and predicted maximum crack width after FFTDNN testing phase

7.4 Recurrent Neural Network

Here the RNN was utilized to predict the load-deflection analysis in non-strengthened and CFRP strengthened RC slab. This was also useful to predict the crack width at maximum load for the CFRP strengthened RC slab.

7.4.1 RNN for load-deflection analysis of non-strengthened RC slab

The architecture of the selected network is shown in Figure 7.27. The selected RNN architecture is included of three hidden layers with 11, 5, and 1 neuron in first, second and third hidden layer respectively. The RNN with the selected architecture was trained and the value of performance function (Figure 7.28) and correlation of determination R^2 (Figure 7.29) in training stage was $4.34e-6$ and 0998 respectively.

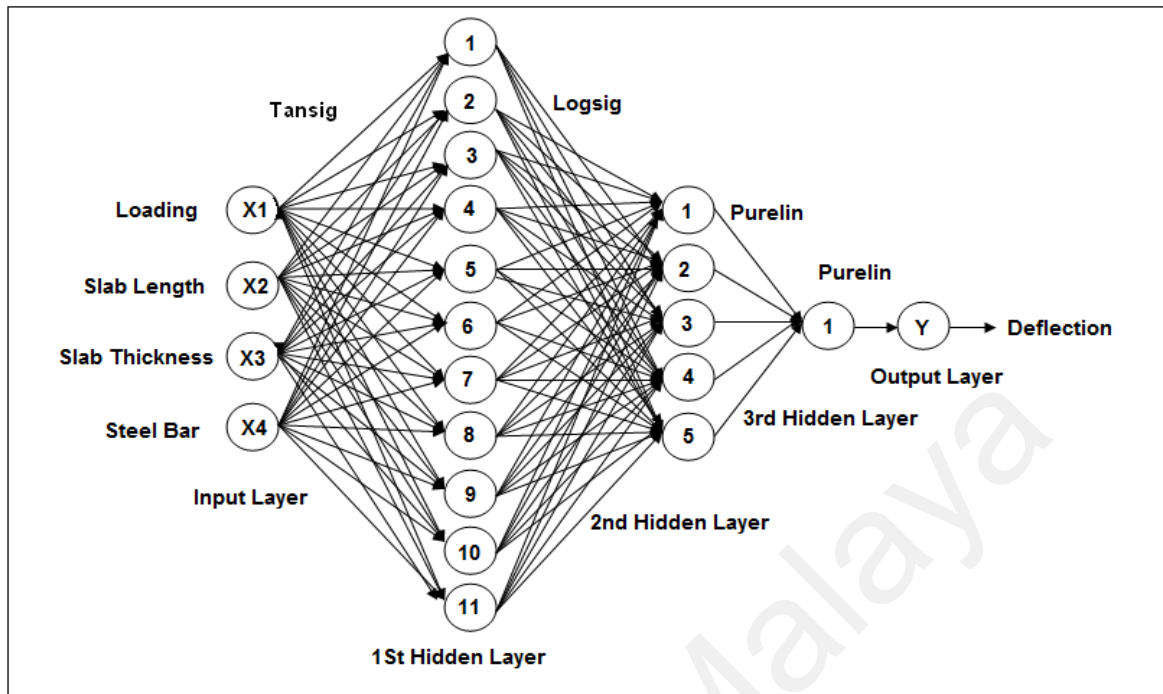


Figure 7.27: The selected network architecture for non-strengthened RC slab using RNN

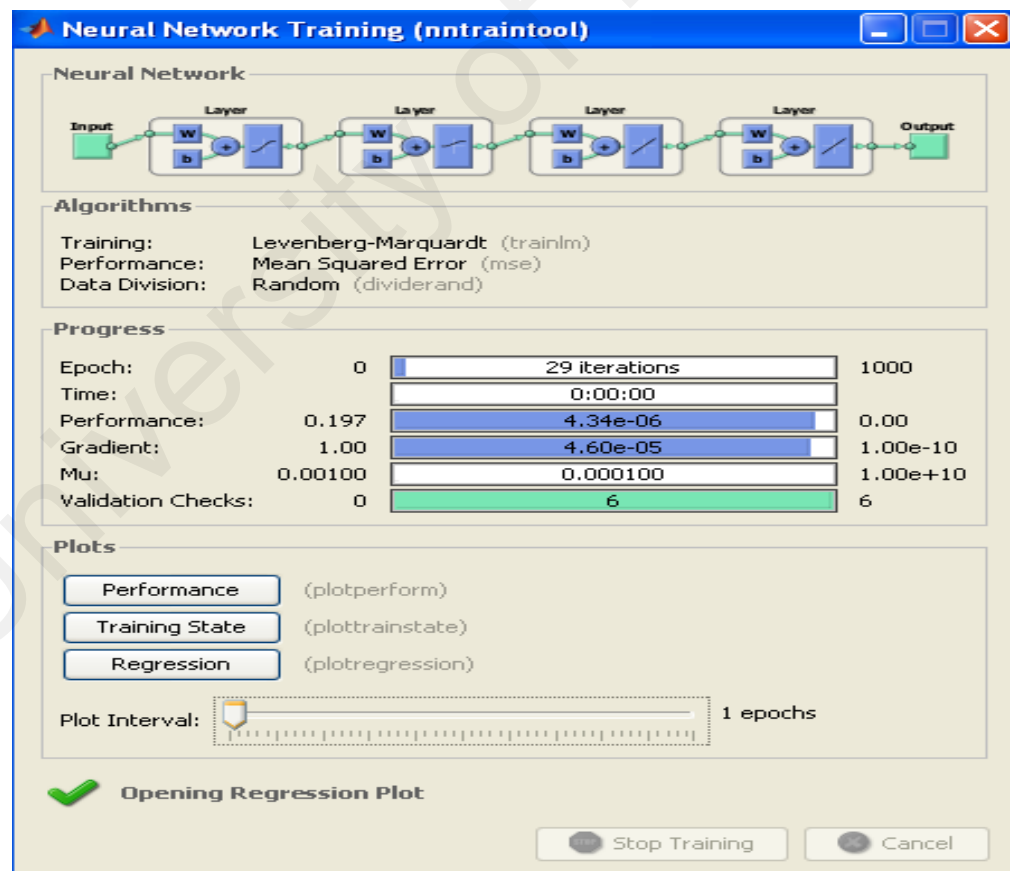


Figure 7.28: RNN running procedure in training stage for non-strengthened RC slab

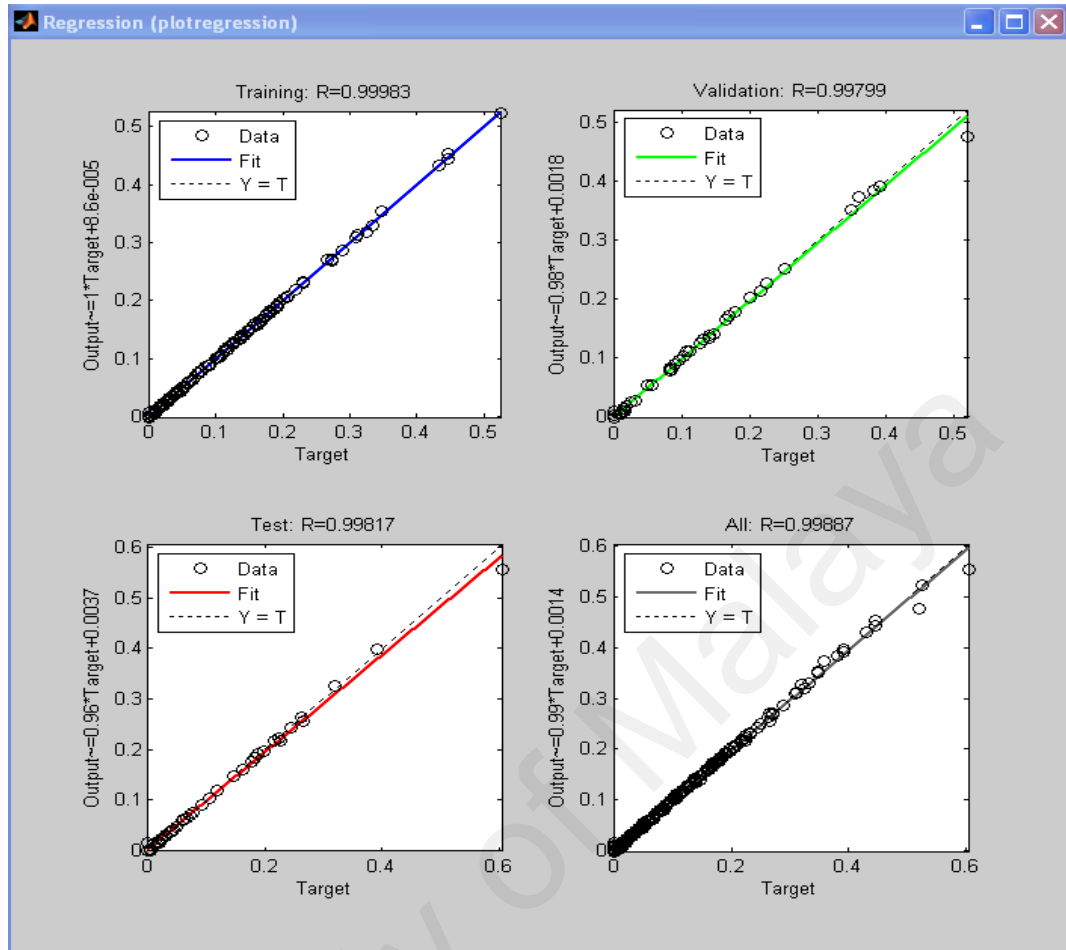


Figure 7.29: The values of correlation of coefficient in network generation for non-strengthened RC slab

The generated network was simulated for 16 testing data of slab 100-3T10-1800 and the RNN output for mid-span deflection was compared with the experimental results. The value of MSE performance function is calculated as well as shown in Table 7.11. The simulated data show a correlation of determination R^2 of 0.98 by comparing the RNN testing output for mid-span deflection with experimental results as shown in Figure 7.30.

Table 7.11: The RNN testing MSE for predicted deflection of slab 100-3T10-1800

Neurons (n)	Exp. Deflection Δ_{Exp} (mm)		Network Deflection Δ_{Net} (mm)		$\frac{\Delta_{Net}}{\Delta_{Exp}}$	E= $\Delta_{Exp}-\Delta_{Net}$	E ²
	Real	Normalized	Real	Normalized			
1	0	0	0	-0.00698	-	0.007	4.87E-05
2	0.53	0.014	0.47	-0.0124	0.89	0.026	6.97E-04
3	0.84	0.022	0.70	-0.0184	0.83	0.040	1.63E-03
4	1.14	0.03	0.96	0.02538	0.85	0.005	2.14E-05
5	1.52	0.04	1.30	0.03411	0.85	0.006	3.47E-05
6	2.17	0.057	2.00	0.05257	0.92	0.004	1.96E-05
7	3.15	0.083	2.91	0.07648	0.92	0.007	4.25E-05
8	4.18	0.11	4.28	0.11276	1.03	-0.003	7.61E-06
9	5.28	0.139	5.34	0.14052	1.01	-0.002	2.30E-06
10	6.35	0.167	5.83	0.1533	0.92	0.014	1.88E-04
11	7.52	0.198	6.03	0.1588	0.80	0.039	1.54E-03
12	8.44	0.222	7.05	0.18549	0.84	0.037	1.33E-03
13	9.5	0.25	8.18	0.21524	0.86	0.035	1.21E-03
14	10.75	0.283	9.53	0.25074	0.89	0.032	1.04E-03
15	12.08	0.318	11.31	0.29763	0.94	0.020	4.15E-04
16	13.3	0.35	13.64	0.35891	1.03	-0.009	7.94E-05
MSE= $\sum E^2/n$							0.000052

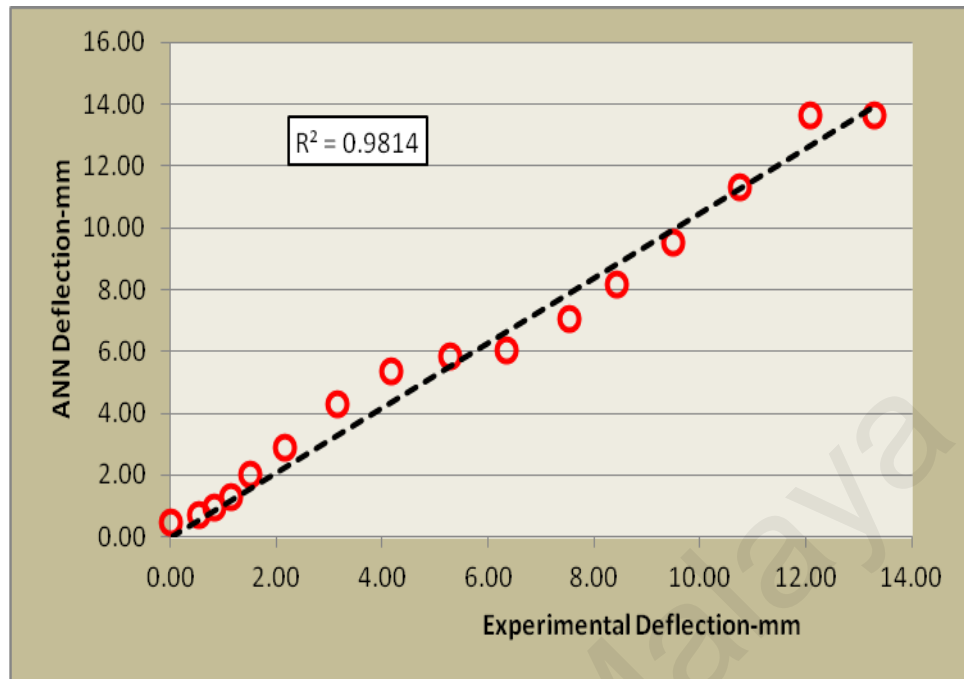


Figure 7.30: A comparing between experimental results and RNN output for mid-span deflection of slab 100-3T10-1800

7.4.2 RNN for load-deflection analysis of CFRP strengthened RC slab

The architecture of selected network is included of one hidden layer with 11 neurons. The transfer function in hidden layer and output were TANSIG and PURELIN respectively. The training process is presented in Figure 7.31 with a MSE performance function of 0.000809.

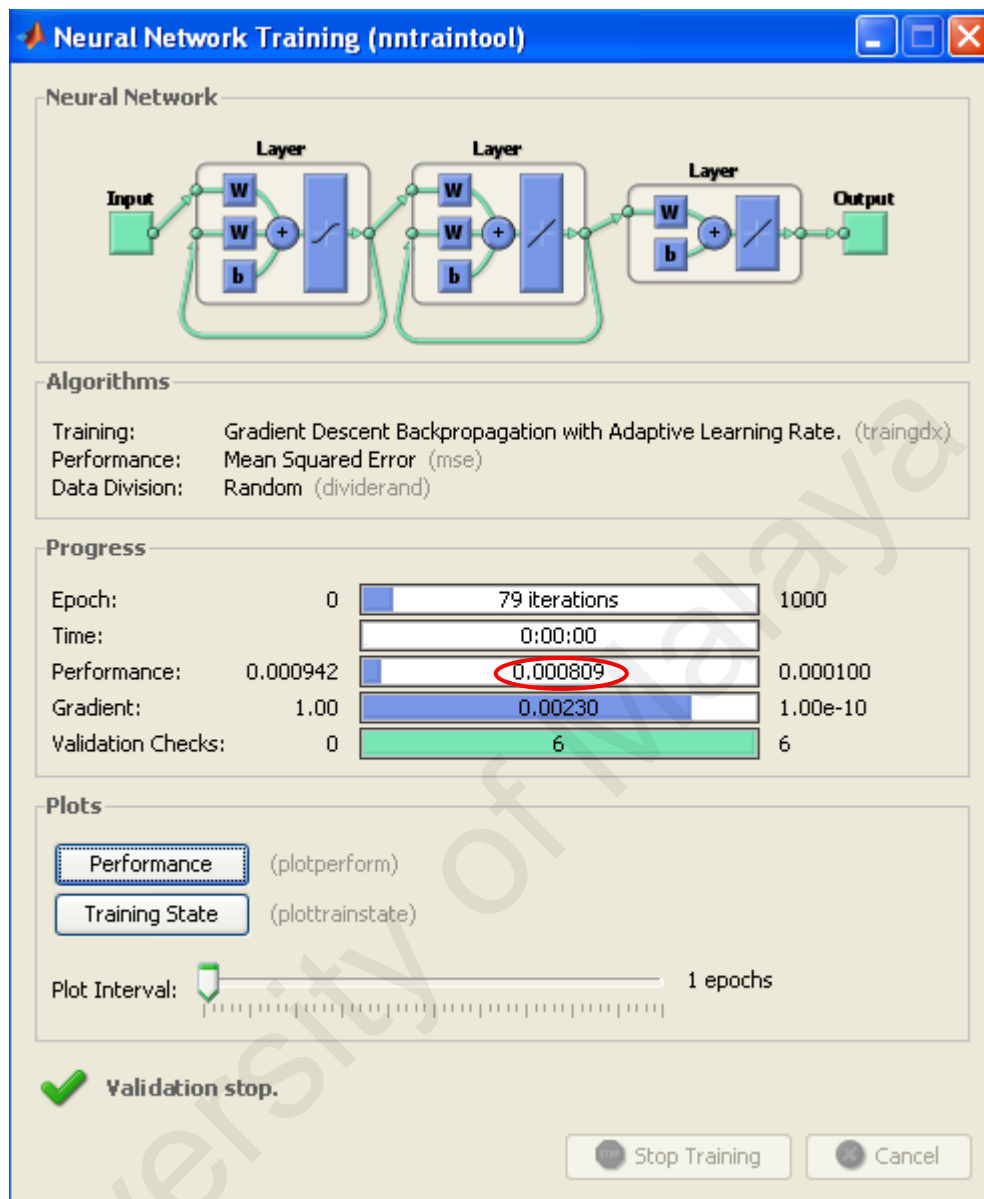


Figure 7.31: RNN training for load-deflection prediction of CFRP strengthened RC slab

The correlation of determination R^2 between experimental results and predicted deflection in training phase was 0.990 (Figure 7.32). The load-deflection data for sample S812-1100 were applied to simulate for the testing network. The RNN testing MSE between for predicted deflection in testing phase was 0.0018 (Table 7.12). Figure 7.33 shows the evaluation between experimental and predicted deflection of slab S812-1800 that indicated a correlation of determination R^2 equivalent to 0.998.

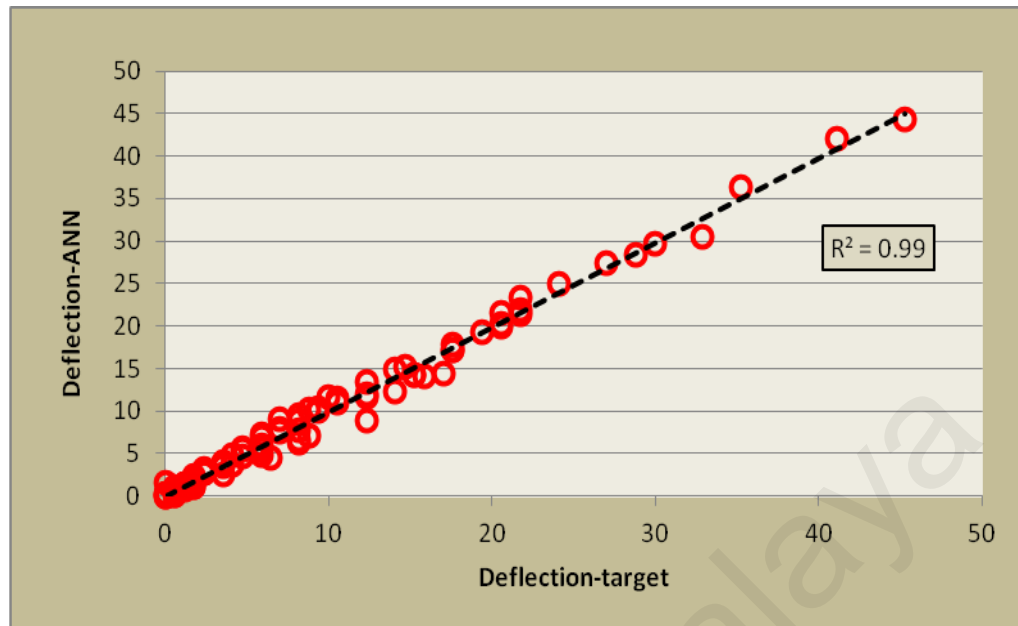


Figure 7.32: Evaluation between experimental and predicted deflection on CFRP strengthened RC slab after RNN training phase

Table 7.12: The RNN testing MSE for predicted mid-span deflection of slab S812-1100

Neurons (n)	Exp. Deflection Δ_{Exp} (mm)		Network Deflection Δ_{Net} (mm)		$\frac{\Delta_{Net}}{\Delta_{Exp}}$	E= $\Delta_{Exp}-\Delta_{Net}$	E^2
	Real	Normalized	Real	Normalized			
1	0	0.1	-0.10	0.10	-	0.0017	0.000003
2	1.32	0.12	1.45	0.13	1.19	-0.0102	0.000103
3	1.83	0.13	2.03	0.14	1.16	-0.0100	0.000100
4	3	0.15	3.61	0.16	1.05	-0.0115	0.000133
5	4.2	0.17	4.76	0.18	0.96	-0.0111	0.000123
6	5.8	0.19	6.19	0.21	0.88	-0.0153	0.000235
7	9.1	0.25	10.06	0.27	0.87	-0.0213	0.000454
8	15.1	0.35	15.56	0.36	0.91	-0.0149	0.000221
9	20.3	0.44	21.59	0.47	1	-0.0275	0.000758
10	31	0.63	30.06	0.61	0.92	0.0183	0.000336
MSE= $\sum E^2/n$							0.0018

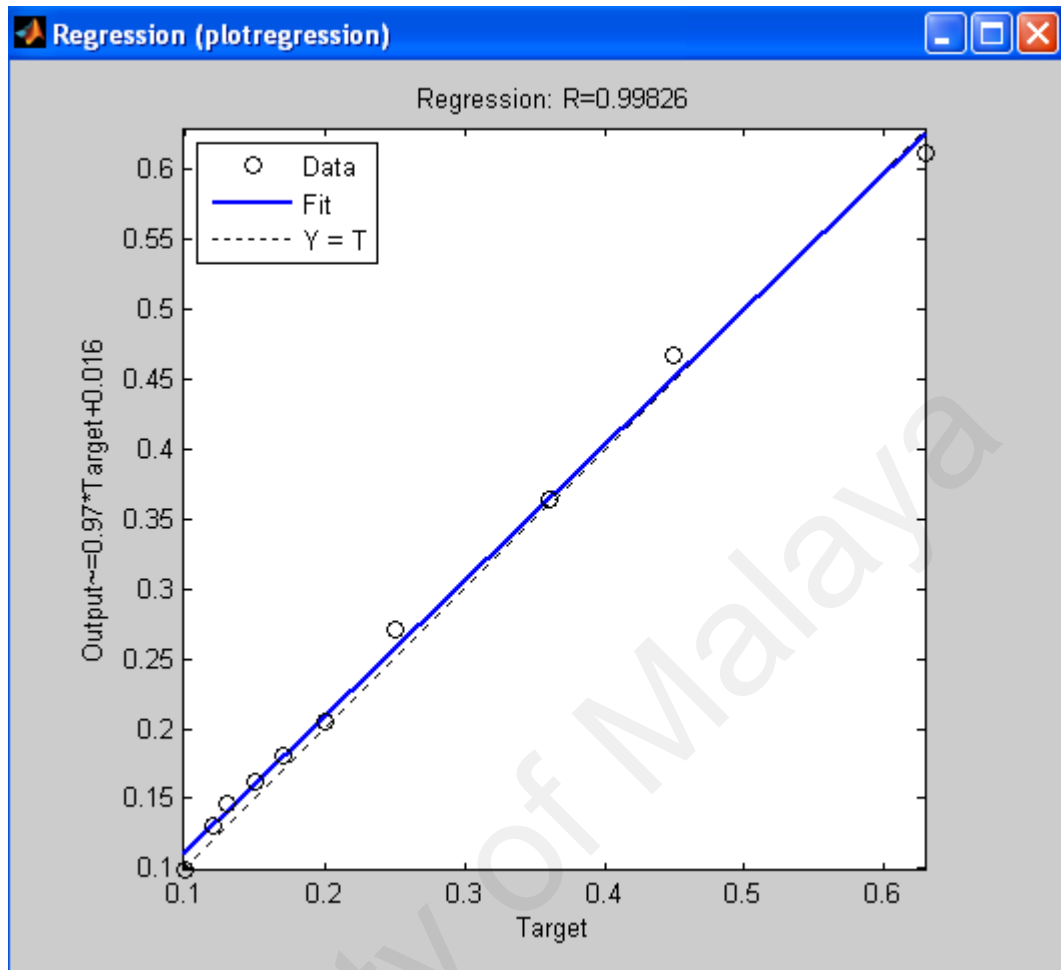


Figure 7.33: Evaluation between experimental and predicted deflection of slab S812-1100 after RNN testing phase

7.4.3 Using RNN for prediction of crack width

A single hidden layer with 8 neurons was the architecture of the selected network for this part for prediction of loading crack width (Figure 7.34). Tansig and Purelin were the chosen transfer function in the hidden layer and output layer respectively. The selected network was trained with a MSE performance function of 0.00116 (Figure 7.35).

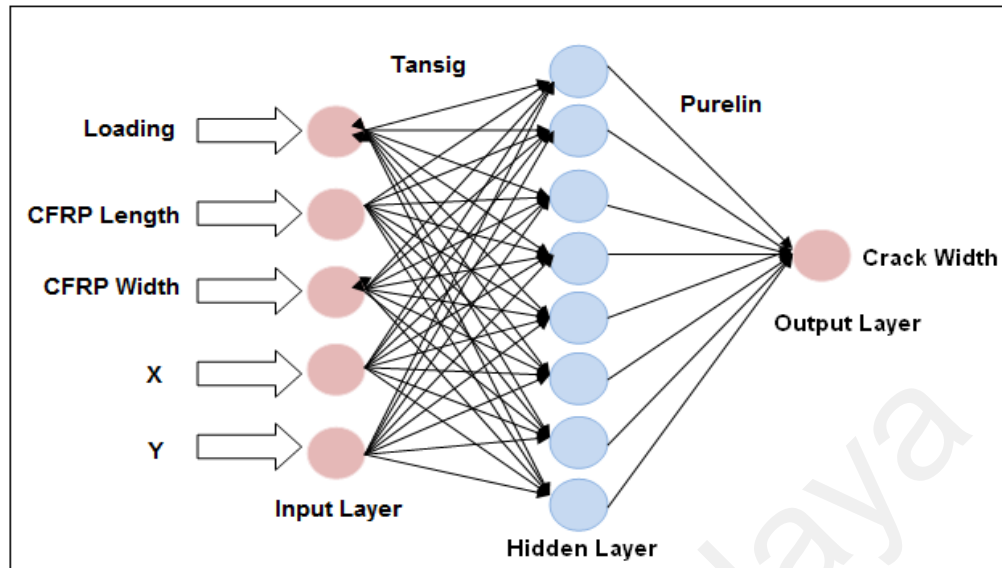


Figure 7.34: The selected RNN architecture for crack width prediction

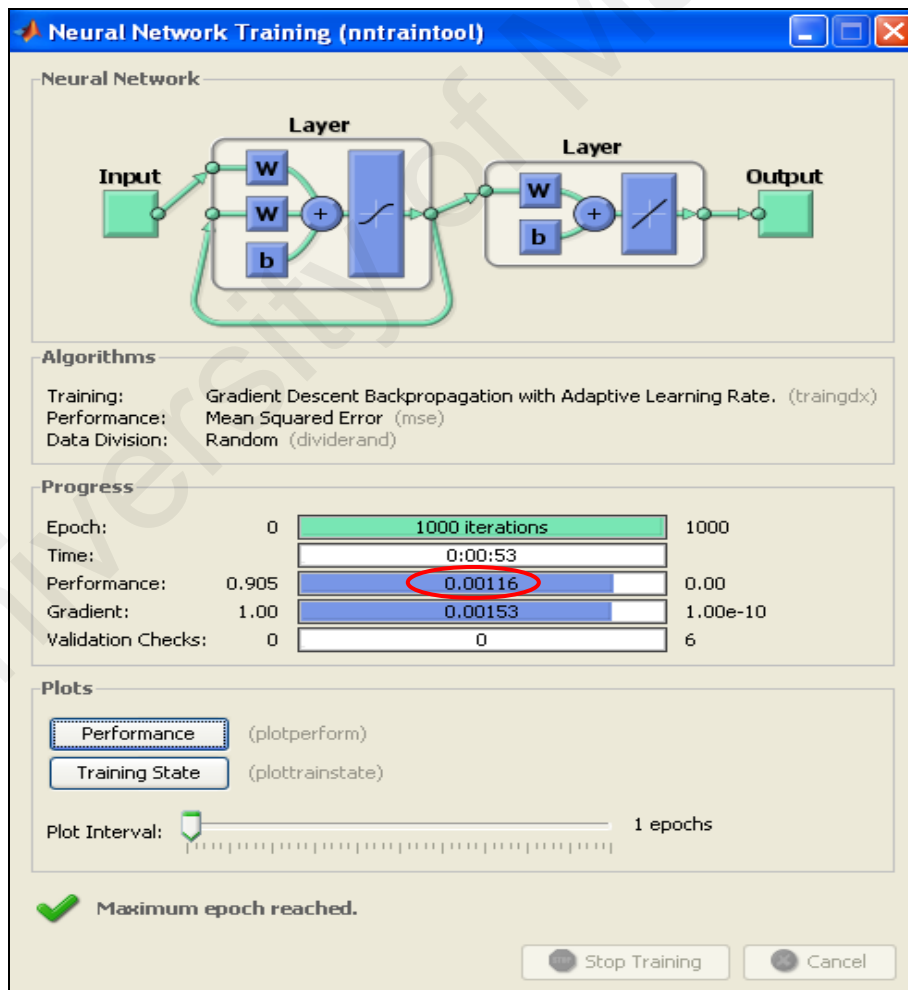


Figure 7.35: RNN training for crack width prediction in maximum applied loading on CFRP strengthened RC slab

In the training phase, the experimental and predicted loading crack widths were compared together and presented in Figures 7.36 and 7.37. The results show that the generated network can be trained to achieve good harmony with the experimental results with a correlation of determination R^2 equivalent to 0.92.

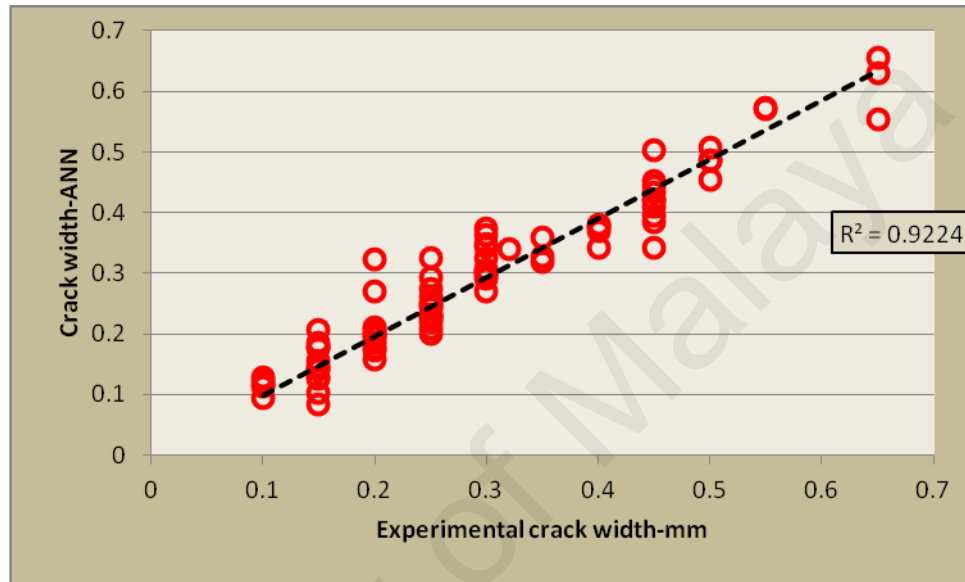


Figure 7.36: Evaluation between experimental and predicted crack width after RNN training phase

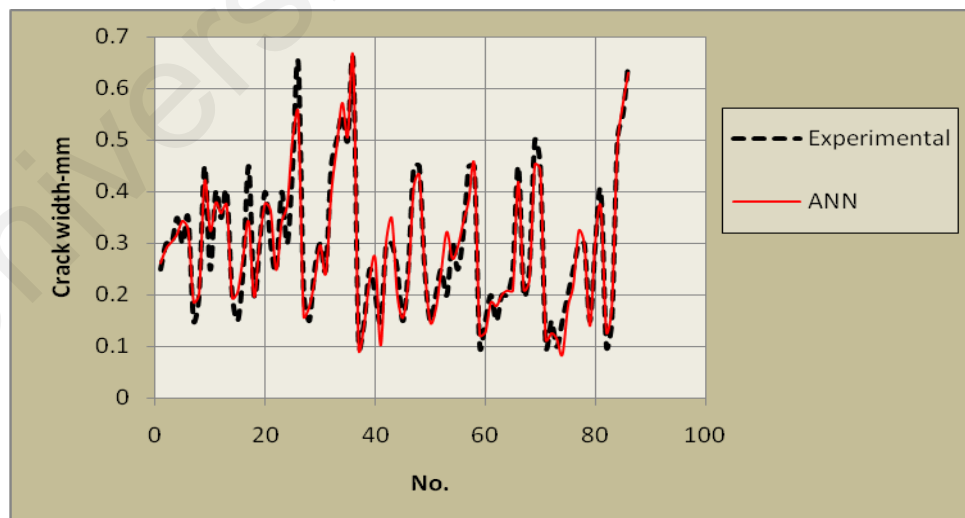


Figure 7.37: A comparison between RNN output and experimental results for crack width after training

The generated network was applied to find the maximum loading crack width. Seven inputs were simulated and the network outputs were compared with the experimental crack width. The testing correlation of determination R^2 between experimental and predicted crack width at maximum loading was 0.96 (Figure 7.38). A comparison between experimental and predicted loading crack width is presented in Figure 7.39. The results with a MSE performance function equivalent to 0.0026 gives an indication that the predicted result using RNN is in good agreement with experimental results (Table 7.13).

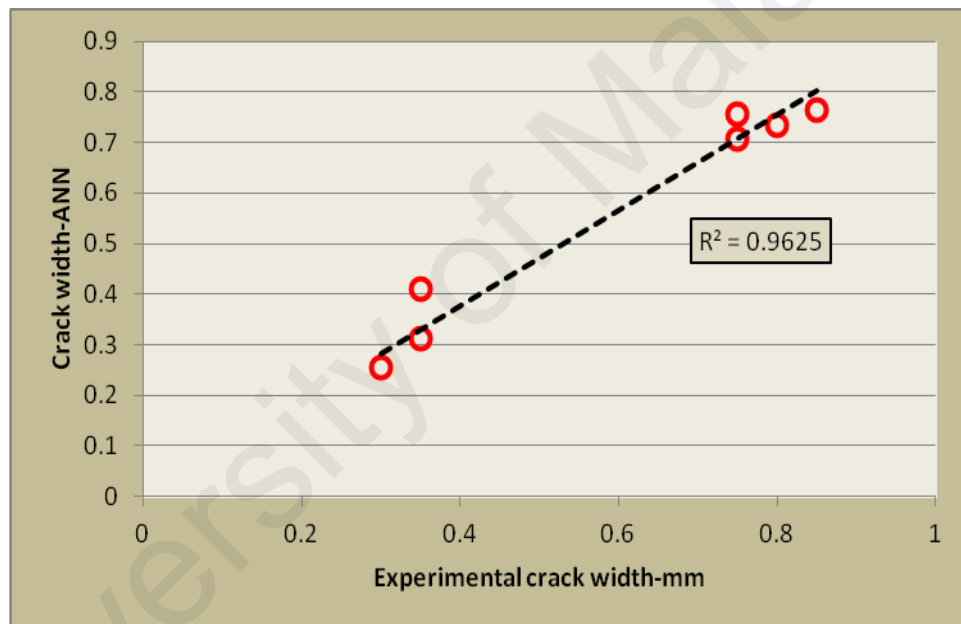


Figure 7.38: Plot of experimental crack width at maximum load versus crack width from RNN

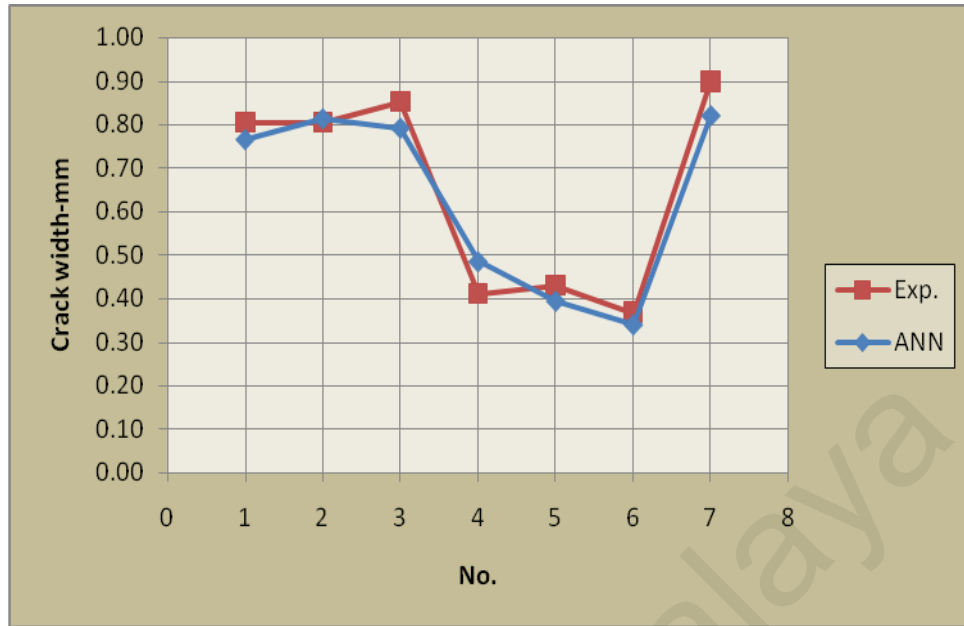


Figure 7.39: A comparison between RNN output and experimental results for maximum loading crack width after testing process

Table 7.13: The RNN testing MSE for crack width prediction of CFRP strengthened slab

Slab	Exp. Deflection Δ_{Exp} (mm)		Network Deflection Δ_{Net} (mm)		$\frac{\Delta_{Net}}{\Delta_{Exp}}$	$E = \frac{\Delta_{Exp} - \Delta_{Net}}{\Delta_{Net}}$	E^2
	Real	Normalized	Real	Normalized			
S512-700	0.75	0.81	0.71	0.76	0.95	0.041	0.0017
S512-1100	0.75	0.81	0.76	0.81	1.01	-0.007	0.0000
S512-1500	0.8	0.85	0.73	0.79	0.91	0.062	0.0038
S812-700	0.35	0.43	0.41	0.48	1.17	-0.056	0.0031
S812-1100	0.35	0.43	0.31	0.39	0.89	0.035	0.0012
S812-1500	0.3	0.38	0.26	0.34	0.87	0.042	0.0018
WCFRP	0.85	0.90	0.76	0.82	0.89	0.080	0.0065
$MSE = \sum E^2/n$							0.0026

7.5 Summary

Four networks namely FBNN, GRNN, FFTDNN, and RNN were applied for load-deflection prediction of non-strengthened and CFRP strengthened RC slab and other output from published studies. The results of the generated SNN using insufficient and sufficient training data are presented in Table 7.14 and Table 7.15 respectively. Also, the results of the use of internal dynamic space in case of sufficient training data is presented in Table 7.16. The experimental data used for network generation from this study and other published studies are classified as following:

- (1) Maximum deflection prediction for the non-strengthened one-way RC slab
- (2) Deflection prediction for the CFRP strengthened one-way RC slab
- (3) Compressive strength prediction on lightweight concrete –Appendix A
- (4) The first crack analysis of CFRP strengthened RC slab- Appendix B
- (5) Crack width prediction of RC beam under short term loading- Appendix C
- (6) Load-deflection analysis prediction on the non-strengthened one-way RC slab
- (7) Load-deflection analysis prediction on the CFRP strengthened one-way RC slab
- (8) Compressive strength prediction on lightweight mortar –Appendix A
- (9) Tensile strength prediction on lightweight mortar–Appendix A
- (10) Elastic modules prediction of high strength concrete- Appendix C
- (11) Load-deflection curve prediction of high strength concrete deep beam- Appendix C
- (12) Loading crack width prediction on the CFRP strengthened one-way RC slab

Also, a comparison between experimental deflection and predicted by GRNN and FEA outputs for the non-strengthened and CFRP strengthened RC slab is illustrated in Table

7.17. The GRNN was generated with insufficient data in training phase. In addition, a comparison between experimental mid-span deflection and predicted deflection by FEA, FBNN, GRNN, FFDNN, and RNN for non-strengthened and CFRP strengthened RC slab are presented in Table 7.18 and Table 7.19 respectively.

Table 7.14: The generated GRNN using insufficient data for network training

Network	Net Checking		Experimental Work				Case Study
			(1)	(2)	(3)	(4)	(5)
GRNN	R ²	Tr	0.82	0.83	0.874	0.989	0.987
		Ts	0.82	0.78	0.942	0.971	0.958
	MSE ×10 ⁻²	Tr	0.74	0.89	0.28	0.032	0.056
		Ts	0.11	0.2	0.04	0.03	0.017

Table 7.15: The generated GRNN and FBNN using sufficient data for network training

Network	Net Checking		Experimental Work				Case Study	
			(6)	(7)	(8)	(9)	(10)	(11)
GRNN	R ²	Tr	0.894	0.83	0.902	0.964	0.8	0.988
		Ts	0.96	0.776	0.934	0.905	0.83	0.984
	MSE ×10 ⁻²	Tr	0.083	0.89	0.69	0.2	0.45	0.008
		Ts	0.13	0.14	0.57	1.06	1.05	0.1
FBNN	R ²	Tr	0.999	0.95	0.992	0.992	0.883	0.999
		Ts	0.97	0.99	0.95	0.95	0.872	0.992
	MSE ×10 ⁻²	Tr	0.0376	0.697	0.029	0.029	0.052	0.00415
		Ts	0.022	0.84	0.032	0.032	0.049	0.0619

Table 7.16: The generated FFTDNN and RNN using sufficient data for network training

Network	Net Checking		Experimental Work		
			(6)	(7)	(12)
FFTDNN	R ²	Tr	0.995	0.987	0.814
		Ts	0.99	0.977	0.97
	MSE ×10 ⁻²	Tr	9.65e ⁻³	8.4e ⁻³	0.238
		Ts	0.008	0.21	0.8
RNN	R ²	Tr	0.99	0.99	0.92
		Ts	0.98	0.99	0.964
	MSE ×10 ⁻²	Tr	4.34e ⁻⁴	0.081	0.116
		Ts	0.0052	0.18	0.26

Table 7.17: A comparison between experimental mid-span deflection and predicted by FEA and GRNN using insufficient data for training

No.	(1)						(2)						
	Max. Deflection in non-strengthened slab						Deflection on slab S512-700						
	Exp.	FEA	GR	FEA / Exp	GR / Exp	Error %	Exp.	FEA	GR	FEA / Exp	GR / Exp	Error %	
1	7.13	6.38	7.63	0.89	1.07	-7	1.22	1.1	1.15	0.90	0.95	5.7	
2	8.51	9.2	7.8	1.08	0.92	8	4.68	3.5	5.3	0.75	1.13	-13	
3	10	12.1	9.06	1.21	0.91	9	14.96	12.6	17.1	0.84	1.14	-14	
4	-	-	-	-	-	-	21.16	21	18.8	0.97	0.93	11	
5	-	-	-	-	-	-	24.1	23.7	21.0	0.96	0.87	12.9	
Mean error						8%	Mean error						11.3%

Table 7.18: A comparison between experimental mid-span deflection and predicted by FEA, FBNN, GRNN, FFTDNN, and RNN using sufficient data for non-strengthened RC slab (100-3T10-1800)

No.	Deflection						FEA / Exp	FB / Exp	GR / Exp	FTTD / Exp	R / Exp	Error %			
	Exp.	FEA	FB	GR	FTTD	R						FB	GR	FTTD	R
1	0	0	0	0.54	0	0	-	-	-	-	0	0	0	0	
2	0.53	0.64	0.39	0.57	0.48	0.47	1.21	0.74	1.07	0.91	0.89	26.4	7.5	-9.4	11.3
3	0.84	0.94	0.66	0.98	0.74	0.7	1.12	0.79	1.17	0.88	0.83	21.4	16.7	-11.9	16.7
4	1.14	1.19	0.91	1.37	0.97	0.96	1.04	0.80	1.20	0.85	0.84	20.2	20.2	-14.9	15.8
5	1.52	1.65	1.38	1.79	1.61	1.3	1.1	0.91	1.18	1.06	0.86	9.2	17.7	5.9	14.5
6	2.17	2.25	1.99	2.47	2.43	2	1.04	0.92	1.14	1.12	0.92	8.3	13.8	12.0	7.8
7	3.15	3.54	2.73	3.63	3.42	2.91	1.12	0.87	1.15	1.09	0.92	13.3	15.2	8.6	7.6
8	4.18	4.55	3.63	4.51	4.47	4.28	1.09	0.87	1.08	1.07	1.02	13.2	7.9	6.9	-2.4
9	5.28	5.6	4.55	4.90	5.55	5.34	1.06	0.86	0.93	1.05	1.01	13.8	-7.2	5.1	-1.1
10	6.35	6.9	5.65	5.53	6.63	5.83	1.09	0.89	0.87	1.04	0.92	11.0	-12.9	4.4	8.2
11	7.52	7.96	6.81	6.12	7.72	6.03	1.07	0.91	0.81	1.03	0.80	9.4	-18.6	2.7	19.8
12	8.44	9.05	7.83	6.79	8.92	7.05	1.08	0.93	0.80	1.06	0.84	7.2	-19.5	5.7	16.5
13	9.5	10.3	9.02	7.86	10.24	8.18	1.08	0.95	0.83	1.08	0.86	5.1	-17.3	7.8	13.9
14	10.75	11.3	10.17	8.72	11.69	9.53	1.05	0.95	0.81	1.09	0.89	5.4	-18.9	8.7	11.3
15	12.08	13.4	12.65	9.44	13.33	11.31	1.11	1.05	0.78	1.10	0.94	-4.7	-21.9	10.3	6.4
16	13.3	14.4	14.6	10.2	15.06	13.64	1.14	1.10	0.77	1.13	1.03	-9.8	-23.3	13.2	-2.6
Mean Error %											10.5	14.9	8	9.7	

Table 7.19: A comparison between experimental mid-span deflection and predicted by FEA, FBNN, GRNN, FFTDNN, and RNN using sufficient data for CFRP strengthened RC slab

No.	Deflection-mm						FEA / Exp	FB / Exp	GR / Exp	FTTD / Exp	R / Exp	Error %			
	Exp.	FEA	FB	GR	FTTD	R						FB	GR	FTTD	R
1	0	0	0.1	0	0.75	0	-	-	-	-	0	0	0	0	
2	1.32	1.12	1	0.99	1.28	1.45	0.85	0.76	0.75	0.97	1.10	24	25	3	-10
3	1.83	2.1	1.9	2.3	2.1	2.03	1.15	1.04	1.26	1.15	1.11	-4	-26	-15	-11
4	3	2.9	2.9	3.69	3.33	3.61	0.97	0.97	1.23	1.11	1.20	3	-23	-11	-20
5	4.2	4.6	4.4	4.9	4.02	4.76	1.10	1.05	1.17	0.96	1.13	-5	-17	4	-13
6	5.8	6	6.2	6.2	4.95	6.19	1.03	1.07	1.07	0.85	1.07	-7	-7	15	-7
7	9.1	9.4	10.6	10	8.04	10.1	1.03	1.16	1.10	0.88	1.11	-16	-10	12	-11
8	15.1	14.4	16.1	14	13.75	15.56	0.95	1.07	0.93	0.91	1.03	-7	7	9	-3
9	20.3	21.9	23.3	18.2	20.8	21.6	1.08	1.15	0.90	1.02	1.06	-15	10	-2	-6
10	31	30.1	34.8	25	30.5	30.1	0.97	1.12	0.81	0.98	0.97	-12	19	2	3
Mean Error %											9.3	14.4	7.3	8.4	

The network predicted results in Tables 7.14 to Table 7.19 are classified as follows:

1. The GRNN predicted the experimental results in this research and other published study by maximum agreement with experimental results in situation where insufficient data is available for network training. The deflection ratio of FEA/Exp and GRNN/Exp varied in the range of 0.89 to 1.21 and 0.91 to 1.07, respectively, for non-strengthened RC slab (120-2T10-1800, 100-2T10-1800, and 90-3T10-1350) and 0.75 to 0.97 and 0.87 to 1.14 for CFRP strengthened RC slab (S512-700). The mean error for deflection calculation of non-strengthened RC slab and CFRP strengthened RC slab was 8 and 11.3 % respectively.
2. The generated GRNN with sufficient training data predicted the mid-span deflection in acceptable agreement with the predicted output by FBNN as well as shown in Figures 7.40 and 7.41. The MSE performance function between target and predicted by GRNN was in acceptable range.

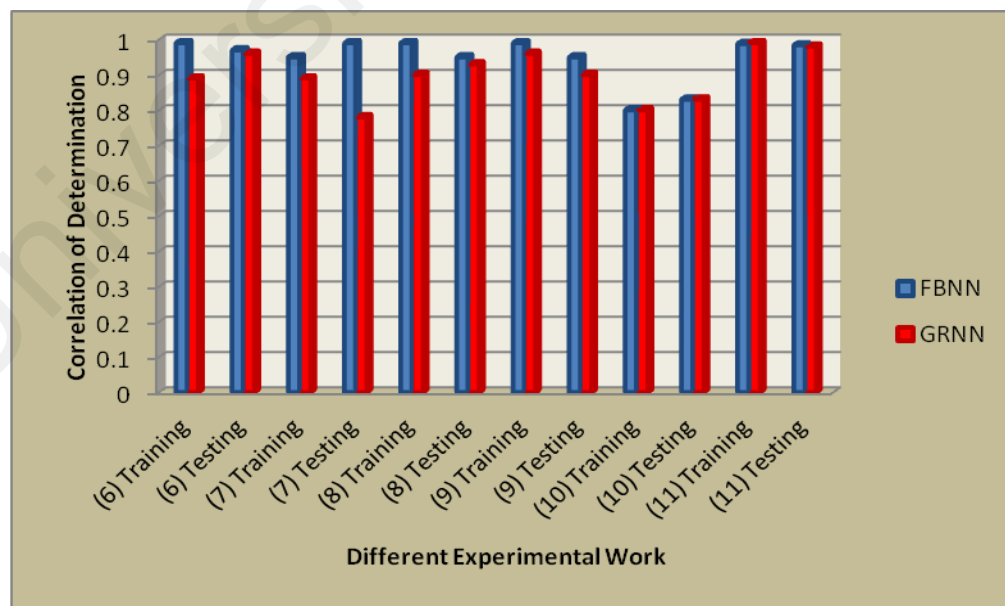


Figure 7.40: The correlation of determination R^2 comparison between generated FBNN and GRNN with sufficient data for various experimental works in Table 7.15.

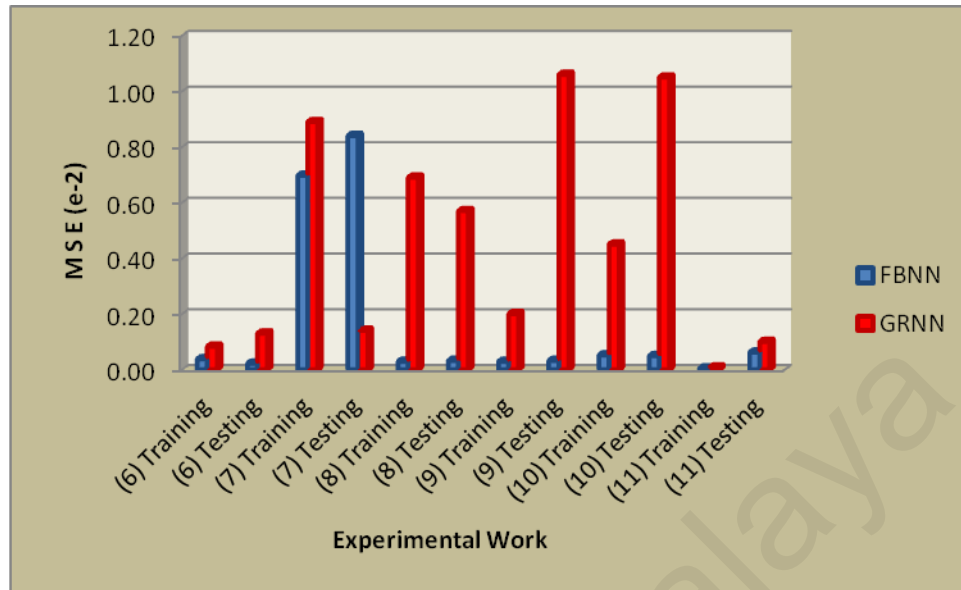


Figure 7.41: The MSE comparison between FBNN and GRNN modeling for the experimental works in Table 7.15.

The value of deflection for non-strengthened and CFRP strengthened RC slab was predicted by GRNN with mean error of 14.9 and 14.4 % respectively.

- FFTDNN and RNN were capable to predict mid-span deflection of non-strengthened and CFRP strengthened RC slab by creating an internal dynamic space during network generation. The ratio of mid-span deflection for FEA/Exp, FBNN/Exp, GRNN/Exp, FFTDNN/Exp, and RNN/Exp Was varied in the range of 1.04 to 1.21, 0.74 to 1.1, 0.77 to 1.34, 0.91 to 1.13, and 0.83 to 1.03, respectively, for non strengthened RC slabs (100-3T10-1800). These ratio was varied in the range of 0.85 to 1.15, 0.76 to 1.15, 0.68 to 1.3, 0.97 to 1.15, and 0.97 to 1.11, respectively, for CFRP strengthened RC slab (S812-1100). The value of mean error for deflection prediction by FBNN, GRNN, FFTDNN, and RNN was 10.5, 14.9, 8, and 9.7% respectively for non-strengthened RC slab and 9.3, 14.4, 7.3, and 8.4 respectively for CFRP strengthened RC slab.

The results of mean error for mid-span deflection by FBNN, GRNN, FFTDNN, and RNN are compared together for non-strengthened and CFRP strengthened RC slab as well as shown in Figure 7.42. It is observed that the dynamic neural network results for prediction of mid-span deflection is better than static neural network.

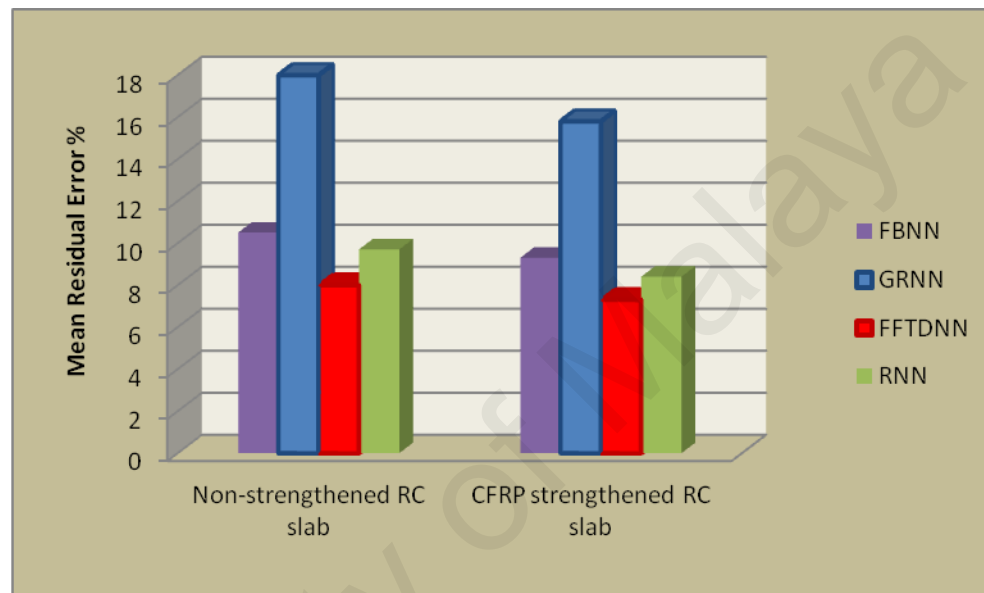


Figure 7.42: Mean residual error of the various modeling for non-strengthened and CFRP strengthened RC slab

CHAPTER 8

8. CONCLUSION AND RECOMMENDATION

8.1 Conclusion

The following conclusions are obtained from current research:

1. In the case of insufficient data for network training, the GRNN predicted the mid-span deflection of non-strengthened and CFRP strengthened RC one-way slabs with a testing coefficient of determination of 0.82 and 0.78 respectively. The ratio between predicted deflection by GRNN and experimental output varied in the range of 0.91 to 1.07 for non-strengthened RC slab and 0.87 to 1.14 for CFRP strengthened RC slab. The mean error for deflection calculation of non-strengthened RC slab (120-2T10-1800, 100-2T10-1800, and 90-3T10-1350) and CFRP strengthened RC slab (S512-700) was 8% and 11.3 % respectively. It is evident that GRNN was able to predict the load-deflection analysis with an acceptable accuracy in situation where insufficient data is available. So, GRNN is an adequate modelling method for the big dimension of structural elements due to difficulty in acquiring sufficient experimental data.
2. In the case of sufficient data for network training, the FBNN and GRNN showed training coefficient of determination of 0.99 and 0.89 respectively, in predicting the load-deflection analysis for non-strengthened one-way RC slabs (100-3T10-1800); and 0.95 and 0.83, respectively, for CFRP strengthened one-way RC slabs (S812-1100). The ratio between predicted deflection for FBNN/Exp. and GRNN/Exp. were in the range of 0.74 to 1.10 and 0.77 to 1.18, respectively, for non-strengthened RC

slab and 0.76 to 1.16 and 0.75 to 1.26, respectively, for CFRP strengthened RC slab. This shows that GRNN solves the problems in acceptable technique when the number of data is sufficient for network training.

3. The FFTDNN and RNN predicted the mid-span deflection with training coefficient of determination of 0.995 and 0.99, respectively, for non-strengthened one-way RC slabs; and 0.98 and 0.99, respectively, for CFRP strengthened one-way RC slabs (S812-1100). The ratio of mid-span deflection for FFTDNN/Exp and RNN/Exp was varied in the range of 0.91 to 1.13, and 0.83 to 1.03, respectively, for non strengthened RC slabs and 0.97 to 1.15, and 0.97 to 1.11, respectively, for CFRP strengthened RC slab.
4. FFTDNN, RNN, FBNN, and GRNN predicted the load-deflection analysis with mean error 8, 9.7, 10.5, and 14.9% respectively for non-strengthened RC slab (100-3T10-1800) and 7.3, 8.4, 9.3, 14.4% respectively for CFRP strengthened RC slab(S812-1100). It is obvious that using FFTDNN and RNN modelling provided outstanding performance over the FBNN and GRNN for load-deflection analysis of CFRP strengthened RC slab. This results show that by creating DNNs using internal dynamic space give more accurate result in compare to SNN method.
5. The following applications were for measuring up of the ANNs approaches in other published experimental results:
 - (i) The results of the generated GRNN on lightweight concrete and other researcher's experimental outputs showed that GRNN are suitable for cases where training data are generally insufficient.

- (ii) For the cases where training data is sufficient for network generation, GRNN was able to predict the results in acceptable and accurate technique in comparison with FBNN.
- (iii) FFTDNN and RNN were able to predict the crack width of CFRP strengthened RC slab with an acceptable agreement with experimental results.

8.2 Contribution

This research contributes and explores many things which are as follows:

- 1 Using static and dynamic neural network as analytical method for deflection prediction of non-strengthened and CFRP strengthened RC slabs
- 2 Using GRNN for prediction in situation where insufficient data are available for network training.
- 3 Using FFTDNN and RNN as dynamic neural networks to predict the load-deflection analysis of non-strengthened and CFRP strengthened one-way RC slabs using internal dynamic space during network generation.
- 4 Using GRNN as SNN to predict load-deflection curves of non-strengthened and CFRP strengthened RC slabs and comparing with the results of the dynamic neural network.

8.3 Recommendation

The study would play pivotal role in using ANNs to predict mid-span deflection of non-strengthened and CFRP strengthened RC slabs. Following future works are recommended which could be benefitted from this study:

- 1 Using GRNN as analytical technique for prediction in other static problems in Civil Engineering.
- 2 Using external effects for making nonlinear space and so dynamic training during network generation by using time dependent data.
- 3 Using other methods of dynamic neural networks, such as Distributed Feed-forward Time-delay Neural Networks (DFTDNNs) and Hopfield Recurrent Neural Networks (HRNNs) for prediction of time sequence problems in Structural Engineering.
- 4 Using DNNs for analysis of reinforced concrete and steel frames under earthquakes and wind loads.
- 5 Using DNNs for analysis prediction of bridge structures under movable live loads, earthquakes, and wind.
- 6 Using sensitivity analysis to show the effect of input parameters on network training.
- 7 Using a method to develop network equation based on trained neural network to predict the training range without using trained ANN.

REFERENCES

- Abed, M. M., El-Shafie, A., and Osman, S.A. (2010). Creep Predicting Model in Masonry Structure Utilizing Dynamic Neural Networ. *Journal of Computer Science*, 6(5), 597-605.
- Abhijit, M., and Sudip, N.B. (1995a). Artificial neural networks in prediction of mechanical behavior of concrete at high temperature. *Department of Civil Engineering, Indian Institute of Technology, Bombay 400076, India*.
- Adhikary, B. B., and Mutsuyoshi, H. (2006). Prediction of shear strength of steel fiber RC beams using neural networks. *Construction and Building Materials*, 20(9), 801-811.
- Al-Sayed, S. H., Al-Salloum, Y.A., Almusallam, T.H. and Amjad, M.A. (1996). Evaluation of service load deflection for beams reinforced by GFRP bars. *Proceedings of the Second International Conference on Advanced Composite Materials in Bridges and Structures, CSCE, Montreal*, 165-172.
- Amen, A., Laurent, M., Manuel, L., and Patric, H. (2008). Strengthening slab using externally-bonded strip composite. *Composite Structures*, 39, 1125-1135.
- American Concrete Institute, A. C. I. (1996). State of the art report on Fiber Plastic Reinforcement for concrete structures. *ACI 440-R-96, Detroit*.
- Arnesen, A., Sorensen, S. I. and Bergan, P.G. . (1980). Nonlinear Analysis of Reinforced Concrete. *Computers & Structures*, 12, 571-579
- Barai, S. V., and Pandey, P.C. (1996). Time-delay neural networks in damage detection of railway bridges. *Advances in Engineering Software*, 28, 1-10.
- Bazant, Z. P., and Cedolin, L. (1983). Finite Element Modeling of Crack Band Propagation. *Journal of Structural Engineering, ASCE*, 109(1), 69-93.
- Beale, M. H., Hagan, M.T., and Demuth, H.B. (2011). Neural Network Toolbox in MATLAB. *The MathWorks, Inc*.
- Benmokrane, B., Chaallal, O., and Masmoudi, R. (1996). Flexural response of concrete beams reinforced with FRP reinforcing bars. *ACI Structural Journal*, 90(1), 364-373.

- Bischoff, P. H. (2005). Re-evaluation of Deflection Prediction for Concrete Beams Reinforced with Steel and Fiber Reinforced Polymer Bars. *ASCE Journal of Structural Engineering*, 131(5), 752-767.
- Branson, D. E. (1977). Deformation of Concrete Structures. *United States of America. McGraw-Hill International Book Company.*
- BS 8110-1:1997. Structural use of concrete. Code of practice for design and construction *British Standards Institution.*
- Caglar, N., Elmas, M., Yaman, Z.D., and Saribiyik, M. (2007). Neural networks in 3-dimensional dynamic analysis of reinforced concrete buildings. *Construction and Building Materials*, 22(5), 788-800.
- Carlos, A. C., and Maria M.L. (2006). Sensitivity analysis of reinforced concrete beams strengthened with FRP laminates. *Cement and Concrete Composites*, 28, 102-114.
- Celikoglu, H. B., and Cigizoglu, H.K. (2006). Public transportation trip flow modeling with generalized regression neural networks. *Advances in Engineering Software*, 38, 71-79.
- Celikoglu, H. B., and Cigizoglu, H.K. (2007). A dynamic network loading process with explicit delay modelling. *Transportation Research Part C*, 15, 279-299.
- Cevik, A., and Guzelbey, I.H. (2008). Neural network modeling of strength enhancement for CFRP confined concrete cylinders. *Building and Environment*, 43(5).
- Chami, G. A., Thériault, M., and Neale, K.W. (2007). Creep behavior of CFRP strengthened reinforced concrete beams. *Constr. Build. Mater*, 23(4), 1640-1652.
- Chamia, G., Thériault, M., and Neale, K.W. (2007). Creep behaviour of CFRP-strengthened reinforced concrete beams. *Construction and Building Materials*, 23(4), 1640-1652.
- Chen, H. M., Tsai, K.H., Qi, G.Z., Yang, J.C.S., and Amini, F. (1995). Neural networks for structural control. *Journal of Computational Civil Engineering*, 9, 168-176.
- Chen, W. F. (1976). Plasticity in Reinforced Concrete. *McGraw-Hill, New York.*
- Christopher, K., Zhongfan, C.S., and Lee, K.L. (2002). Effect of size on the failure of FRP strengthened reinforced concrete beams. *Advances in Building Technology*, 797-801.
- Clarke, J. K., and Waldron, P. (1996). The reinforcement of concrete structures with advanced composites. *Struct Eng* 74(3), 283-288.

- Darwin, D., and Pecknold, D.A. (1977). Analysis of Cyclic Loading of Plane R/C Structures. *Computers & Structures*, , Vol. 7(1), 137-147.
- Demir, F. (2007). Prediction of elastic modulus of normal and high strength concrete by artificial neural networks. *Construction and Building Materials*, 22(7), 1428-1435.
- Dias, W. P. S., and Pooliyadda,S.P. (2001). Neural networks for predicting properties of concretes with admixtures. *Constr. Build. Mater*, 15, 371-379.
- Dotroppe, J. C., Schnobrich, W.C., and Pecknold, D.A (1973). Layered Finite Element Procedure for Inelastic Analysis of Reinforced Concrete Slabs. *IABSE Publication*, 33-34.
- Dutta, S., and Shekar, S. (1993). Bond rating: a non-conservative application of neural networks. *Robert R*.
- El-Shafie, A., Noureldin,A.,Taha,M.R., Aini, H., and Basri, H. (2008). Performance enhancement for masonry creep predicting model using recurrent neural networks. *Eng Int Syst*, 3, 199–208.
- EN 1992-1-1 EUROPEAN STANDARDS, E. (2004). Design of Concrete Structures, Part 1-1: General Rules and Rules for Buildings, . *British Standards Institute, London*.
- Foreta, G., and Limam, O. (2008). Experimental and numerical analysis of RC two-way slabs strengthened with NSM CFRP rods. *Construction and Building Materials*, 22(10), 2025-2030.
- GangaRao, H. V. S., and Faza, S.S (1993). Pre and post-cracking deflection behaviour of concrete beams reinforced with fiber-reinforced plastic rebars. *Proceedings of the First International Conference on Advanced Composite Materials in Bridges and Structures, CSCE, Montreal,*, 151-160.
- Garrett, J. H., Ghaboussi, J., and Wu, X. (1992). Neural Networks, Expert System for Civil engineers. *Knowledge Representation, ASCE, New York, N.Y.*, 104-143.
- Ghaboussi, J., Garrett, J. H., and Wu,X. (1991). Knowledge-Based Modeling of Material Behavior with Neural Networks. *ASCE J. Engineering Mechanics Division*, 117(1), 132-152.
- Guang, H., and Zong,J. (2000). Prediction of compressive strength of concrete by neural networks. *Cement Concrete Res* 30(1245–1250).
- Güneyisi, E., Gesoğlu,M., Özturan,T., and Özbay,E. (2007). Estimation of chloride permeability of concretes by empirical modeling: Considering effects of cement type, curing condition and age. *Construction and Building Materials*, 23(1), 469-481.
- Hawley, D. D., Johnson, J.D.,& Raina, D. (1990). Artificial Neural System: A New Tool Financial Decision Making. *Financial Analysts Journal*, 63-72

- Hebb, D. O. (1949). *The Organization of Behavior*. Wiley, New York.
- Hedong, N., Vasquez,A., and Vistasp,M.K (2006). Effect of material configuration on strengthening of concrete slabs by CFRP composites. *Composites*, 37, 213-226.
- Hedong, N., Vasqueza,A., and Karbhari,V.M. (2006). Effect of material configuration on strengthening of concrete slabs by CFRP composites. *Composites Part B: Engineering*, 37(2-3), 213-226.
- Hegazt. (1996). Predicting Load-Deflection Behavior of Concrete slab Using Neural Networks. *Proc. 3rd Canadian Conference on Computing in Civil and Building Engineering*.
- Ishak, S., Kotha, P., and Alecsandru, C. (2003). Optimization of dynamic neural networks performance for short-term traffic prediction. *Proceedings of the Transportation Research Board 82nd Annual Meeting, Washington, DC*.
- ISIS Canada. (2001). Design Manuals Parts 1 – 4, Intelligent Sensing of Innovative Structures. *University of Manitoba, Winnipeg*.
- Jamal, A. A., Elsanosi,A., and Abdelwahab,A. (2007). Modeling and simulation of shear resistance of R/C beams using artificial neural network. *Journal of the Franklin Institute*, 334(5), 741-756.
- Jiang, J., and Mirza, F.A. (1997). Nonlinear analysis of reinforced concrete slabs by a discrete FE approach. *Computers & Structures*, 65(4), 585-592.
- Jofriet, J. C., and McNeice, G.M (1971). Finite Element Analysis of RC Slabs. *Journal of Structural Division, ASCE*, 97, 785-806.
- Kaiser, H. P. (1989). Strengthening of reinforced concrete with epoxy-bonded carbon-fiber plastics. *Doctoral Thesis, Diss. ETH, Nr. 8918, ETH Zurich, Ch-8092 Zurich, Switzerland*.
- Kasperkiewicz, J., Racz,J., and Dubrawski,A. (1995). HPC strength prediction using artificial neural network. *J. Computing in Civ. Engrg, ASCE*, 9(4), 279 – 284.
- Kendrick, R., Acton, D., and Duncan, A. (1994). Phase-diversity wave-front sensor for imaging systems. *Applied Optics*, 33, 6533-6547.
- Kerh, T., and Yee,Y.C. (2000). Analysis of a deformed three-dimensional culvert structure using neural networks. *Advances in Engineering Software*, 31(5), 367-375.
- Kiang, H. T., and Zhao,H. (2004). Strengthening of Openings in One-Way Reinforced-Concrete Slabs Using Carbon Fiber-Reinforced Polymer Systems. *Journal of Composites for Construction*, 8(5), 393-403.

- Kwak, H. G., and Kim,S.P. (2002). Nonlinear analysis of RC beams based on moment-curvature relation. *Computers & Structures*, 80, 615-628.
- Li, Q. S., Liu, D.K., Fang, J.Q., Jeary, A.P., and Wong, C.K. (1999). Using neural networks to model and predict amplitude dependent damping in building. *wind and structures*, 2(1), 25-40.
- Limam, O., Forest,G., and Ehrlacher,A. (2003). RC two-way slabs strengthened with CFRP strips: experimental study and a limit analysis approach. *Composite Structures*, 60, 467-471.
- Lin, C. S., and Scordelis,A.C. (1975). Nonlinear Analysis of RC Shells of General Form. *Journal of Structural Division, ASCE*, 101, 523-538.
- Lingras, P., and Mountford, P. (2001). Time delay neural networks designed using genetic algorithms for short term inter-city traffic forecasting. In L. Monostori. *J. Vancza and A. Moonis (eds.)*.
- Liu, X., and Gan, M. (1991). A Preliminary Design Expert System (SPRED-1) Based on Neural Network. *Artificial Intelligence in Design'91, Butterworth-Heineman Ltd., Oxford*, 785-800.
- Mahesh, P., and Surinder, D. (2008). Modeling Pile Capacity Using Support Vector Machines and Generalized Regression Neural Network. *Journal of Geotechnical & Geoenvironmental Engineering* 134(7), 1021.
- Mahmut, F., and Mahmud,G. (2009). Generalized Regression Neural Networks and Feed Forward Neural Networks for prediction of scour depth around bridge piers. *Advances in Engineering Software*, 40(8).
- Manish, A. K., and Gupta,R. (2005). Concrete compressive strength prediction using ultrasonic pulse velocity through artificial neural networks. *Automation in Construction*, 15(3), 374-379.
- Mansour, M. Y., Dicleli,M., Lee,J.Y., and Zhang,J. (2004). Predicting the shear strength of reinforced concrete beams using artificial neural networks. *Engineering Structures* 26, 781-799.
- Mehmet, I. (2007). Modeling ultimate deformation capacity of RC columns using artificial neural networks. *Engineering Structures*, 29(3), 329-335 neural networks.
- Meier, U. (1987). Bridge repair with high performance composite materials. *Mater Technik*, 15, 125-128.
- Meyer, C., and Okamura, H. (1985). (1985). "Finite Element Analysis of Reinforced Concrete Structures". *Proceedings of the US-Japan Joint Seminar on Finite Element Analysis of Reinforced Concrete, Tokyo, Japan*.
- Minsky, M., & Papert, S. (1969). Perceptrons. *MIT Press*.

- Moselhi. (1992). Potential Applications of Neural Networks in Construction. *Can. Journal of Civ. Engrg.*, 19, 521-529.
- MS. (1989). Malatsian Standard, Specification For Portland Cement (Ordinary and Rapid-Hardening) Part 3: Chemical Analysis *MS 522: Part 3*.
- Mukesh, D. (1996). Introduction to neural networks: Application of neural computing for process chemists, part 1. *Journal of Chemical Education*, 73, 431-434.
- Mukherjee, A., and Deshpande, J.M. (1995). Modelling Initial Design Process using Artificial Neural Networks. *ASCE Computing in Civil Engineering*.
- Murat, P., Özbaya,E., Öztaşb,A., and Yuce,M.I. (2005). Appraisal of long-term effects of fly ash and silica fume on compressive strength of concrete by neural networks. *Construction and Building Materials*, 21(2), 384-394.
- Nelles, O. (2001). Nonlinear system identification. *Springer, Germany*.
- Ngo, D., and Scordelis, A.C. (1967). Finite Element Analysis of Reinforced Concrete Beams. *Journal of ACI*, 65(3), 152-163.
- Niu, H., Vasquez, A., and Karbhari, V.M. (2006). Effect of material configuration on strengthening ofconcreteslabs by CFRPcomposites. *Composites Part B: Engineering*, 37(2-3), 213-226.
- Öztaş, A., Pala,M., Özbay,E., Kanca,E., Çağlar,N., and Bhatti, M.A. (2006). Predicting the compressive strength and slump of high strength concrete using neural network. *Construction and Building Materials*, 20(9), 769-775.
- Pannirselvam, N., Raghunath,P.N., and Suguna,K. (2008). Neural Network for Performance of Glass Fibre Reinforced Polymer Plated RC Beams. *American J. of Engineering and Applied Sciences*, 1(1), 82-88.
- Rajasekaran, S., Ramasamy,J.V., and Fabin, M.F. (1995b). Artificial Neural Network for Preliminary Area of Truss Configuration. *Proc., National Conference on Civil Engineering Materials and Structures*, 402-408.
- Razaqpur, A. G., Svecovà, D., and Cheung, M.S. (2000). Rational method for calculating deflection of Fiber-Reinforced Polymer Reinforced Beams. *ACI Structural Journal*, 97(1), 175-184.
- Rosenblatt. (1962). Principles of neurodynamics; perceptrons and the theory of brain mechanisms. *Washington: Spartan Books*.
- Scanlon, A., and Murray,D.W. (1974). Time Dependent Reinforced Concrete Slab Deflections. *Journal of the Structural Division, ASCE*, 100, 1911-1924.

- South African Bureau of Standards (SABS) 0100-1. (1992). The Structural Use of Concrete – Part 1: Design. *South African Bureau of Standards, Pretoria*.
- Specht. (1990). Probabilistic neural networks. *Neural Netw*, 3, 109–118.
- Teychenne, D., Franklin, RE., and Erntroy, HC. (1988). Design of normal concrete mixes. *Departement of Environment, HMSO*.
- Timoshenko, S., and Goodier, J.N. (1951). Theory of Elasticity. *McGraw-Hill, New York*.
- Topcu, I. B., and Saridemir, M. (2007). Prediction of properties of waste AAC aggregate concrete using artificial neural network *Comput. Mater. Sci*, 41, 117-125.
- Tsung-yi, P., Ru-yih, W., and Jih-sung, L. (2007). A deterministic linearized recurrent neural network for recognizing the transition of rainfall–runoff processes. *Advances in Water Resources*, 30(8), 1797-1814.
- VanLuchene, R. D., and Roufei, S. (1990). Neural Networks in Structural Engineering. *Microcomputers in Civil Engineering*, 5, 207-215.
- Waleed, A., Thanoon, M.S., Jaafar, M., Razali, A., and Noorzaei, K.J. (2005). Repair and structural performance of initially cracked reinforced concrete slabs. *Construct. Build. Mater*, 19, 595-603.
- Wang, C., Shih, C., Hong, S., and Hwang, W. (2004). Rehabilitation of Cracked and Corroded Reinforced Concrete Beams with Fiber-Reinforced Plastic Patches. *Journal of Composites for Construction* 219-228.
- Wehenkel, L. (1996). Contingency severity assessment for voltage security using non-parametric regression techniques. *IEEE Transactions on Power Systems*, 11, 101-111.
- Werbos, P. J. (1974). Beyond Regression: New Tools for Prediction and Analysis in the Behavioral Sciences. *PhD thesis, Harvard University*.
- Williams, T., and Gucunski, N. (1995). Neural networks for backcalculation of modula from SASW test. *Journal of Computing in Civil Engineering, ASCE*, 9, 1-9.
- Wium, J. A., and Eigeaar, E.M. (2010). An Evaluation of the Prediction of Flat Slab Deflections *34th International Symposium On Bridge And Structural Engineering, Venice*.
- Yasdi, R. (1999). Prediction of road traffic using a neural network approach. *Neural computing and applications*, 8, 135-142.
- Yeh, C. (2007). Modeling slump flow of concrete using second-order regressions and artificial neural networks. *Cement and Concrete Composites*, 29(6), 474-480.

- Yost, R. J., Goodspeed,P.E.,and Schmeckpeper,E.R. (2011). Flexural Performance of Concrete Beams Reinforced With FRP Grids. *Journal of Composites for Construction*, 18-25.
- Yun, S. Y., Namkoong,S., Rho,J.H., Shin,S.W. and Choi,J.U. (1998). A performance evaluation of neural network models in traffic volume forecasting. *Mathematic Computing Modelling*, 27(9-11), 293-310.
- Zhang, T. (2009). Biaxial bending analysis of the slabs under concentrated loads. *International Conference on Engineering Competition.IPPP Xplore*, 213-216.

University of Malaya

APPENDIX A

A. MECHANICAL PROPERTIES OF LIGHTWEIGHT MIXTURE

A.1 Lightweight Aggregate

The lightweight aggregate used in this part was scoria with the specific gravity of less than 1 gr/cm³. The chemical analysis of the scoria as lightweight aggregate is given in Table A.1.

Table A.1: Chemical analysis of the used scoria

Chemical Formulas	Sio ₂	Al ₂ O ₃	Fe ₂ O ₃	Cao	Mgo	So ₃	Thermal Gradient
Percent	67.96	16.2	2	3.36	0.8	0.75	5.82

Water absorption is one of the important physical properties in the porous material. Water absorption has direct relation with the size of grain, type of surface opening, irregularity of opening and time. Water absorption versus time is shown in Figure A.1.

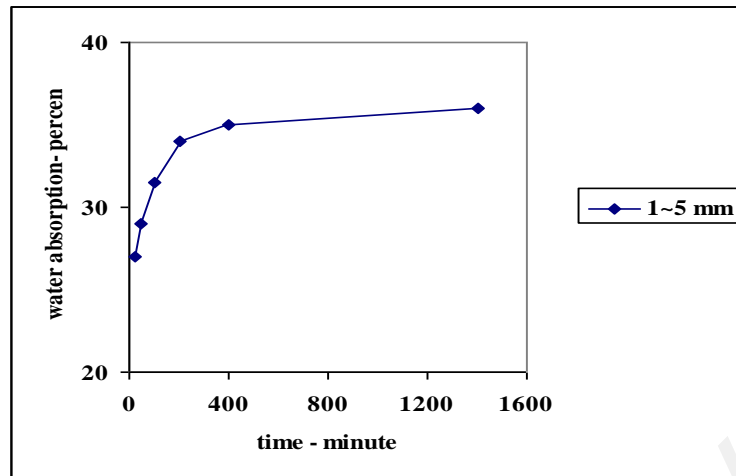


Figure A.1: Water absorption vs. time

Numerous of pores have caused difference between dry and saturated density. The specific gravity of dry and saturated scoria as lightweight material is shown in Table A.2.

Table A. 2: Specific gravity dry and saturated aggregates

Grain Density –kg/m ³	0 – 3.16	3.16 – 3.4	3.4 – 3.8	3.4 – 1 , 1.2
Dry on Oven	765	738	683	676
Saturated	1262	1144	1058	1041

After the test on scoria, the specific gravity of dried and saturated grains, with the size between 0 to 4.75 mm, were 760 and 1260 kg/m³ respectively. Grain size test is shown Figure A.2.

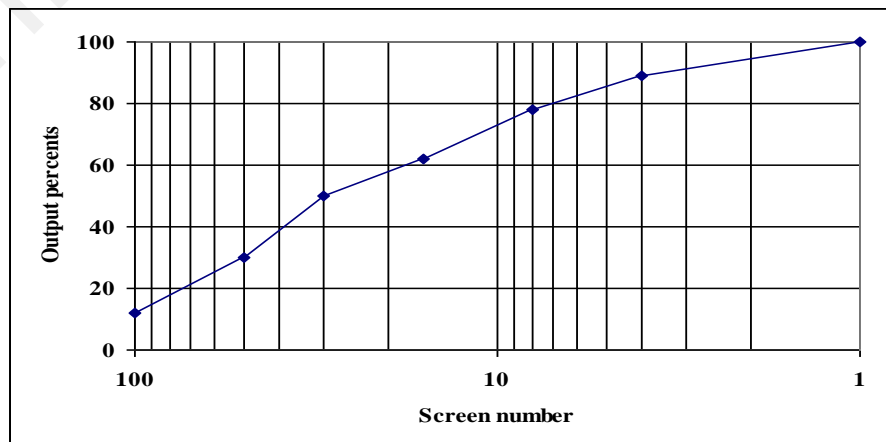


Figure A. 2: Grain size curve of the scoria

A.2 Mixture Design

In this study, the mixture of absolute volume method has used. With having water and cement amounts and by using of absolute volume method can extract the amount of aggregates. It is assumed that the volume of compacted mix is equal to total absolute volumes of It's constituents.

$$\frac{C}{\gamma_C} + \frac{W}{\gamma_W} + \frac{A}{\gamma_A} = 1 \quad (\text{A.1})$$

In this formula C is the amount of cement, W is the amount of water and A is the amount of aggregate (sand + gravel + scoria) in kg/m³ of concrete.

A.2.1. Lightweight Concrete

In order to study below parameters, 96 of lightweight samples in the shape of cylinder 15*30 (cm) were made to determine compressive strength and tensile strength. The schedule of lightweight construction is given in Table A.3. All samples were made of normal water and the average of compressive strength and tensile strength were obtained from five similar samples.

The results of the concrete mix design have presented in Tables A.4 to A.7.

Table A.3: The Schedule of Lightweight Concrete Construction

Parameters	Concrete Samples
Scoria Instead of Sand in Lightweight Concrete - %	0, 20, 30, 40
Water-Cement Ratio	0.50,0.55, 0.60
Cement Content in Compressive Sample – kg/m ³	300, 350 ,400
Cement Content in Tensile Sample – kg/m ³	350
Curing Time - Days	7&28

Table A.4: Mix design for 0% scoria instead of sand (ordinary concrete)

$\frac{W}{C}$	Cement Content- Kg/m^3	Aggregates (Kg)		$\frac{A_g}{C}$	$\frac{A_{Sa} + A_{Sc}}{C}$	Density Kg/m^3
		Sand	Gravel			
0.50	300	766.38	1149.57	3.83	2.55	2320
0.50	350	725.84	1088.76	3.11	2.41	2300
0.50	400	685.30	1027.96	2.57	1.70	2350
0.55	300	751.23	1126.85	3.76	2.50	2300
0.55	350	708.17	1062.26	3.04	2.02	2180
0.55	400	665.11	997.67	2.49	1.66	2150
0.60	300	736.09	1104.14	3.68	2.45	2275
0.60	350	690.51	1035.76	2.96	1.97	2150
0.60	400	644.92	967.38	2.42	1.60	2200

Table A. 5: Mix design for 20% scoria instead of sand in concrete

$\frac{W}{C}$	Cement Content- Kg/m^3	Aggregates (Kg)			$\frac{A_g}{C}$	$\frac{A_{Sa} + A_{Sc}}{C}$	Density Kg/m^3
		Scoria	Sand	Gravel			
0.50	300	111.15	444.62	1149.57	3.83	1.85	2109.39
0.50	350	105.27	421.10	1088.76	3.11	1.50	2120.53
0.50	400	99.40	397.58	1027.96	2.57	1.24	2131.67
0.55	300	108.96	435.83	1126.85	3.76	1.82	2113.55
0.55	350	102.71	410.85	1062.26	3.04	1.47	2125.39
0.55	400	96.47	385.87	997.67	2.49	1.21	2137.22
0.60	300	106.76	427.04	1104.14	3.68	1.78	2117.72
0.60	350	100.15	400.60	1035.76	2.96	1.43	2130.24
0.60	400	93.54	374.15	967.38	2.42	1.17	2142.77

Table A.6: Mix design for 30% scoria instead of sand in concrete

$\frac{W}{C}$	Cement Content- Kg/m^3	Aggregates (Kg)			$\frac{A_g}{C}$	$\frac{A_{Sa} + A_{Sc}}{C}$	Density Kg/m^3
		Scoria	Sand	Gravel			
0.50	300	146.59	342.04	1149.57	3.83	1.63	2042
0.50	350	138.84	323.95	1088.76	3.11	1.32	2057
0.50	400	131.08	305.86	1027.96	2.57	1.09	2071
0.55	300	143.69	335.28	1126.85	3.76	1.60	2048
0.55	350	135.46	316.06	1062.26	3.04	1.29	2063
0.55	400	127.22	296.85	997.67	2.49	1.06	2079
0.60	300	140.80	328.52	1104.14	3.68	1.56	2053
0.60	350	132.08	308.18	1035.76	2.96	1.26	2069
0.60	400	123.36	287.83	967.38	2.42	1.03	2086

Table A.7: Mix design for 40% scoria instead of sand in concrete

$\frac{W}{C}$	Cement Content- Kg/m^3	Aggregates (Kg)			$\frac{A_g}{C}$	$\frac{A_{Sa} + A_{Sc}}{C}$	Density Kg/m^3
		Scoria	Sand	Gravel			
0.50	300	174.39	261.58	1149.57	3.83	1.45	1989.59
0.50	350	165.16	247.74	1088.76	3.11	1.18	2007.06
0.50	400	155.94	233.91	1027.96	2.57	0.97	2024.54
0.55	300	170.94	256.41	1126.85	3.76	1.42	1996.11
0.55	350	161.14	241.71	1062.26	3.04	1.15	2014.68
0.55	400	151.34	227.01	997.67	2.49	0.95	2033.25
0.60	300	167.49	251.24	1104.14	3.68	1.40	2002.64
0.60	350	157.12	235.68	1035.76	2.96	1.12	2022.30
0.60	400	146.75	220.12	967.38	2.42	0.92	2041.95

A.2.2. Lightweight Mortar

In order to study below parameters, 210 mortar samples in the shapes of cylinder 15*30 (cm) were made to determine compressive strength and tensile strength. The water – cement ratio was 0.55 and the cement content was 350 kg/m³. The schedule of the experimental work has shown in Table A.8. As we consider, different percentage of scoria instead of sand from 5 to 100% by increasing 5% in each step, have been studied to find compressive and tensile strength after 3, 7, 14, 28, & 90 curing days. All samples were made of normal water and the average of compressive strength and tensile strength were obtained from 3 similar samples. The mortar mixture design is shown in Table A.9.

Table A.8: The Schedule of Lightweight Mortar Construction

Parameters	Mortar Samples
Scoria Instead Sand in Lightweight Mortar - Percent	0 ,5,10,15, 20, 25,30,35,40,45,50,55, 60,65,70,75,80,85,90,95 and 100
Water-Cement Ratio	0.55
Cement Content in Compressive Sample – kg/m ³	350
Cement Content in Tensile Sample – kg/m ³	350
Curing Time - Days	3,7,14,28 and 90

Table A.9: Mix design for different percentage of scoria instead of sand in mortar

Scoria %	Sand Kg/m ³	Scoria Kg/m ³	Density Kg/m ³	Aggregate Kg/m ³
0	1543.2	0.0	2051	1543.2
5	1339.1	70.5	1901	1409.6
10	1167.6	129.7	1851	1297.4
15	1021.4	180.2	1695	1201.6
20	895.3	223.8	1599	1119.1
25	785.4	261.8	1551	1047.1
30	688.7	295.2	1497	983.9
35	603.1	324.7	1479	927.9
40	526.7	351.1	1380	877.8
45	458.1	374.8	1341	833.0
50	396.2	396.2	1286	792.4
55	340.1	415.6	1265	755.7
60	288.9	433.3	1261	722.2
65	242.0	449.5	1223	691.5
70	199.0	464.3	1167	663.4
75	159.3	478.0	1158	637.4
80	122.7	490.7	1121	613.4
85	88.7	502.5	1119	591.1
90	57.0	513.4	1081	570.4
95	27.6	523.6	1078	551.1
100	0.0	533.1	1043	533.1

A.3 Experimental Results

A.3.1. Lightweight Concrete

The experimental results for compressive and tensile strength of concrete made with 0, 20, 30, and 40 % scoria instead of sand and different cement content 300, 350, and 400 Kg/m³ and various water cement ratio 0.50, 0.55, and 0.60 are given in Table A-10. The relationship between compressive strength and cement content has shown in Figures A-3 to A-6. The experimental results shown that the maximum compressive strength in concrete creates in 350 Kg/m³ cement content. The relationship between compressive

strength and the percentage of scoria instead of sand in different cement content is given in Figures A-7, A-8, and A-9. It is obvious that by increasing the percentage of scoria instead of sand, the compressive strength of concrete decreased. The acceptable squared coefficient of determination between data proves the well accuracy of experimental work. Figure A-10 has presented decreasing in tensile strength of concrete by increasing the percentage of scoria instead of sand. They also prove that by increasing the water cement ratio the compressive and tensile strength decreased. The relationship between tensile strength and squared compressive strength, 7 and 28 days age, has given in Figures A-11 and A-12. The squared coefficient of determination between data is more than 0.8. Figures A-13, A-14, and A-15 have presented relationship between slump and different percentages of scoria for different water cement ratio and cement content. The results have shown decreasing in slump by increasing in percentage of scoria instead of sand in concrete. This predictable experimental results presented acceptable rang of slump in 0.55 water cement ratio by increasing the percentage of scoria instead of sand in produced concrete.

Table A.10: The experimental results for compressive and tensile strength of concrete

Scoria instead of sand-%	Cement Content	Compressive Strength-MPa						Tensile Strength-MPa					
		7 Days			28 Days			7 Days			28 Days		
		0.5	0.55	0.6	0.5	0.55	0.6	0.5	0.55	0.6	0.5	0.55	0.6
0	300	21	20	18	31.5	31	28.5	-	-	-	-	-	-
0	350	23.5	23	18.5	33.5	32	29	2.85	2.6	2.45	4	3.6	3.4
0	400	20	19	18	30.5	29	26.5	-	-	-	-	-	-
20	300	20	17.5	16.5	29	26	24	-	-	-	-	-	-
20	350	21	19	17	30	27	24	2.75	2.4	1.95	3.75	3.4	2.85
20	400	19.5	16.5	14.5	26	24	23	-	-	-	-	-	-
30	300	18	17	15	25	24	22.5	-	-	-	-	-	-
30	350	20	18.5	15.5	25.5	24	23.5	2.55	2.4	1.7	3.15	2.9	2.75
30	400	18.5	18	14	24.5	22.5	21	-	-	-	-	-	-
40	300	15.5	15.5	14	24	24	22	-	-	-	-	-	-
40	350	17.5	16	14.5	25.5	24.5	23	2.4	2	1.6	2.95	2.7	2.6
40	400	16	15	12.5	24	23	20	-	-	-	-	-	-

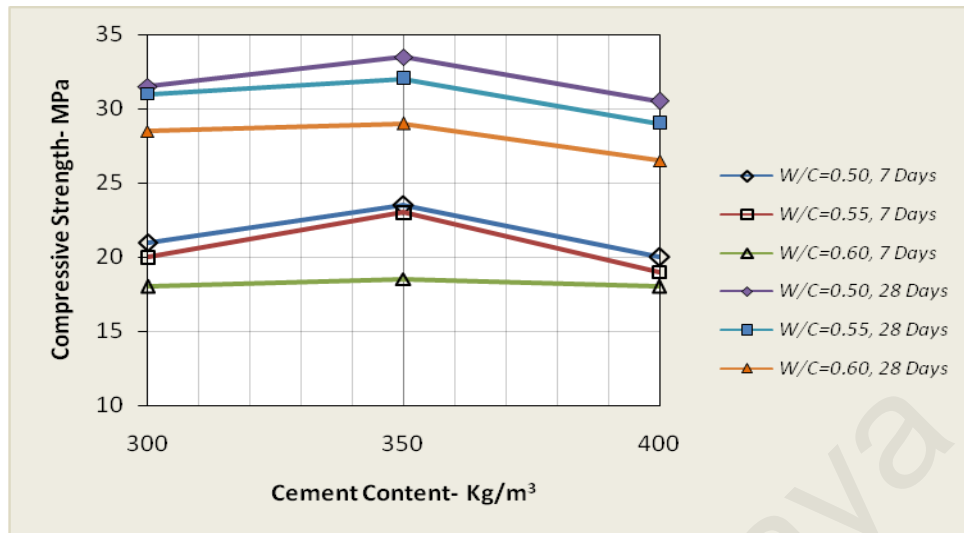


Figure A.3: Relationship between cement content and compressive strength for the concrete made with 0% scoria instead of sand

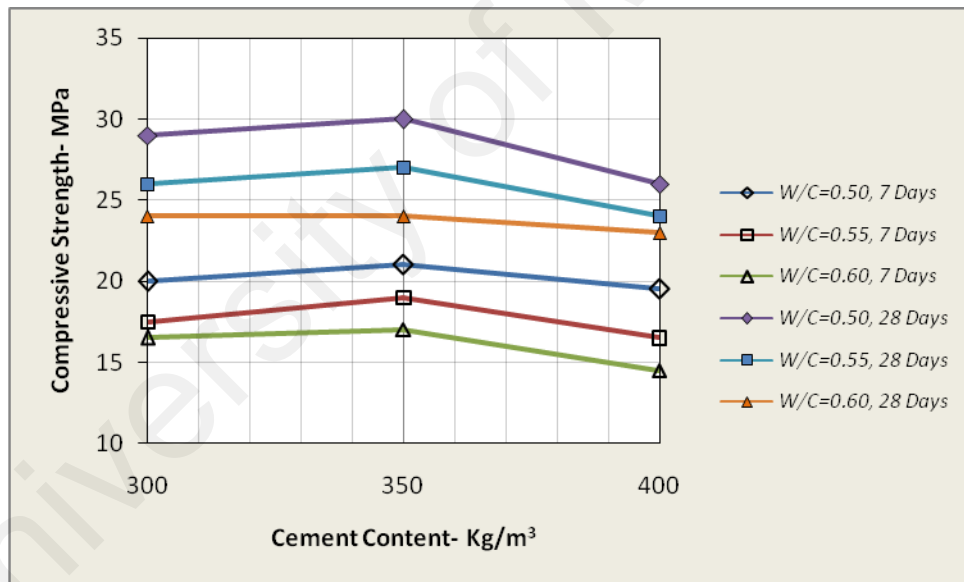


Figure A.4: Relationship between cement content and compressive strength for the concrete made with 20% scoria instead of sand

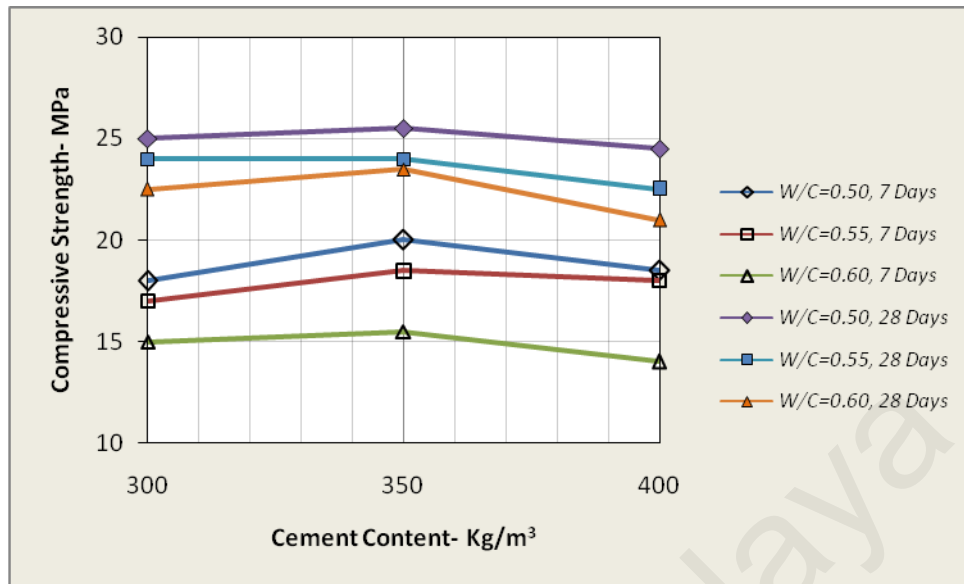


Figure A.5: Relationship between cement content and compressive strength for the concrete made with 30% scoria instead of sand

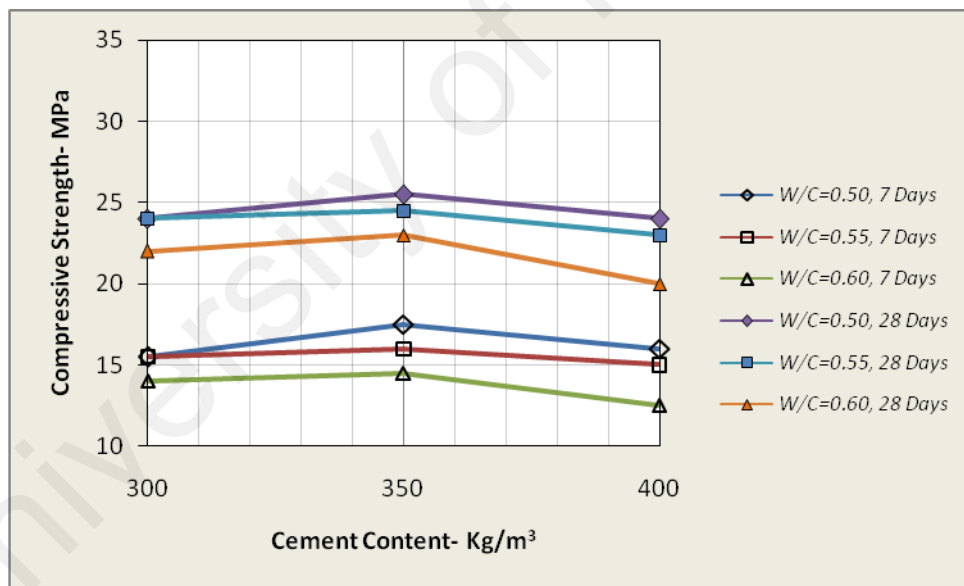


Figure A.6: Relationship between cement content and compressive strength for the concrete made with 40% scoria instead of sand

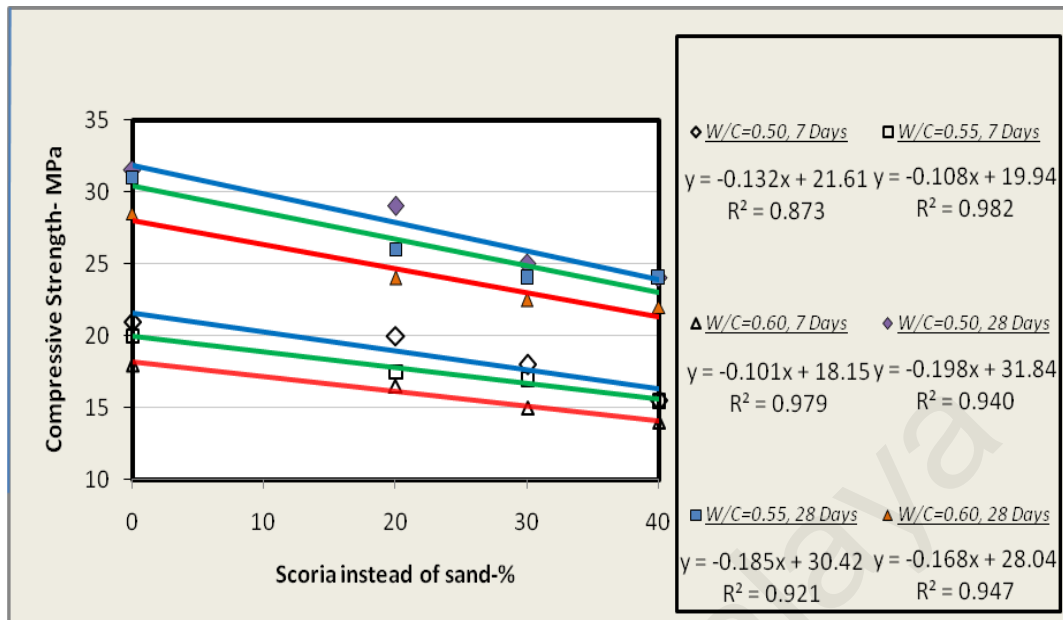


Figure A.7: Relationship between percentage of scoria instead of and compressive strength with 300 Kg/m³ cement content

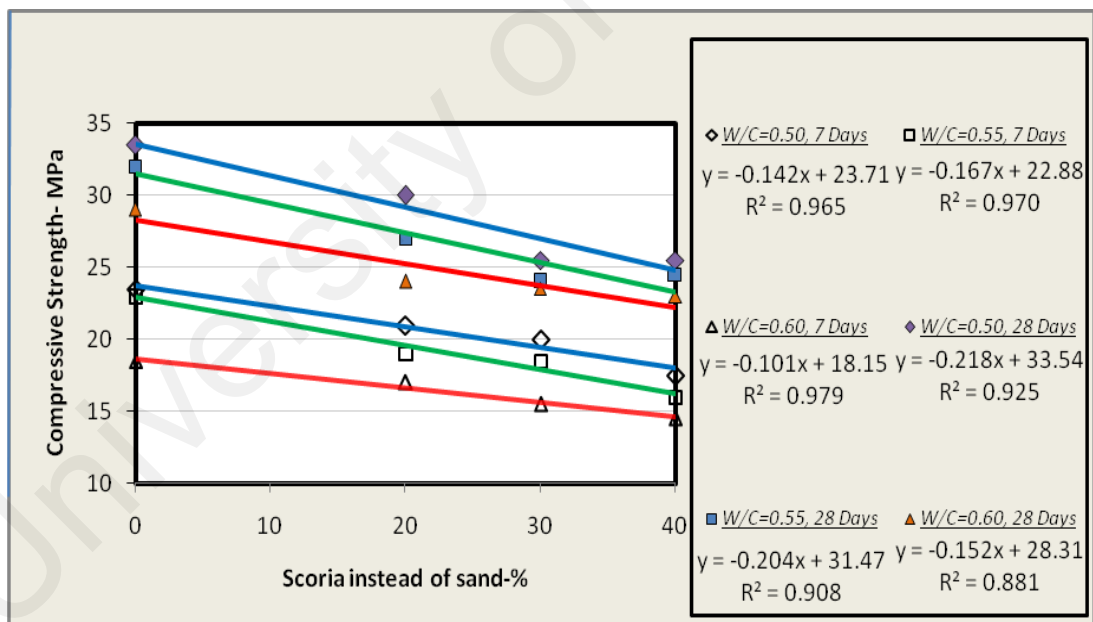


Figure A.8: Relationship between percentage of scoria instead of and compressive strength with 350 Kg/m³ cement content

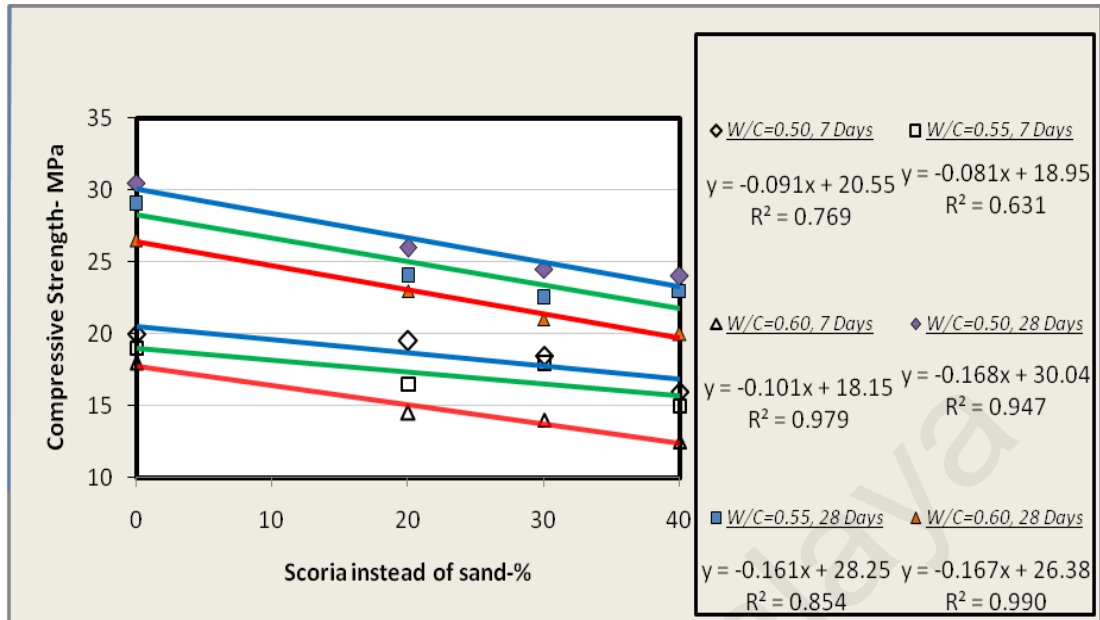


Figure A.9: Relationship between percentage of scoria instead of and compressive strength with 400 Kg/m³ cement content

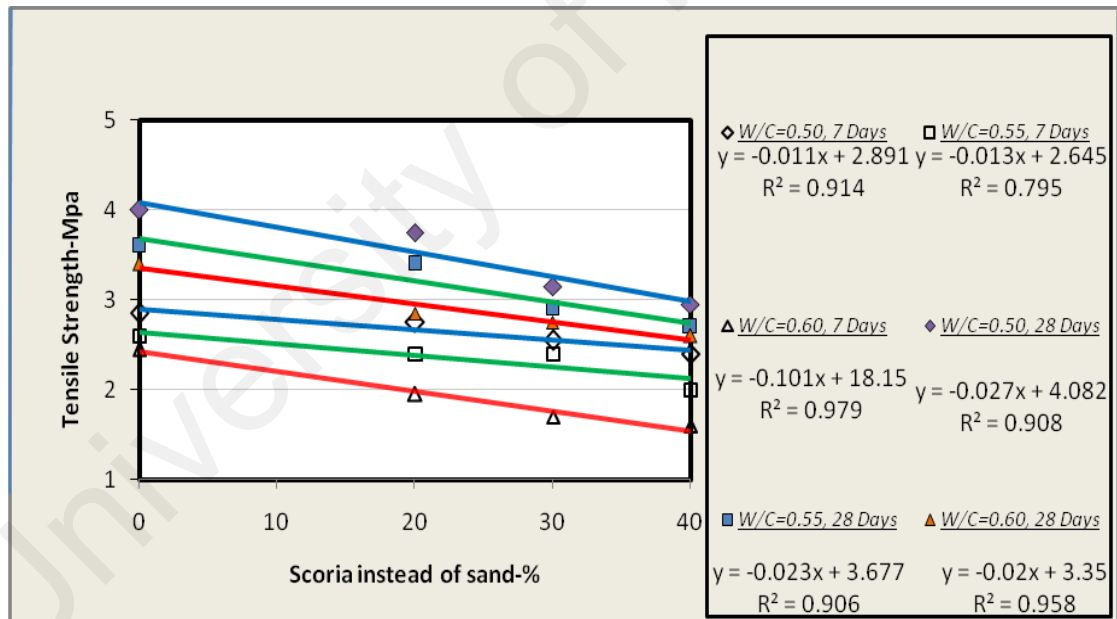


Figure A.10: Relationship between percentage of scoria instead of and tensile strength with 350 Kg/m³ cement content

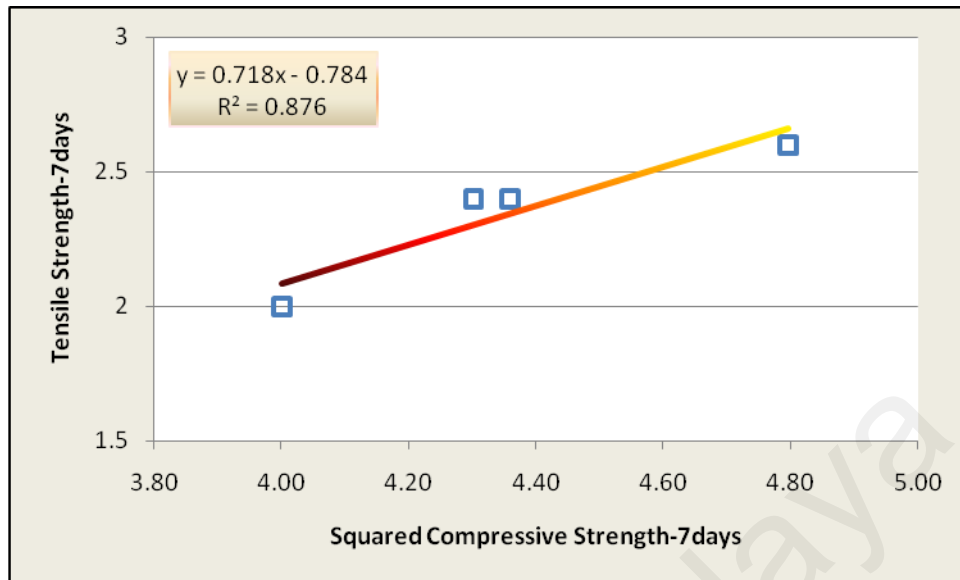


Figure A.11: Relationship between squared compressive strength and tensile strength for the concrete– 7 days

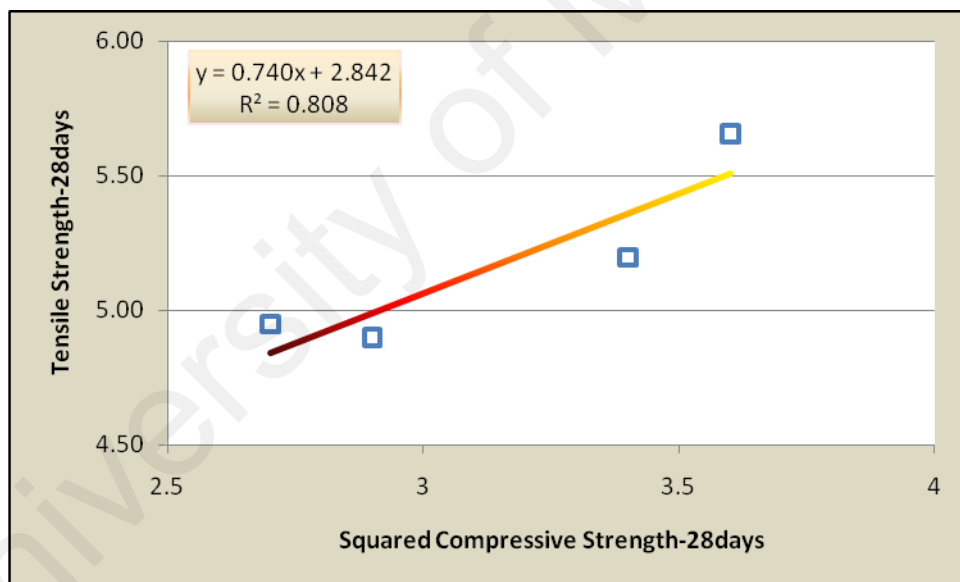


Figure A.12: Relationship between squared compressive strength and tensile strength for the concrete – 28 days

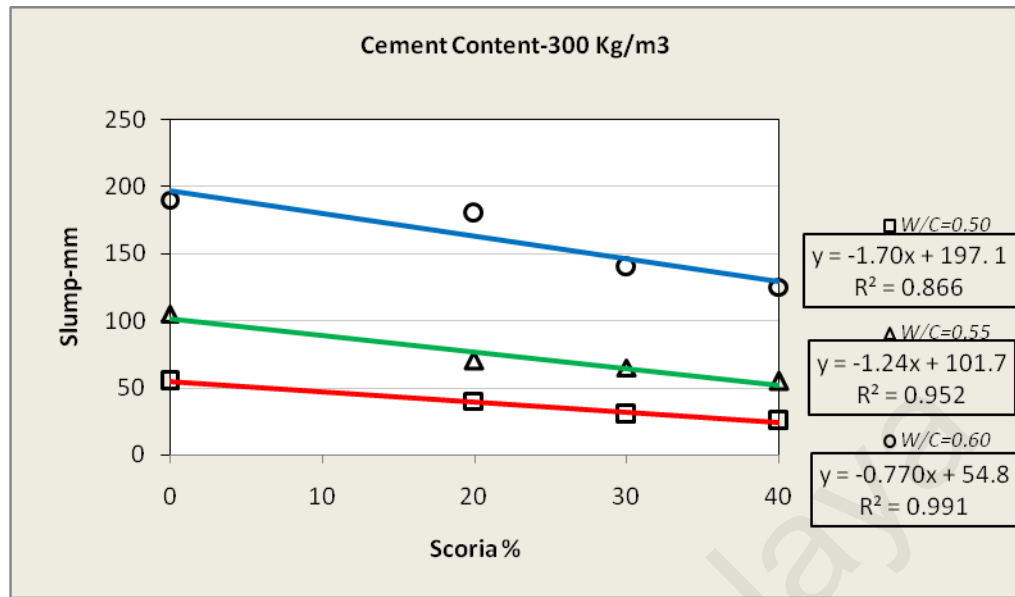


Figure A.13: Relationship between slump and percentage of scoria instead of sand for concrete with 300 kg/m³ cement content

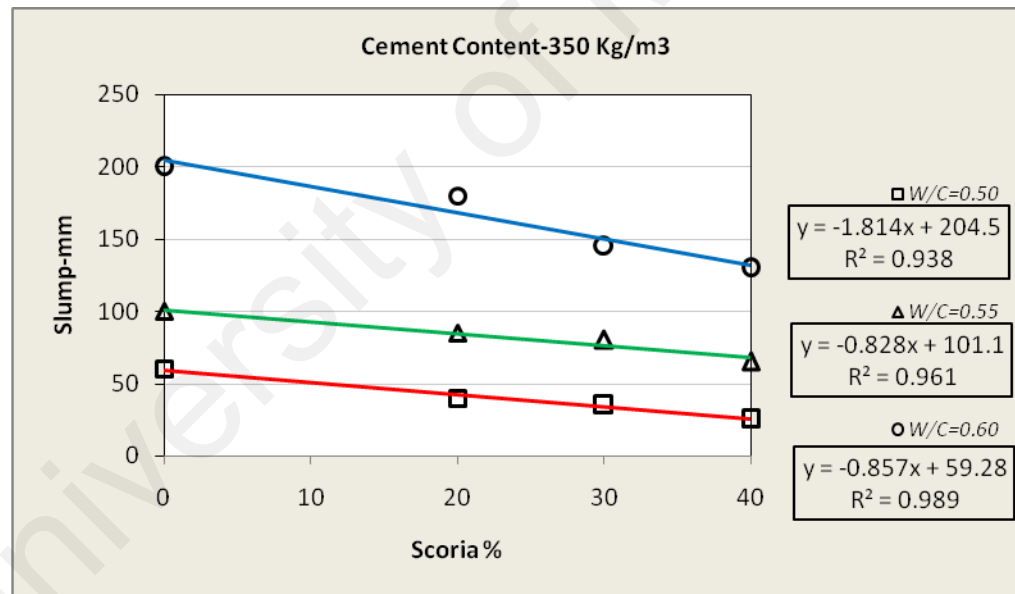


Figure A.14: Relationship between slump and percentage of scoria instead of sand for the concrete with 350 kg/m³ cement content

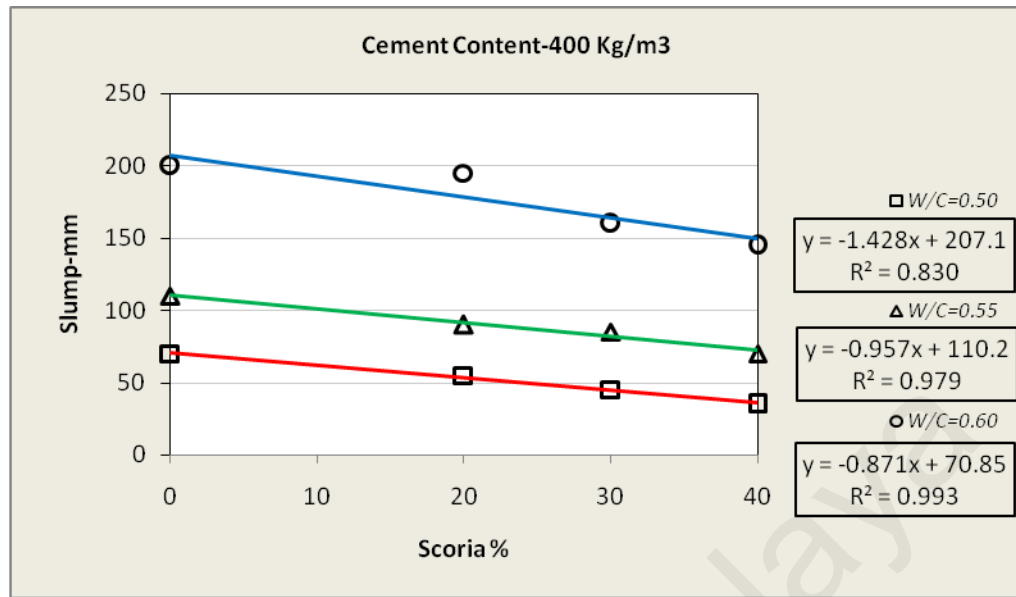


Figure A.15: Relationship between slump and percentage of scoria instead of sand for the concrete with 400 kg/m3 cement content

University of Malaysia

A.3.2. Lightweight Mortar

The experimental results of mechanical strength and density of different percentage of scoria instead of sand in mortar is given in Table A.11. The lightweight mortar made by 0, 5, 10, 15, 20, 25, 30, 35, 40, 45, 50, 55, 60, 65, 70, 75, 80, 85, 90, 95, and 100 percentage of scoria instead of sand and 0.55 water-cement ratio and 350 kg/m³ cement content. The selected cement content and cement ratio has found due to experimental result of concrete made with 0, 20, 30, & 40 % scoria instead of sand on the lightweight concrete section. The compressive and tensile strength of the mortar in 3, 7, 14, 28, & 90 is given in Figures A-16 and A-17. They have shown 10% and 21% reduce in compressive and tensile strength by completely replacing scoria instead of sand. The relationship between scoria instead of sand and density has shown in Figure A.18. This figure presented 45% reduce in density by increasing 100% scoria instead of sand. The mortars made with $\geq 60\%$ scoria instead of sand with specific gravity $\leq 1300 \text{ Kg/m}^3$ (BS EN 1996) are lightweight mortar.

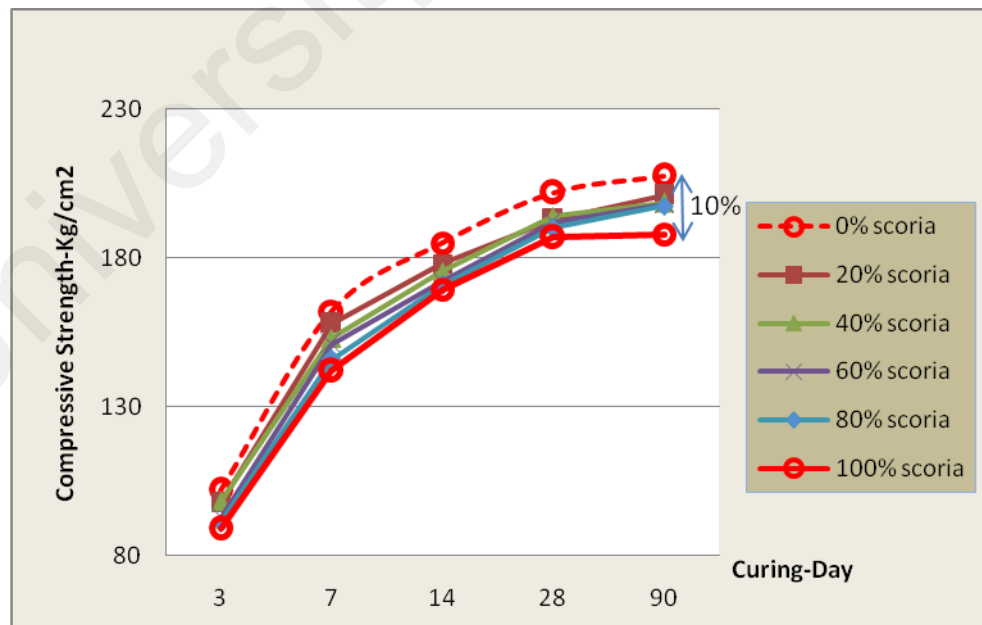


Figure A.16: Compressive strength of mortar made with different percentage of scoria instead of sand

Table A.11: The experimental results for compressive strength (CS), tensile strength (TS) and density of lightweight mortar made with different percentage of scoria instead of sand

No.	Scoria %	3 Days		7 Days		14 Days		28 Days		90 Days		Density Kg/m ³
		CS	TS	CS	TS	CS	TS	CS	TS	CS	TS	
1	0	102	11.5	162	20	185	23	202	24	207.5	25.4	2051
2	5	98.5	11	162	19	186	23	201	25	208	25	1901
3	10	98	11.5	160.6	19	180	22	195	23	200	25	1851
4	15	99.5	11	157	18.5	183	22.5	195	23.5	202	24.5	1695
5	20	97.5	11	158	18	178	22	193	22.5	201	24	1599
6	25	96	10.5	161	18.5	179	21	195	22	202	24.6	1551
7	30	95	10.4	154	18	175	21	194.5	22	199	23.4	1497
8	35	96.5	11	156.5	18.4	174.5	22.5	193	23	201	23	1479
9	40	98	11.6	153	18	175.5	22.7	194	23.5	198.5	23.5	1380
10	45	99.5	10	153	17.5	173	22	192.5	22	203	23	1341
11	50	93	10.5	151.7	17.5	174.5	21.5	193	22.5	201.5	23.5	1286
12	55	89	10.5	150	17	175.5	20	192	21	197.6	22	1265
13	60	92.5	10	151	17	172	21	192	22	198	23.5	1261
14	65	93	10.5	150	17.5	173.5	21	190	21	201	22.5	1223
15	70	88	11	148.7	17.5	171.5	20	190.5	21.5	199.5	23	1167
16	75	88.5	10.6	151.5	17	172	21	189.5	21	196	22.5	1158
17	80	91	11	146	16.5	171	20	190.	20.5	197.5	21	1121
18	85	89.5	9	147	16	165	20	188.	20	196	21.5	1119
19	90	88	9.6	144.4	16.5	167.5	18	187.5	19.5	194	21.5	1081
20	95	87.5	9	141.5	16	168.6	20	186.	19	195.6	21	1078
21	100	89	9.6	142	16	169.5	19	186.8	19	188	20	1043

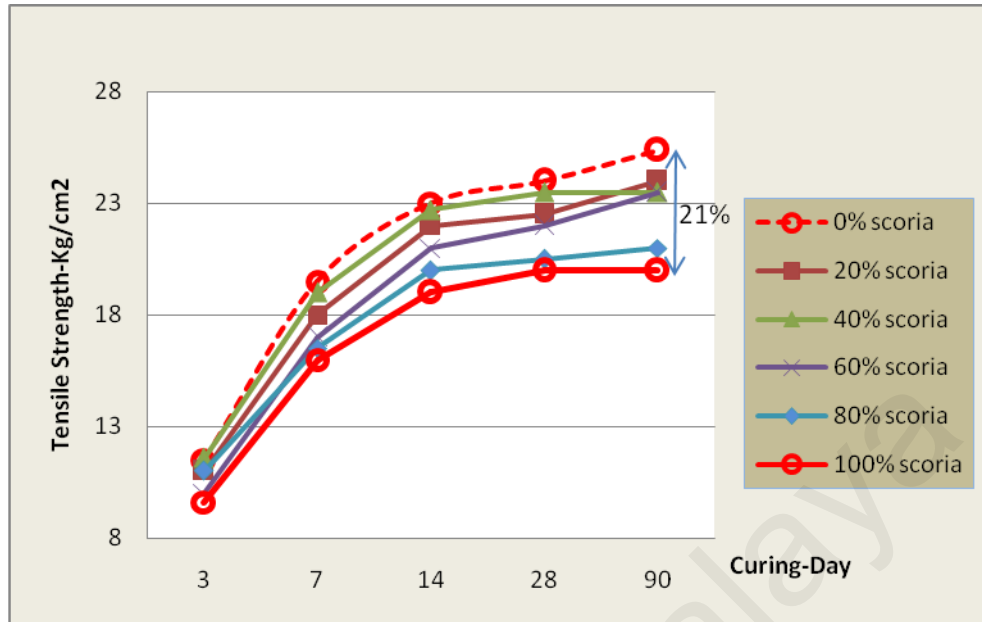


Figure A.17: Tensile strength of mortar made with different percentage of scoria instead of sand

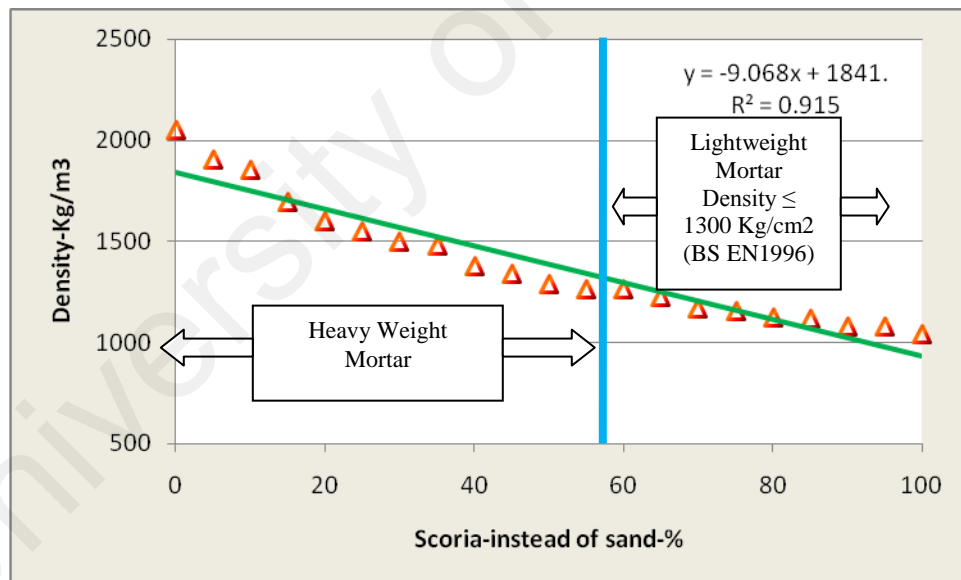


Figure A.18: Density of mortar made with different percentage of scoria instead of sand

The relationship between compressive and tensile strength and the percentage of scoria instead of sand in lightweight mortar has shown in Figures A-19 and A-20. In these figures have shown by increasing scoria instead of sand in mortar the compressive and tensile strength has decreased. In Figures A.21 and A.22, the relationship between squared

compressive strength and tensile strength has shown. The squared coefficient of determination calculated between data was 0.918 for the 28-day mixture and 0.904 for the 7-day mixture. It proves the adequate agreement between experimental data.

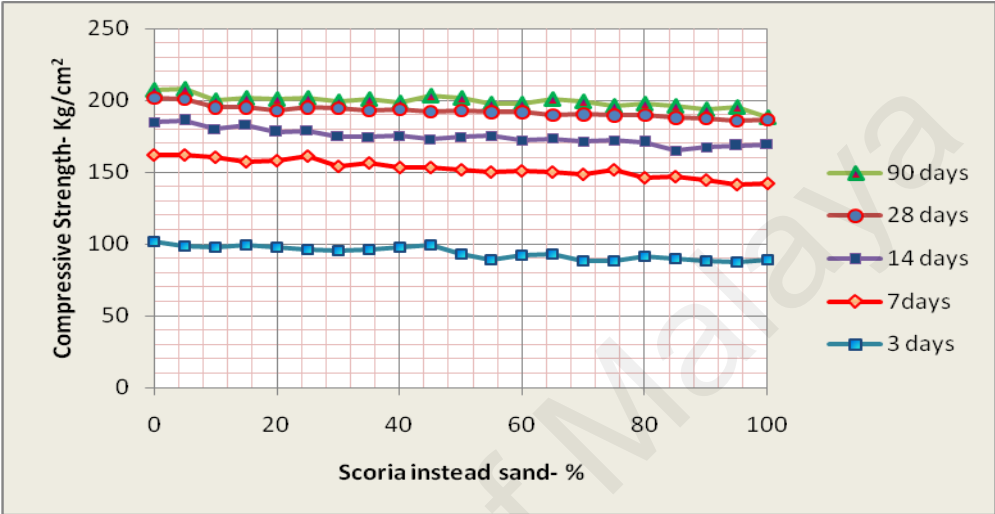


Figure A. 19: Relationship between compressive strength and percentage of scoria instead of sand

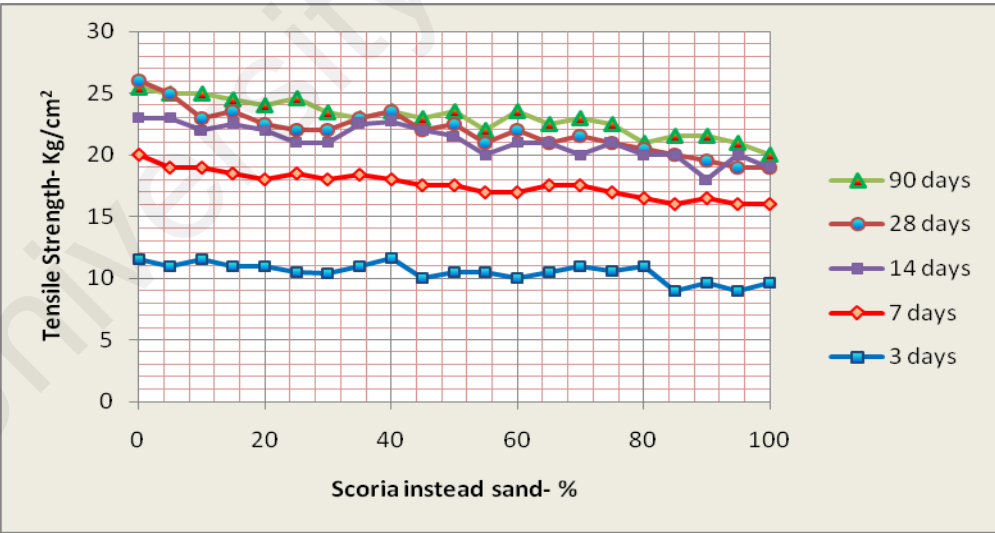


Figure A. 20: Relationship between tensile strength and percentage of scoria instead of sand

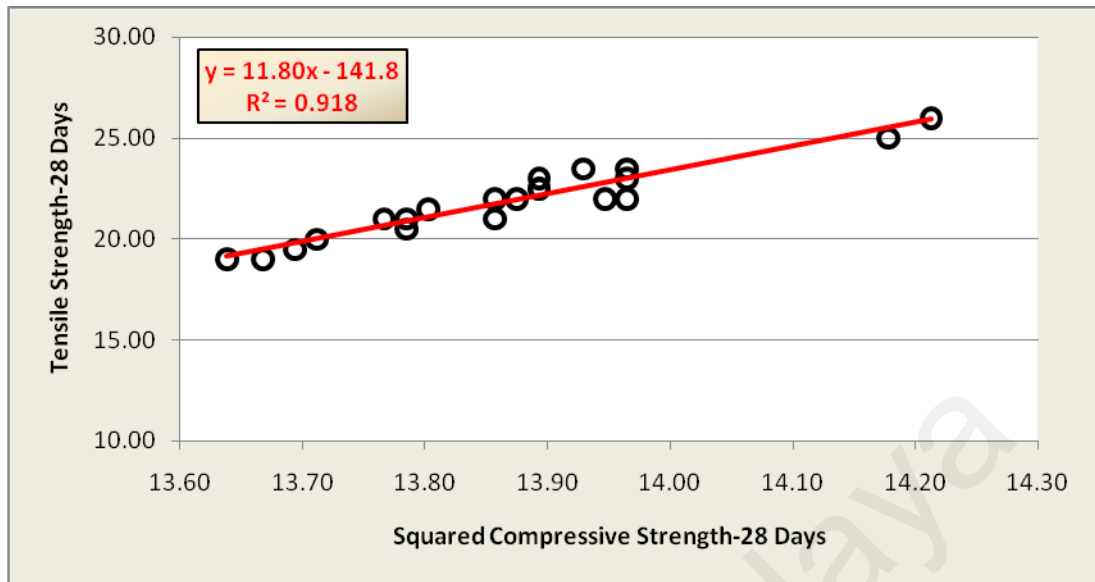


Figure A. 21: Relationship between squared compressive strength and tensile strength – 28 days

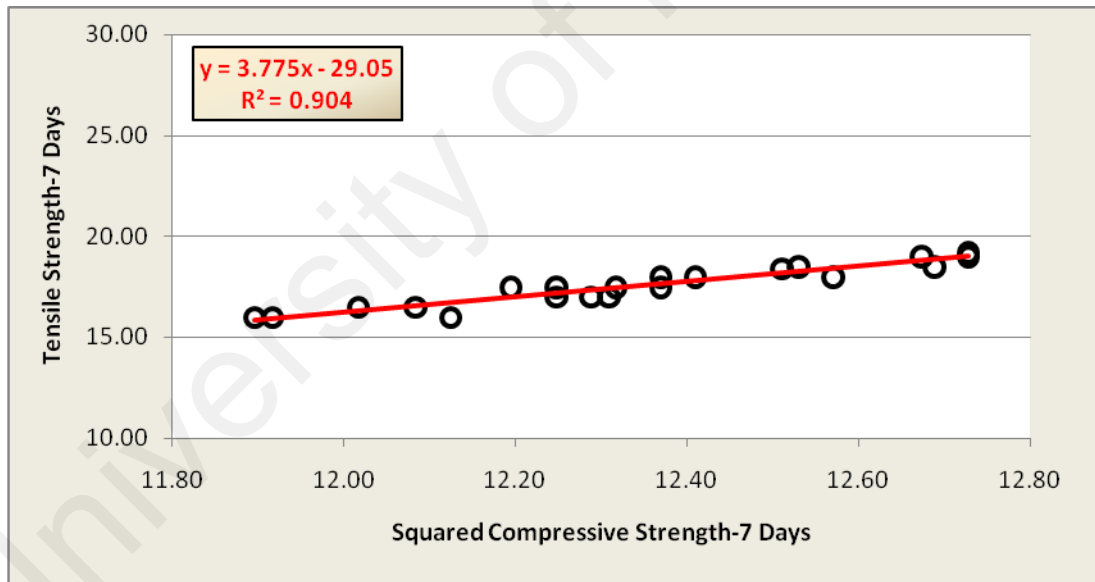


Figure A.22: Relationship between squared compressive strength and tensile strength – 7 days

A.4 Feed-forward Back-propagation Neural Networks

Feed-forward Back-propagation Neural Networks (FBNNs) applied for the mechanical strength prediction of lightweight mortar and concrete made with different percentage of scoria instead of sand.

A.4.1. Lightweight Concrete

In this part, eight networks with different structures were studied to identify the optimal result as well as shown in Table A.12. The cement content, water cement ratio, and the percentage of scoria instead of sand were input data and concrete compressive strength was network output. The different data arrangements (DA) given in Figures A.23 were applied as important parameter to test different networks. The other parameters such as training function, adaption learning function, performance function, number of hidden layer, transfer function in hidden layer, and transfer function in output layer, were considered to find the best network.

Table A.12: Properties of applied FBNN

Net Market	Training function	Adaption learning function	Number of Neurons in Hidden layer	Transfer function in Hidden layer	Transfer function in Output layer	Data Arrangement in Figure
N1	TRAINLM	LEARNGD	18	TANSIG	TANSIG	DA1
N2	TRAINLM	LEARNGD	17	TANSIG	TANSIG	DA2
N3	TRAINBR	LEARNGD	10	TANSIG	LOGSIG	DA3
N4	TRAINBR	LEARNGDM	9	TANSIG	LOGSIG	DA1
N5	TRAINBR	LEARNGD	10	LOGSIG	LOGSIG	DA3
N6	TRAINBR	LEARNGD	9	LOGSIG	LOGSIG	DA3
N7	TRAINBR	LEARNGD	10	LOGSIG	LOGSIG	DA2
N8	TRAINBR	LEARNGD	10	LOGSIG	LOGSIG	DA1

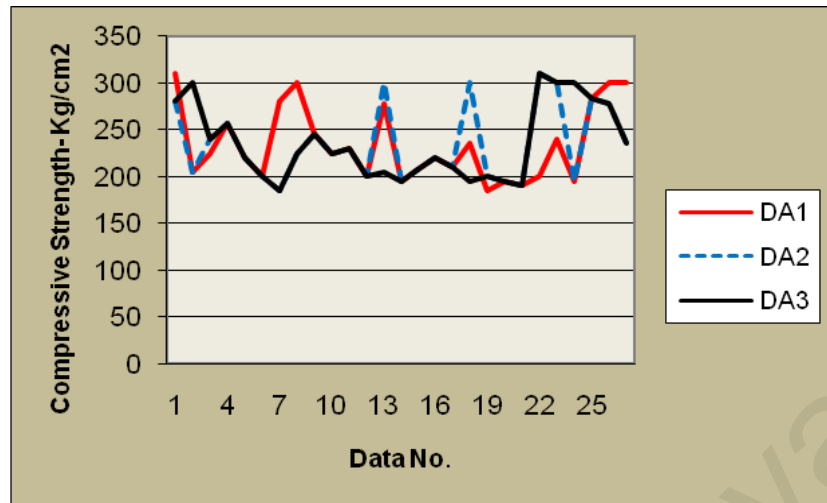


Figure A.23: Applied Data Arrangement (DA) in FBNN generation

The minimum error was extracted using the MSE method for eight networks, as shown in Figure A.24. The coefficient of determination is shown in Table A.13. Network N8, with 10 neurons in the hidden layer, is considered to have the minimum error and maximum correlation coefficient, close to 1. For this network, the input data arrangement was the important parameter in comparing with the networks N7 & N5. In networks N7 & N5 all other parameters are similar to network N8. However, the created network N8 is more knowledgeable than either N7 or N5.

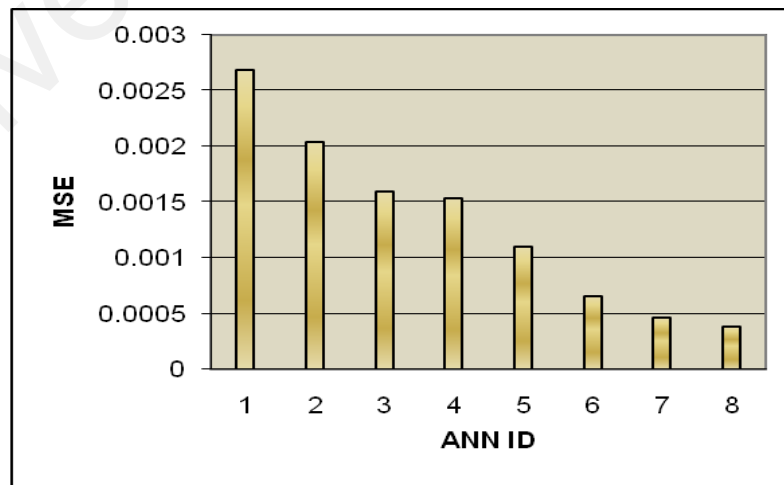


Figure A.24: Mean squared error (MSE) for 8 classified neural networks

Table A.13: The amount of MSE & R^2 for 8 classified neural network on FBNN method

Neural Network ID	R^2	MSE
N1	0.6848	0.002682
N2	0.9846	0.002038
N3	0.9486	0.001591
N4	0.9694	0.001529
N5	0.9261	0.001102
N6	0.9612	0.000652
N7	0.9551	0.000464
N8	0.9639	0.00038

According to the calculated MSE and R^2 in Table A.13, neural network No.8, with a means squared error equal to 0.00038 and squared coefficient of determination equal to 0.9639, was the best network. The network architecture is shown in Figure A.25.

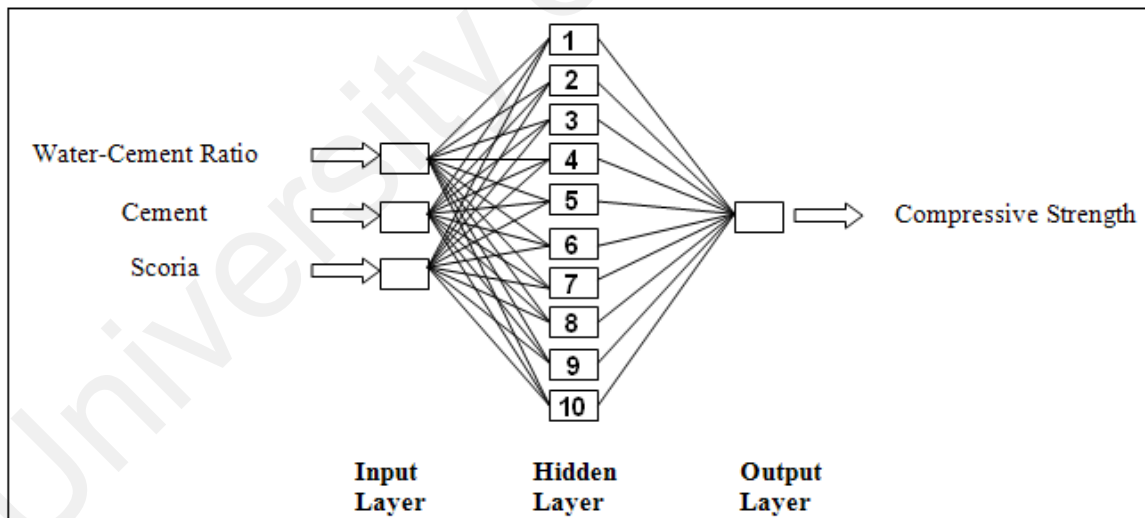


Figure A.25: Layer Architecture of the selected FBNN

In Figure A.26, the network output data and experimental results for the compressive strength are compared.

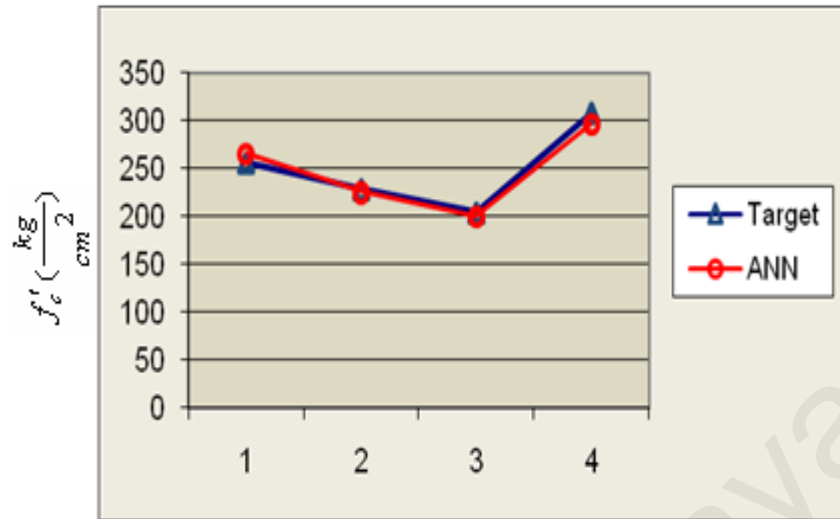


Figure A.26: FBNN evaluation between target and predicted compressive strength

The squared coefficient of determination and RMSE in the training phase of the selected network was 0.945 and 0.0215.

A.4.2. Lightweight Mortar

In this part, a multilayer feed-forward back-propagation neural network by using different training and learning functions, 1 & 2 hidden layers with different neurons, and log-sigmoid/Purelin as transfer function was adopted. The root mean square error (RMSE) applied to compare between predicted results and targets. The neural network information is given in Table A.14.

Table A.14: ANNs Information

The Number of Data	105 data = 80 (Training) + 15 (Validation) + 10 (Testing)
Input Layer	(Scoria - %) & (Curing - day)
The number of Neurons in Hidden Layers(HNs)	$3 \leq \text{HNs} \leq 15$
Output Layer	Compressive & Tensile Strength
Net Architecture	(2-HN ₁ -2) & (2-HN ₁ -HN ₂ -2)
Network Type	Multilayer Feed-Forward
Net Algorithm	Back-Propagation
Training Function	Trainbr & Trainlm
Learning Function	LEARNGD & LEARNGDM
Output Transfer Function	Log-Sigmoid & Purelin
Hidden Transfer Function	Log-Sigmoid & Tangent Sigmoid
Performance Function	RMSE

According to information given in Table A.14, 52 different networks have generated as well as shown in Tables A.15, A.16, A.17, and A.18. The net calculation report presented in Table A.15 investigated for the 3, 7, 11, & 15 neurons in the hidden layer, Trainbr & Trainlm as training function, Learngd and Learngdm as learning function, and sigmoid as output transfer function. The network calculation sheet shown in Table A.16 is generated for the 5, 10, & 15 neurons in one hidden layer network, trainlm and learngdm as training and learning function, and Purelin as output transfer function. Tables A.17 and A.18 presented the calculation for network with two hidden layers and different neurons. In both calculation reports, the training and learning function are similar but the output transfer function is different. The validations of the created networks are performed on the testing output after training.

Table A.15: Networks Calculation Report for one Hidden Layer and LOGSIS as output Transfer Function

Train Func	Learn Func	Transfer Func	RMS error & R ²	The number of neurons in hidden layer							
				3		7		11		15	
				Train	Test	Train	Test	Train	Test	Train	Test
Trainbr	L GD	Logsig	RMS	0.153	0.161	0.152	0.159	0.157	0.161	0.170	0.162
			R ²	0.841	0.886	0.882	0.843	0.822	0.875	0.894	0.767
		Tansig	RMS	0.145	0.161	0.167	0.160	0.139	0.161	0.142	0.159
			R ²	0.860	0.902	0.841	0.866	0.843	0.827	0.706	0.806
	L GDM	Logsig	RMS	0.157	0.159	0.147	0.161	0.158	0.159	0.146	0.161
			R ²	0.869	0.849	0.867	0.826	0.869	0.875	0.830	0.844
		Tansig	RMS	0.655	0.625	0.171	0.161	0.167	0.161	0.161	0.166
			R ²	0.841	0.909	0.866	0.870	0.717	0.791	0.74	0.79
Trainlm	L GD	Logsig	RMS	0.154	0.213	0.160	0.155	0.141	0.158	0.135	0.154
			R ²	0.87	0.85	0.884	0.9	0.886	0.865	0.87	0.89
		Tansig	RMS	0.16	0.158	0.186	0.213	0.17	0.154	0.138	0.163
			R ²	0.881	0.887	0.856	0.878	0.9	0.87	0.914	0.865
	L GDM	Logsig	RMS	0.149	0.161	0.154	0.155	0.152	0.154	0.142	0.171
			R ²	0.869	0.893	0.881	0.908	0.909	0.889	0.906	0.855
		Tansig	RMS	0.165	0.154	0.144	0.154	0.138	0.155	0.159	0.154
			R ²	0.903	0.892	0.905	0.855	0.879	0.978	0.879	0.902

Table A.16: Networks Calculation Report for one Hidden Layer and PURELIN as output Transfer Function

Neurons in hidden layer	Training & learning Function: TRAINLM & LEARN GDM				Transfer Function Logsig=L, Tansig=T
	R ²			Training RMSE	
	Training	Validation	Testing		Hidden Layer
5	0.994	0.991	0.989	0.0294	L
	0.997	0.993	0.996	0.0214	T
10	0.996	0.984	0.995	0.0233	L
	0.997	0.994	0.997	0.020	T
15	0.998	0.992	0.993	0.0368	L
	0.998	0.993	0.996	0.0227	T

Table A. 17: Networks Calculation Report for two Hidden Layers and LOGSIS as output Transfer Function

Neurons in hidden layer		Training & learning Function: TRAINLM & LEARNGDM				Transfer Function Logsig=L , Tansig=T	
HL1	HL2	R ²			Training RMSE	1 st hidden	2 nd hidden
		Training	Validation	Testing			
5	10	0.882	0.913	0.896	0.153	L	T
		0.881	0.891	0.93	0.145	T	T
5	5	0.886	0.897	0.907	0.152	L	T
		0.887	0.919	0.92	0.139	T	T
10	5	0.907	0.862	0.855	0.147	L	L
		0.887	0.863	0.922	0.153	T	L
		0.897	0.883	0.875	0.143	T	T

Table A.18: Networks Calculation Report for two Hidden Layers and PURLIN as output Transfer Function

Neurons in hidden layer		Training & learning Function: TRAINLM & LEARNGDM				Transfer Function Logsig=L , Tansig=T	
HL1	HL2	R ²			Training RMSE	1 st hidden	2 nd hidden
		Training	Validation	Testing			
5	10	0.997	0.975	0.991	0.029	L	T
		0.997	0.996	0.992	0.022	T	T
5	5	0.99	0.98	0.994	0.032	L	T
		0.996	0.990	0.989	0.024	T	T
10	5	0.998	0.996	0.982	0.017	L	L
		0.997	0.992	0.989	0.0243	T	L
		0.997	0.992	0.996	0.0286	T	T

According to the RMSE and data coefficient of determination for network output, the two following network presented in Table A.19 is selected.

Table A.19: The parameters and RMSE of selected network

Net Architecture	Neurons & Transfer Func in hidden layer		Training Function	Learning Function	Output Transfer Function	R ² (All)	RMSE	
	HL1	HL2					Train	Test
2-10-2	10 Tansig	-	Trainlm	Learngdm	Purelin	0.996	0.020	0.027
2-10-5-2	10 Tansig	5 Logsig	Trainlm	Learngdm	Purelin	0.992	0.017	0.018

A comparison between the experimental and predicted compressive strength and tensile strength by the aforementioned network (2-10-2) and (2-10-5-2) are shown in Figures A.27

and A.28. These Figures presented that the experimental and predicted results are close together.

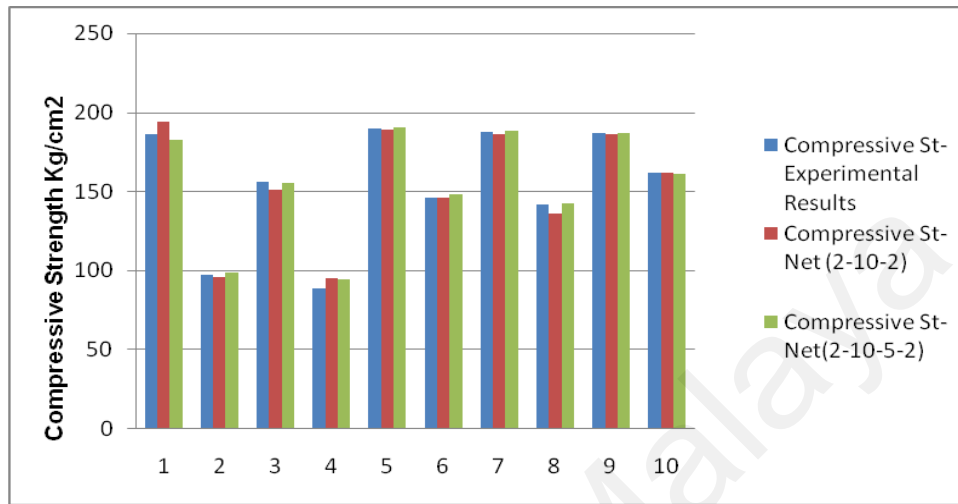


Figure A.27: Evaluation of target and predicted compressive strength by FBNN

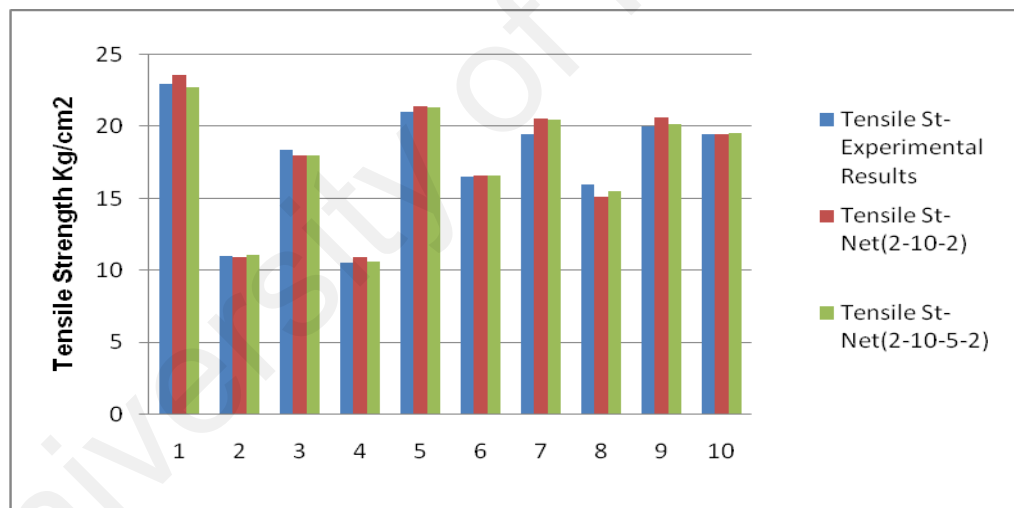


Figure A.28: Evaluation of target and predicted tensile strength by FBNN

The relationship between squared compressive strength and tensile strength of network output is given in Figure A.29. The coefficient of determination closed to 1 presented the effective relation between them in both networks 2-10-2 and 2-10-5-2.

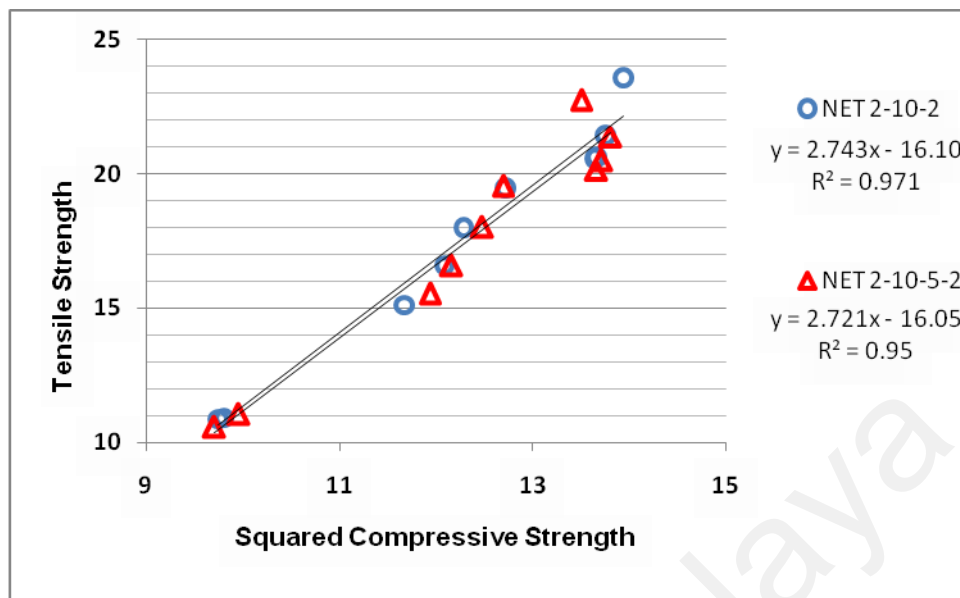


Figure A.29: Relationship between squared compressive strength and tensile strength predicted by FBNN

A.5 Generalized Regression Neural Network (GRNN)

In this part, Generalized Regression Neural Network (GRNN) utilized for the mechanical strength prediction of lightweight mortar and concrete and prediction of the load-deflection analysis of RC one-way slab.

A.5.1. Lightweight Concrete

In this part, 32 data applied for the network training and 4 data for testing. The percentages of scoria instead of sand, cement content, and water cement ratio were as input layers and compressive strength was as output layers. The predicted compressive strength had good agreement with the experimental results as well as shown in Figures A.30, A.31, and A.32. The squared correlation coefficients between data in network training and testing were 0.910 and 0.953 respectively. Also, the amount of MSE for predicted data in training and testing phase were 0.0028 and 0.00044 respectively. So, the generated GRNN can

predict the compressive strength of lightweight concrete made with different percentage of scoria instead of sand.

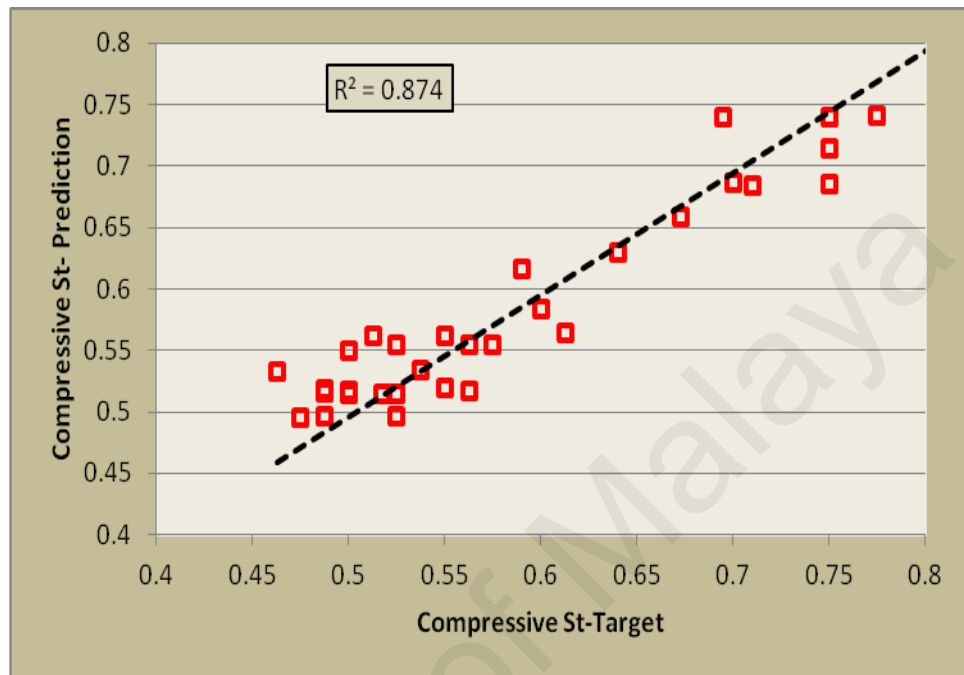


Figure A.30: Evaluation of predicted compressive strength of lightweight concrete in GRNN training phase

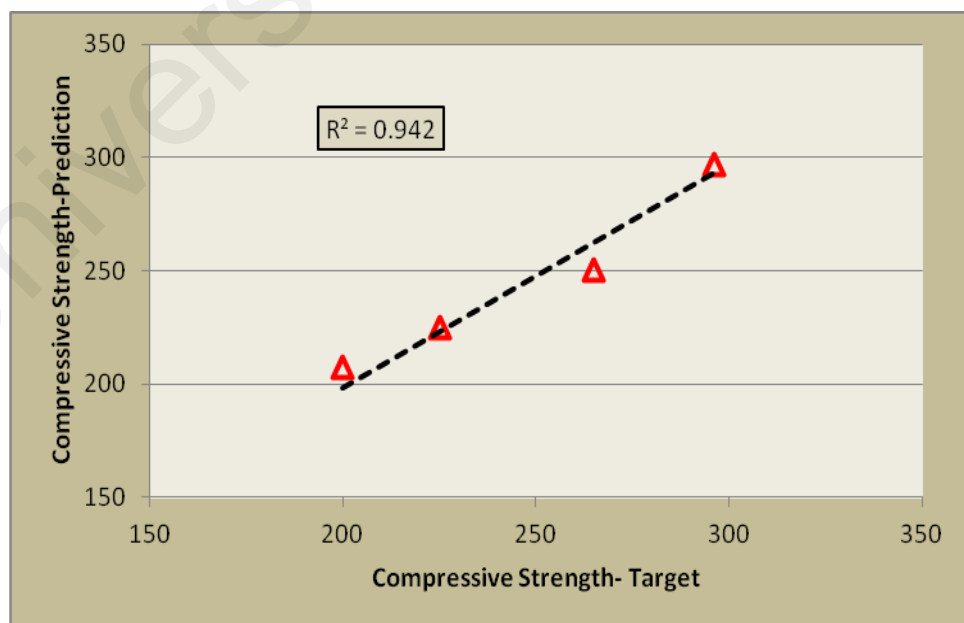


Figure A.31: The squared coefficient of determination between target and predicted compressive strength of lightweight concrete in GRNN testing phase

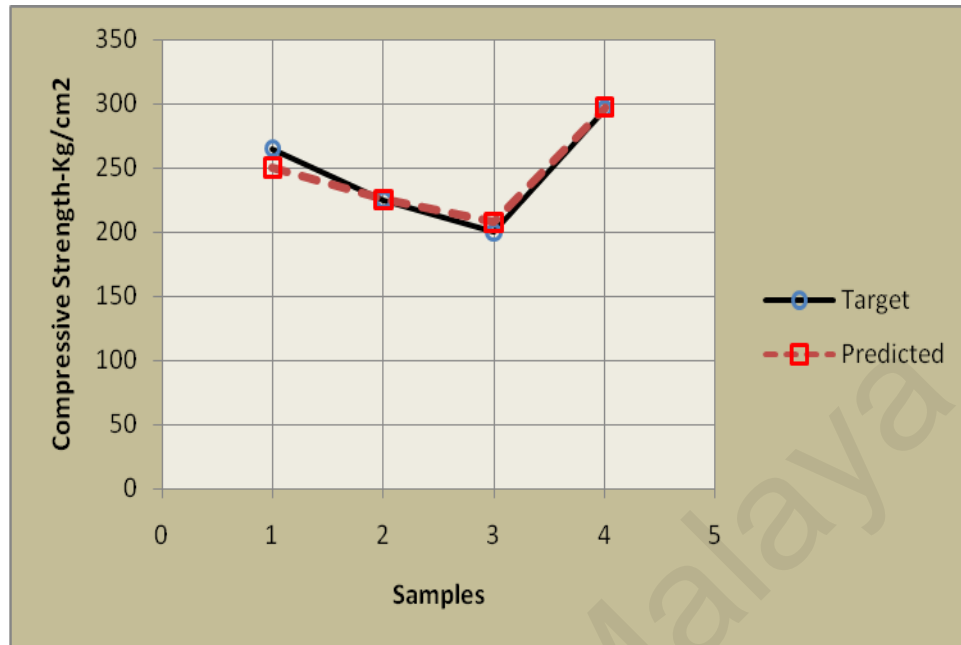


Figure A. 32: GRNN respond for compressive strength of lightweight concrete in compare with compressive strength as target

As results, the generated GRNN can predict the experimental results in normal and small number of training data available with minimum error and maximum coefficient of determination between data.

A.5.2. Lightweight Mortar

Totally 90 data applied for network creation by considering 80 data for training and 10 data for testing. The percentages of scoria instead of sand and curing time were as input layers and compressive and tensile strength were as output layers by two different networks generation. The good agreement between predicted compressive strength and target in training phase is shown in Figure A.33. The squared coefficient of determination was 0.902.

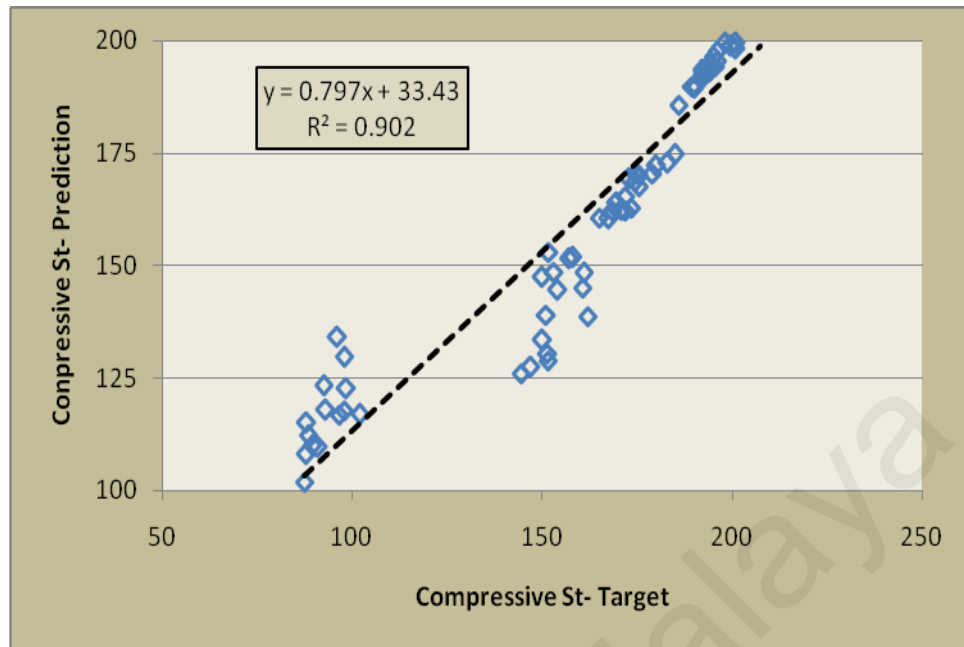


Figure A.33: Evaluation of predicted compressive strength of lightweight mortar in GRNN training phase

The amounts of MSE & RMSE in training stage were 0.0069 and 0.083 respectively. In the testing phase, the predicted compressive strength is in good agreement with the experimental results as well as shown in Figures A.34 and A.35. The amount of squared coefficient of determination between target and predicted compressive strength in testing stage was 0.934. MSE and RMSE in testing stage were 0.0057 and 0.0755 respectively.

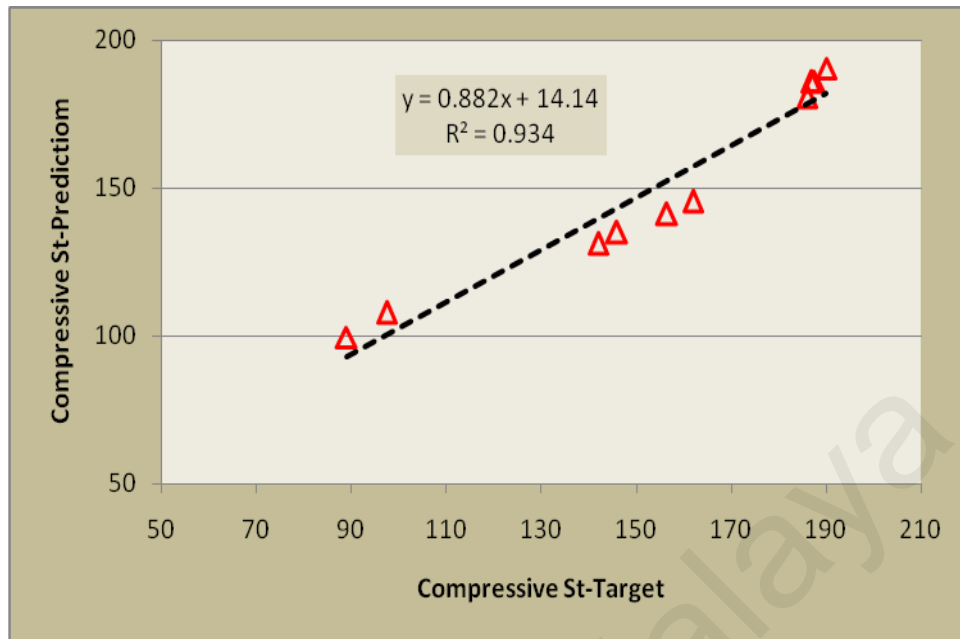


Figure A.34: The squared coefficient of determination between target and predicted compressive strength of lightweight mortar in GRNN testing phase

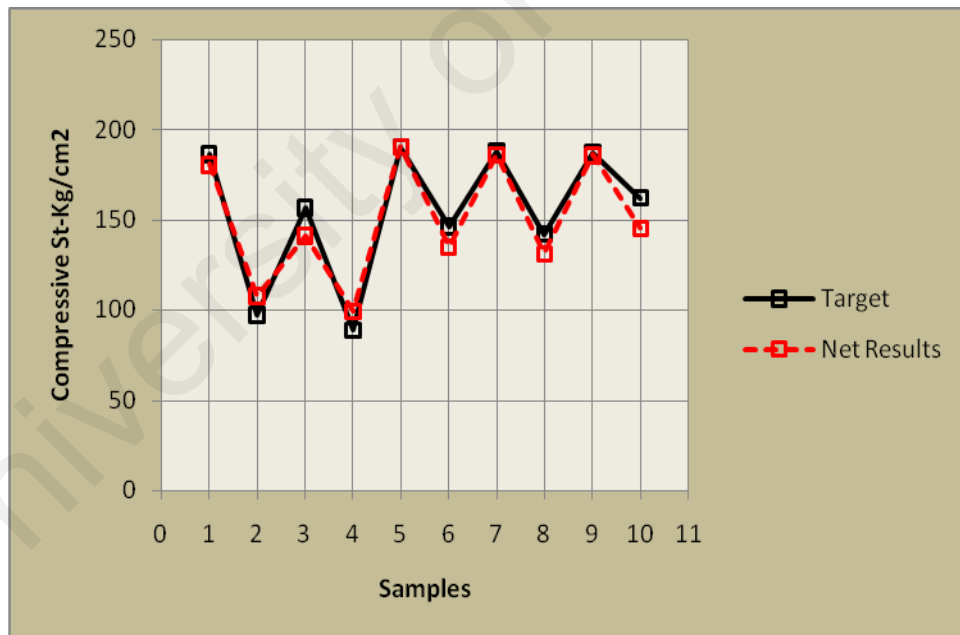


Figure A.35: GRNN respond for compressive strength of lightweight mortar in compare with target

The GRNN respond for the tensile strength in compare with the experimental results are presented in Figures A.36, A.37, and A.38. In network training, the selected network indicated 0.964, 0.002, & 0.0447 for squared correlation coefficient, MSE, and RMSE

respectively. The amount of squared correlation coefficient, MSE, and RMSE in network testing was 0.905, 0.0106, and 0.103 respectively.

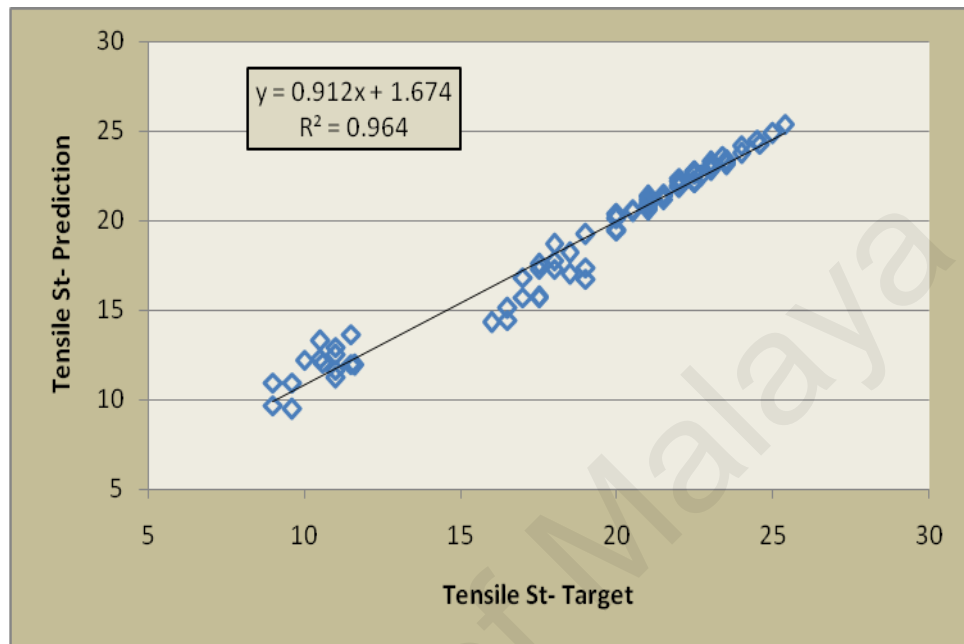


Figure A.36: Evaluation of predicted tensile strength of lightweight mortar in GRNN training phase

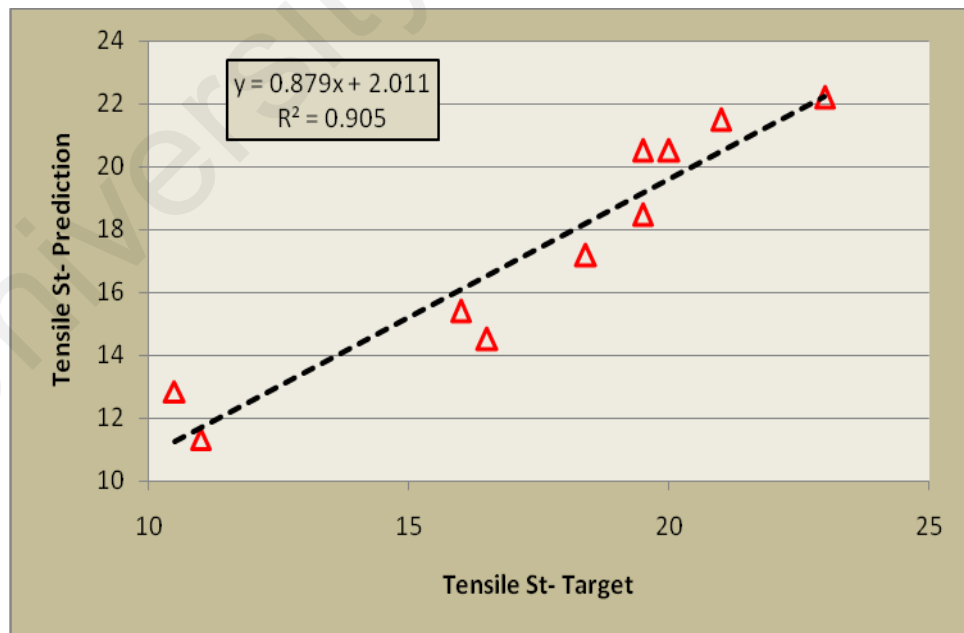


Figure A.37: The squared coefficient of determination between target and predicted tensile strength of lightweight mortar in GRNN testing phase

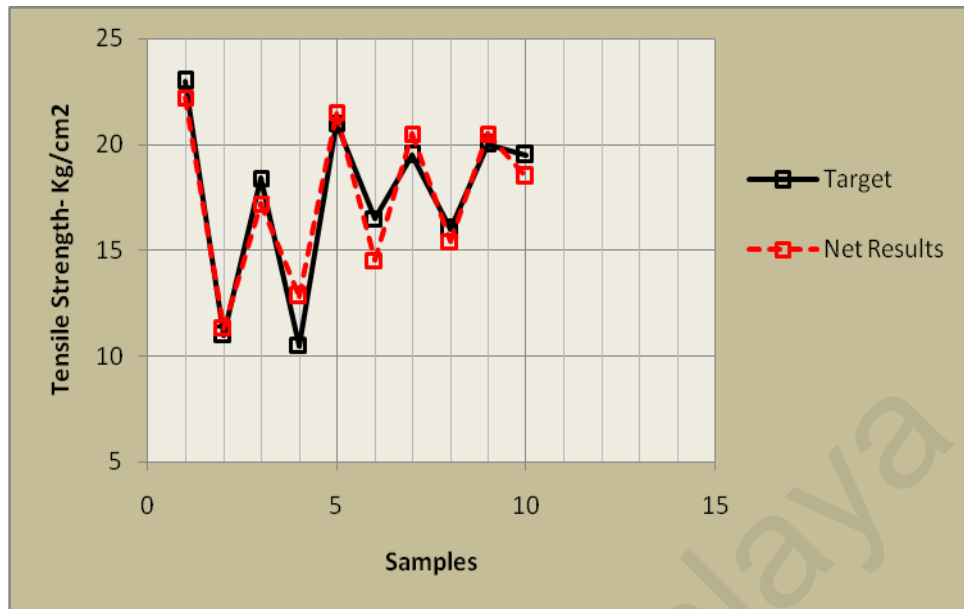


Figure A.38: GRNN respond for tensile strength of lightweight mortar in compare with experimental results as target

The predicted tensile strength from generated GRNN is in good agreement with experimental results introduced as target.

University of Malaysia

APPENDIX B

B. FIRST CRACK ANALYSIS OF CFRP STRENGTHENED RC SLAB

Six slabs with dimensions being 1800×400×120 (mm) with an equal percentage of steel bars and different lengths and width of CFRP, as shown in Table B.1 were tested and compared with a similar sample without CFRP. Before sampling, the strain gauges were installed on the bending region of the steel bar and covered by silicon adhesive for water isolation. After casting, the samples were cured using gunny bags and water for 28 days. Then, the CFRP was attached on the tensile surface of the concrete. Finally, the strain gauges were attached on the CFRP and the compressive side of the concrete before testing. The loading and instrument setups are indicated in Figure B.1.

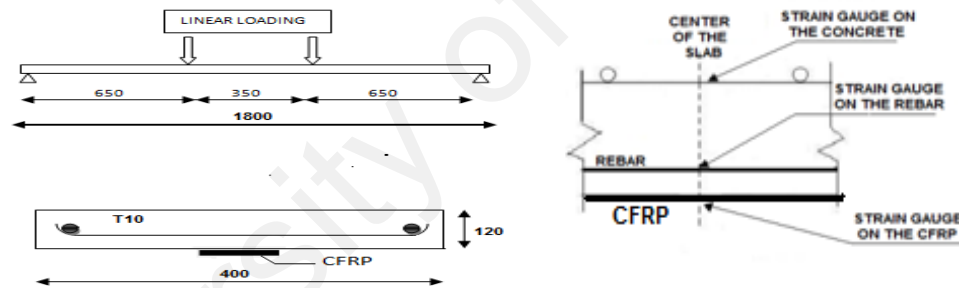


Figure B.1: Loading and Instrument Setup

Table B.1: The Tested Samples

Samples Market	CFRP Type	Steel	CFRP		
			Thickness (mm)	Width (mm)	Length (mm)
CFRP-1	S512	2T10	12	50	700
CFRP-2	S512	2T10	12	50	1100
CFRP-3	S512	2T10	12	50	1500
CFRP-4	S812	2T10	12	80	700
CFRP-5	S812	2T10	12	80	1100
CFRP-6	S812	2T10	12	80	1500
CFRP-0	WCFRP*	2T10	-	-	-

*Without CFRP

B.1. Experimental Results

The experimental results for first crack loading for the different slabs are shown in Table B.2 and Figure B.2 - B.6. The first crack load for CFRP-1, CFRP-2, CFRP-3, CFRP-4, CFRP-5, and CFRP-6 were 23.52, 24.12, 24.72, 29.3, 29.58, and 30.19KN with 8%, 10%, 13%, 34%, 35.9%, and 38.74% increase in capacity, respectively, in comparison with the slab without CFRP (CFRP-0). The results indicate that by increasing the length and thickness of the CFRP the first crack load will improve. The deflections in the first crack load were 5.94, 5.04, 4.95, 4.7, 4.6, and 4.46 mm with 8%, 21.8%, 23.25%, 27.24%, 28.8%, and 31% reduction for CFRP-1, CFRP-2, CFRP-3, CFRP-4, CFRP-5, and CFRP-6, respectively. In the strengthened slabs, the stress on the steel bar, concrete, and CFRP were 1990, 567, and 2750 microns for CFRP-1, 1941, 573, and 2678 microns for CFRP-2, 1881, 792, and 2615 microns for CFRP-3, 2226, 661, and 3239 microns for CFRP-4, 2201, 666, and 3199 microns for CFRP-5, and 2158, 982, and 3183 microns for CFRP-6, respectively. Indeed, by increasing the length of the CFRP, the stress on the steel bar and CFRP were decreased and the stress on the compressive surface of the concrete was increased. As can be seen in the first crack loading, the load, deflection, and strain were improved by increasing the length, thickness and width of CFRP.

Table B.2: The experimental Result

Slab Market	First Crack				
	Crack load	Crack deflection	Steel Strain	Concrete strain	CFRP Strain
	P_{cr_KN}	Δ_{cr_mm}	$\epsilon_s_μ$	$\epsilon_c_μ$	$\epsilon_{CF}_μ$
CFRP-0	21.76	6.46	2430	494	-
CFRP-1	23.52	5.94	1990	567	2750
CFRP-2	24.12	5.04	1941	573	2678
CFRP-3	24.72	4.95	1881	792	2615
CFRP-4	29.3	4.7	2226	661	3239
CFRP-5	29.58	4.6	2201	666	3199
CFRP-6	30.19	4.46	2158	982	3183

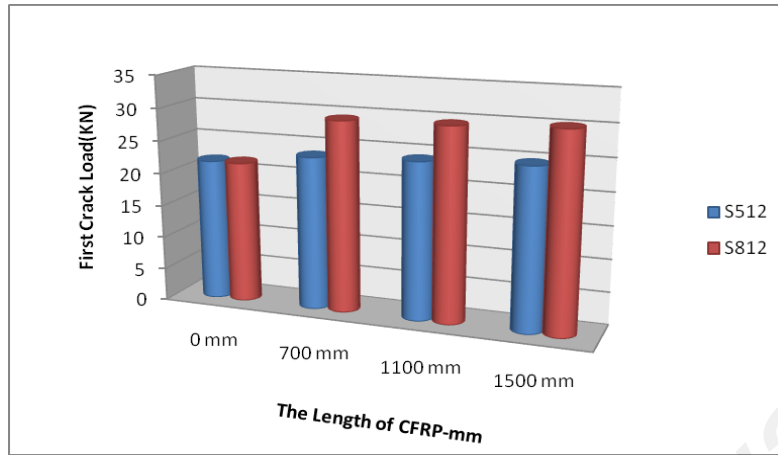


Figure B.2: The First Crack Loading

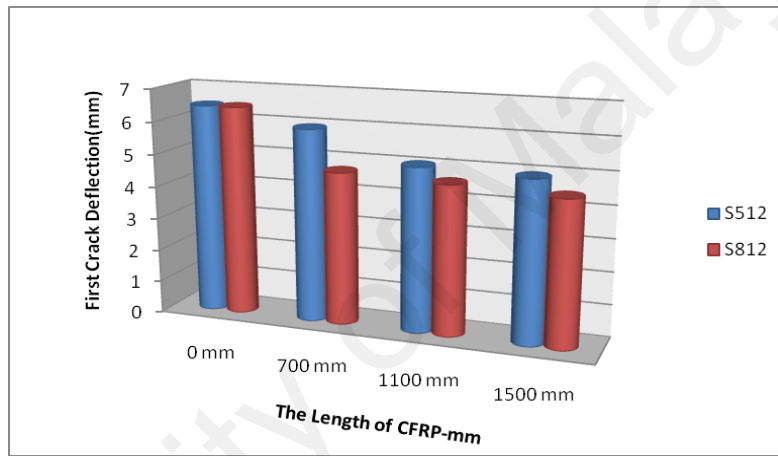


Figure B.3: The First Crack Deflection

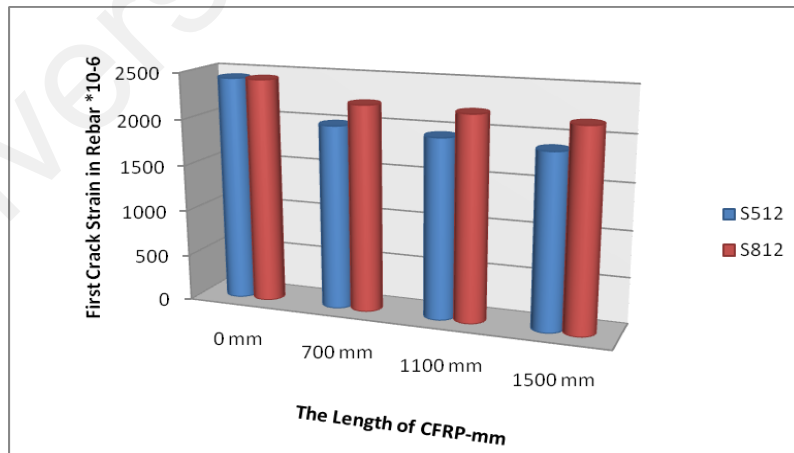


Figure B. 4: First Crack Strain in Steel Bar

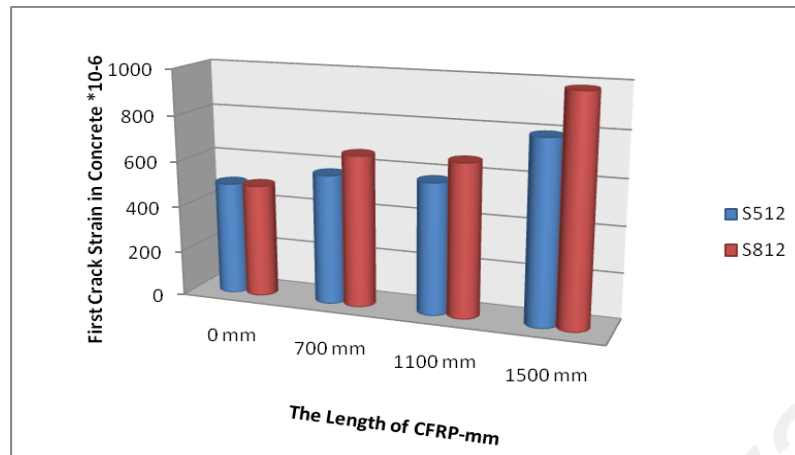


Figure B.5: First Crack Strain on Concrete

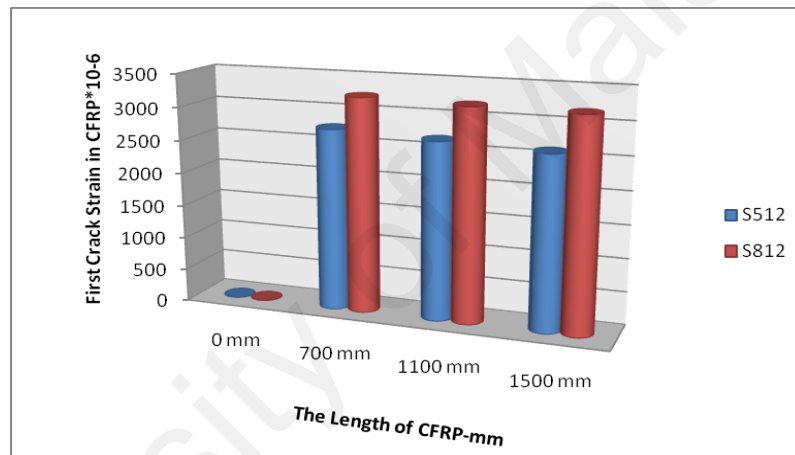


Figure B.6: First Crack Strain on CFRP

B.2. General regression neural network

GRNN is a neural network architecture that can solve any activity approximation problem. Five sets of extracted data were considered to generate an optimum network. The five different attempts to extract data for training and testing are indicated in Table B.3. For example, for the best generated network, set number 5, the predicted results of network for the CFRP-2 and CFRP-4 are indicated in Figures B.7 and B.8 respectively, and compared with the experimental results. In these Figures, the GRNN results for five parameters of analysis – loading, deflection, steel bar strain, strain on concrete, and strain

on CFRP – in the first crack are shown and compared with the experimental results. The network predicted and the experimental results are close with minimum error and maximum correlation coefficient. In addition, The Mean Square Error (MSE) of the predicted results for the set number 5 in training and testing stage are shown in Table B.4. As we see, the error for the constructed network is extremely low.

Table B.3: The different extracted data for network generation

Set No.	Training data	Testing data
1	CFRP-0, CFRP-1, CFRP-2, CFRP-3, & CFRP-4	CFRP-5 & CFRP-6
2	CFRP-0, CFRP-1, CFRP-3, CFRP-5, & CFRP-6	CFRP-2 & CFRP-4
3	CFRP-2, CFRP-3, CFRP-4, CFRP-5, & CFRP-6	CFRP-0 & CFRP-1
4	CFRP-1, CFRP-2, CFRP-3, CFRP-5, & CFRP-6	CFRP-0 & CFRP-4
5	CFRP-0, CFRP-1, CFRP-3, CFRP-5, & CFRP-6	CFRP-2 & CFRP-4

Table B.4: The MSE & RMSE in testing stage

MSE	P_{cr_KN}	Δ_{cr_mm}	$\varepsilon_s_μ$	$\varepsilon_c_μ$	$\varepsilon_{CF}_μ$	Mean
Training	7.01E-04	3.78E-06	1.26 E-06	3.007E-05	0.000847	3.167E-04
Testing	0.000298	6.02E-06	8.86E-05	4.96E-05	0.001081	0.000305

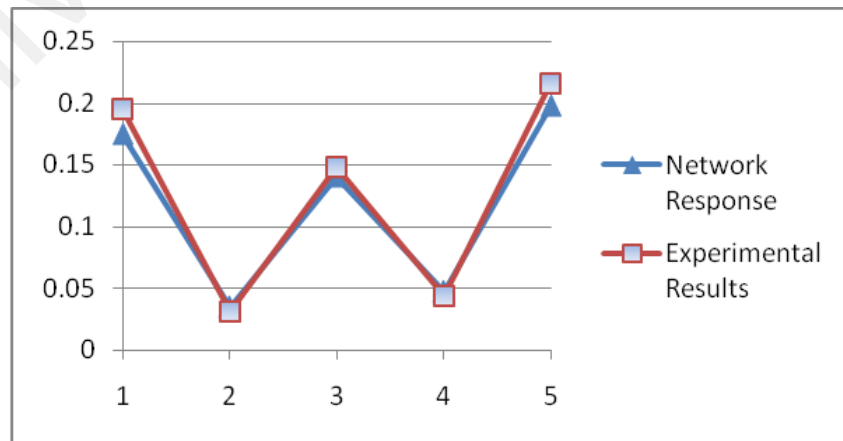


Figure B.7: Network Response in Comparison with Experimental Results for CFRP-2

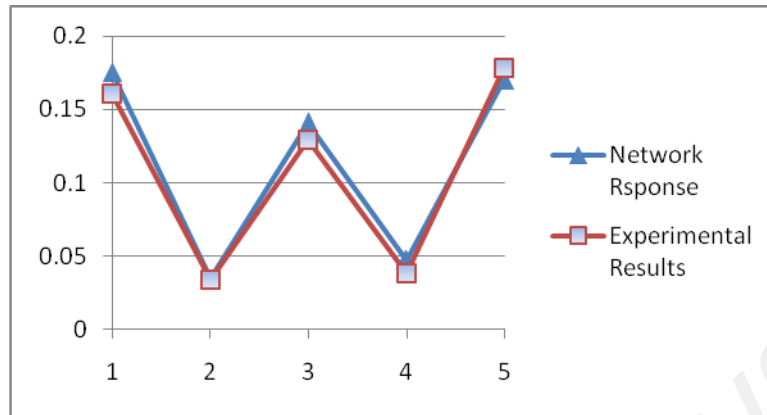


Figure B.8: Network Response in Comparison with Experimental Results for CFRP-4

The mean coefficient of determination between data used in network and real data for the samples CFRP-2 and CFRP-4 were 0.971 and 0.989 in testing and training respectively. The output results of the generated GRNNs produced experimental results of 2.89%, 1.45%, 1.98%, 1.23%, and 3.45% root mean squared error for the first crack loading, deflection, steel bar strain, strain on concrete, and strain on CFRP, respectively.

APPENDIX C

C. OTHER PUBLISHED EXPERIMENTAL WORK

C.1. Prediction of elastic modulus of high strength concrete

This study is investigated on using Support vector machine (SVM) to forecast elastic modulus of normal and high strength concrete. The elastic modulus predicted by SVM was compared with the experimental data and other prediction models as well as shown in Tables C.1 and C.2. The amount of ANN error for each data used in training and testing are presented in these tables.

Table C.1. Comparison of errors estimated by SVM and other models for training data from HSC

f_c (MPa)	E_c (GPa)	ACI 363	CEB	NS 3473	Wee	Gesoglu	Regression	Fuzzy	ANN	SVM
63.2	41.8	-8.4	-0.4	-8.8	-1.3	-3.3	-1.7	0.4	0.8	2.9
70.2	43.0	-8.2	-0.4	-9.0	-0.9	-2.2	-0.9	0.0	0.9	0.0
65.1	41.5	-7.9	0.4	-8.3	-0.4	-2.5	-0.8	0.8	1.2	2.5
70.5	40.4	-5.7	2.4	-6.5	1.6	0.4	1.6	2.8	3.6	2.4
71.5	41.4	-6.6	1.7	-7.0	0.8	0.0	0.8	2.1	2.9	1.7
63.6	42.6	-9.4	-1.3	-9.4	-1.7	-3.8	-2.1	-0.4	0.0	2.1
85.9	45.0	-7.2	0.5	-9.0	0.0	0.9	0.9	0.5	0.5	0.0
90.2	44.4	-5.8	1.8	-7.5	1.3	2.7	2.2	1.8	1.3	1.3
85.9	44.3	-6.6	1.3	-8.0	0.9	1.3	1.3	1.3	1.3	0.4
81.2	43.9	-7.0	0.9	-8.3	0.4	0.4	0.9	0.9	1.3	0.0
88.1	44.5	-6.2	1.3	-8.0	0.9	1.8	1.8	1.3	1.3	0.9
81.6	43.8	-7.0	0.9	-8.3	0.4	0.4	0.9	1.3	1.3	0.0
84.8	47.2	-9.9	-1.9	-11.3	-2.4	-1.9	-1.4	-1.9	-1.9	-2.4
85.6	45.6	-8.2	0.0	-9.6	-0.5	0.0	0.0	0.0	0.0	-0.9
96.2	46.6	-7.0	0.5	-9.3	0.0	2.3	1.4	0.5	0.9	0.0
46.4	35.2	-5.6	2.8	-5.3	1.4	-3.2	0.0	2.8	1.4	0.0
73.9	41.6	-6.2	1.7	-7.1	1.2	0.4	1.2	2.1	2.9	1.2
87.6	44.5	-6.7	1.3	-8.0	0.9	1.8	1.8	1.3	1.3	0.9
93.1	45.4	-6.4	1.4	-8.2	0.9	2.3	1.8	1.4	2.3	0.9

f_c (MPa)	E_c (GPa)	ACI 363	CEB	NS 3473	Wee	Gesoglu	Regression	Fuzzy	ANN	SVM
95.3	45.2	-5.9	1.8	-8.1	1.4	3.2	2.7	1.8	2.3	1.4
102.1	46.1	-5.5	1.8	-7.8	1.4	4.1	3.2	2.3	1.4	0.9
102.8	46.7	-6.1	1.4	-8.4	0.9	3.7	2.8	1.9	0.9	0.5
106.3	48.4	-7.3	0.0	-9.7	0.0	2.9	1.9	0.5	-0.5	-1.5
104.2	46.3	-5.6	1.9	-7.9	1.9	4.6	3.2	2.3	1.4	0.9
94.6	47.3	-8.0	-0.5	-9.9	-0.9	0.9	0.5	-0.5	0.0	-0.9
94.0	46.3	-7.4	0.5	-9.3	0.0	1.9	1.4	0.5	1.4	0.0
96.6	46.5	-7.0	0.5	-9.3	0.5	2.3	1.9	0.9	0.9	0.0
91.5	45.9	-7.3	0.5	-9.2	0.0	1.4	1.4	0.5	1.4	0.0
91.7	46.0	-7.4	0.5	-9.2	0.0	1.4	0.9	0.5	1.4	0.0
119.9	49.1	-5.9	1.5	-9.3	1.0	5.9	3.9	2.0	0.0	0.5
125.6	50.9	-6.6	0.0	-10.2	0.0	5.6	3.1	1.0	0.0	0.0
77.2	47.1	-10.8	-3.3	-12.2	-4.2	-3.8	-3.3	-2.8	-2.4	-3.8
66.5	46.8	-12.6	-4.7	-13.1	-7.0	-5.6	-5.6	-4.2	-3.7	-3.3
70.7	47.3	-12.3	-4.3	-13.2	-6.1	-5.2	-5.2	-4.3	-3.3	-4.3
61.8	45.4	-12.3	-4.1	-12.7	-7.3	-5.0	-5.4	-3.6	-3.2	0.0
68.9	47.6	-13.3	-5.2	-13.8	-7.1	-5.7	-5.7	-4.8	-3.8	-4.3
62.2	45.4	-12.3	-4.1	-12.7	-7.3	-5.0	-5.4	-3.6	-3.2	0.0
75.8	43.0	-7.3	0.9	-8.2	-0.4	0.0	0.4	0.9	1.7	0.0
67.7	48.2	-14.0	-5.8	-14.5	-8.2	-6.7	-6.7	-5.3	-4.8	-4.8
53.6	46.2	-14.8	-6.9	-14.8	-11.1	-7.9	-8.8	-5.5	-6.5	0.0
92.9	46.4	-7.4	0.0	-9.3	1.4	0.0	0.9	0.5	0.9	0.0
94.0	48.3	-9.2	-1.4	-11.1	0.0	-1.9	-0.5	-1.4	-1.0	-1.9
97.7	47.0	-7.1	0.5	-9.4	2.4	0.0	1.4	0.5	0.5	0.0
102.0	48.8	-8.3	-1.0	-10.7	1.5	-1.0	0.5	-0.5	-1.0	-2.0
86.2	47.1	-9.4	-1.4	-10.8	-1.4	-1.9	-1.4	-1.4	-1.4	-2.4
87.9	43.0	-5.2	2.6	-6.5	3.4	2.2	3.4	3.0	2.6	2.2
82.7	45.4	-8.2	-0.5	-9.5	-0.5	-0.9	-0.5	-0.5	0.0	-1.4
79.1	44.7	-8.5	-0.4	-9.4	-0.9	-0.9	-0.4	0.0	0.4	-0.9
86.6	46.1	-8.3	-0.5	-9.7	0.0	-0.9	0.0	-0.5	-0.5	0.5
85.5	44.3	-6.6	0.9	-8.4	1.3	0.4	1.3	1.3	1.3	-5.3
91.1	46.8	-8.4	-0.5	-9.8	0.5	-0.9	0.0	-0.5	0.5	-0.9
96.7	53.2	-13.8	-5.9	-16.0	-4.3	-6.4	-4.8	-5.9	-5.9	-6.4
91.2	49.3	-10.8	-3.0	-12.3	-2.0	-3.5	-2.5	-3.0	-2.0	-3.5
83.8	45.9	-8.7	-0.9	-10.1	-0.9	-1.4	-0.5	-0.5	-0.5	-1.4
87.1	47.7	-10.0	-1.9	-11.4	-1.4	-2.4	-1.4	-1.9	-1.9	-2.4
93.2	46.2	-7.4	0.5	-9.2	1.8	0.0	1.4	0.5	1.4	0.0

f_c (MPa)	E_c (GPa)	ACI 363	CEB	NS 3473	Wee	Gesoglu	Regression	Fuzzy	ANN	SVM
86.9	46.1	-8.3	-0.5	-9.7	0.0	-0.9	0.0	-0.5	-0.5	-0.9
90.7	48.1	-9.6	-1.9	-11.5	-1.0	-2.4	-1.0	-1.9	-1.0	-2.4
89.5	47.6	-9.5	-1.4	-10.9	-1.0	-1.9	-1.0	-1.4	-1.9	-1.9
87.8	45.4	-7.3	0.5	-9.1	0.9	0.0	0.9	0.5	0.5	0.0
95.2	50.8	-11.7	-4.1	-13.7	-2.5	-4.1	-3.0	-3.6	-3.0	-4.1
92.2	50.0	-11.0	-3.5	-13.0	-2.5	-4.0	-3.0	-3.5	-2.5	-4.5
97.6	49.3	-9.4	-2.0	-11.8	0.0	-2.5	-1.0	-2.0	-1.5	-2.5
87.5	48.5	-10.7	-2.9	-12.1	-2.4	-3.4	-2.4	-2.4	-2.9	-3.4
80.4	43.2	-6.5	1.3	-7.8	0.9	0.9	1.3	1.7	1.7	0.4
86.5	44.2	-6.6	1.3	-8.0	1.8	0.9	1.8	1.3	1.3	0.9
83.9	44.3	-7.1	0.9	-8.4	0.9	0.4	0.9	0.9	1.3	0.0
80.9	44.6	-8.0	0.0	-8.9	-0.4	-0.4	0.0	0.4	0.4	-0.9
85.7	45.1	-7.7	0.5	-9.0	0.5	0.0	0.9	0.5	0.5	-0.5

Table C. 2: Comparison of errors estimated by SVM and other models for testing data from HSC.

f_c (MPa)	E_c (GPa)	ACI 363	CEB	NS 3473	Wee	Gesoglu	Regression	Fuzzy	ANN	SVM
69.7	41.5	-7.1	1.2	-7.5	0.4	-0.8	0.4	1.7	2.5	1.7
78.3	44.3	-8.0	0.0	-9.3	-0.4	-0.9	-0.4	0.0	0.4	-0.9
82.6	44.2	-7.1	0.9	-8.4	0.4	0.4	0.9	0.9	1.3	0.0
65.8	40.8	-6.9	1.2	-7.3	0.4	-1.6	0.0	1.6	2.4	3.3
100.6	45.8	-5.5	1.8	-7.8	1.8	4.1	3.2	2.3	1.8	0.9
92.8	45.8	-6.9	0.9	-8.7	0.5	1.8	1.4	0.9	1.8	0.0
93.6	47.1	-8.0	-0.5	-9.9	-0.9	0.9	0.5	0.0	0.5	-0.9
71.5	48.0	-13.0	-4.8	-13.9	-6.7	-5.8	-5.8	-4.8	-3.8	-3.4
59.1	40.9	-8.6	-0.4	-8.6	-4.1	-1.2	-1.6	0.4	0.4	3.3
57.9	44.5	-12.5	-4.0	-12.5	-8.0	-4.9	-5.8	-3.1	-3.6	1.8
93.7	50.5	-11.6	-4.0	-13.6	-2.5	-4.0	-3.0	-3.5	-3.0	-4.0
85.3	45.0	-7.7	0.5	-9.0	0.5	0.0	0.9	0.5	0.5	0.0
99.7	47.6	-7.6	0.0	-10.0	1.9	-0.5	1.4	0.5	0.0	-1.0
85.1	44.7	-7.2	0.4	-8.5	0.9	0.0	0.9	0.9	0.9	0.0
90.3	45.0	-6.8	1.4	-8.1	2.3	0.9	1.8	1.4	0.9	0.9
87.2	41.1	-3.3	4.5	-4.9	4.9	4.1	4.9	4.9	4.5	4.1
84.5	45.3	-7.7	0.0	-9.5	0.0	-0.5	0.0	0.0	0.0	-0.9
77.0	47.2	-11.3	-3.3	-12.3	-3.8	-4.2	-3.3	-4.7	-2.4	-2.4
86.0	43.8	-6.1	1.8	-7.4	1.3	2.2	2.2	0.0	1.8	1.3
86.0	42.3	-4.7	3.0	-6.3	2.5	3.4	3.4	1.7	3.4	2.5

Using Generalized Regression Neural Networks (GRNNs) for elastic modulus prediction and comparing with the results of ANN are the objective of this part. 69 data applied for training and 20 data utilized for testing. The high compressive strength of concrete and elastic modulus considered as input and output layer respectively. The amount of MSE in training and testing for both ANN and GRNN is shown in Table C.3. The GRNN results showed MSE equal 0.45 & 1.05 % in network training and testing.

Table C.3: MSE comparison between GRNN and ANN done by

Network	MSE	
	Training	Testing
ANN	5.186 e-4	4.99 e-4
GRNN	0.0045	0.0105

A comparison between target and predicted by GRNN for Elastic modulus in training and testing phase are shown in Figure C.1 and C.2. The maximum difference between target and predicted elastic modulus in GRNN training and testing was 3.2 & 2.6 GPa.

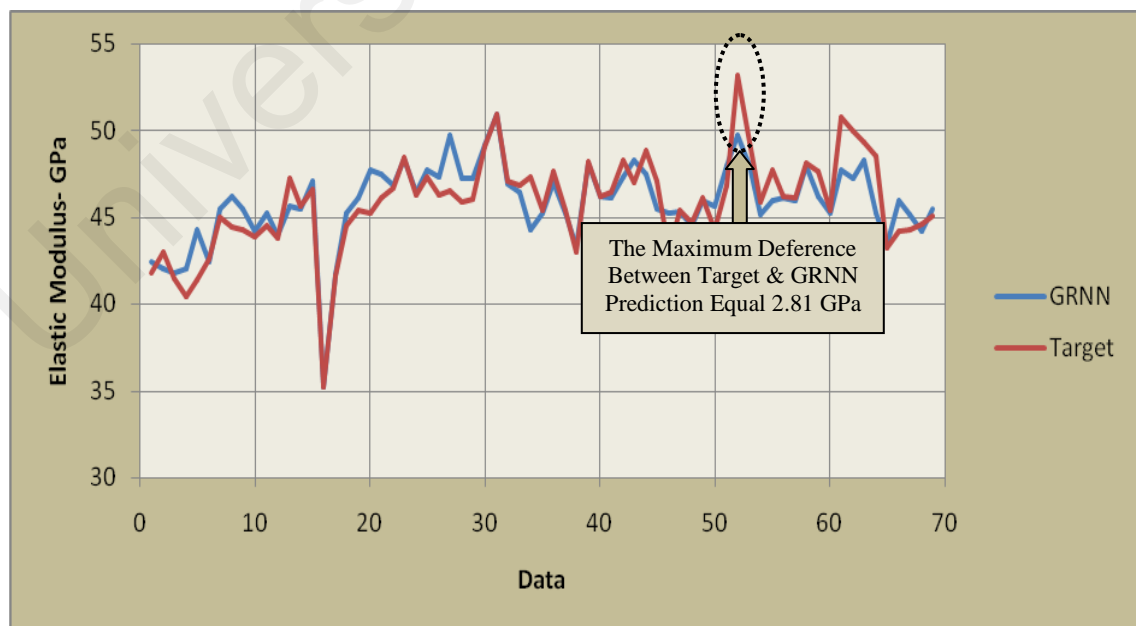


Figure C.1: Evaluation of target and predicted Modulus of Elasticity in GRNN training

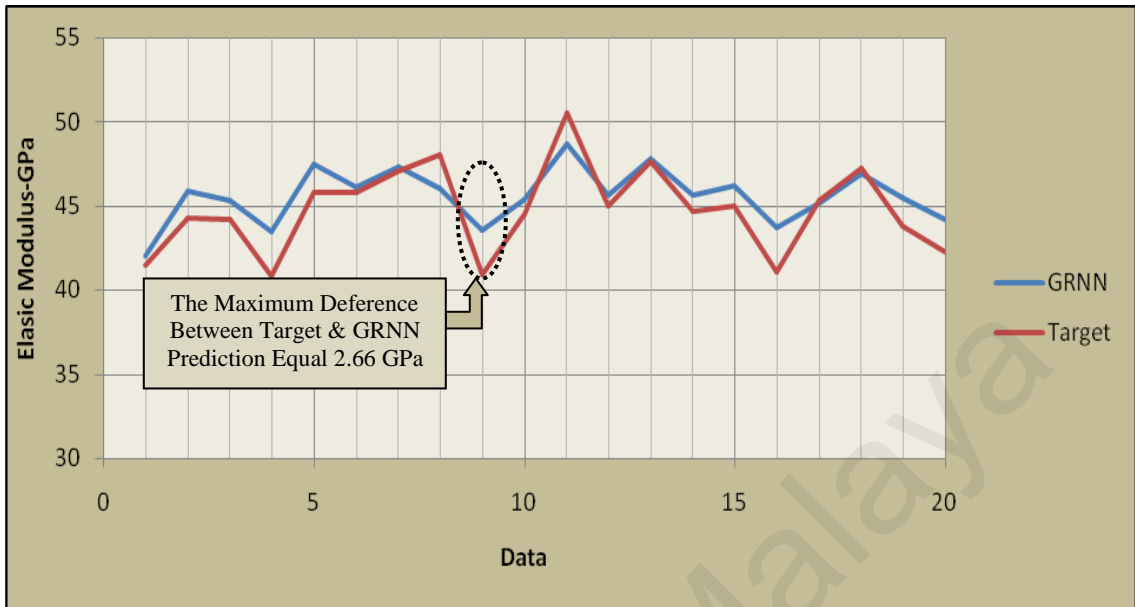


Figure C.2: Evaluation of target and predicted Modulus of Elasticity in GRNN testing
 A.2. Prediction of crack width of RC beam under short time loading

University of Malaysia

C.2. Crack width prediction of RC beam under short time loading

The schedule of the experimental work and sample detail are shown in Table C.4 and Figure C.3.

Table C.4: The schedule of RC beam sampling

Specimen	No. of Bars	Bar Diam. (mm)	Steel Area (mm ²)	c_b (mm)	c_s (mm)	s (mm)
B1-a	2	16	400	40	40	150
B1-b	2	16	400	40	40	150
B2-a	2	16	400	25	25	180
B2-b	2	16	400	25	25	180
B3-a	3	16	600	25	25	90
B3-b	3	16	600	25	25	90

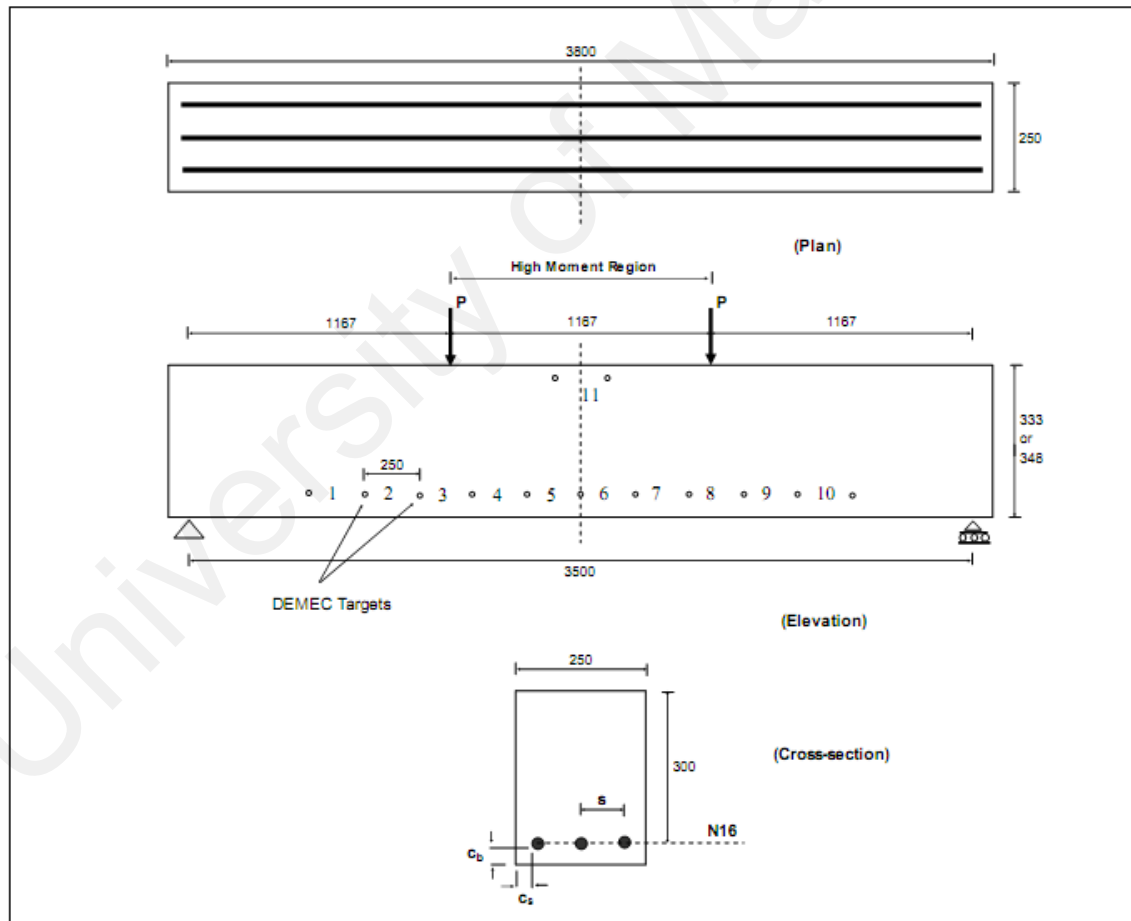


Figure C.3: The loading and instrument setup for the RC beam

The measured experimental crack width in the high moment region (H.M.R) of the beam B2-b is applied for the GRNN generation as well as shown in Table C.5.

Table C.5: The measured experimental crack width in the (H.M.R) of the beam B2-b

Load (kN)	C ₃₋₂ (mm)	C ₄₋₁ (mm)	C ₅₋₁ (mm)	C ₅₋₂ (mm)	C ₆₋₁ (mm)	C ₇₋₁ (mm)	C ₈₋₁ (mm)
0							
10							
20							
25				0.08			
30	0.08		0.08	0.10	0.10	0.05	0.08
35	0.10		0.10	0.15	0.15	0.08	0.13
40	0.15		0.10	0.15	0.18	0.08	0.15
45	0.15		0.13	0.18	0.18	0.13	0.18
50	0.18		0.13	0.23	0.25	0.15	0.20
55	0.20	0.05	0.15	0.28	0.28	0.18	0.20
60	0.25	0.08	0.15	0.28	0.33	0.20	0.23
65	0.28	0.08	0.15	0.30	0.38	0.23	0.25
70	0.30	0.13	0.18	0.30	0.43	0.25	0.28
Distance from C.L. (mm)	521	255	220	95	167	402	569

The loading and crack distance from center of the beam is considered as network input layer and the crack width as output layer. 63 data used for training and 7 data for testing. The MSE for network training and testing after simulation were $5.6161e^{-4}$ & 0.00017 respectively. A comparison between target and simulated crack width of RC beam on short time applied loading are shown in figures C.4, C.5, C.6, and C.7. The evaluation of the results presented good agreement between data after network generation.

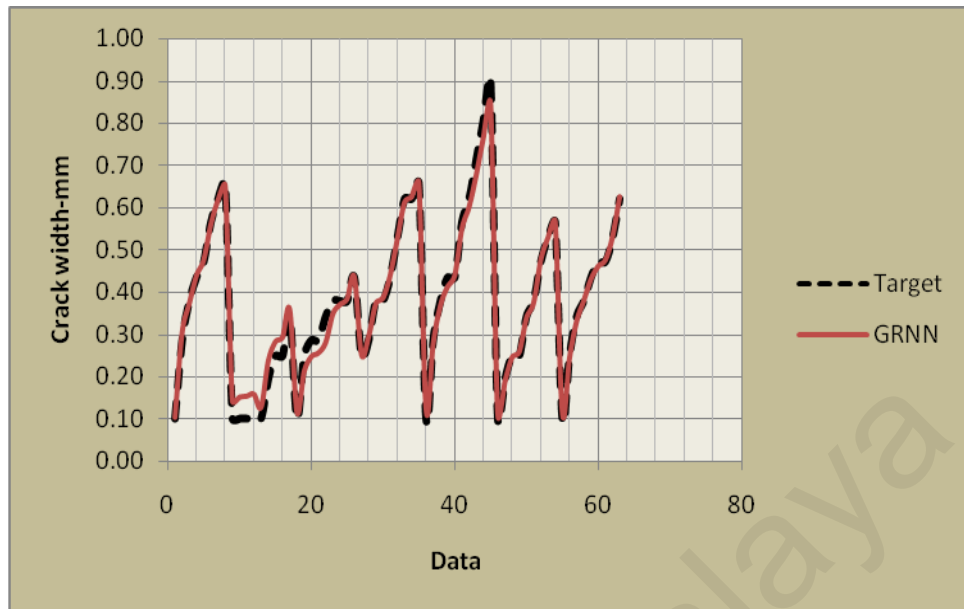


Figure C.4: An evaluation between target and predicted crack width after GRNN training

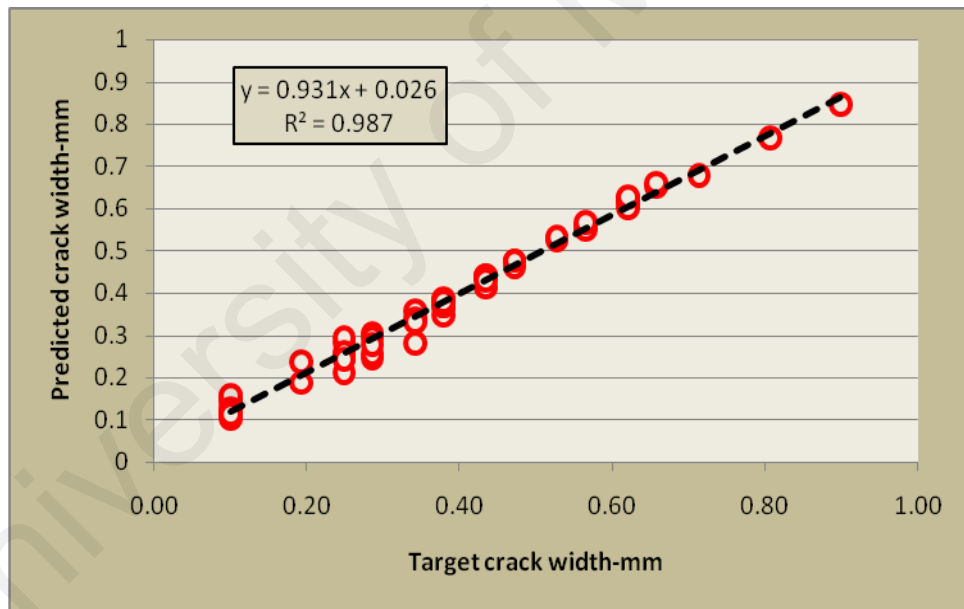


Figure C.5: An comparison between target and predicted crack width after GRNN training to calculat squared correlation coefficient

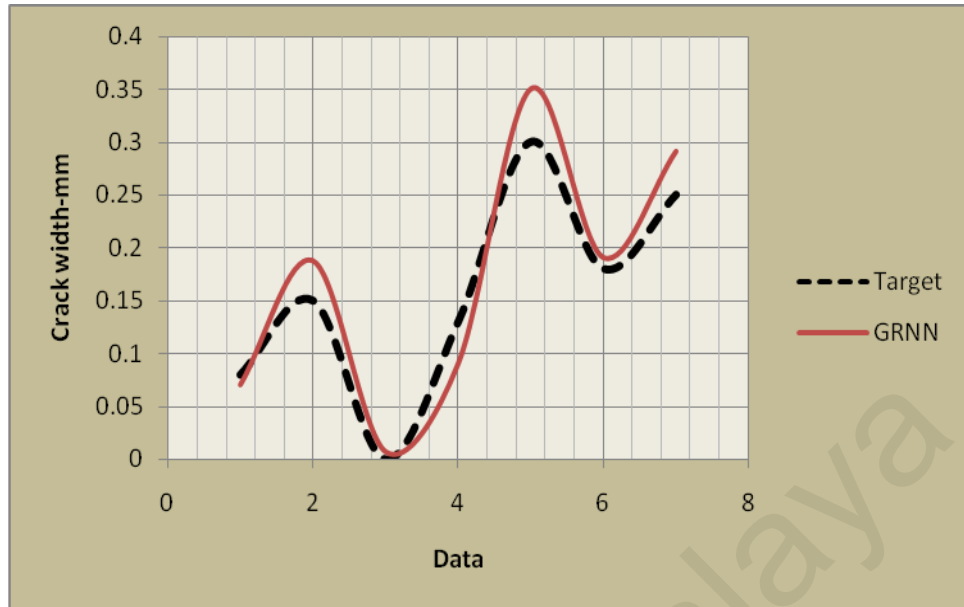


Figure C.6: An evaluation between target and predicted crack width after GRNN testing

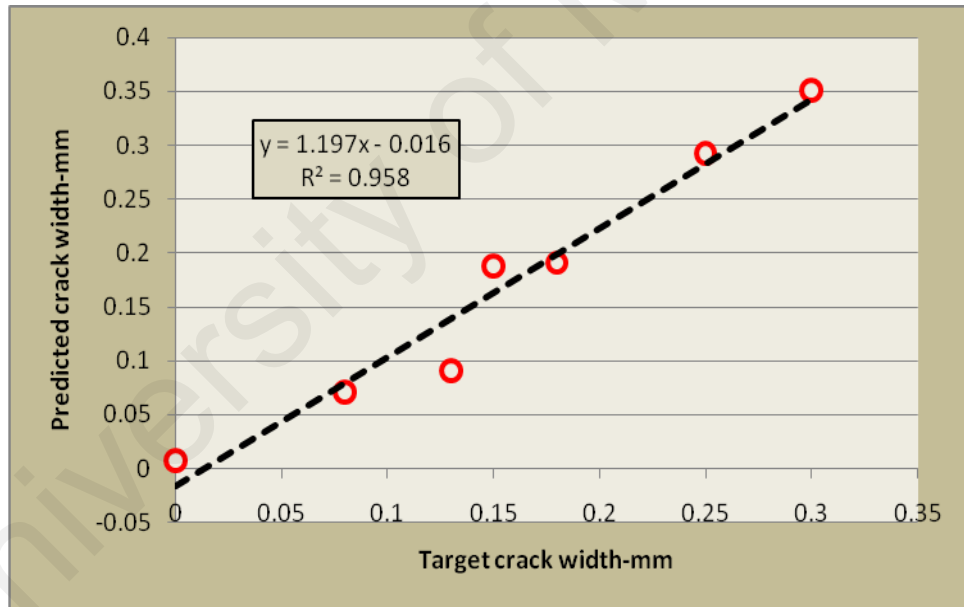


Figure C.7: An comparison between target and predicted crack width after GRNN testing to calculate squared correlation coefficient

The mentioned data used to generate feed forward back propagation neural network (FBNN). The MSE in network training and testing were 0.000243 & 0.0017 respectively. A comparison between predicted results by ANN and GRNN in testing phase are shown in Figure C.8. As we can see, when the number of data for FBNN generation is not enough,

the GRNN can predict the results with minimum error and maximum correlation coefficient .

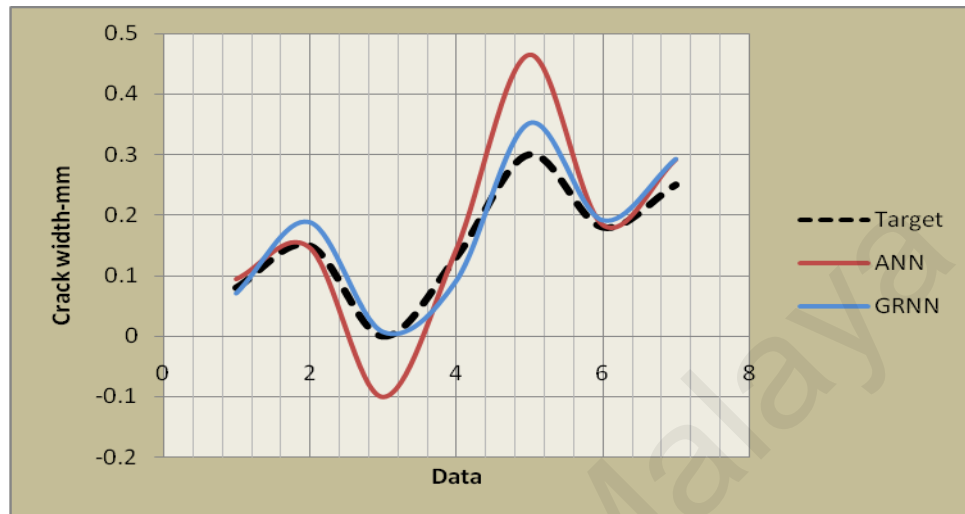


Figure C.8: An evaluation between target and predicted crack width after GRNN & ANN testing

C.3. Load-Deflection Analysis of High Strength Concrete Deep Beam

The data are arranged in a format such that 10 input parameters cover the geometrical and material properties of the HSC deep beam and the corresponding output value is the deflection prediction. All deep beams had a section of 500 mm depth and 200 mm width and 1500 mm length. The beam details and the geometrical parameters of beams are schematically determined in Figure C.9. The different parameters of mentioned deep beam are given in Table C.5.

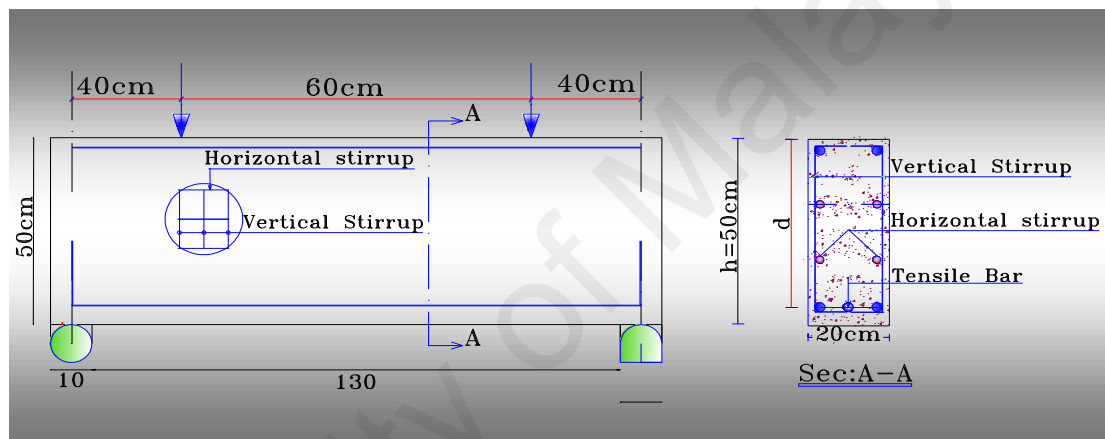


Figure C.9: Detail of tested beam

Table C.6: Different parameters of six deep beams

Item	Parameters								
	F_{cu}	a/d	L_0/d	f_{yv}	f_{yh}	A_v/b_{sv}	A_h/b_{sh}	ρ	f_y
B1	91.5	0.804	2.985	353	353	0.0064	0.00424	0.002191	353
B2	91.5	0.798	2.965	353	353	0.0064	0.00424	0.00269	614.4
B3	91.1	0.746	2.772	353	353	0.0064	0.00424	0.00409	618
B4	93.72	0.7575	2.81	353	353	0.00636	0.006697	0.00604	590.35
B5	79.1	0.851	2.979	614.4	614.4	0.00785	0.00982	0.008088	585.54
B6	87.5	0.769	2.857	614.4	614.4	0.00785	0.00982	0.00938	523.64

f_{cu} =28 days cylindrical strength of concrete

a =shear span ; d =effective depth; L_0 =overall length of tested beams; b =the beam width

f_{vy} =the yield strength of vertical web reinforcement, f_{hy} =the yield strength of horizontal web reinforcement

A_v =the area of vertical web reinforcement, s_v = the distance of vertical web reinforcement

A_h =the area of horizontal web reinforcement, s_h = the distance of horizontal web reinforcement

ρ =the tensile bar percentage, f_y = the tensile bar yield strength and p =applied load in each incremental loading stage

The output load-deflection of deep beam B2 applied for ANN testing and the other deep beam output used for verifying and training. Totally 1084 data have utilized to create network, 954 data for training, 99 data for verifying, and 31 data for testing. 20 networks with different hidden layer and network function have selected that the best 5 networks have indicated in Table C.7. In every 20 networks used 10 neurons in input layer (F_{cu} , a/d , L_0/d , f_{vy} , f_{hy} , A_v/bs_v , A_h/bs_h , ρ , f_y , & Loading) and 1 neuron in output layer (deflection) named network output. Feed-forward back propagation (FFBP) was the end construct for ANN.

Table C.7: properties of the selected network

Net. Market.	Neurons in Hidden Layer			Training Function	Adaption Learning Function	Training Function In hidden layer			Transfer Function in output layer
	H1	H2	H3			H1	H2	H3	
Net.1	10	1	-	TRAINBR	LEARNGDM	Tansig	Logsig	-	Purelin
Net.2	10	10	-	TRAINBR	LEARNGDM	Tansig	Logsig	-	Tansig
Net.3	10	5	-	TRAINBR	LEARNGDM	Tansig	Logsig	-	Purelin
Net.4	15	5	-	TRAINBR	LEARNGDM	Tansig	Logsig	-	Purelin
Net.5	15	5	-	TRAINBR	LEARNGD	Tansig	Logsig	-	Purelin

The Mean Squared Error (MSE) presented in Figure C.10. All net error is acceptable and the net.4 has the minimum MSE. The coefficient of determination for the 5 networks, as well as shown in Table C.8, was acceptable and close to 1.

Table C.8: Network Correlation Coefficient

Network	Net.1	Net.2	Net.3	Net.4	Net.5
Correlation of determination (R^2)	0.986	0.990	0.985	0.992	0.990

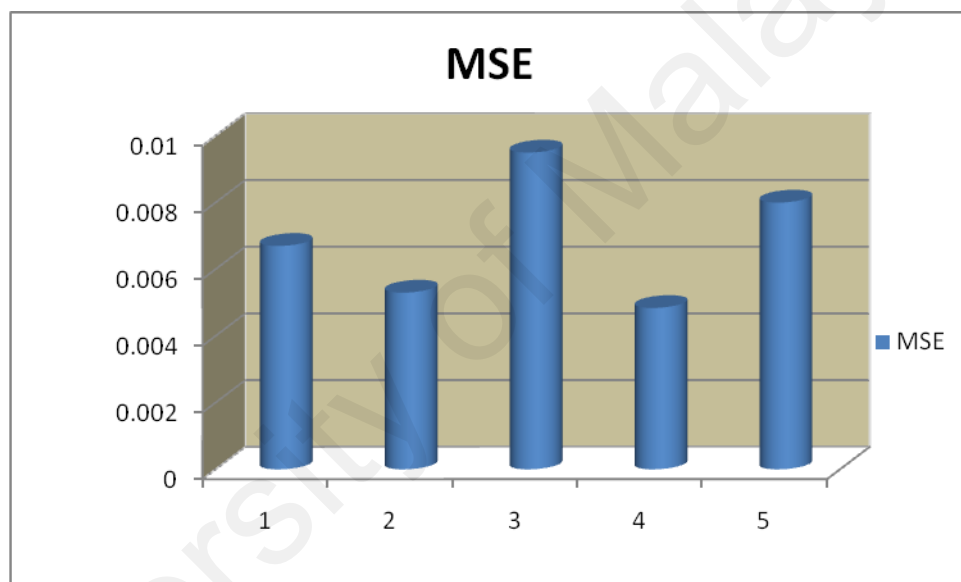


Figure C.10: The amount of mean square error (MSE) for 5 evaluated networks

As we can see, the feed forward backprop neural network, 10-15-5-1 (10 inputs, 15 neurons in first hidden layer, 5 in second hidden layer and 1 output) as net architecture, TRAINBR training function, LEARNNGDM learning function, TANSIG and LOGSIS as training function in first and second layer, PURLIN transfer function in output layer can predict the load-deflection diagram with minimum error less than 1% and maximum coefficient of determination close to 1.

The mentioned data applied for GRNN generation to predict mid span deflection of the high strength concrete deep beam. The results of the generated network in training and testing phase gave mean square error equal to $2.48e^{-5}$ and $7.11e^{-4}$. In this part, the produced GRNN concluded better results than ANN in case of enough data. It is because the gathered data were in elastic region of load-deflection curve. An comparison between target and simulated GRNN output for load-deflection on high strength concrete deep beam is shown in figure C.11.

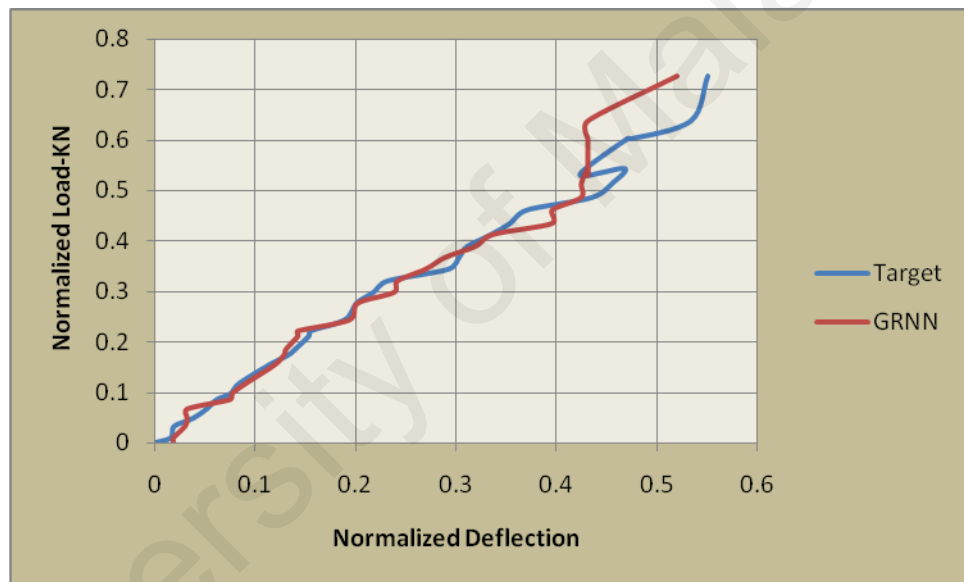


Figure C.11: An comparison between target and predicted load-deflection by GRNN

D. The Results of the LUSAS Finite Element Analysis

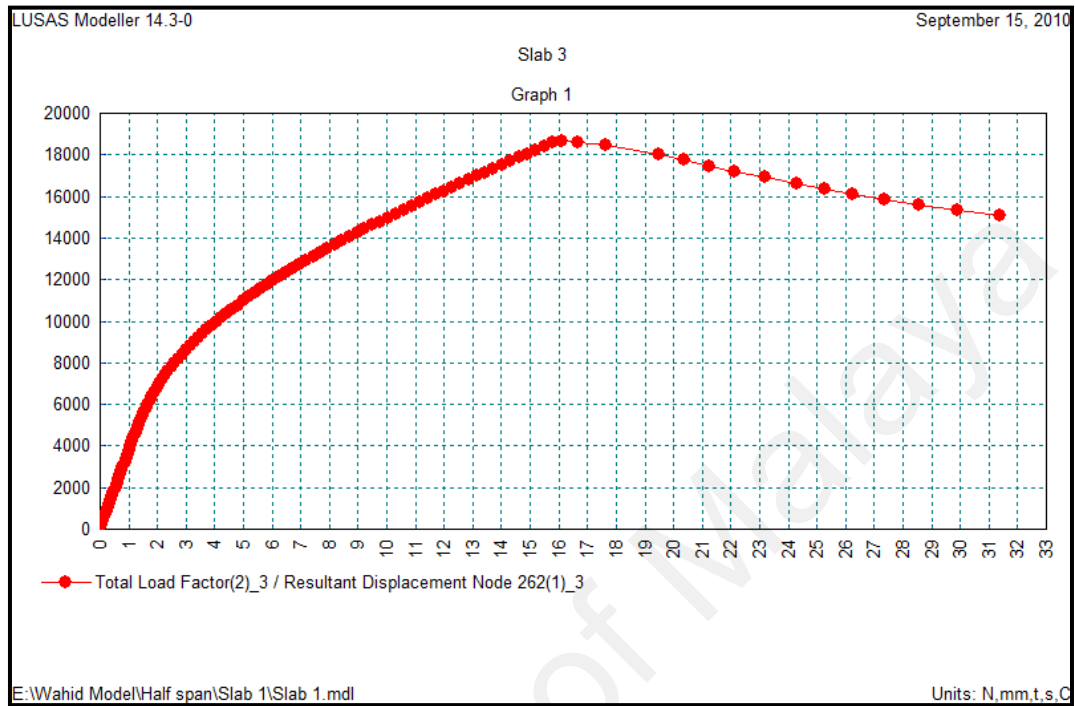


Figure E.1: Load-deflection curve for the sample 120-4T10-2400

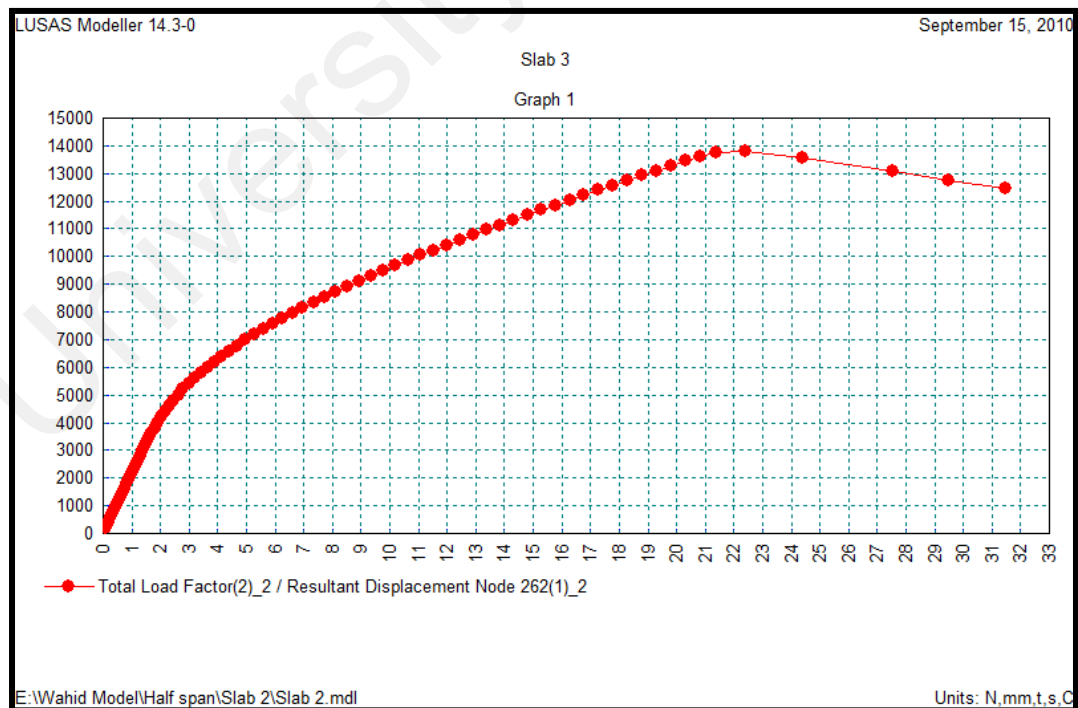


Figure E.2: Load-deflection curve for the sample 100-4T10-2400

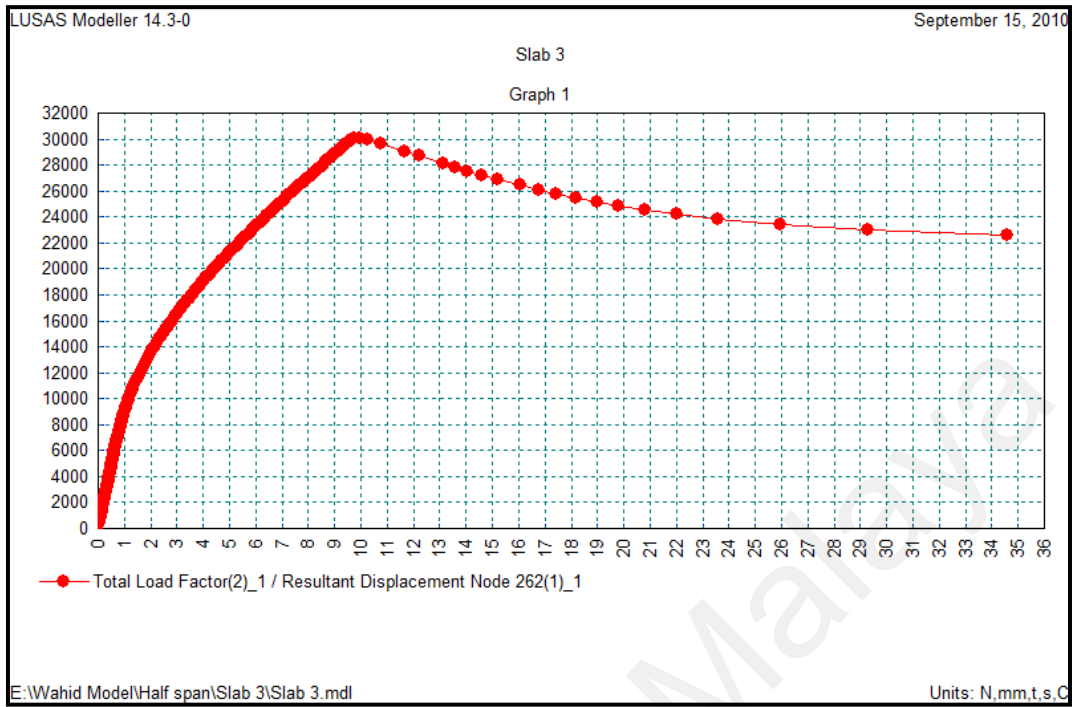


Figure E.3: Load-deflection curve for the sample 120-5T10-1800

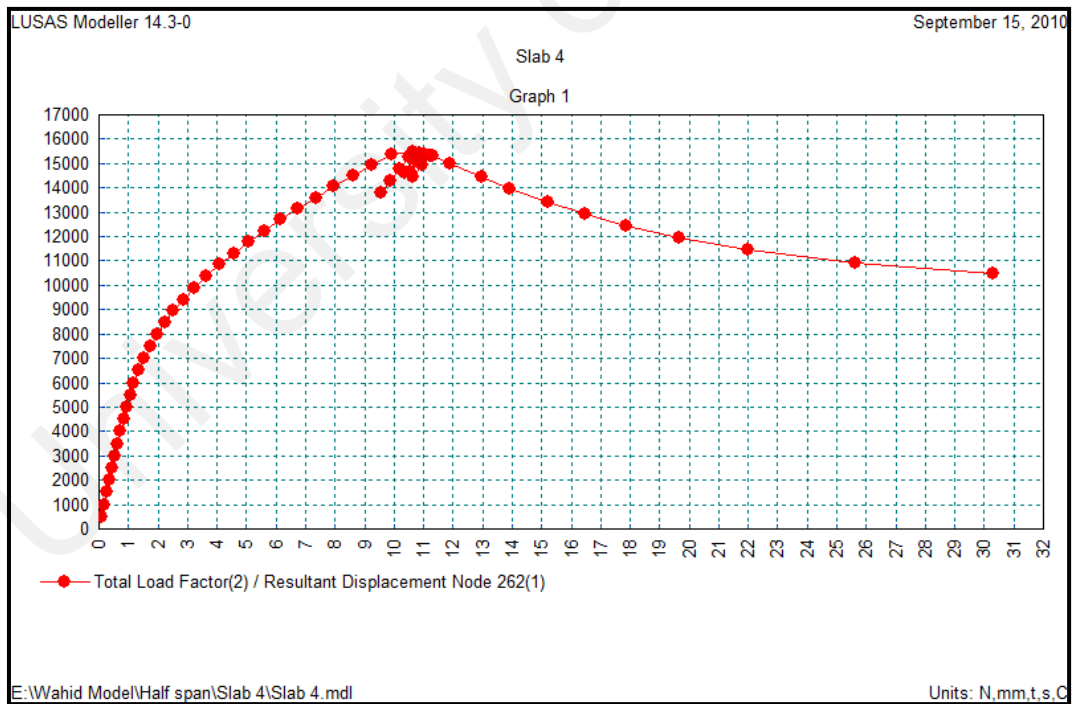


Figure E.4: Load-deflection curve for the sample 100-3T10-1800

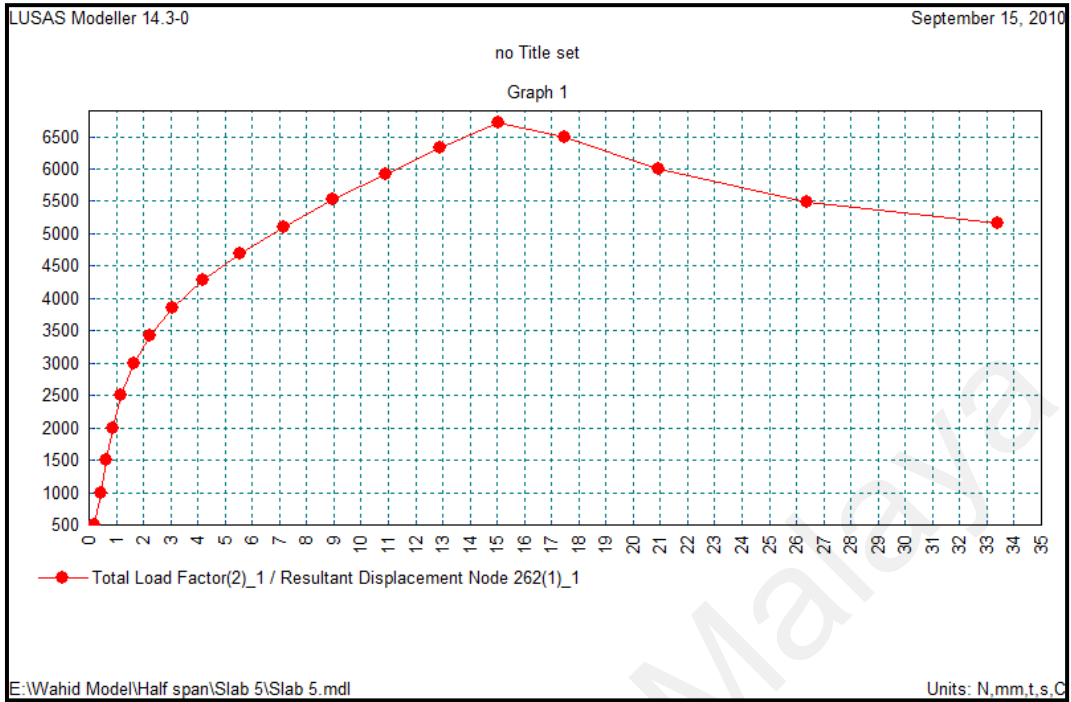


Figure E.5: Load-deflection curve for the sample 55-2T10-1350

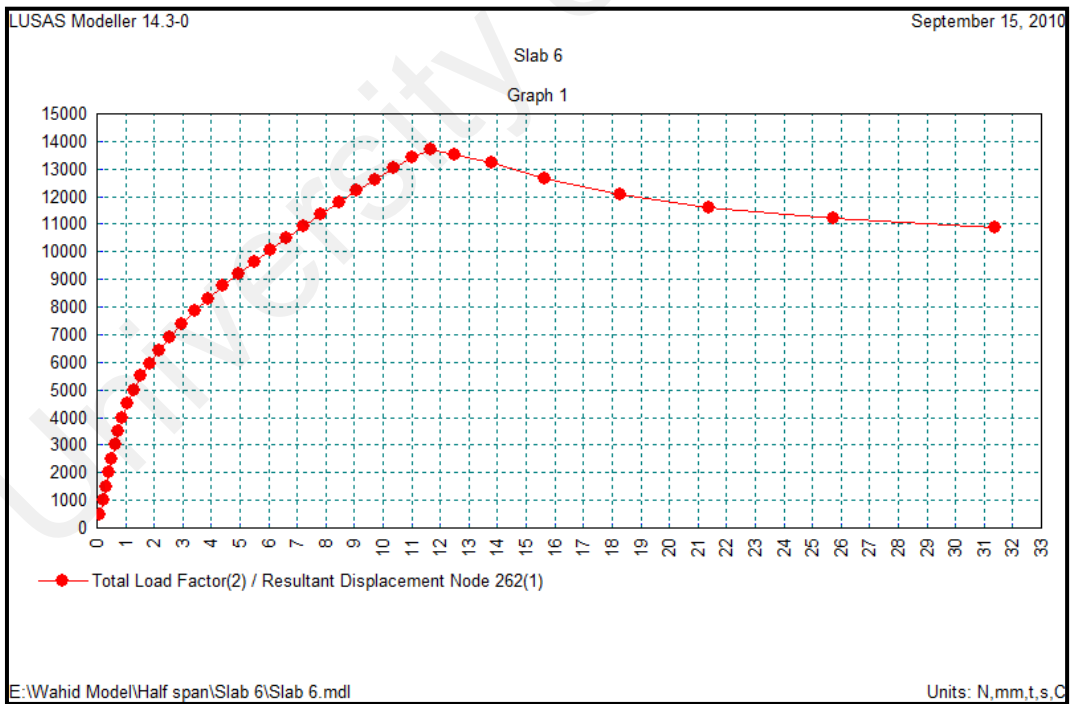


Figure E.6: Load-deflection curve for the sample 70-3T10-1350

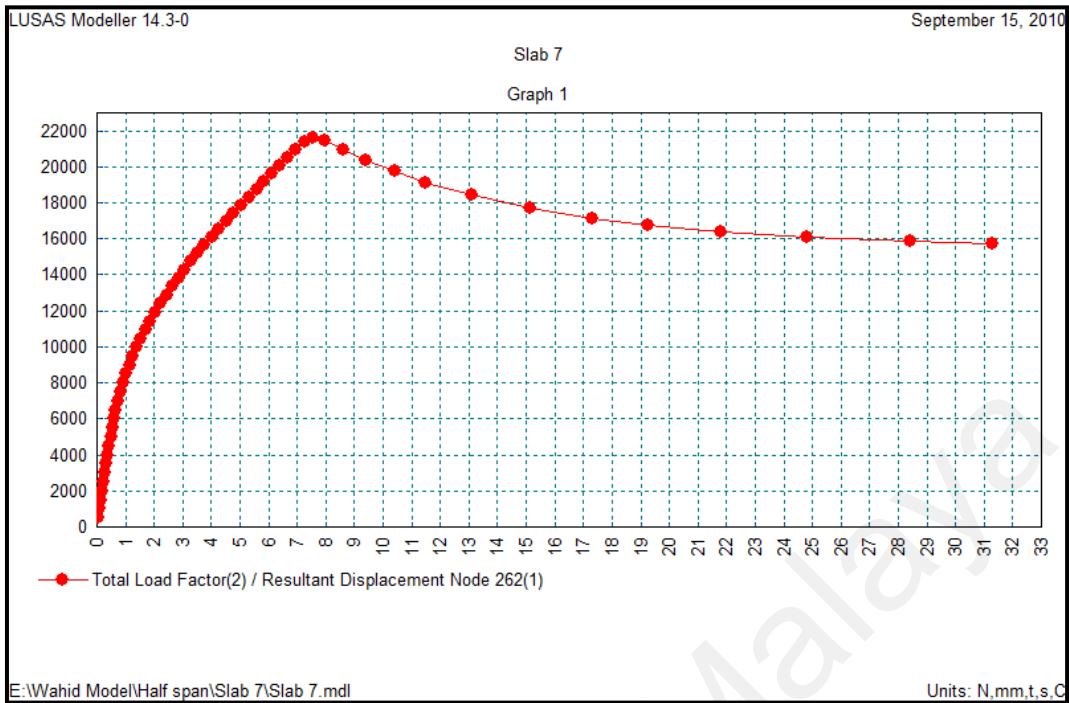


Figure E.7: Load-deflection curve for the sample 90-4T10-1350

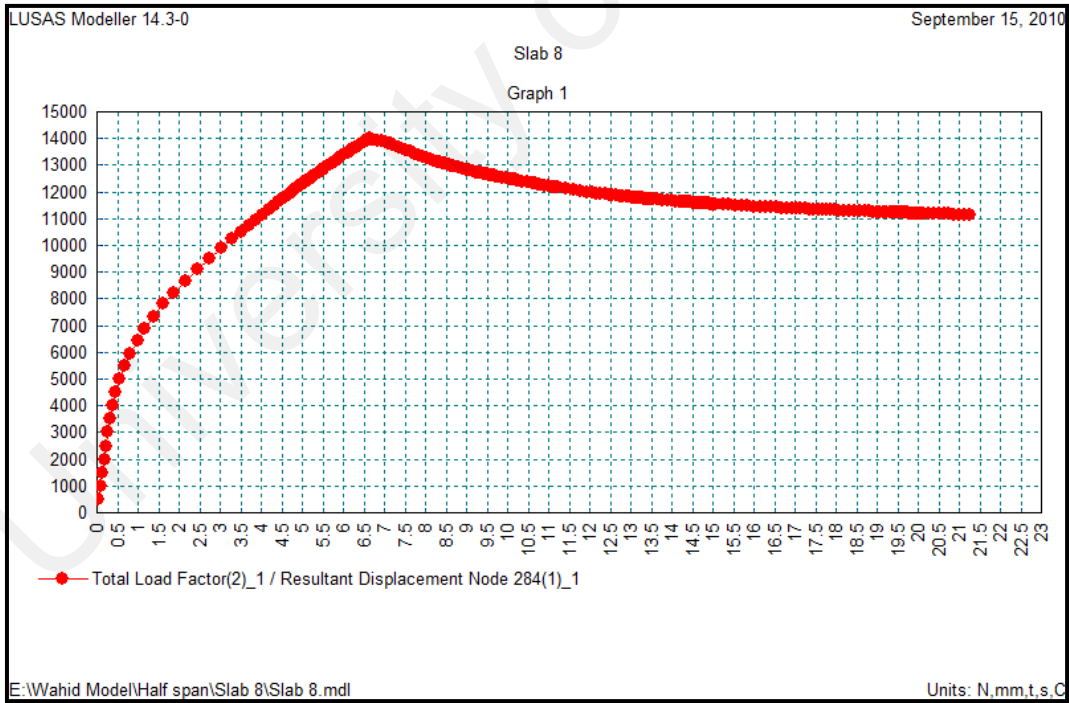


Figure E.8: Load-deflection curve for the sample 55-3T10-860

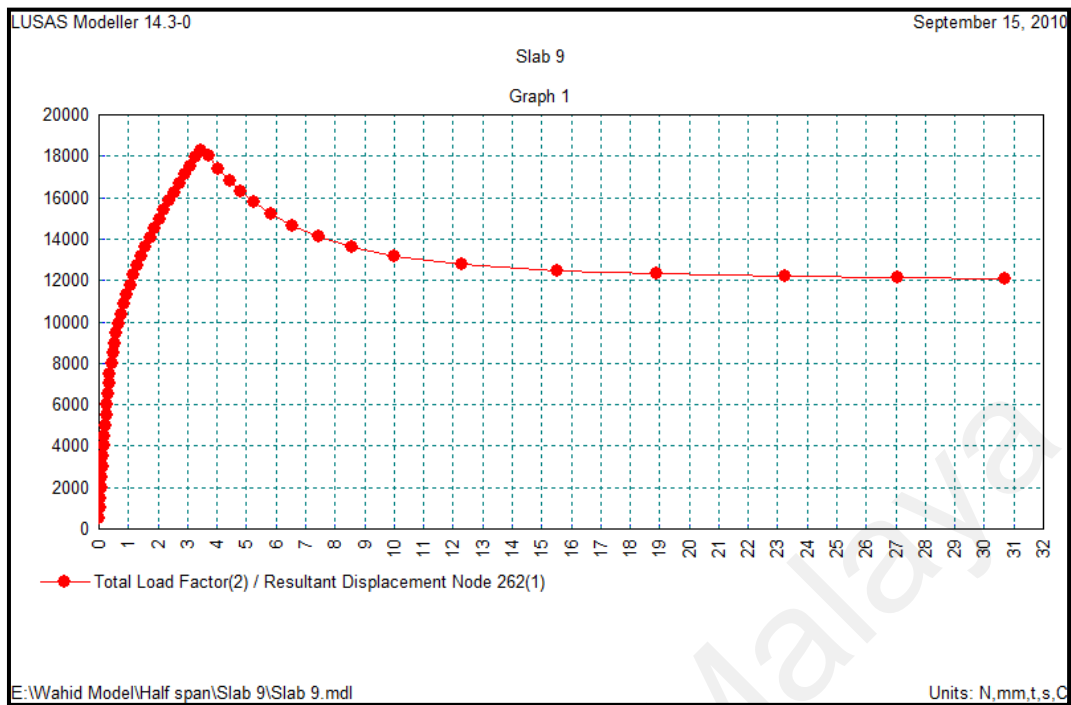


Figure E.9: Load-deflection curve for the sample 70-2T10-860

University of Malaya

E. Normalized Experimental Results Applied for NN

E. 1. Non-strengthened RC Slab

Table E.1: Normalized experimental load-deflection analysis for 19 non-strengthened RC slabs

1		2		3		4		5		6	
100-3T10-2400		120-3T10-2400		120-4T10-1800		120-3T10-1800		120-2T10-1800		100-2T10-1800	
Def	Load										
0.000	0.000	0.000	0.000	0.000	0.000	0.000	0.000	0.000	0.000	0.000	0.000
0.008	0.015	0.004	0.031	0.004	0.030	0.004	0.030	0.016	0.030	0.012	0.030
0.016	0.032	0.006	0.061	0.007	0.061	0.008	0.061	0.021	0.061	0.016	0.061
0.023	0.046	0.009	0.091	0.010	0.092	0.011	0.091	0.024	0.091	0.020	0.092
0.031	0.061	0.012	0.122	0.014	0.121	0.014	0.121	0.027	0.122	0.023	0.122
0.048	0.091	0.016	0.152	0.017	0.152	0.017	0.153	0.030	0.152	0.027	0.152
0.066	0.121	0.021	0.182	0.021	0.182	0.020	0.182	0.033	0.182	0.038	0.182
0.084	0.152	0.030	0.212	0.025	0.212	0.024	0.213	0.036	0.212	0.052	0.212
0.106	0.182	0.041	0.243	0.030	0.243	0.028	0.243	0.041	0.242	0.067	0.243
0.137	0.212	0.056	0.273	0.035	0.273	0.033	0.273	0.053	0.273	0.085	0.273
0.174	0.242	0.078	0.303	0.042	0.303	0.038	0.303	0.062	0.303	0.099	0.303
0.216	0.273	0.106	0.333	0.048	0.333	0.043	0.334	0.076	0.334	0.117	0.333
0.263	0.303	0.135	0.364	0.055	0.364	0.050	0.364	0.089	0.364	0.146	0.364
0.324	0.333	0.165	0.394	0.061	0.394	0.058	0.394	0.102	0.394	0.162	0.394
0.382	0.364	0.199	0.424	0.068	0.424	0.065	0.424	0.114	0.424	0.177	0.424
0.447	0.394	0.231	0.455	0.075	0.455	0.072	0.455	0.126	0.455	0.192	0.455
0.526	0.424	0.272	0.485	0.082	0.485	0.080	0.486	0.137	0.485	0.208	0.485
0.605	0.439	0.310	0.515	0.089	0.515	0.087	0.515	0.147	0.515	0.225	0.500
0.658	0.439	0.348	0.546	0.096	0.546	0.094	0.546	0.158	0.546	0.242	0.485
0.737	0.433	0.391	0.576	0.103	0.576	0.102	0.576	0.168	0.576	0.395	0.424
0.816	0.429	0.447	0.606	0.110	0.606	0.109	0.606	0.187	0.606	0.711	0.364
0.921	0.425	0.579	0.576	0.118	0.637	0.122	0.636	0.263	0.576		
1.000	0.424	0.789	0.545	0.125	0.667	0.130	0.667	0.526	0.515		
				0.132	0.697	0.141	0.697				
				0.140	0.727	0.151	0.727				
				0.147	0.758	0.168	0.758				
				0.154	0.788	0.211	0.727				
				0.162	0.818	0.289	0.697				
				0.169	0.849	0.474	0.652				
				0.176	0.879	0.658	0.621				
				0.183	0.909	0.789	0.606				
				0.188	0.940						
				0.195	0.970						
				0.206	1.000						
				0.316	0.939						
				0.526	0.848						
				0.632	0.818						

Continue Table E.1: Normalized experimental load-deflection analysis for 19 non-strengthened RC slabs

7		8		9		10		11		12	
100-3T10-1800		100-4T10-1800		55-2T10-1350		55-3T10-1350		55-4T10-1350		70-3T10-1350	
Def	Load	Def	Load	Def	Load	Def	Load	Def	Load	Def	Load
0.000	0.000	0.000	0.000	0.000	0.000	0.000	0.000	0.000	0.000	0.000	0.000
0.007	0.030	0.003	0.031	0.011	0.031	0.005	0.030	0.010	0.030	0.008	0.031
0.012	0.061	0.006	0.061	0.024	0.061	0.043	0.061	0.028	0.061	0.013	0.061
0.016	0.091	0.009	0.092	0.053	0.091	0.088	0.091	0.048	0.091	0.018	0.091
0.021	0.121	0.013	0.121	0.105	0.121	0.131	0.121	0.088	0.121	0.029	0.121
0.030	0.152	0.018	0.152	0.211	0.152	0.184	0.152	0.140	0.152	0.050	0.152
0.044	0.182	0.025	0.182	0.368	0.182	0.231	0.182	0.181	0.182	0.076	0.182
0.058	0.212	0.037	0.213	0.474	0.197	0.276	0.212	0.225	0.212	0.108	0.212
0.073	0.243	0.049	0.243	0.658	0.182	0.325	0.242	0.272	0.242	0.142	0.243
0.088	0.273	0.061	0.273	0.921	0.167	0.372	0.273	0.312	0.273	0.180	0.273
0.104	0.303	0.073	0.303			0.431	0.303	0.349	0.303	0.224	0.303
0.117	0.333	0.091	0.334			0.579	0.280	0.391	0.333	0.266	0.333
0.132	0.364	0.104	0.364			0.684	0.267	0.432	0.364	0.333	0.364
0.149	0.394	0.117	0.394			0.789	0.258	0.521	0.394	0.447	0.333
0.167	0.424	0.127	0.424					0.711	0.371	0.789	0.303
0.184	0.455	0.143	0.455					0.789	0.358		
0.199	0.485	0.154	0.485								
0.217	0.515	0.165	0.515								
0.229	0.546	0.178	0.546								
0.260	0.576	0.190	0.576								
0.316	0.561	0.202	0.606								
0.368	0.545	0.217	0.636								
0.447	0.530	0.231	0.667								
0.526	0.515	0.245	0.697								
		0.266	0.727								
		0.289	0.712								
		0.342	0.673								
		0.421	0.636								

Continue Table E.1: Normalized experimental load-deflection analysis for 19 non-strengthened RC slabs

13		14		15		16		17		18		19	
70-2T10-1350		90-3T10-1350		90-2T10-1350		55-3T10-860		55-2T10-860		70-2T10-860		70-3T10-860	
Def	Load	Def	Load	Def	Load	Def	Load	Def	Load	Def	Load	Def	Load
0.000	0.000	0.000	0.000	0.000	0.000	0.000	0.000	0.000	0.000	0.000	0.001	0.000	0.000
0.016	0.031	0.010	0.030	0.006	0.030	0.008	0.030	0.005	0.030	0.001	0.031	0.001	0.031
0.021	0.061	0.014	0.061	0.012	0.061	0.011	0.061	0.009	0.061	0.001	0.062	0.002	0.061
0.024	0.091	0.017	0.091	0.017	0.091	0.014	0.091	0.012	0.091	0.002	0.092	0.002	0.093
0.027	0.122	0.021	0.121	0.021	0.121	0.016	0.121	0.015	0.122	0.003	0.121	0.003	0.122
0.032	0.152	0.026	0.152	0.026	0.152	0.020	0.152	0.020	0.152	0.004	0.152	0.005	0.153
0.043	0.182	0.032	0.182	0.030	0.182	0.026	0.182	0.026	0.182	0.005	0.182	0.008	0.182
0.058	0.213	0.040	0.212	0.034	0.212	0.039	0.212	0.038	0.212	0.008	0.212	0.010	0.212
0.082	0.243	0.049	0.243	0.037	0.243	0.053	0.242	0.051	0.242	0.010	0.244	0.013	0.242
0.105	0.273	0.059	0.273	0.041	0.273	0.073	0.273	0.075	0.273	0.014	0.274	0.017	0.273
0.132	0.303	0.070	0.303	0.050	0.303	0.092	0.303	0.096	0.303	0.017	0.303	0.020	0.303
0.161	0.333	0.080	0.333	0.061	0.334	0.118	0.333	0.115	0.333	0.022	0.334	0.024	0.334
0.191	0.364	0.091	0.364	0.070	0.364	0.145	0.364	0.141	0.364	0.026	0.364	0.027	0.364
0.219	0.394	0.101	0.394	0.083	0.394	0.171	0.394	0.188	0.333	0.030	0.395	0.031	0.394
0.251	0.424	0.112	0.424	0.098	0.424	0.211	0.424	0.246	0.310	0.034	0.424	0.035	0.424
0.288	0.455	0.126	0.455	0.111	0.455	0.289	0.394	0.395	0.274	0.038	0.455	0.038	0.455
0.319	0.485	0.138	0.485	0.119	0.485	0.395	0.382			0.041	0.486	0.042	0.485
0.359	0.515	0.150	0.515	0.140	0.515					0.049	0.516	0.045	0.516
0.374	0.515	0.167	0.546	0.155	0.545					0.055	0.546	0.048	0.546
0.658	0.500	0.181	0.576	0.357	0.515					0.066	0.576	0.052	0.576
0.921	0.455	0.200	0.606	0.379	0.485					0.076	0.606	0.056	0.606
		0.217	0.637	0.405	0.455					0.095	0.636	0.059	0.637
		0.234	0.667							0.158	0.591	0.063	0.667
		0.263	0.697							0.289	0.530	0.066	0.697
		0.375	0.667							0.526	0.485	0.071	0.728
		0.509	0.624									0.087	0.758
		0.661	0.591									0.158	0.667
		0.748	0.576										
		0.991	0.539										

E.2. CFRP Strengthened RC Slab

Table E.2: Normalized experimental load-deflection analysis for 7 CFRP strengthened RC slabs

1		2		3		4		5		6		7	
WCFRP		S512-700		S512-1100		S512-1500		S812-700		S812-1100		S812-1500	
Def	Load	Def	Load	Def	Load	Def	Load	Def	Load	Def	Load	Def	Load
0.10	0.10	0.10	0.10	0.10	0.10	0.10	0.10	0.10	0.10	0.10	0.10	0.10	0.10
0.14	0.30	0.10	0.12	0.10	0.12	0.10	0.12	0.12	0.25	0.27	0.12	0.12	0.22
0.21	0.43	0.11	0.16	0.11	0.16	0.11	0.16	0.13	0.35	0.32	0.13	0.13	0.25
0.24	0.47	0.11	0.20	0.11	0.20	0.11	0.20	0.16	0.41	0.36	0.15	0.13	0.29
0.25	0.50	0.11	0.23	0.11	0.23	0.11	0.23	0.17	0.44	0.40	0.17	0.16	0.34
0.31	0.58	0.12	0.28	0.12	0.25	0.12	0.25	0.20	0.49	0.44	0.20	0.17	0.38
		0.13	0.35	0.13	0.28	0.13	0.28	0.24	0.53	0.52	0.25	0.20	0.41
		0.14	0.38	0.14	0.32	0.14	0.32	0.34	0.64	0.60	0.36	0.24	0.51
		0.16	0.41	0.16	0.35	0.16	0.35	0.39	0.64	0.67	0.45	0.34	0.58
		0.18	0.44	0.18	0.41	0.18	0.41			0.76	0.63	0.37	0.59
		0.20	0.47	0.20	0.45	0.20	0.45			0.61	0.70	0.47	0.65
		0.22	0.50	0.22	0.50	0.22	0.50					0.59	0.72
		0.25	0.52	0.24	0.54	0.24	0.54					0.70	0.79
		0.27	0.55	0.26	0.58	0.26	0.58					0.80	0.86
		0.31	0.58	0.28	0.60	0.28	0.60					0.87	0.90
		0.35	0.60	0.31	0.62	0.31	0.62						
		0.40	0.63	0.36	0.65	0.36	0.64						
		0.43	0.64	0.40	0.68	0.40	0.66						
		0.45	0.64	0.45	0.71	0.45	0.68						
				0.47	0.71	0.47	0.70						
						0.51	0.71						
						0.56	0.73						
						0.61	0.75						
						0.66	0.76						

APPENDIX F

F. Artificial Neural Networks (ANNs)

Artificial Neural Network (ANN) consist of mufti thousand sample units processing that have parallel connection and are following together in mufti layers. The effect of a local link named the weight of the connection. ANN gets random amounts of the weight of local connection. In the teaching process, these neurons will reclaim until final teaching between input and output relationship. The structure of a multi input neuron has shown in Figure F.1 that (P) and (a) is input and output layer respectively.

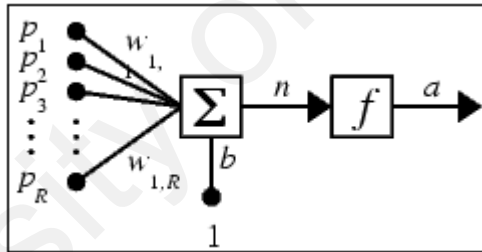


Figure F.1: The structure of multi input layer

The effect of (P) on (a) is defined by the weight (W).

$$W = [W(1,1) \ W(1,2) \ \dots \ W(1,R)] \quad P = \begin{bmatrix} P(1) \\ P(2) \\ P(3) \\ \cdot \\ \cdot \\ \cdot \\ P(R) \end{bmatrix} \quad (F.1)$$

The other input is 1 (the constant amount) that will be multiplied in bias (b) and then will be added with WP. The conclusion defines pure input (n) for function (f) that is calculated by below formula:

$$n = \sum_{i=1}^R P_i W(1,i) + b = WP + b \quad (\text{F.2})$$

The output of neuron is defined by:

$$a = f(WP + b) \quad (\text{F.3})$$

Where:

W = Weight or the effect of interior connection
P = Input matrix
b = bias

Bias in network cause interaction between inputs and outputs layer be more easily than network without bias.

ANN is a data-processing method that neurons process the data. The signals translate the interconnection links which possess a corresponding weight. The weight has multiplied along with the incoming signal for any typical neural net. The output signal has obtained by applying activations to the net input.

The neural net can be a single layer or a multilayer net. The structure of the single artificial neural net has shown in Figure F.2.

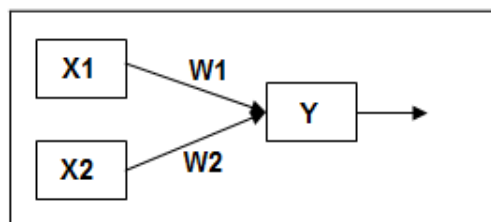


Figure F.2: A Simple Artificial Neural Network

It shows a single artificial neural net with two input neurons (x_1, x_2) and one output (y). The interconnected weights given by w_1 and w_2 . In a single layer net, there is a single layer of weighted interconnections.

A multilayer network may be used to enhance the flexibility of the network in data processing and allocate to generate network for the estimate of high complex non-linear functions with less link weights.

In a MNN, each neuron is linked to every other nearby neuron in the next layer. They can perform arbitrary complex input/output mapping or decision surfaces separating different patterns. A three-layer MNN has shown in Figure F.3. In MNN, neurons are structured into three different layers:

- (1) Input layer includes input neurons which get external signals.
- (2) Hidden layers transfer the information received from the input nodes to the output layer.
- (3) Output layer receives signals from the hidden layer and convert them into a calculated amount of the output.

This classic neural network is interesting because neurons in the hidden layers are free to create their own rendition of the input.

MNNs support an increase in computational power over a single-layer neural system unless there is a nonlinear activation function between layers.

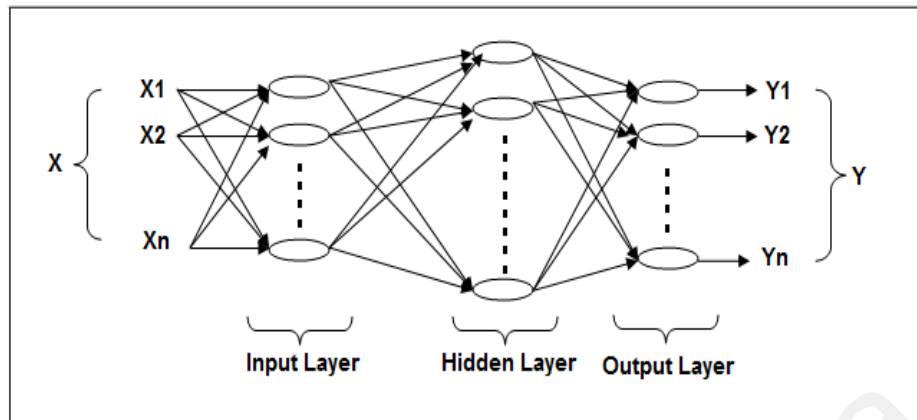


Figure F.3: A Three-Layered Static Artificial Neural Network

ANN can predict several output in a network generation, but it gives more perfect predictions when a single output is modeled. Also, the network generation will be stronger if the network be consisted of less variable inputs.

F.1. Types of Artificial Neural Network

Feed-Forward Back-propagation, Feed-Forward Time Delay, Feed-Forward Distributed Time Delay, Hopfield, Layer Recurrent, LVQ, NARX, Generalized Regression, Radial Basis, Self-Organizing, Probabilistic, Perception and so on are different kind of neural network that can be defined based on following elements:

F.1.1. Applications

The application of the neural network is defined as following:

- (1) **Classification:** The task of pattern respect is to allocate an input pattern to one of many classes. Feed forward is the network using in this kind of application.
- (2) **Clustering:** An algorithm investigates the similarity between patterns and places similar patterns in a cluster. Simple Competitive, Adaptive Resonance Theory, and

Kohonen Self-Organizing Map are the networks using in the clustering applications.

- (3) **Association:** Network training for pattern remembering is the most important objective, so that when an unclear version of a particular pattern is applied, the network associates it with the closest one in its memory and presents the original version of that particular pattern. The network used in association application is Hopfield Network.
- (4) **Prediction:** The aim is to predict some future values of the time-sequenced information. Back propagation, Delta Bar Delta, Extended Delta Bar Delta, Directed Random Search, Higher Order Neural Network, and Self Organizing Map into Back Propagation are the networks used in prediction problems. Back Propagation is the more popular network in prediction.

F.1.2. Net Connection Type

- (1) **Static (feed-forward):** The information moves in only forward direction from input to output. The output of any layer does not have any effect on the same layer. In the other work, there is no feed back or loop.
- (2) **Dynamic (feedback):** The signals move in both directions, forward and back. These kinds of networks are very powerful and can get extremely complicated. Feedback networks as Dynamic network reaches an equilibrium point by continuously changing in their state. They stay at the equilibrium status until the input changes and a new equilibrium needs to be found. The Feedback architectures are also referred to interactive or recurrent, although the later term is often applied to represent the connection of the feedback in single-layer groups.

F.1.3. Net Topology

- (1) **Single layer:** The network consists of input and output layer.
- (2) **Multilayer:** The network consists of input, hidden, and output layer.
- (3) **Recurrent:** In recurrent neural network (RNN), the connection between unites forms a directed loop.
- (4) **Self-organized:** This neural network uses a neighborhood function to preserve the topological properties of the input space.

F.1.4. Network Learning Methods

Supervised Learning: The network includes an external teacher to make easy training by showing the perfected response for a given data. Supervised learning algorithms improves the network prediction capabilities by weight changing due to use the difference between the predicted and preferred target.

This kind of the learning consisted of training data made up of N input—output examples:

$$T = \{(X_i, d_i)\}_{i=1}^N \quad (\text{F.4})$$

Where:

X_i is the input vector of the i^{th} example (Scalar).

d_i is the desired response of the i^{th} example (Scalar).

N is the size of the samples

By the training samples definition, y_i the actual network output is calculated. The accuracy of the network output is tested by the mean square error formula:

$$E(n) = \frac{1}{N} \sum_{i=1}^N (d_i - y_i)^2 \quad (\text{F.5})$$

Unsupervised Learning: The neural network with unknown target vector for each input vector is named as unsupervised training. The unsupervised network is complex and difficult to employ. The unsupervised neural network is called self-organizing network or self-learning networks due to the network ability to carry self-learning. The network uses no external teacher and base on local data. In this method of network learning, x is some input data given to network to minimize the f output function.

Reinforced Learning: Reinforcement learning is defined in terms of an agent interacting with an environment. In this method, x input data is not given and the network is generated by an agent's interactions with the environment. The plan is to find out a strategy for selecting procedures that minimizes some measure of a long-term cost. The environment's dynamics and the long-term cost for each strategy are usually unknown, but can be estimated.

F.2. Neuron Model and Net Architecture

F.2.1. Neuron Model

The neuron model is defined as simple and multiple neurons. A simple neuron without and with bias is shown in Figure F.4.

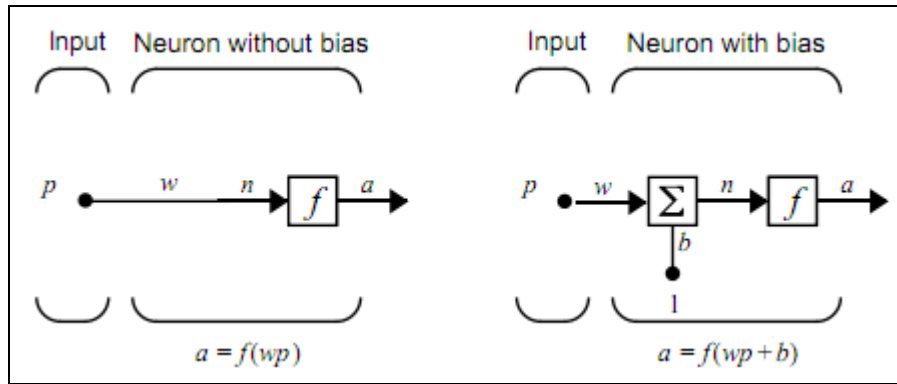


Figure F.4: Simple neuron with and without bias

The model of the simple neuron consisted of the input “p”, weight “w”, and bias “b” as scalar parameters that the output “a” again scalar parameter is created by using transfer function. In the multiple neurons modeling, the input layer is layer number 0 and N is the number of the weight for the both hidden and output layers. The model of the two layers multi-layer neurons is shown in Figure F.5.

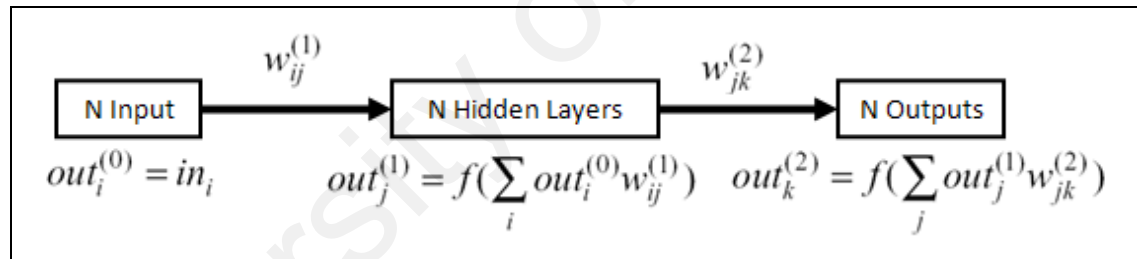


Figure F.5: Multiple neurons modeling

The input layer can be defined as R-elements input vector which are affected by the matrix weight and is transmitted to be summed in summing junction to create output vector by using transfer function.

F.2.2. Network Architectures

The net layer architecture is defined in two cases of one-layer and multiple layers network.

F.2.2.1. A Layer of neurons

The R input elements and S neurons in one-layer network are shown in Figure

F.6.

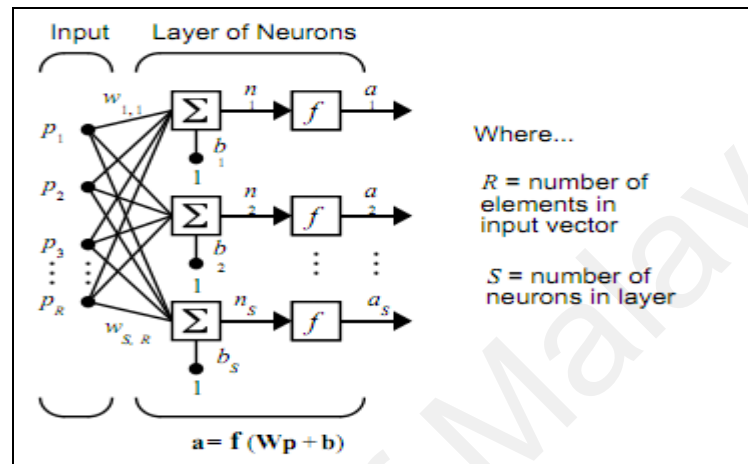


Figure F.6: One-layer network architecture

As we can see, in this kind of the network each element such as $p_1, p_2, p_3, \dots, p_R$ is connected to each neuron input such as $n_1, n_2, n_3, \dots, n_s$ through the following weight matrix W .

$$\mathbf{W} = \begin{bmatrix} w_{1,1} & w_{1,2} & \dots & w_{1,R} \\ w_{2,1} & w_{2,2} & \dots & w_{2,R} \\ \dots & \dots & \dots & \dots \\ w_{S,1} & w_{S,2} & \dots & w_{S,R} \end{bmatrix} \quad (\text{F.6})$$

It is important that the number of inputs to a layer (R) can be different from the number of neurons (S). A layer is not forced having equal number of inputs and neurons.

F.2.2.2. Multiple layers of neurons

In this network can have several layers that the detail of each layer included of weight matrix “ W ”, bias vector “ b ”, and output vector “ a ”. The weight matrices, output

vectors, etc., for each of these layers are append the number of the layer as a superscript to the variable of interest. The three layers network is shown in Figure F.7. Each neuron in input layer is connected to the each neuron in first layer affected by the first weight matrix. And also, the each neuron in 1st layer is connected to neurons in 2nd layer affected by the second weight matrix and so on. A constant input 1 is fed to the biases for each neuron.

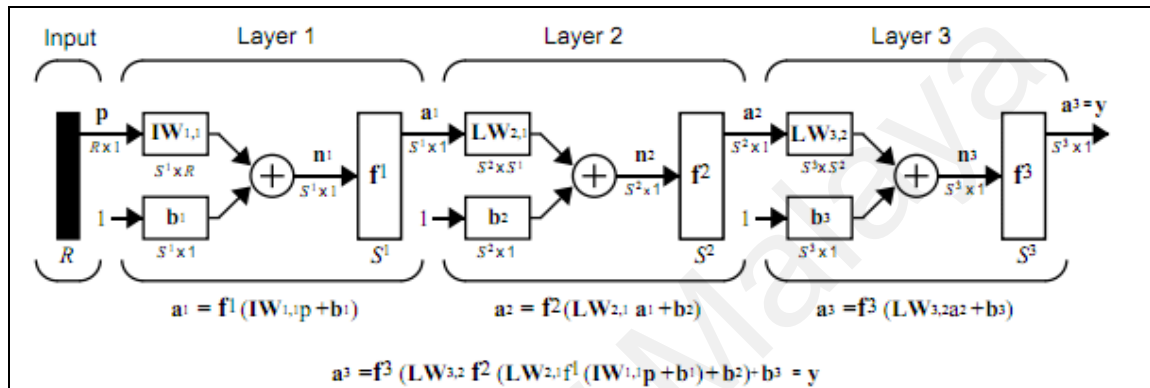


Figure F.7: Three-layer network architecture

F.2.3. Data Structures

In this section, the effect of the input data structure in network simulation is discussed. The data structure in static and dynamic neural network is defined as following:

Static Neural Network: The data definition occurs at the same time as concurrent vectors

Dynamic Neural Network: The data definition occur sequentially in time as sequential vectors

F.2.3.1. Simulation with concurrent inputs in a static network

Simulation in static network that has no feedback or delay is the simplest network simulation. In this case, the input treats as concurrent. In other word, it is not concerned for input vector to occur in the particular time. Also, the problems are even made simpler by

assuming the network included only one input vector. A single matrix of concurrent inputs is defined to static network to create a single matrix of concurrent outputs.

F.2.3.2. Simulation with sequential inputs in a dynamic network

When the network has delays, the network input would normally be a sequence of input vectors that happen in a certain time arrange. To demonstrate this case, a simple network that includes one delay is used.

F.2.3.3. Simulation with concurrent inputs in a dynamic network

By applying a set of concurrent inputs instead of a sequence of inputs, the network response will be completely different. The results will be same if each concurrent input apply to the separate network and compute one output. It is important to be considered that no need to assign any initial condition for net delay.

In two latest sections, the sequential and concurrent inputs are applied to dynamic networks. But, in the first section, the concurrent inputs were applied to static networks. In addition, it is possible to apply sequential inputs to static networks. The network simulation results will not be different, but it can have an effect on the way in which the network is trained. This issue will be obvious in the next section.

F.2.4. Training Styles

The two following training styles are explained in this part:

Incremental Training: Each time that the inputs are presented to network, the weights and biases of the network will be updated.

Batch Training: The weights and biases are only updated after all of the inputs are presented.

F.2.4.1. Incremental training

This training style can be applied for the both static and dynamic neural network, though it is more generally used with dynamic networks, such as adaptive filters.

In the incremental training, the weights and biases are updated while each input is applied. So, the functional adapt is used and the input and target are presented as sequences. As we discussed before, the simulation results for the static network in both cases of the concurrent and sequential input vectors will be same. It is because in case of using functional adapt, the weight is updated by incremental training mode if the input vectors are as a cell array of sequential vectors. But if the input is applied as a matrix of concurrent vectors, the weights are updated only after all inputs are applied as presented in next section.

F.2.4.2. Batch training

The batch training can be applied for the static and dynamic network. In this training, the weight and bias are updated after all of the input data and target are presented. The batch training can be completed by using either adapt or train, although the training is the best option. The incremental training can only be completed with adopt function, but the training can be used in the batch training. In the static networks, the training is simple as following:

- **Train:** The network is trained in batch mode and the input is changed to concurrent vectors, even if they are originally passed as a sequence.
- **Adapt:** The input format find out the method of training. For the input passed as a sequence, the incremental mode training is used. For the input passed as concurrent vectors, the network is trained in batch mode.

In the dynamic network, the batch mode training is typically done with train only.

F.3. Back-Propagation Algorithm

Back-propagation Neural Networks (BPNN) with commonly network architecture has applied to design special class of layered feed-forward named multilayer perceptron (MLP). BPNNs are training algorithms in a supervised style. The Input-output pairs are used to train a network until the network can approximate a function. A back-propagation network normally starts out with a casual set of weight. The weight will be changed in each process of input-output pair. During the feed-forward computation, each neuron performed two mathematical processes and each pair involves of two phases: a forward pass and a backward pass. In the forward pass a sample input presents to the network to process follow and reach to the output layer. The first process inserts input signals and products the weights coefficients and also computes the weight sum of the input node. In the backward pass, the output due to the forward pass compares with the known target and computes the evaluated error for the output units. The second unit is a non-linear component named neuron activation function that recognizes nonlinear function and transforms the sum of weighted signal into an output value. The back-propagation algorithm revises the weights in each input-output set by propagation the error back to the network using a widely used learning mechanism to change the weights and biases. After

training the generated network can be tested for the new input-output pairs. A neuron as a small computing part given in Figure F.8, takes the input signals X_1, X_2, \dots , develops them and then transmits the output Y .

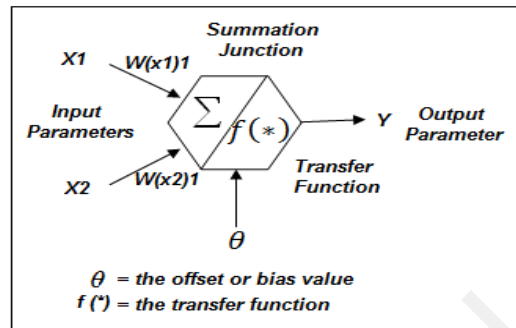


Figure F.8: Nonlinear model of a neuron

As we can see, the three essential mechanism of a nonlinear model of a neuron consisted of:

- i) a set of connecting links which are each characterized by a specific weight
- ii) a summation junction
- iii) an transfer function

For illustration, the defined signals, activation function, weigh coefficient, error and so on in a three layer artificial neural network are given in Figure F.9. The teaching of network is an iterative process and the weights coefficients of nodes are modified in each iterative process by using new data from training data set.

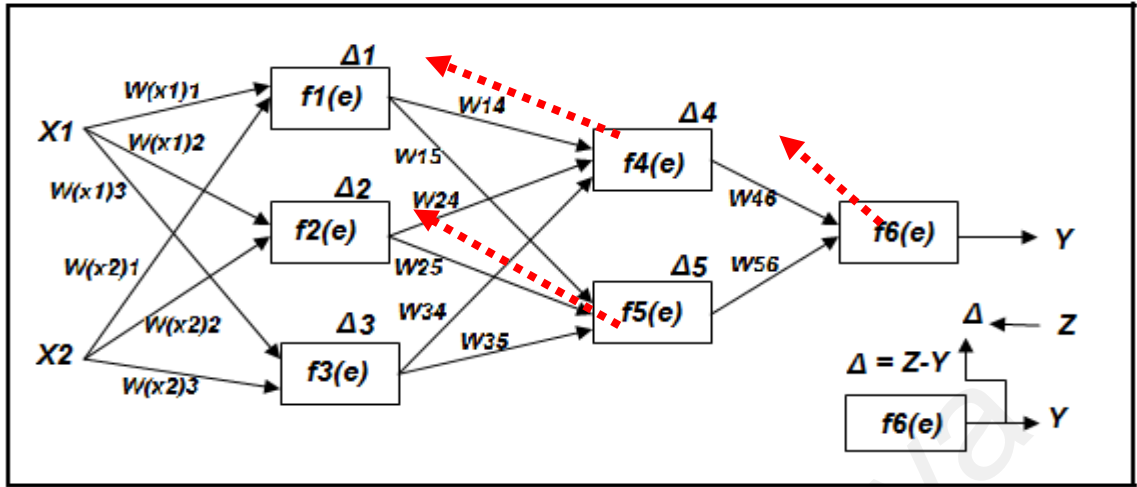


Figure F.9: A Three-Layered Static Artificial Neural Network

The training process consisted of:

- 1) Determine the primary value for weights
- 2) Each neuron in input layer transfers the signals $(x_i, i = 1, \dots, n)$ to all neurons in hidden layer.
- 3) Each hidden layer $(Z_i, i = 1, \dots, p)$ sums all the weighted signals from input and applies the activation function to calculate the output signals on output layer.

$$y_1 = f_1(w_{(x1)1}x_1 + w_{(x2)1}x_2)$$

$$y_2 = f_2(w_{(x1)2}x_1 + w_{(x2)2}x_2)$$

$$y_3 = f_3(w_{(x1)3}x_1 + w_{(x2)3}x_2)$$

$$y_4 = f_4(w_{(x1)4}x_1 + w_{(x2)4}x_2)$$

$$y_5 = f_5(w_{(x1)5}x_1 + w_{(x2)5}x_2)$$

(F.7)

- 4) Each output layer $(y_k, k = 1, \dots, m)$ sums the weighted signals transmitted from hidden layer and apply the activate function to calculate output signal.

$$y_6 = f_6(w_{(x1)6}x_1 + w_{(x2)6}x_2)$$

(F.8)

- 5) Each output layer calculates the error by comparing the target patterns and the response of the training pattern.

(F.9)

$$\Delta = Z - Y$$

- 6) The weights' coefficients w_{mn} used to propagate errors back for all network layers. Each hidden unit sums the input errors which are connected to the hidden unit.

$$\begin{aligned}\Delta_1 &= W_{14} \Delta_4 + W_{15} \Delta_5 \\ \Delta_2 &= W_{24} \Delta_4 + W_{25} \Delta_5 \\ \Delta_3 &= W_{34} \Delta_4 + W_{35} \Delta_5 \\ \Delta_4 &= W_{46} \Delta \\ \Delta_5 &= W_{56} \Delta\end{aligned}\tag{F.10}$$

- 7) When the error signal for each neuron is computed, the weights coefficients of each neuron input node may be modified. In formulas below df/de represents derivative of neuron activation function (which weights are modified). Coefficient η influences network training speed.

$$\begin{aligned}W'_{(x1)1} &= W_{(x1)1} + \eta \Delta_1 \frac{df_1}{de} x_1 \\ W'_{(x2)1} &= W_{(x2)1} + \eta \Delta_1 \frac{df_1}{de} x_2 \\ W'_{(x1)2} &= W_{(x1)2} + \eta \Delta_2 \frac{df_2}{de} x_1 \\ W'_{(x2)2} &= W_{(x2)2} + \eta \Delta_2 \frac{df_2}{de} x_2 \\ W'_{(x1)3} &= W_{(x1)3} + \eta \Delta_3 \frac{df_3}{de} x_1 \\ W'_{(x2)3} &= W_{(x2)3} + \eta \Delta_3 \frac{df_3}{de} x_2 \\ W'_{14} &= W_{14} + \eta \Delta_4 \frac{df_4}{de} y_1\end{aligned}\tag{F.11}$$

$$W'_{24} = W_{24} + \eta \Delta_4 \frac{df_4}{de} y_2$$

$$W'_{34} = W_{34} + \eta \Delta_4 \frac{df_4}{de} y_3$$

$$W'_{15} = W_{15} + \eta \Delta_5 \frac{df_5}{de} y_1$$

$$W'_{25} = W_{25} + \eta \Delta_5 \frac{df_5}{de} y_2$$

$$W'_{35} = W_{35} + \eta \Delta_5 \frac{df_5}{de} y_3$$

$$W'_{46} = W_{46} + \eta \Delta_6 \frac{df_6}{de} y_4$$

$$W'_{56} = W_{56} + \eta \Delta_6 \frac{df_6}{de} y_5$$

The training process will be stopped when the total error touches to a minimum value or limits to the number of training.

F.3. Radial-Basis Function

Radial-basis function (RBF) is another popular layered feed-forward network which has important common estimate properties. The architecture of the RBF consisted of two layers: hidden layer and liner output layer. The RBF networks apply memory-based learning for their design that learning is viewed as a curve-fitting problem in high-dimensional space as following:

1. Finding a surface in a multidimensional space to supply a most excellent fit to the training data.
2. Generalization is equal to apply the multidimensional surface to interpolate the test data.

The some fundamental different between RBF networks and perceptrons are:

- i) MLP are general approximators, whereas RBF networks are local approximators.

- ii) MLP can have various numbers of hidden layers, whereas RBF networks have only a single hidden layer.
- iii) The output layer of a MLP can be linear or nonlinear; whereas RBF network is always linear.
- iv) The activation function of a MLP computes the inner product between the input signal vector and the pertinent synaptic weight vector, whereas the activation function of the hidden layer in an RBF network computes the Euclidean distance between the input signal vector and parameter vector of the network.

The generalized regression neural network and probabilistic neural network are defined in Radial Basis networks.

F.4. Recurrent Network Function

In Recurrent Neural Networks (RNN), arbitrary connections in both feed-forward and feedback between neurons are allowed. The Elman Network and Hopfield Network are two kind of the network in case of recurrent function.

F.4.1. Elman Network

Elman networks consisted of two-layer back-propagation networks and a feedback connection from the hidden layer output to its input. The feedback connection lets Elman networks to recognize and create temporal patterns, as well as spatial patterns. The architecture of the Elman Network forms of TANSIG and PURELIN transfer function in hidden and output layer respectively. Having enough neurons in hidden layer are important in Elman Network. The training in the Elman network can be done either of two functions, *train* or *adapt*. In the *train* function, the following process in each epoch occurs:

- i. The all input series is applied to the network, and its outputs are calculated and compared with the target series to produce an error series.
- ii. For each sequence, the error series are back-propagated to get *gradients* of errors for each bias and weight.
- iii. The found gradient is used to revise the weights with the back-prop training function selected by the user. Traingdx is the recommended function.

In the *adopt* function, the following process in each step occurs:

- i. The input vectors are applied to the network, and it produces an error.
- ii. The generated error is back-propagated to get gradients of errors for each bias and weight.
- iii. The approximate found gradient is applied to renew the weights with the learning function selected by the user. Learnngdm is the recommended function.

F.4.2. Hopfield Network

Hopfield networks are constructed of artificial neurons which have N inputs. For each input x_i there is a weight w_i associated. There is also an output. The status of the output is maintained, until the neurons are updated. Updating the neuron involves of the following process:

- i. The value of each input, x_i is calculated and the weighted sum of all inputs are calculated as following formula:

(F.12)

$$\sum x_i w_i$$

- ii. The state of the output for neuron is set to +1 if the weighted input sum is bigger or equal to 0. It is set to -1 if the weighted input sum is smaller than 0.
- iii. A neuron keeps its output status until it is updated again.

The architecture of the Hopfield network is consisted of the saturated linear transfer function Satlins as well as shown in Figure F.10.

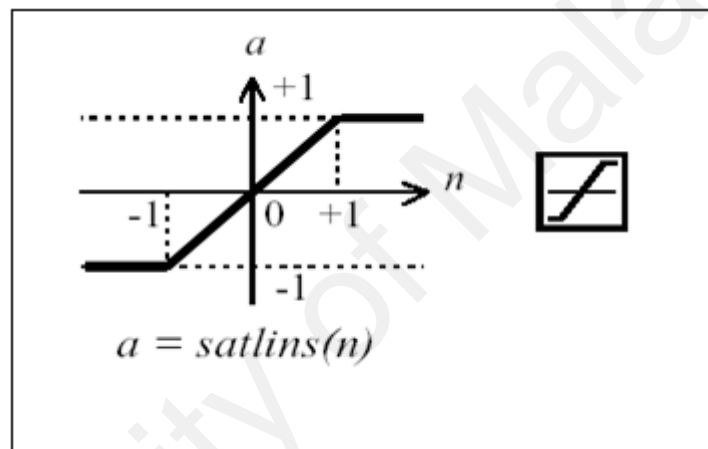


Figure F.10: Satlins transfer function applied in Hopfield network

For inputs less than -1 the Satlins transfer function produces -1. For inputs in the range -1 to +1 it simply returns the input value. For inputs bigger than +1 it produces +1. This network can be experienced with one or more input vectors which are defined as initial network conditions. After initial network conditions, the network generates an output which is then feedback to turn into input. This procedure is repeated more and more until the output become stable.

Published Paper

Razavi SV, Jumaat MZ, and EI-Shafie AH(2011), Using Generalized Regression Neural Network (GRNN) for Mechanical Strength Prediction of Lightweight Mortar, Computers and Concrete, (ISI). Accepted.

Razavi SV, Jumaat MZ, and EI-Shafie AH (2011). General Regression Neural Network (GRNN) for the First Crack Analysis Prediction of Strengthened RC One-way Slab by CFRP. Int J. of Physical Sciences. (ISI). 6(10):2439-2446.

Razavi SV, Jumaat MZ, and EI-Shafie AH (2011). Artificial Neural Network for Mechanical Strength Prediction of Lightweight Mortar. Scientific Research and Essays. (ISI). 6(16): 3406-3417

Halvaeyfar MR, Jumaat MZ, and Razavi SV. (2011). Nonlinear Analysis of Load-Deflection Testing of Reinforced One-way Slab Strengthened by CFRP and Using ANN for Prediction. Int J. of Physical Sciences. (ISI). 6(13):3054–3061

Razavi SV and Jumaat MZ (2011). Application of Artificial Neural Network for prediction of Lightweight Concrete. IGRDG Journal. 2(1).

Razavi SV (2010). GR & FFB Neural Network for Presentation of Strengthened RC Slab by using CFRP. The 5th Civil Engineering Conference in The Asian Region and Australian Structural Engineering